# Sea Breeze Circulation in the Auckland Region: Observational Data Analysis and Numerical Modelling

**A thesis**
**submitted in partial fulfilment**
**of the requirements for the degree**
**of**
**Doctor of Philosophy in Environmental Science**
**in the**
**University of Canterbury**

by

**Basit A. Khan**

**University of Canterbury**
**March, 2010**

# Abstract

The main aim of this research is to improve our knowledge of the sea breeze circulation in the complex coastal environments, where more than one mesoscale circulations occur. Interaction of these circulations with each other and with external factors such as topographical features and large scale winds leads to pronounced changes in the thermodynamic structure of the boundary layer. The variations in sea breeze circulation also have distinct effect on the pollutant transport and dispersion mechanisms in the coastal urban areas. In this research, dynamic and thermodynamic characteristics of the sea breeze circulation and their associated air pollution potential have been investigated by utilizing observational data for two summer periods and numerical modelling techniques. Effect of some external factors such as gradient flow and terrain elevation has also been examined. Observed meteorological and air quality data was obtained from a number of monitoring sites within and around Auckland while Advanced Weather Research & Forecasting (WRF) and 'The Air Pollution Model' (TAPM) were employed to simulate meteorology and pollutant dispersion in Auckland. WRF is used to investigate the thermally induced mesoscale circulation while TAPM has been employed to examine the pollutant dispersion in the region. Both models were validated against observed data from six different sites within Auckland. Validation results of WRF and TAPM are also compared with surface meteorology. Validation and inter-comparison of the two models show that WRF performed better than TAPM for all the surface meteorology variables. WRF showed a positive bias in predicted winds speed and relative humidity and a cold bias in the near surface Temperature. TAPM on the other hand under-predicted surface winds, while near surface temperature and relative humidity are similar to WRF.

Results show that the sea breeze occurred around 20% of the two summer periods of 2006 and 2007. Both observed data analysis and the numerical modelling results confirmed the existence of two thermally induced systems in the Auckland region. Bay breezes are initiated in the morning hours (0800 – 1000 hours) from small bodies of water (Manukau, Waitemata, and Kaipara Harbour, and along the Hauraki Gulf coastline), followed by mature sea breezes from the main bodies of water (Tasman Sea

and larger Hauraki Gulf area) in the late morning. The cessation of sea breezes started after 1600 hours. Frequency of sea breeze days was the highest under coast-parallel gradient winds (southeast and northwest), with speeds < 6 m $s^{-1}$. The predicted depth of the sea breeze inflow ranged between 200 and 600 m, while the depth of the return flow was in the range of 200 – 500 m. Sensible heat flux is an important control in the development of sea breeze over the region. Coastal mountain ranges helped early onset of the sea breeze, but also inhibited inland propagation. Strong jet-like westerly winds along the coastline near the Manukau Harbour are due partly to the narrow opening at the Manukau Head, reduced friction over the harbour water, and divergence of wind due to coastline shape. Gradient winds significantly affect the evolution of the sea breeze and modify many of its dynamics, such as the sea breeze inflow layer, return flow, inland penetration, sea breeze head, etc. Under northerly gradient flow northeast sea breeze lasts longer while under southerly gradient flow cessation of the westerly sea breeze was delayed.

Over both east and west coasts, WRF predicted anticlockwise rotation, especially under easterly gradient wind conditions. However, inland stations near Manukau Harbour show partial and complete clockwise rotation, which is primarily due to orographic features of the region. The diurnal rotation of the sea breeze system may contribute to recirculation of pollutants in the morning hours under coast-parallel gradient wind conditions. Pollutants that are emitted during morning peak traffic hours and advected towards Manukau Harbour by the remnants of the land breeze may be returned by bay breezes in the mid morning hours.

Mixed layer height over land before arrival of the sea breeze also varied a lot and ranged between 600 to 1400 m. A convective internal boundary layer (CIBL) forms in the surface layer after arrival of the sea breeze. The CIBL under coast parallel gradient winds was relatively shallow (200 – 400 m), while under coasts-normal gradient winds (southwest and northeast), the predicted depth was in the range of 400 to 500 m. However, the inland extent of the CIBL was greater under coast-normal winds, especially under south-westerly gradient winds. The ground level concentration of air pollutants thus can be increased during sea breeze inflow over the region.

Both bay breeze and mature sea breeze contribute towards development, extent and strength of the sea breeze convergence zones (SBCZs). Gradient winds and terrain play an important role in the position and strength of SBCZs. Under strong south-westerly gradient flow, a SBCZ is formed along the eastern coastline, while under north-easterly gradient winds a SBCZ is formed along the west coastline. During coast-parallel gradient winds the SBCZ is formed in the middle of landmass, and is then gradually displaced eastward or westward depending on the balance between large scale PGF and surface friction effect. In addition to SBCZs, terrain and coastline-induced convergences were also evident. Higher ground level concentrations of pollutants are expected under coast-normal gradient winds, when SBCZs are formed in the middle of the land mass and the wind speed of the sea breeze inflow and the sea breeze front is relatively low. This may increase pollution concentration, especially in the evening hours, to unacceptable levels. Results of this research suggest that given the size, synoptic meteorology and specific geography of the region, significant recirculation of pollutants is not likely to happen to contribute to next day's pollution. The pollutant concentration may increase in the SBCZs, but their ability to recirculate the pollutants requires more extensive research.

A closed sea breeze circulation cell is unlikely to form in this region due to topographical influences and a strong gradient wind effect. The pollutant plume is expected to be advected in the return flow over the peaks of higher terrain and via the top of the convergence zones, but its remixing in the onshore flow is subject to many factors such as gradient wind speed and direction, direction of the return flow and nature (size and state) of the pollutant. In appropriate conditions, pollution levels may reach to unhealthy levels under coast-parallel gradient wind condition.

**I, dedicate this thesis to my mother Ejaz-un-Nissa,**
**and my wife Humaira.**

# Acknowledgement

I wish to offer my profound gratitude to my supervisors Dr. Peyman Zawar-Reza and Professor Andrew Sturman, for their unending support, advise, guidance and encouragement throughout this research. I am especially indebted to Professor Andrew Sturman for encouraging me to undertake this research. Dr. Peyman always went beyond the student–supervisor relationship and provided help and support in both personal and research problems. In particular I am grateful to both of my supervisors for bailing me out with commercial projects when I was had financial difficulties. A big thanks also goes out to the head of the Geography Department, Wendy Lawson, for providing administrative support and helping me in winning the doctoral scholarship.

The department of Geography provided a relaxed, friendly and comfortable research environment that I enjoyed a lot in the last few years. My especial thanks go to the department's IT team, especially Steven Sykes and John Thyne were always quick to respond to any computing requirements. I am also grateful to Anna Petrie and Marney Brosnan for providing administrative support and organizing artistic and colourful events. Though all of the Geography Department's staff are friendly and supportive, a personality that no newcomer can forget is that of Henry Connor. I always enjoyed talking to him and greatly appreciated his comments and advice on how to improve the quality of my research.

Being part of the Centre for Atmospheric Research of the University of Canterbury (UCAR), I gained a whole lot of experience. Despite coming from different cultural and academic backgrounds the researchers at UCAR work and enjoy like a family. I am greatly thankful to Steve George, Zahid, Mikhail Titov, Mike Green, Tim Appelhans and Marwan Kuturji for their valuable advices, help and support throughout this research. Marwan in particular become a close friend over time and often inspired me and surprised me with his intelligence, creative thinking and positive energy. I would also like to thank the National Institute of Water and Atmospheric Research (New Zealand) and Auckland Regional Council for providing meteorological and air pollution data for the Auckland region. Also many thanks to James Sturman of NIWA

for providing sea surface temperature data around New Zealand. Modelling tools have never been error free and probably would never achieve the title of ‘user friendliness’, researchers in this field, therefore, always require an efficient help desk. In case of WRF (ARW), this role is being performed by the ‘WRF help’. I greatly appreciate ‘WRF help’ team at University Corporation of Atmospheric Research (UCAR USA) for their help and support to researchers for trouble shooting WRF (ARW).

Finally, I want to thank my family and friends, who were always there for me. Most importantly I want to thank my wife for her patience and support.

## Contents

**List of Appendices**

## List of Tables

## List of Figures

# 1. Introduction

## 1.1 Background

In this thesis, the dynamic and thermodynamic structure of the sea breeze and its potential effect on the air quality of the Auckland region has been investigated. The effect of topography and large-scale winds on the sea breeze circulation that results in variations in the pollutant transport and dispersion mechanisms has also been examined. Mesoscale circulations arising from diurnal thermal differential of land and water are amongst most intensively studied meteorological processes. This is partly due to the effect of these circulations on the local weather and air quality of coastal urban areas, where large part of the human population lives as 13 of the world's 20 most populous metropolitan areas are situated along sea coasts, estuaries or large lakes (Arritt 1987; Miller et al. 2003). The complexity of the sea-breeze phenomenon gave rise to much interest in the understanding of the dynamics of the boundary layer during sea-breeze events (Miller et al. 2003; Simpson 1994). The structure, behaviour and characteristics of the sea-breeze system are crucial not only due to its meteorological significance but also due to its air quality implications in the coastal regions. Therefore, an understanding of the three dimensional thermodynamic characteristics of the sea breeze circulation is important for the evaluation of pollutant transport and dispersion within the boundary layer. This is especially true in complex coastal environments such as the Auckland region where interaction of surface features and large scale winds with a variety of sea breeze phenomena, such as sea breeze convergence zones, convective internal boundary layer, and diurnal wind rotation, may further complicate the dispersion of pollutants (McKendry 1989).

The complex terrain of the Auckland region, with large and small bodies of water on both sides of the isthmus and an undulating and indented coastline, gives rise to an equally complex boundary layer structure that, combined with mesoscale sea-land breeze circulations, and large scale winds, produces complex wind patterns. Sea-land circulation is the dominant feature of the summer time local meteorology of the region and due to its role in local weather and air quality, the sea breeze circulation may have significant effects for social, commercial and environmental aspects of society. The complexity of local and mesoscale winds offers a great challenge for local weather and air quality forecasting for the region. The efforts to improve our understanding of mesoscale phenomena such as the land-sea breeze have been greatly hampered by the lack of observational data of several key boundary layer properties such as the atmospheric boundary layer height, low-level jets and thermodynamic structure of the sea breeze circulation. The sparse network of observational meteorological sites and their ability to sample the state of the atmosphere only at single points limits our ability to comprehend the entire extent of any particular meteorological phenomenon. In this context, the numerical modelling technique provides a powerful and convenient tool for understanding the complex three dimensional structure, stratification and dynamics of the planetary boundary layer (PBL) at a larger scale (Talbot et al. 2007). Mesoscale numerical models can be used to identify regions of diminished/enhanced air quality based on consideration of areas of convergence/divergence, weak/strong winds and increased/decreased PBL depth. Modelling techniques can also be utilized as a guide, in optimal network design, for example, siting of acoustic sounders may be based on consideration of the PBL depth field (Bell & Fisher 1995; McKendry 1989; Sutton 1996).

A number of observational and numerical modelling studies have been conducted since 1980's in the Auckland region to investigate the sea breeze phenomenon and its overall impact on the air quality of the region. Amongst these, probably the most comprehensive observational study on sea breeze circulation was conducted by McGill (1987). In this study, McGill (1987) analysed data for three summer periods (12 months) of 1979, 1980 and 1981. The sea breeze days from these 12 months of summer data were identified using a method developed by Mathews (1982). The study addressed the development, onset and decay of the sea breeze, sea breeze convergence

zones and the effect of gradient winds on the mesoscale circulation. The vertical structure of sea breezes was also discussed. However, primary focus of this study was on sea breeze dynamics (sea breeze inflow, return flow, sea breeze convergence zone etc.), the thermal structure of the atmosphere during a sea breeze event was totally ignored. Additionally, the affect of sea breeze dynamics on the air quality of the region were also not discussed. Previous numerical studies of sea breeze circulation and associated air pollution have used a variety of different numerical tools. Amongst these the simplest but the least accurate was probably the box model applied by Wratt et al. (1990). Although model chemistry was represented reasonably accurately, the meteorological fields were poorly represented, yet they are critical for transport and dispersion of pollutants in a given area (Sutton 1996). McKendry (1989) and McKendry (1992) employed a mesoscale meteorological hydrostatic model developed at Colorado State University (CSU) to study the variations in the planetary boundary layer and development of sea breeze convergence zones during a sea breeze event. Results of these studies were in general agreement with the previous observation studies. The CSU model was developed for the study of thermally-forced, terrain-induced mesoscale phenomena with hydrostatic approximations. Various studies show its ability to accurately simulate mesoscale phenomena (e.g. Pielke 1974), but many of its shortcomings make it inappropriate for use in the complex terrain of the Auckland region. The hydrostatic approximation used in the CSU model retains only gravity and vertical pressure gradient forces and assumes that the acceleration term in the vertical momentum equation is much smaller than the pressure gradient and buoyancy terms and can be ignored. This is appropriate for scales greater than 10 km (Pielke 1984), but at smaller scales from local to mesoscale processes such as the sea-land breeze circulation, vertical acceleration cannot be ignored and a non-hydrostatic model is desirable to accurately simulate this mesoscale phenomenon (Miao 2006). The CSU model uses the Deardorff (1974) prognostic equation to estimate the PBL depth. However, Physick & Abbs (1989) found that the prognostic equation suggested by Deardorff did not accurately simulate the convective internal boundary layer growth during sea breeze inflow. Additionally, it is difficult to specify surface properties in the model setup, and the simulation was run without taking into account variations in surface characteristics. This would have direct impact on the magnitude of latent and sensible heat fluxes and thus the predicted PBL depth (McKendry 1989). The inability

of the model to update the lateral boundary conditions with the evolving large scale synoptic situation also undermined the accuracy of results. Finally, McKendry (1989) concluded that considering the complexity of the region, application of simple Gaussian and 'box' approaches for air quality assessment are inadequate in Auckland.

Ridley (1992) and Ridley (1995) employed a Lagrangian Particle Dispersion Model (LPDM) with meteorological fields obtained from the modified version of CSU model to simulate particle dispersion in the sea breeze convergence zone over Auckland. The model accurately represented the wind field and pollutant advection but the major drawback was the limitation of the LPDM, to handle only a small number of point sources. This limitation hampered the results of the study of a region where more than 70% of the pollutants come from traffic emissions (Sutton 1996).

Considering the shortcomings in the above modelling approaches, Sutton (1996) utilized a mesoscale, non-hydrostatic Eulerian model named 'Regional Atmospheric Modelling System (RAMS)' coupled with a Eulerian component to model sea breezes and pollutant dispersion. Unlike a Lagrangian model that specifies the point source at a particular point inside the gird, a Eulerian model specifies the source over the entire grid cube. However, low resolution and errors in the RAMS code undermined confidence in the model results. More recently, Gimson (2005) employed two Eulerian based models namely 'The Air Pollution Model' (TAPM) and California Photochemical Grid Model 'CALGRID' to simulate local flows such as the sea breeze and cold air drainage to investigate their role in the air quality of the Auckland region. Results of Gimson's study suggest that the sea breeze convergence zone in Auckland coincides with periods of elevated ozone ($O_3$) and peaks in nitrogen dioxide ($NO_2$). However, the study was limited to the investigation of sea breeze convergence zones only.

In summary, previous numerical modelling studies of sea-land breezes suggest application of mesoscale, non-hydrostatic models with improved PBL and land surface parameterization, along with better representation of land surface characteristics. For pollution dispersion, Lagrangian and/or Eulerian approaches were recommended instead of the Gaussian or 'box model' approach (McKendry 1989; Sutton 1996).

Taking the past work into consideration, a comprehensive research programme was designed to study the sea breeze circulation and its potential effect on the air quality of the region. The experimental design was based on the recommendations of McKendry (1989) who suggested intensive observational study along with numerical modelling of the local meteorology that would test the veracity of the model results, but more importantly respond to questions that observational data may not be able to answer due to its inherent limitations. Along with the data analysis of two summer period of five months each (November, December, January, February, and March) of 2006 and 2007, two mesoscale numerical models, namely the Advanced Research Weather Research and Forecasting WRF(ARW) modelling system and 'The Air Pollution Model' (TAPM), have been employed. WRF is used as the main modelling tool to investigate the thermodynamic structure of the sea breeze, while TAPM is primarily used to investigate pollution dispersion in the Auckland region. Additionally, the performance of both WRF and TAPM is also evaluated. A detailed description of both of these models is provided in Chapter 5.

## 1.2 Main Aim and Objectives

The aim of this thesis is to improve our understanding of the sea breeze circulation in the complex coastal environments and its role in the air quality over a narrow peninsula shape land mass such as Auckland where sea breeze occurs on both sides of the isthmus. The effect of various external factors (both meteorological and topographical) on various sea breeze characteristics has also been. A detailed description of the geography, weather and climate of the Auckland region is provided in Chapter 3. This thesis has three dimensions: one is the investigation of the sea breeze circulation itself; second is the effect of external factors such as gradient winds and topography; and third is the effects of the sea breeze circulation on the air quality of the Auckland region. Within this framework the specific objectives for this research are defined as follows:

a) ***To examine the frequency, onset and decay of the sea breeze****:* Sea breeze evolution is affected by a number of factors. In the Auckland region, very few studies have examined sea breeze occurrence for more than one summer period. Probably the only major study in this respect was completed by McGill (1987). The onset and decay time of the sea breeze inflow is not

only significant from a local weather perspective, but it is important for air quality applications.

b) ***To investigate the dynamic and thermodynamic structure of the sea breeze:*** The general behaviour of the sea breeze circulation depends on its various characteristics/components. Amongst these, sea breeze convergence zones, the convective internal boundary layer, diurnal rotation of wind direction, and sea breeze inflow and return flow are important from an urban air quality perspective. An investigation of these sea breeze characteristics will help in determining their role in enhancement or inhibition of pollutant concentration.

c) ***Inter-comparison of WRF and TAPM performance in simulating the sea breeze:*** TAPM is widely used in Australia and has been applied in most of the large urban areas in New Zealand. In the Auckland region, TAPM has been employed for a variety of air pollution and meteorological studies. However, WRF is still a relatively new model for New Zealand and has not been extensively tested for modelling mesoscale meteorological processes at such a fine resolution (500 m). A comparison of both model results would improve our understanding of the differences in predictive power of the two models, as well as their treatment of different meteorological variables (e.g. temperature, wind velocity, moisture) in the coastal environment of the Auckland region.

d) ***To examine the effect of large scale winds on the sea breeze circulation***: Interaction of various characteristics of the sea breeze such as sea breeze inflow, diurnal wind rotation, convective internal boundary layer with large scale winds results in complex wind flows and significant modifications in sea breeze characteristics. An investigation of these interactions between synoptic forcing and sea breeze characteristics is necessary to understand the sea breeze and its effect on the pollution potential of the region.

e) ***To examine the effect of topography on the sea breeze circulation***: Topography has a major effect on the onset, decay and strength of the sea breezes. Various sea breeze characteristics, for example diurnal wind rotation and sea breeze convergence zones are also significantly affected by

topographical features. An understanding of the effect of terrain features is desirable to comprehend variations in the sea-land circulation.

## 1.3 Thesis Structure

As outlined above, the main focus of this thesis is to investigate the sea breeze phenomenon, with its non-linear interactions with external factors and impact on the air quality of the Auckland region, by means of observational data analysis and numerical modelling techniques. The thesis has been organized in eight chapters.

The first Chapter discusses the background, establishes the rationale, and sets aims and objectives for the research. The next two chapters (2 and 3) provide a detailed overview of the sea breeze circulation and local meteorology of the Auckland region, while focusing on the daytime circulation. The air quality implications of the sea breeze characteristics are also discussed in sufficient detail. The next four chapters (4, 5, 6 and 7) are the core of this research and provide a detailed analysis of the sea breeze circulation and its air quality implications by utilizing observed data and various real and idealized numerical experiments.

Chapter 4 analyses the observational data for 2006 and 2007. The data were obtained from various observational sites within the Auckland region. First, the sea breeze and non-sea breeze days were identified based on a simple assumption that any summer day was a sea breeze day if onshore flow occurred on both sides of the peninsula. Various statistical techniques were then used to assess the differences between sea breeze and non-sea breeze days. The important characteristics of the sea breeze circulation are also discussed in this chapter. A case study for a selected high air pollution day is also included.

In Chapter 5, the mesoscale numerical modelling technique was used to investigate the kinematic and thermodynamic structure of the sea breeze and associated pollution dispersion. In these numerical modelling studies two mesoscale numerical models (Advanced Research WRF and The Air Pollution Model), are employed to investigate the sea breeze phenomenon. Both models were run in non-hydrostatic mode and without data assimilation. The WRF model was used to study the major characteristics

of the sea breeze circulation, while TAPM was employed to investigate pollution dispersion over the Auckland region. Both models were first validated against the observed data from six automated weather stations (AWS) within the Auckland region.
Chapter 6 examines the effects of gradient winds on the sea breeze circulation. For this purpose four idealized simulations were run with four different gradient winds imposed in the initial model setup. Modifications of sea breeze characteristics due to variations in the large scale winds were then studied.

Chapter 7 addresses the topographic influences on sea breeze circulation. In this chapter, two WRF simulations were analysed. The first simulation was run with topography and the second simulation was run without topography. The background wind was removed from both simulations to eliminate the effect of the large scale winds.

Chapter 8 provides a summary of the four analysis chapters (4, 5, 6 and 7) and concludes the results with recommendations for future work.

### 1.3.1 Time

The clock time used in this thesis is New Zealand Standard Time (NZST) unless, defined otherwise. Therefore both ‘hour’ and ‘NZST’ refers to New Zealand Standard time without daylight saving adjustment. In some instances universal clock time (UTC) is used and identified by using ‘Z’ or ‘UTC’ as suffix to the time/hour. The UTC is approximately 12 hours behind NZST.

# 2. The Sea Breeze System

## 2.1 Introduction

Sea and land breezes are thermally forced, mesoscale atmospheric circulations often observed along the coasts of oceans, lakes and islands. Sea breezes occur along nearly every coast around the world (Avissar et al. 1989). Sea and land breezes are well studied phenomena. Perhaps the first documented account of sea-land breezes was found in the writings of Aristotle in the $4^{th}$ century B.C., who referred to these circulations as 'alternating winds' (Neumann & Mahrer 1973). Although sea-land breezes are most common in subtropical latitudes, they have also been observed in the Arctic (e.g. Kozo, 1982). Sea and land breezes are produced due to the distinct differential response of land and water to daytime heating and nocturnal cooling. Thermal gradient between land and sea which is the main driving force behind the mesoscale circulation is attributed to variations in specific heat capacity of land and water, heat transfers (vertical and horizontal) and vapour flux rates (Bureau of Meteorology-Australia 1977a; Miller et al. 2003; Thompson 1998). Sea breezes typically form during spring, summer and autumn months. The cool ocean air begins its inland journey during the mid to late-morning hours, when daytime land temperatures exceed adjacent water temperatures by an average of about 3°C to 6°C (Comet 1999; Simpson 1994). The wind direction associated with the sea breeze is directed inland along the surface pressure gradient, which is oriented perpendicular to the coastline. Solar heating increases the pressure gradient by lowering the pressure over the land relative to that over water. Consequently, sea breeze penetration reaches a maximum and winds are strongest at this time (Oke 1987; Thompson 1998). Afternoon is the most

active time of the day when the sea breeze circulation intensifies as daytime solar heating reaches its maximum although coastal regions that experience intense sea breeze in the afternoon, peak temperature in these regions occur much before that in the late morning (Simpson 1994). In mid-latitudes sea breeze depth reaches up to 500 m, and often twice that in the tropics, while the inland extent of the sea breeze front ranges between 10 and 200 kilometres (Thompson 1998). The sea breeze circulation slowly diminishes in the late afternoon, so that one or two hours after sunset the sea breeze dies away altogether. At night-time the land cools, and the process reverses itself with the formation of a land breeze circulation. Sometimes, a disconnected sea-breeze front continues to advance farther inland during the night over the growing nocturnal stable boundary layer causing a bore (a propagating solitary wave with characteristics similar to an hydraulic jump), a phenomenon known as the Morning Glory in Australia and is traditionally associated with convergence of two sea breeze fronts (Clarke 1984; Stull 2003). The oppositely directed night time offshore flow of the land breeze is much weaker than a sea breeze and due to less available energy rarely achieves half of sea breeze wind speed, and is often reinforced by slope effects (Thompson 1998). In a convective environments a land breeze front can also be developed over the ocean and sometimes initiates nocturnal convection along the land breeze front over the ocean (University Corporation of Atmospheric Research 2008).

Although the underlying mechanism of thermally induced circulations is the same, the characteristics of the circulation may considerably differ from one region to another in terms of onset, intensity, direction, phase change, inland extent etc. In addition to land-water thermal differential, the variations in sea-land circulation are attributed to local, mesoscale and synoptic atmospheric conditions, latitudinal position, coastline shape, land surface characteristics (e.g. soil type, soil texture, soil moisture, soil temperature etc.), topography and land cover (Abbs & Physick 1992; Clarke & Arritt 1995; Hong et al. 1995; Mahfouf et al. 1987; Miao et al. 2003; Miller et al. 2003). For example the prevailing large scale synoptic weather patterns have a direct effect on the strength, persistence and inland penetration of sea and land breezes (Adams 1997; Avissar et al. 1989; McKendry 1992; Miller et al. 2003; Zhong & Takle 1993). In addition to large scale synoptic winds sea breezes can also interact with other external meteorological phenomena e.g. temperature inversions, separate sea breeze systems from some other

nearby coast, boundary layer convection, horizontal roll vortices, urban heat islands and synoptic scale cold fronts (Atkins et al. 1995; Frietas et al. 2006; Lin et al. 2008; McGill 1987; McKendry 2003; Miller et al. 2003; Pielke 1974). In general the strength of sea breezes is proportional to the magnitude of the land and sea temperature difference, as well as the direction and the strength of the prevailing synoptic flow (Comet 1999). Many empirical studies have used temperature information for examining the occurrence of sea breezes. For example, McKendry and Roulet (1994) reported that all sea breezes observed on the western shore of James Bay (Canada) were associated with inland temperatures > 20$^{o}$C. Biggs & Graves (1962) developed an early lake (sea) breeze index that compares the background wind to the land-sea temperature contrast:

$$\text{L-B Index} = |U|^2 / C_p \Delta T$$

Where 'U' is the near-surface wind speed, $C_p$ is the specific heat coefficient of dry air at constant pressure (1.004 J $g^{-1}$ $K^{-1}$) and $\Delta T$ is the difference between the inland air temperature and the temperature of the water surface. If the L-B Index is large then the inertial force will be large and a lake (sea) breeze will not develop. However, if the L-B Index is small, then the buoyant force will be relatively large, and the lake (sea) breeze can move inland. Biggs & Graves (1962) found that the critical L-B Index range lies between 2.7 and 3.2, and values within this range correctly predict the occurrence/non-occurrence of the lake breeze 97% of the time.

## 2.2 Structure and Dynamics of the Sea Breeze System

The sea-land circulation is often thought to be a simple and easily understood system, but in reality it is incredibly complex mesoscale meteorological process. The sea breeze system consist of phenomena that occur on several spatial (Miller et al. 2003) and temporal scales. The structure of the sea breeze includes a sea breeze circulation cell and its associated phenomenon such a sea breeze head, a sea breeze inflow current, a sea breeze front, a return flow and Kelvin-Helmholtz Billows (Figure 2.1). When sea breeze moves over land, it modifies the vertical thermal structure of lower boundary layer that leads to a shallow well mixed convective internal boundary layer. Additionally development of sea breeze circulation results in various dynamic processes such as diurnal rotation of near surface winds and sea breeze convergence

zone (SBCZ) etc. This section briefly discusses some of the important characteristics of a sea breeze system.

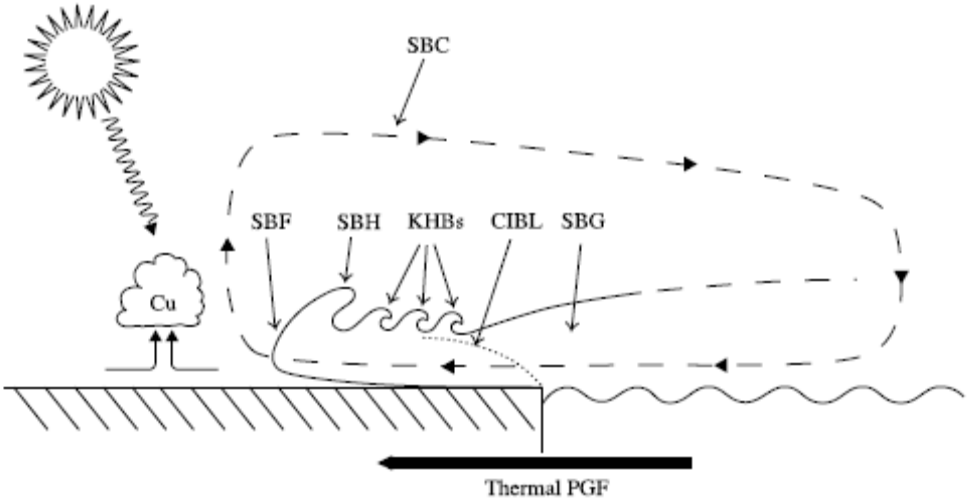


Figure 2.1: The Sea breeze system (SBS), adopted after (Miller et al. 2003)
* SBC: Sea breeze circulation cell; SBF: Sea breeze front; SBH: Sea breeze head; KHB: Kelvin-Helmholtz Billows; CIBL: Convective internal boundary layer; SBG: Sea breeze gravity wave (sea breeze inflow current).

### 2.2.1 Sea Breeze Circulation Cell (SBC)

Sea breeze circulation is simply a response of the lower atmosphere to balance the mesoscale horizontal and vertical pressure gradient that is resulted from thermal differences between land and sea. Miller (2003), has defined the sea breeze circulation cell as "A vertically rotating mesoscale circulation, with shoreward flow near land surface, rising air currents inland, a (usually) seaward return flow near 900 hPa and a diffused sinking currents several kilometres out to sea". The horizontal extent of the SBC is to both landward and seaward direction; however, under weak or zero gradient winds, the SBC extension over the water is more than over land due mainly to the reduced frictional force over sea (Abbs & Physick 1992; Finkele 1995).

The SBC may not be a mass conservative closed system as found by Estoque (1962). Various studies in different parts of the world found that in certain condition the return flow was either not generated at all or it was incomplete and insufficient to counterbalance the low level sea breeze inflow (Banta et al. 1993; Estoque 1962; Miller et al. 2003). The upper limit of the circulation varies from a few hundred metres to 1 or 2 km, depending on synoptic conditions (Xian & Pielke 1991a).

### 2.2.2 The Sea Breeze Inflow (SBI) Current

The sea breeze inflow (SBI) corresponds to the low level inland propagating flow of cool, moist marine air behind the sea breeze front (Miller et al. 2003; Talbot et al. 2007). When fully developed, surface (10 m height) wind speeds in the marine, inflow portion of the sea breeze at the coast range from 1 to 10 m $s^{-1}$ with typical values of 6 m $s^{-1}$. Wind speed of the onshore flow increases with the square-root of the land-sea temperature difference (Oke 1992; Stull 2003). Due to its similarity with the cold fronts, the inland movement of the leading edge of the cold dense marine air inflow is sometimes referred to as a mesocale cold front (Simpson 1994). The vertical extent of the sea breeze inflow is usually defined by the zero onshore wind component (Abbs & Physick 1992). The depth of the onshore flow behind the front ranges between about 300 and 2500 m (Barbato 1975).

### 2.2.3 The Diurnal Rotation of Sea Breeze

As the sea-breeze circulation evolves the surface wind oscillates back and forth between onshore and offshore, reversing directions over the diurnal cycle. The Coriolis force induces an oscillating along-shore wind component that lags the onshore-offshore component by 6 hours (or 1/4 cycle). Hence, the diurnal wind vector rotates throughout the course of the day causing the direction of the circulation to turn to the right of coast-normal in the Northern Hemisphere and to the left of the coast-normal in the Southern Hemisphere. For example, along a meridional coastline, with ocean to the west in the Southern Hemisphere, the diurnal component of the surface wind tends to be westerly (onshore) during afternoon, southerly (alongshore) during the evening, easterly (offshore) at night and northerly (alongshore) in the morning. The diurnal wind component and the mean 24 hour average surface winds are additive, so that if the mean wind is blowing from the south, the surface wind speed will be high in the evening (around sunset) when the mean wind and the diurnal wind component are in the same direction. At sunrise, the surface wind speed will tend to be low when the diurnal wind component is from the north (opposite to the mean gradient wind) (Bureau of Meteorology-Australia 1977a,b; Stull 2003). If a weak synoptic-scale gradient wind exists with a component parallel to the shore, then the surface wind can be approximated as the vector sum of the synoptic and sea-breeze components, and as described in Section 2.3.1, the whole circulation can become helical with the horizontal

axis over the shoreline (Stull 2003). At latitudes greater than $20^{o}$, the Coriolis force becomes strong enough to considerably affect the direction of sea breeze as the circulation develops. The strength of the sea breeze component increases in the afternoon, and as a result, the Coriolis force increases and the sea breeze effect may become directed more nearly parallel to the coast (Bureau of Meteorology-Australia 1977a,b)

### 2.2.4 The Sea Breeze Front (SBF)

A sea-breeze front is the leading landward edge of the advancing cool marine air (sea breeze inflow current), and behaves similarly to a weak advancing cold front or a thunderstorm gust front (Stull 2003) (Miller 2003). It is often associated with sharp changes in temperature, moisture, and wind speed and direction (Miller et al. 2003). Its approach may be marked by low level convergence, temperature drop, an increase in humidity, upward motion and development of fair weather cumulus clouds (Cu). A line of thunderstorms may be triggered if the atmosphere is convectively unstable. The sea-breeze front usually advances at approximately 3/4 of the surface wind speed (Stull 2003).

Based on the above properties the temporal and spatial evolution of a SBF can be categorized either as a) a thermodynamic sea breeze front or b) a kinematic sea breeze front (Atkins et al. 1995; Miller et al. 2003). Thermodynamic SBFs are characterized by marked changes in the mean thermodynamic properties of the air within the planetary boundary layer (PBL) that are created by the interaction between SBF and Horizontal Convective Rolls (HCRs). The kinematic sea breeze fronts are characterized by maximum convergence especially in the first 100 m AGL. Although it is unlikely, if both features (convergence and thermodynamic changes) occur at the same place and at the same time, they can cause strong frontogenesis. In cases of onshore ambient flow the thermodynamic front may be as much as 15 km ahead of the kinematic front while kinematic sea breeze fronts are not clearly defined. In general only an offshore gradient flow exhibit kinematic sea breeze front (Atkins et al. 1995; Miller et al. 2003).

Near capes and peninsulas, sea-breeze fronts from opposite shores converge and collide during the day, producing stronger upward motion that may trigger thunderstorms and

cloud lines along the convergence zone. During the day, the sea breeze front is driven partially by the active conversion of available potential energy to kinetic energy. After sunset, a sea breeze front may be separated from the onshore flow behind the front and can continue to progress hundreds of kilometres inland as an independent entity, known as a bore (Clarke 1984; Miller et al. 2003; Stull 2000). The sea breeze vector at low levels often turns under the influence of the Coriolis force and the baroclinicity between land and sea. If the background synoptic flow is in the same direction as the low level sea-breeze and there are no major barriers to the flow, then the sea breeze front can progress much further inland (over 100 km). The sea breeze front will move slowly or may not form at all if the synoptic-scale flow is offshore and stronger than about 5 m $s^{-1}$ (University Corporation of Atmospheric Research 2008). For synoptic flow parallel to the coastline, some observations indicate that the sea-breeze front becomes broader and more diffused (Stull 2003).

Vertical currents initiated or enhanced by the SBF are associated with cumulus cloud development and thunder storms (Atkins et al. 1995). Vertical currents are also a factor in the dilution of pollutants in the PBL and therefore may have significant implications for dispersion of pollutants in coastal areas. Vertical velocities along the SBF are greatly affected by the strength of the frontal zone and the rate at which the SBF advances inland (Helmis et al. 1995). Downdrafts occur 60% of the time before SBF passage, while updrafts dominate at the SBF passage (Chiba 1993). The magnitude of the downdrafts is ~0.5 m $s^{-1}$ while updrafts range between 0.5 m $s^{-1}$ to 1.0 m $s^{-1}$ (Helmis et al. 1995). Vertical velocities of 1 to 1.5 m $s^{-1}$ have been observed with a sharp frontal zone, while weaker fronts produce updrafts and downdrafts only one third as large. Fast moving fronts produce greater vertical velocities than slow moving fronts. The direction of the ambient flow also affects the magnitude of vertical velocities; for example updrafts reach 2 m $s^{-1}$ when the ambient flow is offshore (Helmis et al. 1995).

### 2.2.5 The Sea Breeze Head (SBH)

The sea breeze head (SBH) is the raised part of the sea breeze inflow current above and immediately behind the SBF. The sea breeze head is created by strong vertical currents within both the continental and marine air masses (Miller et al. 2003). It is similar to the head at the leading edge of a gust front (Miller et al. 2003; Stull 2003). The height

of the SBH is approximately twice the depth of the sea breeze inflow (Simpson 1977), however, the range of variation in this general principle is quite large for example (Nakane & Sasano 1986) measured a sea breeze head of 1300 m depth with a sea breeze inflow of only 300 m. The headwind flattens the SBH and the top of the sea-breeze head often curls back over warmer air from aloft in a large horizontal roll eddy (Stull 2003).

### 2.2.6 Kelvin-Helmholtz Billows (KHBs)

Kelvin-Helmholtz Billows are the result of velocity shear induced Kelvin-Helmholtz instability that occurs near the sea breeze head region and produces multiple vortices near the sea breeze front. These vortices break down into small-scale turbulent eddies at the rear of the SBH and along the upper boundary of the sea breeze inflow current during periods of low static stability (e.g. around midday), known as Kelvin-Helmholtz Billows (KHBs) (Abbs & Physick 1992; Miller et al. 2003; Sha & Kawamura 1991). KHBs appear as vortex rolls in regions of strong shear and cause vigorous mixing between the two (continental and marine) air masses in this region. This KHB induced mixing during midday/afternoon also generates a friction-like force along the top of the sea breeze inflow that slows down the inland penetration of the sea breeze front (Miller et al. 2003; Physick 1980; Sha & Kawamura 1991). With a Richardson number smaller than ~0.25, the midday insolation-induced thermodynamic instability is further enhanced (Atkins et al. 1995). The wavelength of (KHBs) ranges from 0.5 to 1 km along the density interface at the top of the feeder flow behind the head. These waves produce a frictional drag on the sea breeze by entraining low-momentum air from above the interface that slows down the inland progression of the sea breeze. A slowly subsiding return flow occurs over water and completes the circulation as the air is again cooled as it blows landward from the cold water (Stull 2003).

### 2.2.7 Convective Internal Boundary Layer (CIBL)

The convective internal boundary layer (also known as a thermal internal boundary layer) is a well mixed region within the marine air mass over land, adjacent to the Earth's surface that is formed due to the heating of the onshore marine airflow above the ground (Miller et al. 2003; Stull 2003). This convectively unstable air mass forms an internal boundary layer with an unmodified stable marine air mass aloft that acts as a

cap and suppresses vertical motion. The CIBL height grows in depth according to the square root of the distance from the shoreline as the marine air is modified by the heat flux from the warm ground (Miller et al. 2003; Stull 2003). The CIBL is a persistent cause of air pollution problems in coastal regions. Onset of the CIBL results in a significant reduction in the atmospheric mixing depth so that locally generated pollutants that are trapped in the shallow surface layer can quickly reach unhealthy levels (Miller et al. 2003).

Determination of CIBL height is an important component of operational dispersion models since the interaction between this layer and contaminant plumes governs the location and strength of the plumes' footprint (Luhar et al. 1998). The upper limit of the CIBL increases non-linearly with distance from the coast (Miller et al. 2003). Convective internal boundary layer (CIBL) is the result of differences in the surface heat flux between different surfaces (in the sea breeze case, land and water). Venkatram (1977) derived a theoretical equation to estimate the height (h) of the CIBL:

$$h = U_*/U_m \, [2(\theta_{land} - \theta_{Sea})X / \gamma(1-2F)]^{1/2}$$

Where 'h' is the CIBL depth $U_*$ and $U_m$ are the friction velocity and mean wind speeds inside the CIBL, respectively, $\gamma$ is the lapse rate above the boundary layer, F is the entrainment coefficient that ranges from 0 to 0.22, $\theta_{land}$ and $\theta_{sea}$ are the potential air temperatures over land and water, respectively, and X is the fetch on distance from the coastline to the point of measurement (Hsu 1985; Venkatram 1977). Hsu (1988) evaluated the effectiveness of the equation by utilising the data from three different coastal regions at different latitudes and found the results to be in good agreement.

Various studies used potential temperature ($\theta$) and Turbulent Kinetic Energy (TKE) as a measure for the identification of the CIBL. Arritt (1987) and Talbot et al. (2007) defined the CIBL top as a significant increase in the potential temperature lapse rate and a minimum of turbulent kinetic energy. Gamo et al. (1982) and Durand et al. (1989) found that the top of the CIBL was associated with a minimum of turbulent kinetic energy above the gradient discontinuity or $\theta$ inversion. Raynor (1975) also defined the CIBL top as a discontinuity in $\Delta\theta/\Delta z$ or the top of the well mixed layer

(Venkatram 1977). Luhar et al. (1998) used a slab model to calculate the CIBL height and found that the model effectively predicted the CIBL unless the atmosphere is neutrally stable. Studies such as Rayner et al. (1979) have found that a higher CIBL is associated with a low wind speed and stronger ground heat fluxes, while the growth rate of the CIBL is associated with wind shear at the top of the CIBL (Federovich et al. 2001). A positive wind shear (wind momentum above the top of the CIBL is greater than wind momentum within the CIBL) will impede the vertical growth of the CIBL, while a negative wind shear (wind momentum within the CIBL is greater than above it) enhances the growth of the CIBL (Federovich et al. 2001).

### 2.2.8 Sea Breeze Convergence Zone (SBCZ)

The development of sea breeze circulations over peninsulas, irregular coastlines and narrow land masses is often associated with zones of strong vertical motion which may be caused by the interaction of sea breezes from opposite sides, or simply the horizontally convergent flow associated with a convex coastline (Edinger & Helvey 1961; McPherson 1970). Often, these interactions create interesting meteorological phenomena. For example, over Cape York Peninsula, Australia, the collision of sea breezes from opposite sides of the peninsula is responsible for the "morning glory" phenomenon and the North Australian Cloud Line (Clarke 1984; Noonan & Smith 1987). Sea Breeze Convergence lines are also known as regions of storm genesis (Sturman et al. 1999). Over the south Florida peninsula, similar sea breeze convergence zones (SBCZs) have been shown in modelling studies to be the dominant controls on the location of thunderstorm complexes on days not affected by synoptic scale disturbances (Pielke 1974).

## 2.3 Factors Affecting the Sea Breeze

The nature of the sea breeze circulation and its regional structure are often altered by various meteorological and geographical phenomena. Factors like direction and strength of gradient winds, shape and orientation of the coastline, presence of coastal mountains or high terrain, and low-level inversions not only determine the basic characteristics of sea breeze, but they can also dramatically modify this thermally induced mesoscale circulation. In this section, these controls are briefly reviewed (University Corporation of Atmospheric Research 2008).

### 2.3.1 Gradient Winds

Gradient wind plays an important role in determining the shape, shore-relative location, strength and inland penetration of the sea breeze circulation and whether or not a sea breeze will be detectable on land at all (Estoque 1962). The gradient winds may also exert an influence on the behaviour of the sea breeze (Finkele 1995). In general, a strong large scale synoptic flow reduces the likelihood of sea breeze and more likely develops dynamically produced local winds (Sturman & Tapper 2006). Strength of the sea breeze front is measured by the magnitude of the vertical velocity at the sea breeze front or magnitude of the horizontal front-normal temperature gradient. Another measure of intensity of the sea breeze is the available potential energy that takes into account the kinetic energy, velocity, temperature gradient and velocity gradient (Atkins & Wakimoto 1997; Pearson 1975; Pearson et al. 1983). Based on the strength and direction of the large-scale winds, the sea breeze circulation falls into four broad prevailing wind categories. These four categories and their effect on the sea breeze circulation are explained blew.

***a) Sea breeze circulation under onshore gradient winds (Case 1)***

In this case the large scale winds advect the cooler marine air towards land which reduces the thermal gradient between land and sea. The vertical velocities at the sea breeze front are thus weaker, which leads to a weak sea breeze circulation (Estoque 1962). Arritt (1993), in his detailed numerical modelling study of large-scale wind effects on the sea breeze, found that during an onshore gradient wind flow, the frontogenesis term is suppressed, resulting in a weak thermal perturbation of the large-scale flow and thus a weak sea breeze circulation. The inland extent of the sea breeze front under onshore gradient wind conditions is usually much larger than coast parallel and offshore gradient wind conditions. Under onshore gradient winds, the sea breeze is also observed to flow over small mountain ranges (Simpson 1977; Stull 2003). The speed of the sea breeze front is approximated by a linear vector sum of the imposed background wind and sea breeze wind component (Pearson et al. 1983; Stull 2000). Sometimes the resultant wind will be in between the sea breeze and gradient wind directions, while the wind speed can be high (Bureau of Meteorology-Australia 1977a,b). If the onshore synoptic scale winds are too strong, a convective internal boundary layer (CIBL) develops instead of the sea breeze

circulation (Stull 2003).

***b) Sea breeze circulation under offshore gradient winds (Case 2)***

The large scale gradient winds advect warmer air over land towards the sea creating a strong temperature gradient in the lower atmosphere and resulting in a stronger sea breeze circulation (Estoque 1962). This type of sea breeze is preceded by calm conditions as the large-scale pressure gradient force is in equilibrium with the local thermal pressure gradient force (Miller et al. 2003). Arritt (1993) found that the most intense sea breeze circulations are associated with calm to moderate offshore gradient flow, although if the offshore gradient wind is too strong then both vertical and horizontal velocities weaken, eventually reducing the intensity of the sea breeze circulation so that the sea breeze circulation can exist entirely offshore. In general, the inland penetration of the sea breeze front may be delayed under offshore gradient wind flow and in some cases it prevents them reaching the land (Arritt 1993; Estoque 1962; Stull 2003). However, some studies reported that sea breeze fronts often strengthen late in the day when convective mixing has diminished (Physick 1980; Simpson 1977).

***c) Sea breeze circulation under coast-parallel gradient winds with a large-scale low over land. (Case 3).***

In this case, a lower pressure over land and high over sea implies an area of low-level divergence near the coast and over the ocean. Air from aloft sinks into the divergence zone and assists with the initiation of the sea breeze. A landward component is produced due to differences in surface friction that create a perturbation similar to that of onshore gradient flow (Zhong & Takle 1993). There is no calm period prior to the onset of this sea breeze and relative to the Case 4 sea breeze, the sea breeze in Case 3, can reach the coast with an even weaker thermally-induced PGF. The arrival of the sea breeze under Case 3 is marked by a gradual veering of winds. Like the offshore sea breeze (Case 2), the Case 3, sea breeze circulates in a vertical cell, but the along-shore component of the synoptic wind causes the circulation to take on a helical shape rather than a simple loop (Adams 1997; Miller et al. 2003; Zhong & Takle 1993).

***d) Sea breeze circulation under coast-parallel gradient winds with large-scale low over the sea (Case 4).***

In coast-parallel gradient flow, the large-scale low pressure over the sea combined with the cross-shore variation in the surface friction, results in an area of low-level convergence near the coast. This surface convergence prevents air sinking from aloft and inhibits the inland penetration of the sea breeze front (Adams 1997; Miller 2003). With large-scale low pressure over the ocean, a seaward component is induced which leads to perturbed flow similar to an offshore gradient flow (Case 2) (Zhong & Takle 1993). This also implies that a Case 4 sea breeze can only reach the coast with a stronger thermally-induced PGF relative to a Case 3 sea breeze. Arrival of a Case 4 sea breeze is marked by a gradual shift in wind direction. In this case, the wind will back and the vertical rotation of the sea breeze cell will also become helical rather than in a simple loop (Adams 1997; Miller et al. 2003).

### 2.3.2 Temperature Inversions

Inversions play an important role in the development of sea breezes. An inversion tends to limit the vertical extent of the heating to a shallow layer, which typically reduces the strength of the sea breeze. A sea breeze can be stronger on days with a moderate temperature rise through a deep layer than on days with a large temperature rise through a shallow layer. In unstable environments, an inversion may inhibit convection by providing a cap or lid that restricts the ascent of buoyant air parcels. The lift induced by a sea breeze may not be sufficient to break through the inversion and initiate convection. The inversion may also be important in trapping moisture to favour the development of fog and stratus clouds. For example, along the U.S. West Coast, a strong, low-level inversion occurs with a marine boundary layer that is nearly saturated. Under these inversion conditions lifting and/or cooling of the boundary layer frequently leads to the formation of coastal fog or stratus (University Corporation of Atmospheric Research 2008).

### 2.3.3 Terrain

Local topography and surface characteristics have large influence on the evolution of local and mesoscale flows such as sea and land breezes. In the coastal regions where coastal hills runs parallel to the coast, it is difficult to differentiate between the sea

breeze and effects of slope heating and cooling, as both occur simultaneously (Sturman & Tapper 2006). When the sea breeze is coupled with the upslope winds, the SBC is strengthened by the topography (Miao et al. 2003). The temperature gradient between the coastal plain and shore facing hills also affects the strength of the sea breeze. If temperature of the hill slopes varies with the same diurnal period as that of the coastal plain, this will strengthen the sea breeze system, as well as change the temporal evolution of the sea breeze by an early onset and later cessation. However, if the surface temperature of the mountainous terrain is lower than the coastal plain (for example, slopes covered with clouds or fog or snow), the hill will act as a barrier and the sea breeze will be either confined to the coastal plain (Asai & Mitsumoto 1978; Miller et al. 2003) or the cool, dense, marine air mass tends to go around the hill rather than over it (Miao et al. 2003). When the opposing breezes meet on the opposite (lee) side of the hill, they may form a sea breeze convergence zone (SBCZ) close to the mountains (Miao et al. 2003). In the presence of convection these SBCZ's cause clouds and rainy weather over the land. Skies often remain cloud free over the ocean (Ahrens 2007). The proximity of mountains and associated valleys to the coast may also contribute to earlier onset and later end of the sea breeze by producing mountain-valley circulations that add to the sea breeze strength (Miao et al. 2003). The mountains and valleys tend to determine the distribution of heating and the locations into which the sea breeze front can penetrate. Afternoon hot spots are located in inland valleys and tend to draw the sea breeze inland (University Corporation of Atmospheric Research 2008).

Over peninsulas and narrow landmasses with ocean on both sides, the sea breeze system forms on opposite sides of the landmass and leads to sea breeze convergence at the centre of the landmass, although the location and intensity of the convergence zones is influenced by many other factors, such as large scale winds, surface characteristics and topographical height of the terrain. Results of Xian and Pielke (1991b) suggest that the thermal forcing over a narrow peninsula or island with width <100 km is insufficient for developing a deep well-organized mesoscale circulation and both sea breeze systems would be weak, while a landmass > 150 km across is too wide for the two opposite systems to reach each other before sunset so that the associated convergence region in the centre of the landmass is weakened. In the evening hours

during stable atmospheric conditions, when opposing sea breeze flows meet each other, they may produce undular bores (Clarke 1984). In Florida, the light west wind (2 m $s^{-1}$ – 4.5 m $s^{-1}$) keeps the sea breeze fronts confined to the eastern coast and prevents them moving onshore or even forming at all. With prevailing east winds, they actually help push the sea breeze front as much as half way across the peninsula (NOAA 2008). On smaller peninsulas, such as at the northern tip of New Zealand, quite often sea breezes from the opposite coasts collide. In these situations, two lines of thunderstorms may form and combine into a single but intense, short-lived thunderstorm line (NOAA 2008).

In complex terrain a number of sea breeze systems may be produced, although their location, intensity and temporal extent may differ from each other. Inland topographic features may cause channelling of the low-level flow, thus creating areas of enhanced convergence and upward vertical motion. The point where these different sea breeze systems converge, can produce intense vertical motion over land (Melas et al. 1998; Miller et al. 2003).

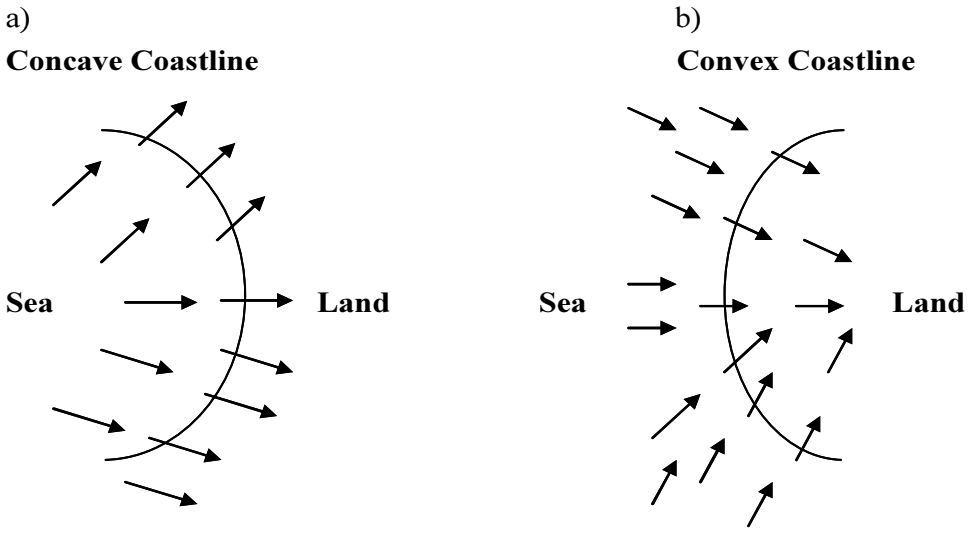


Figure 2.2: Effect of coastline shape on sea breezes a) divergence, and b)convergence over land

The coastline shape may either enhance or diminish the convergence and convection found along the sea breeze front. Onshore flow for a concave coastline, such as a bay, becomes divergent (Figure 2.2a). A divergent flow suppresses lifting along the sea breeze front. However, over a convex coastline, onshore flow enhances convergence

and uplift along the sea breeze front (Figure 2.2b). Capes and points are examples of convex land-water boundaries that are commonly associated with increased convection and thunderstorms activity (Abbs & Physick 1992; Baker et al. 2001; Purdom 1976; University Corporation of Atmospheric Research 2008).

### 2.3.4 Land and Sea Surface Temperatures and Soil Moisture

Soil moisture and land and sea surface temperature have significant effects on the temperature gradient between land and sea. A decrease in soil moisture leads to higher surface temperature on land and higher horizontal and vertical wind components that result in a stronger sea breeze, whereas higher moisture content leads to relatively colder land temperature and lighter sea breezes (Baker et al. 2001; Miao et al. 2003; Schumann et al. 1991). In some lake-breeze experiments, Segal and Pielke (1985) and Aritt (1987) found that water surface temperature has little effect on lake breeze development, as long as the water is cold enough that the surface layer over the lake is stably stratified. If the water is warmer, the more vigorous fluxes due to convective turbulence may suppress the lake breeze. Sea surface coastal upwelling that brings colder water to the surface also enhances the cross-shore temperature gradient.

### 2.3.5 Sea Water Upwelling

A rather less studied phenomenon is the temperature variation due to coastal upwelling that brings the colder water to the surface (Miller 2003). Franchito et al. (1998) and Apel (1987) found stronger sea breezes during periods of coastal upwelling and weaker when there was no upwelling. In the South Island of New Zealand, observational and modelling study over the east coast of Canterbury region, also found stronger sea breezes during periods of coastal upwelling (McKendry et al. 1988). If the upwelling is strong, it will keep sea level temperatures relatively colder than land even at night. Thus the lack of temperature reversal may then encourage the sea breeze to continue through the night (Oke 1992).

### 2.3.6 Urban Heat Island Effect (UHI)

The urban heat island (UHI) is a widely acknowledged, observed and researched phenomenon as it is a direct consequence of human activities. Moreover, it has a significant influence on the local meteorology and dispersion of pollutants emitted in

the urban airshed. The main cause of the UHI is modification of the land surface due to the urban built environment. Urban development, concrete structures, asphalt, emission of pollutants and excess heat from anthropogenic activities, increases temperature in the cities and urban areas and forms a temperature gradient between the urban and surrounding rural areas. The temperature difference is usually larger at night than during the day and larger in winter than in summer (Yoshikado 1992). This urban-rural temperature difference results in a dome of warm air over urban areas with a centre height that goes up to 300 m over the hottest part of the city (Lin et al. 2008). Partly as a result of the UHI effect, urban areas experience relatively low wind speeds, less sunlight and ultraviolet radiation, while temperature, cloud cover and rainfall are higher than surrounding rural areas. If the SBS develops near a coastal city, it will interact with the city's urban heat island. Previous studies such as Bureau of Meteorology-Australia (1977b), Bureau of Meteorology-Australia (1977a), Yoshikado (1992) and Sturman et al. (1999), suggest that the presence of the UHI increases the sea breeze velocity during daytime and weakens the land breeze during the night time, and hence has a significant impact on air pollution diffusion and dispersion (Lin et al. 2008; Yoshikado 1992). The sea breeze accelerates as the size of the inland urban area increases (Ohashi & Kida 2001). The UHI also causes the SBC to last longer (Ohashi & Kida 2001), and the interaction may result in unusually regular and persistent lines of clouds, such as the Kampachi Street cloud line in downtown Tokyo (Kanda et al. 2001).

## 2.4 Air Pollution Potential of Sea Breezes

Most of the mega cities, industrial centres and large populations of the world reside close to the coasts, which leads to extraordinarily high levels of pollutant emissions in coastal areas. Sea breeze exerts both direct and indirect control on the fate of pollutants released into the coastal regions. Examples of direct controls are the landward transport of pollutants by elements of the sea breeze system, trapping and increasing concentration of pollutants in shallow convective internal boundary layers, and replacement of polluted continental air with relatively clean marine air (Miller et al. 2003). The sea breeze characteristics such as inland penetration distance and updraft and downdraft velocity are of crucial importance for air quality applications and emergency response air pollution modelling in coastal urban areas. Since cities near the

ocean usually experience sea breezes by noon, their highest temperature usually occurs much earlier than in inland cities. In the cold oceanic air relative humidity rises as the temperature drops. When relative humidity increases to above 70%, water vapour begins to condense upon particles of sea salt or industrial smoke, producing haze that in addition to health implications, also has an adverse visual impact on the urban air quality of the coastal region. If the rising warm air along the cold sea breeze front is sufficiently moist, a line of cumulus clouds may form along it. If the air is conditionally unstable, thunderstorms may also form (Ahrens 2007).

Sea and land breezes tend to disperse pollutants in a very complex manner (Haigh 1992; Sutton 1996). Weak sea breezes and their convergence zones increase pollutant concentration (McGill 1987). Oke (1992) argued that sea breezes are not good pollution ventilators for three reasons: first, the wind speed is usually low (less than 7 m $s^{-1}$); second, they are closed circulation systems; and third, they exhibit a diurnal reversal in the direction of the flow. As a result, during the SBC pollutants emitted into the surface layer can be recirculated several times over the near-shore area (Lyons 1972). That is, pollutants are carried aloft in the frontal regions or SBCZ and disperse in the return flow. A fraction of these pollutants drifts seawards, and at a short distance from the coast it may be partly caught in the downward current and returned landwards by the sea breeze (Forsdyke 1997), while remaining pollutants reside in an elevated stable layer and remain aloft in the residual layer during the night (Lyons & Olsson 1973). The residual layer often exists for a while in the morning before it collapses into the new mixed layer, and thus pollutants trapped in the residual layer from the previous day's emission increase pollutant concentration on the following day (Stull 2003).

The reversal of the land and sea breezes can also result in pollution emissions being returned to the urban source area. The conditions conducive for the sea breeze are the same as for oxidant formation (such as summer days with low synoptic winds, strong insolation and high temperatures) which may increase photochemical pollution in a given region (McGill 1987; McKendry 1996). Thus the occurrence of high concentrations of pollutants, especially ground-level ozone, in coastal regions is highly correlated with the occurrence of sea breezes and to lesser extent land breezes. Examples of major coastal cities suffering from the above air quality problems include

Los Angeles, Athens, Chicago, Tokyo, Vancouver and Toronto (Sills 1998). However, wind speeds in excess of 5 m $s^{-1}$ enhance dispersion and dilution of pollutants and generally reflect non-sea breeze conditions (Bell & Fisher 1995).

# 3. Weather and Climate of the Auckland Region

## 3.1 Introduction

The Auckland region is located in the North Island of New Zealand at 36$^{o}$ 52' S and 174$^{o}$ 46'E at a narrow isthmus with sea to both the east and the west (Figure 3.1). The total area of the Auckland region from Wellsford in the north to Pukekohe in the south is over 5,000 km$^{2}$ (Auckland Regional Council 2004b). It includes three major harbours (Waitemata, Manukau, and Kaipara) and many tidal waterways. The urban area is confined to a rectangle of about 50 x 20 km oriented north-west to south-east and represents less than 25% of the total land mass (Auckland Regional Council 2004a). Except for the Waitakere, Hunua and Coromandel ranges and South Auckland which is flat, the general topography of land surrounding the Auckland is hilly and undulating, but mostly well under 100 m in altitude. The Auckland isthmus and southern part of the urban area are dotted with numerous small volcanic features. These in many instances affect the local airflow characteristics in the lowest few hundred metres of the atmosphere (Sparrow 1968). In addition to the non-uniform shape of the coasts, the separation between east and west coasts of the Auckland isthmus varies from 10 to 60 km, and leads to competing sea breezes in summer (McGill 1987). The Coromandel Peninsula, Waiheke Island and Great Barrier Island (none of which are included in the region) shelter the waters of the eastern seaboard (Hessell 1988). The Waitakere and Hunua plateaus rise to 480 m and 690 m respectively. The Waitakere Ranges lie to the west and provide some degree of shelter to the western suburbs from the prevailing

westerly conditions. This sheltering effect together with cold air drainage from the slopes of the ranges leads to locally poor dispersion conditions. The land to the north becomes much more dissected into broad ridges and valleys with a general elevation of about 60 m and slopes being generally steeper than on the isthmus (Sparrow 1968). Within the Auckland urban area volcanic cones such as Mount Eden (196 m), One Tree Hill (183 m) and Mount Wellington (137 m) rise above the general level (Sparrow 1968).

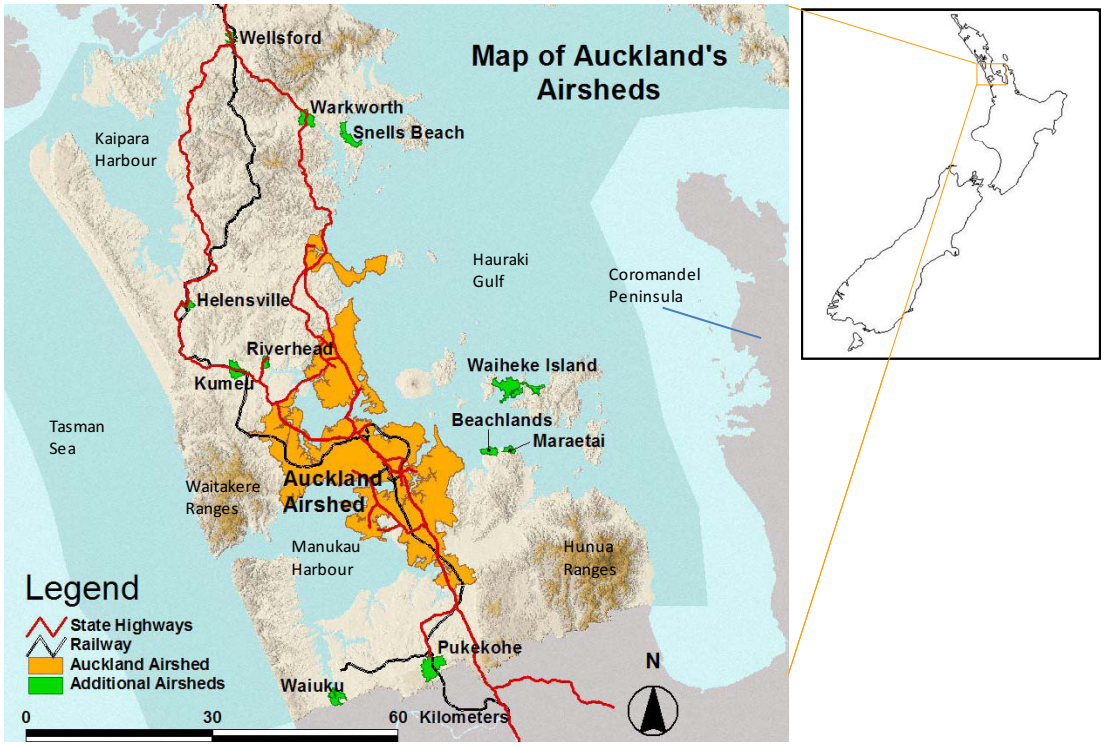


Figure 3.1: Map of the Auckland Region with airsheds defined by the Auckland Regional Council for air quality purposes (Auckland Regional Council 2007a).

Auckland is the fastest growing metropolitan region in Australasia and has the largest urban area in New Zealand. The region houses more than 1.3 million people (30% of the country's total population) with a population forecast of 1.6 million by the year 2017 (ARC 1997; Auckland Regional Council 2004b). The Auckland region is comprised of three districts, namely Franklin, Rodney and Papakura, and four cities, namely Auckland, Manukau, North Shore and Waitakere city. Being the business capital of the country, Auckland houses 38% of the country's businesses. The rate of car ownership in New Zealand is the second highest in the world (ARC 1997). According to ARC (1997) statistics, car ownership is growing twice the rate of

population. Due to the increasing emissions from transport and industry, Auckland has an increasing potential to adversely affect local ecosystems, human health and materials (Taylor et al. 1997). Rapid growth of population, industry and business introduced manifold problems for the urban Auckland, such as traffic congestion, housing requirements, social issues, law and order problems and environmental degradation. Increase in emissions is putting more stress on the Auckland airshed leading to degraded air quality of the region. Although due to the marine environment and generally above average prevailing winds, the general understanding is that everything blows out to the sea. However, certain meteorological processes such as strong inversions in winter and sea-land breezes in summer may restrict ventilation and dispersion of pollutants, and may contribute towards higher pollutant concentrations that could be harmful to human health, ecosystems and materials.

## 3.2 Climate of the Auckland Region

New Zealand lies in the mid-latitude zone of westerly winds, in the path of an irregular succession of anticyclones that migrate eastwards every six to seven days (Hessell 1988). Auckland has a distinct maritime environment. The climate of Auckland can be characterized as temperate to subtropical (McKendry 1996). Its location on the narrow isthmus bordered on opposing sides by the Tasman Sea and Pacific Ocean results in good ventilation (McKendry 1996) and protects Auckland from climatic extremes (Hessell 1988; Hurnard 1980). In winter, the air over Auckland is relatively stable and dispersion is slow, so that pollutant levels may therefore increase (ARC 1995,1997). If the weather is cold and calm during the morning rush hour period, there is potential for pollution events to occur in the afternoon. In summer, sea breezes frequently occur on both sides of the isthmus. The closed circulation and the ability of the sea breeze to inhibit vertical motion are associated with increased air pollution in summer (Brasell 1982; McKendry 1989). The important features of Auckland's climate are discussed below.

### 3.2.1 Winds

The mean high pressure belt in the New Zealand sector of the Southern Hemisphere is centred near $30^{o}$ S, just north of the country (Hessell 1988). Therefore, the prevailing

wind flows over the northern New Zealand at upper levels are from the west or southwest in all seasons. Because of the absence of high ground, the prevailing surface wind over Auckland is from the same direction, although winds from the northeast are also quite common (Hurnard 1980). Auckland is situated to the north of the main North Island's volcanic plateau and it is therefore less exposed to Antarctic air. However, it is more exposed to weather systems of tropical origin (Hessell 1988). Auckland has a relatively high mean wind speeds of 7-8 m $s^{-1}$ (ARC 1997). The most common synoptic winds over Auckland are westerly, south-westerly and north-easterly airflows (ARC 1997; Hessell 1988; Jiang 2000), which provide good ventilation to the Auckland region. However, in winter, Auckland experiences relatively stable atmospheric conditions (ARC, 1995, 1997) that often arise due to subsidence inversions associated with slow moving eastward migrating anticyclones, a characteristic of the region's climate (Jiang 2000). Winds generally decrease for a period in the summer or early autumn and rise to their maximum in spring (Hessell 1988). Calm and near calm morning winds from the south with relatively low morning temperatures and high solar radiation are frequent in Auckland during winter (Jiang 2000). However, Auckland is also vulnerable to strong gusty westerlies accompanied by thunderstorms, most frequently during winter and spring (Hessell 1988).

### 3.2.2 Air Temperature

The mean air temperatures in Auckland are significantly higher than Wellington, Christchurch and other South Island regions, primarily due to Auckland's northerly location. However, the marine setting of Auckland ensures a moderate temperature range, usually without extremes of hot and cold. The region therefore enjoys warm, humid summers and mild winters (Hurnard 1980). Most of the highest air temperatures in the Auckland region occur in the month of February, with a mean maximum of 24°C. The lowest temperatures are observed in the month of July, with a mean minimum of 7°C. In general, the average monthly air temperature ranges from 10.8 °C in July to 19.8 °C in February, with an annual average of 15.1°C (NIWA 2005).

### 3.2.3 Humidity

Relative humidity in the Auckland region is moderate due to its relatively warm climate. However, the vapour pressure which reflects the actual moisture content in the air is above the country' average (Sparrow 1968) and at times gives Auckland an image of an uncomfortably humid environment (Hessell 1988; Hurnard 1980). The monthly mean relative humidity is the highest (>88%) at night time in the cold winter months and the lowest during the summer period (~75%) when the air temperature is high (NIWA 2005). However, the actual moisture content is much higher in summer with an average vapour pressure of 21.6 hPa compared to winter, which is only 14.9 hPa. The variation in relative humidity over the sea is much smaller, with the mean annual figure close to Auckland of around 77% (Hessell 1988).

### 3.2.4 Rainfall

Rain in the Auckland region occurs mainly with northerly winds. The average annual rainfall over most of the city and suburbs is 1200 – 1600 mm (Hurnard 1980), with winter having almost twice as much rain as summer (Hessell 1988). The monthly mean rainfall for winter is 135 mm, while for summer it is 77 mm (NIWA 2005). Auckland's heaviest rainfalls occur when there is a depression to the north or northwest with a strong north to northeast wind flow over the city (Hessell 1988). South-westerlies produce cloudy and showery weather in Auckland, especially in winter when comparatively warm seas tend to destabilize the flow. However, in summer south-westerlies are frequently fine because the lower layers are not destabilized as they are in winter (Hessell 1988).

### 3.2.5 Solar Radiation

The average sunshine hours over most of the Auckland region ranges from 2000 hours to 2100 hours per year (Hessell 1988; NIWA 2005) amounting to about 50% of the total possible sunshine (Hurnard 1980). During summer time, Auckland receives maximum sunshine in the afternoon hours of the day. Generally, there is a significant increase in cloudiness in winter, which reduces the sunshine over Auckland, while solar radiation in summer is three to four times more than winter (Hessell 1988).

### 3.2.6 Sea and Land Breezes

In the Auckland area and most of the North Island, sea breezes occur most frequently from November to March during anticyclonic conditions when the sunshine is the greatest and the synoptic wind flows are weak. The sea breezes occur for up to four days at a time and are observed approximately between 17% to 40% over the five month period (Bell & Fisher 1995; Hessell 1988; McGill 1987; Revell 1978). On a local scale, sea breezes are common but complex events because of the conflicting effects of large areas of open water almost surrounding Auckland region and the uneven terrain of the urban areas. The irregular coast line of the Auckland isthmus adds to the complexity of the sea breezes. The region's main ranges (the Waitakere and Hunua ranges) and synoptic wind direction also cause variations in the sea breeze circulations.

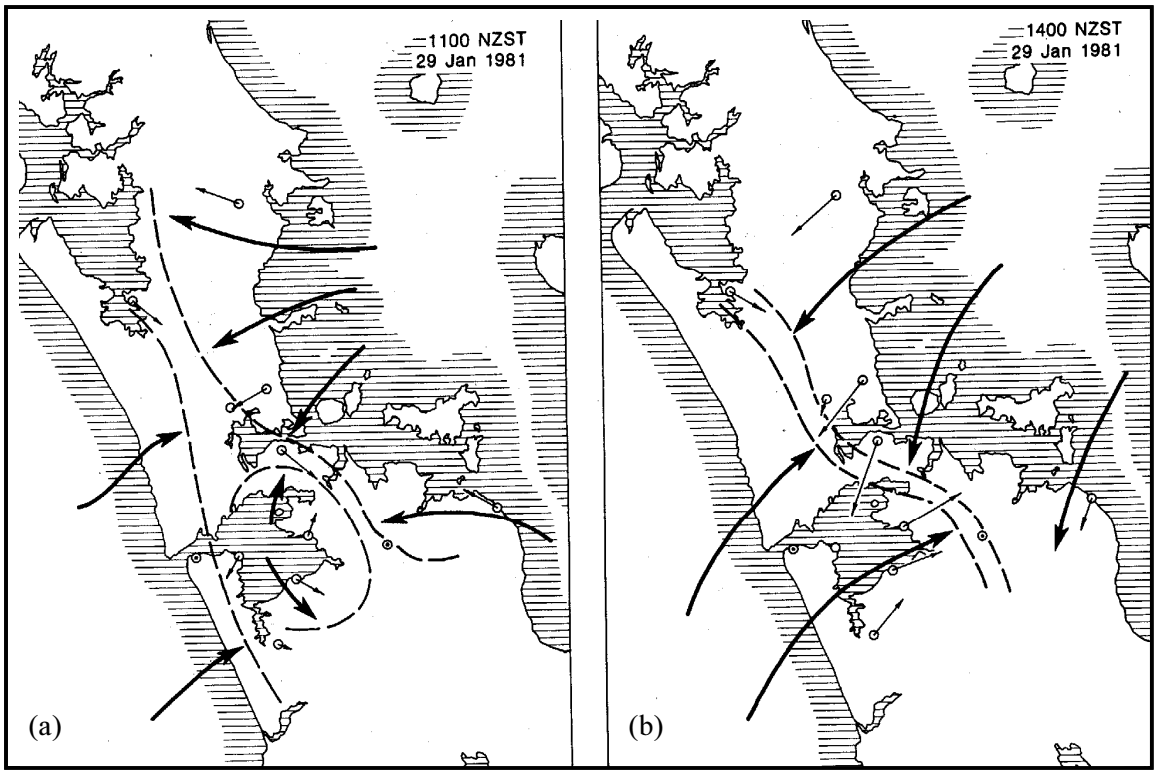


Figure 3.2 General sea breeze circulation patterns, a) Bay breezes at 1100 NZST, and b) mature sea breezes with sea breeze convergence zone (SBCZ) at 1400 NZST. After Hessell (1988).

Sea breeze over Auckland generally occurs simultaneously on both east and west coat of the peninsula. Previous studies (both observational and numerical) reported

existence of two thermally induced circulations in the region: bay breeze from harbours and mature sea breezes from east and west coasts (Figure 3.2a). On a typical sea breeze day, under weak gradient winds (<5 m $s^{-1}$), bay breezes initiate from Manukau, Waitemata and Kaipara Harbours between 0800 – 1100 NZST. As the day proceeds, the increased surface heating also increases the thermal pressure gradient between land and sea that results in the onset of mature sea breezes from both east and west coast. In the afternoon hours, mature sea breezes blowing from the main water bodies in the region (Tasman Sea, Hauraki Gulf, and larger Hauraki Gulf) dominate the region (Figure 3.2b). The sea breeze typically weakens by 1700 hours and dissipates at 2000 hours (Bell & Fisher 1995; McGill 1987; Revell 1978). The depth of the bay breezes is between 200 and 600 m while in the afternoon the depth of mature sea breezes ranged between 400 to 1450 m. The depth of observed return flow also varied considerably ranging from 50 m to 700 m (McGill 1987). At night wind flow reverses from land to sea. These land breezes produce light offshore flow with only 30% of the strength of the sea breezes and occur only 40% of the days that sea breezes occur. After 2200 hours, synoptic winds need to be very low for land breezes to dominate (Bell & Fisher 1995; Haigh 1992). Numerical modelling studies in the Auckland region (e.g. McKendry 1989; McKendry 1992) show good agreement with bay breeze depth , however underestimated the depth of the mature sea breezes from either coast. Several numerical modelling studies have been conducted to study sea breezes in Auckland. The predicted depth of bay breezes was in good agreement with the observed data (~250 to 500 m) with no return flow. However, models generally underestimated the depth of mature sea breezes (predicted sea breezes ~500 to 750 m) over the isthmus with marked return flow between 1000 to 2000 m for both westerly and easterly sea breezes. Despite over-prediction of the return flow the modelled results were consistent with McGill (1987) and Brasell's (1982) that the summertime air pollution meteorology of the Auckland region is influenced by sea breeze effects.

### 3.2.7 Sea Breeze Convergence Zones (SBCZ) Over the Auckland Region

In the Auckland region, the presence of two sea breezes from opposite coasts results in the formation of a sea breeze convergence zone (SBCZ) over the isthmus (McGill 1987; Sutton 1996). The SBCZs are an important feature of the summertime meteorology of the region. Observation and modelling studies of Auckland's sea breeze

(McGill 1987; McKendry 1989,1992,1996; Sutton 1996) suggest that the exact location of convergence zones greatly depends on the geostrophic wind strength and direction.

Synoptic winds influence the location of the SBCZ (McKendry 1996) and cause the convergence zone to migrate. For example, a light south-westerly synoptic wind acts to push the SBCZ out over the Hauraki Gulf, east of Auckland and towards the Coromandel Peninsula while under a northeast gradient winds the easterly sea breeze dominates and the SBCZ were formed along the west coast and south of the Manukau Harbour, triggered by the interaction of sea breezes from the west coast and easterly flow deflected around the Hunua Ranges. Under coast-parallel northwest gradient wind flow, the east coast sea breeze dominates and, the convergence zones would migrate westward while under south-easterly gradient winds (which is also coast-parallel wind direction), the SBCZ may remain inland with no dominating sea breeze. However, under southerly gradient flow, the westerly sea breeze may dominate over the southern half of the Auckland region (McGill 1987; McKendry 1992). In general under weak synoptic pressure gradient, the SBCZ would be approximately down the centre of the land mass (McKendry 1996). Results of the modelling study of Auckland sea breezes show that the interaction between gradient wind direction and the complex coastal configuration is an important control of the intensity, location and dynamics of migratory SBCZs, and on occasions may also induce the formation of a mesoscale cyclonic eddy (McKendry 1992; McKendry & Revell 1991).

Most of the studies conducted in the Auckland region suggest that sea breeze convergence zones may have some role in the horizontal and vertical distribution of pollutants (McGill 1987; McKendry 1996; Ridley 1993; Ridley 1995; Sutton 1996). However, Adeeb & Shooter (2003,2004) found that $O_3$ concentration remains low in the SBCZs during summer as dilution of polluted air occurs due to mixing of polluted east-coast air into the clean west-coast air mass. Contrary to this Ridley (1995) in his numerical modelling study reported inhibition of mixing of east and west coast sea breezes in the SBCZ. Ridley (1995) used a Lagrangian particle dispersion model to assess the pollutant transport mechanisms in the Auckland region. The result of his study suggest that convergence of sea breezes from opposite directions limits the exchange of particles between the two circulations, thus leading to a much higher

concentration in the convergence area. Convergence also results in rapid vertical transport of particles, leading to higher pollutant concentration at the top of the elevated boundary layer. The modelling results show that particles in the return flow may not often be carried offshore, and the potential exists for them to be recirculated or mixed to the surface in the following day's sea breeze (Ridley 1995). Various observational and modelling studies suggest that only weak sea breeze circulations and their convergence zones can be associated with the build up of air pollution (Adeeb & Shooter 2003; McGill 1987; McKendry 1992). The modelling study by McKendry (1989) identified the migratory sea breeze convergence lines as the principal feature contributing to marked spatial and temporal variations in wind and PBL depth. Such convergence zones have been investigated at a larger scale by Noonan and Smith (1987) for the Cape York Peninsula and by Pielke (1974) for South Florida. The simulation results suggest that the dominance of sea breeze circulations over the region leads to recirculation of pollutants that could be an aspect of the local air pollution meteorology that is worthy of further investigation.

The structure and dynamics of the mesoscale circulation are strongly affected by a number of large and small scale meteorological elements, such as gradient winds, topography, soil moisture and sea surface temperature. However, not many studies are available on the sensitivity analysis of sea breezes for the Auckland region. McKendry (1989,1992) investigated the effect of different gradient wind conditions on sea breeze circulation, and especially the strength and orientation of the SBCZs, whereas Sutton (1996) tried to assess the effect of terrain, land and sea surface temperature, but was limited by the complexity of the model and errors in the code. The simulation results of Sutton (1996), however, suggested that topography, especially the higher terrain, can displace a SBCZ up to 20 km from where it would otherwise form, while land and sea surface temperature did not have any considerable effect on SBCZ.

## 3.3 Air Pollution in the Auckland Region

Air quality in the Auckland region is considered good due to the ventilation effect of generally high wind speed and the coastal environment. However, the pollution exceedence record shows that the air quality of the Auckland region is significantly affected by human influences during both winter and summer seasons. Air pollutants

are also responsible for degraded visibility, brown hazes and smog that impacts on quality of life and raises health issues for the public. The Auckland Regional Council has identified areas where air quality is likely, or known to exceed national air quality standards (NES) (Table 3.1). These areas are known as airsheds and identified on the map of the Auckland region in Figure 3.1.

Table 3.1: National Environmental Standards for major pollutant species (Ministry for the Environment 2005)

| **Pollutant** | **Standard** | **Time Average** | **Allowable exceedences per year** |
|---|---|---|---|
| Carbon Monoxide (CO) | 10 mg $m^{-3}$ | 8 hours (running mean) | 1 |
| Fine Particles ($PM_{10}$) | 50 µg $m^{-3}$ | 24 hours | 1 |
| Nitrogen Dioxide ($NO_2$) | 200 µg $m^{-3}$ | 1 hour | 9 |
| Ozone ($O_3$) | 150 µg $m^{-3}$ | 1 hour | 0 |
| Sulphur Dioxide ($SO_2$) | 350 µg $m^{-3}$<br>570 µg $m^{-3}$ | 1 hour<br>1 hour | 9<br>0 |

The important pollutants that impact on air quality in the Auckland region include fine particulates ($PM_{10}$ and $PM_{2.5}$), carbon monoxide (CO), nitrogen oxides ($NO_2$) and Ozone ($O_3$) (Auckland Regional Council 2004b). Other important pollutants emitted into the Auckland airsheds include VOC, $SO_2$ and $CO_2$. Emissions from motor vehicles are the main source of air pollution in the Auckland region. The emission inventory for the Auckland region (2004a) estimates that transport accounted for 78% of the total mass of all ambient pollutants (excluding $CO_2$). The important pollutants that contribute towards higher percentage of traffic emissions include $NO_2$, CO, fine particulate matter, and $SO_2$. Other sources of pollution include home heating, industry, and open air burning. The emission inventory estimates that 48% of $CO_2$ emissions come from transport, 46% from industry and only 6% from domestic sources. There is a significant seasonal variation in $PM_{10}$ emission, mainly because of domestic heating in winter. The total volume of $PM_{10}$ is much higher in winter (29 tonnes $day^{-1}$) than in summer (10 tonnes $day^{-1}$). The increase in $PM_{10}$ during winter is largely from domestic sources, increased from 0.2 tonnes $day^{-1}$ in summer to 18.5 tonnes $day^{-1}$ in winter. The emissions from other sources (transport and industry) are almost constant throughout the year. Ozone is a secondary pollutant as it is not directly emitted from any source. Ozone is either formed by reaction between oxides of nitrogen and hydrocarbon in the

presence of sunlight, or transported from upper layers of the atmosphere as background ozone. The higher surface $O_3$ levels are observed in spring and summer, and the reasons are both local and non-local. The photochemical properties of $O_3$ lead to smog events due to higher solar radiation in summer and spring. In addition to that, increased horizontal and vertical advection of $O_3$ during spring also contributes to higher surface $O_3$ levels. In the Auckland region, annual average ozone concentrations have changed little over the years (Auckland Regional Council 2007b), with maximum $O_3$ concentrations close to the NES (Auckland Regional Council 2009).

The emission inventory of the Auckland region (Auckland Regional Council 2004a) predicted a decrease in $PM_{10}$ emissions in the following years that would be attributed to shifting away from coal and wood for both domestic heating and industrial use. Although PM10 concentration appeared to have decreased over past years at most monitoring sites, in recent years this trend has levelled off (Auckland Regional Council 2007b) and Auckland Regional Council (2009) data for $PM_{10}$ show an increasing trend in $PM_{10}$ concentration. The concentration of $PM_{10}$ has also exceeded both national environmental standards (NES) and Ambient Air Quality Guidelines (AAQG) at urban monitoring sites measured around Auckland (Figure 3.3). The $NO_2$ concentration also increased in the Auckland region over the past decade, which is mainly due to increasing numbers of motor vehicles in the region. Except for the years 2003 and 2006, the number of exceedences for $NO_2$ were above the allowable limit (Figure 3.3).

The average annual concentration of $SO_2$ fluctuated in the last two decades. The variations in $SO_2$ concentration is mainly dominated by coal run industries and diesel vehicles. In recent years $SO_2$ has an increasing trend due to increasing numbers of diesel vehicles. However, concentrations of $SO_2$ measured at monitoring sites across the region are typically less than the NES. Only the concentration of CO has decreased significantly over the last decade (Auckland Regional Council 2009). According to the emission inventory of the Auckland region (Auckland Regional Council 2004a) reduction in CO is attributed to the improved emission control equipment in motor vehicles. Data show that after 2004 there has not been any CO exceedence above the allowable limit (Figure 3.3).

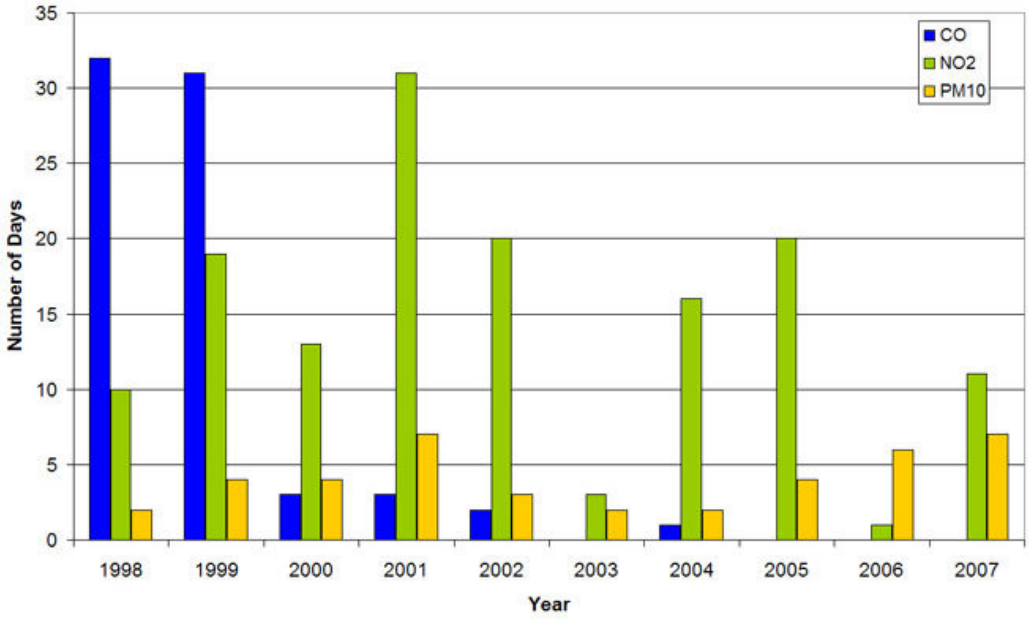


Figure 3.3: Days of exceedences of NES in the Auckland region from 1998 to 2007; After Auckland Regional Council (2009).

### 3.3.1 Pollutant Dispersion during Sea Breeze Days

The observational and modelling work performed around the region shows that meteorological mechanisms behind the pollution episodes during sea breeze events are varied and complex. Several pollutant dispersion mechanisms may exist in the Auckland region. In the first scenario, the polluted air mass is advected seawards, firstly by light synoptic winds and/or remnants of land breezes and drainage flows, and later by elementary sea breeze flow in the morning hours (0700 to 0900 NZST) of the day. The pollutants are advected back towards the receptors by the mature sea breezes in the late morning or the afternoon hours of the day. However, Bell and Fisher (1995) believed that a complete recirculation of pollutants is unlikely in the life time of the day's sea breeze and suggested that the 'next day' mechanism may also occur in the Auckland region. The 'next day' mechanism applies to scenarios of more than one consecutive sea breeze day with weak nocturnal gradient winds. Pollutants that are carried aloft in the frontal regions or in the SBCZ may remain in the stable layer and reside in the residual layer during the night. On the next morning, when the residual layer collapses these pollutants are mixed with the morning emissions and increase the near- surface pollutant concentrations.

# 4. Observational Data Analysis

## 4.1 Introduction

The Auckland region consists of highly irregular coastlines and a rolling hill terrain that results in very complex low level airflow evolution. During summer months the thermodynamic structure of the boundary layer can be highly variable due to development of the thermally induced sea-land circulation. The mesoscale circulation also interacts with large scale wind and topographical features of the region. These interactions significantly affect the boundary layer characteristics. The resultant modified boundary layer poses significant challenges for weather and air quality forecasting in the region. The modified lower boundary layer can remarkably affect the transport and dispersion of pollutants. The main impetus of this chapter is to understand changes in the dynamic and thermodynamic structure of the lower atmosphere over the region during sea breeze episodes. The effect of these variations on the air quality of the region has also been investigated.

The sea breezes in the Auckland region occur on fine days particularly during the summer period between November and March at times when synoptic forcing is weak and the intensity of sunshine is greatest (McGill 1987). Previous studies suggest that the sea breeze over Auckland occurs from 17% to 40% of summer time (McGill 1987; Revell 1978). Observed airflow patterns on days with sea breeze circulations are complex and considered to be the result of the interaction of sea breezes, the synoptic flow, topography and mesoscale heat lows or troughs (Revell 1978). In this observational study 10 months data of two summer periods (November, December,

January, February and March) for the years 2006 and 2007 have been analysed. The study region encompasses the isthmus that varies in width from 10 to 60 km. It has two major harbours (Manukau and Waitemata) and three mountain ranges namely Waitakere Ranges, Hunua Ranges and Coromandel Peninsula. A detailed description of the weather, climate and geography of the Auckland region is provided in Chapter 3.

The surface and vertical sounding data were obtained from four sources: a) the National Institute of Water and Atmospheric Research, b) Auckland Regional Council, c) Meteorological Service of New Zealand, and d) The University of Wyoming web site (USA). Surface meteorological data and upper air data from Auckland Airport were obtained from NIWA, whereas upper air data from balloon flights from Whenuapai were obtained from the Meteorological Service of New Zealand. Vertical sounding data from aeroplane flights at Whenuapai Aerodrome were also downloaded from University of Wyoming (USA). Pollutant and some meteorological data were provided by Auckland Regional Council. Analysis of meteorological conditions and air pollution require availability of good quality data from observational network. Generally, near surface observations (both meteorological and air pollutants) should be representative of free air-conditions over as much of the area as possible. The site should have free exposure to both sunshine and wind from all directions which means absence of any building structures, trees, steep slopes, hollows and other obstructions in the close vicinity of the monitor (Davey & Pielke 2005; WMO 2008). Unfortunately many of the monitors in the Auckland Region do not comply with the requirements of WMO (2008) and Australian standard of ambient air (Standards Australia 1987). In many cases monitors are poorly sited and sheltered by nearby trees, building structures or hilly terrain. For example Lincoln road sampling unit in Henderson is sheltered by nearby trees to the southwest, whereas sampling units at Khyber Pass and Queen Street are sheltered by extensive building structures. Glen Eden although does not have trees or building around but an irregular and hilly terrain acts as obstruction to the wind flow from the northeast. Although extreme care has been taken in the selection of monitoring stations, however, in some cases due to the sparse monitoring network and critical nature of the location of the sampling unit, inclusion of certain noncompliant monitoring sites was unavoidable. This deficiency however, has been recognized and described wherever required in the text. After acquiring the data from sources

mentioned above, a rigorous statistical screening of the data were carried out to check for errors, missing values and its appropriateness for various statistical tests.

## 4.2 Data Screening

Surface winds and temperature data were available from a number of locations in the Auckland region. The hourly averaged surface winds, temperature, pressure and solar radiation data were obtained for the years 2006 and 2007. The data were checked for errors, missing values, outliers, normality and independence. Erroneous data for wind speed and wind direction were identified in 355 cases and therefore replaced with a missing data flag. Temperature and relative humidity data were not available from the Musick Point and North Shore monitoring stations and therefore could not be used for the analysis. The available corrected data were checked for outliers and normality.

**Outliers:** There are various methods in practice to identify outliers. First, mean and 5% trimmed mean (distribution mean without the 5% extreme values) were calculated for wind speed, air temperature, solar radiation and relative humidity to see if there are any significant differences between both means.

Table 4.1: Descriptive statistics of 10 months of summer data for the years 2006 and 2007

| Meteorological Parameter | Mean | 5% Trimmed Mean | Median |
|---|---|---|---|
| u velocity | 1.00 | 1.07 | 1.35 |
| v velocity | 0.453 | 0.466 | 0.580 |
| Wind speed | 4.4 | 4.2 | 3.80 |
| Air temperature | 18.0 | 18.0 | 18.0 |
| Solar radiation | 19.4 | 19.5 | 19.8 |
| Relative humidity | 76.0 | 76.3 | 77.0 |

The highest difference between mean, 5% trimmed mean and median is found with wind speed, whereas air temperature, solar radiation and relative humidity appear to show no significant differences between mean, 5% trimmed mean and median values. Wind speed, however, appears to have outlying cases. Hair Joseph F (2005) has defined outliers as cases with standard score of 4.0 or greater. The standard score

indicates the number of standard deviations an observation is above or below the mean and is defined as:

$$Z_i = (X_i - \mu_i)/\sigma$$

Where "Zi" is the standard score of the observation, "$X_i$" is the observation; "$\mu_i$" is the population mean; and "$\sigma$" is the population standard deviation.

Given this criterion, 98 cases were detected as outliers in the wind speed data, whereas none of the standard scores in air temperature, solar radiation and relative humidity exceeded the threshold standard score value of 4.0. To assess the effect of these 98 outlying cases, basic statistics was calculated with and without these outlying cases (Table 4.2). The difference in mean wind speed with and without outlying cases is 0.03 which is only 0.6% of the mean wind speed. There is no difference in the median values. It was therefore decided to keep the outlying cases for the wind analysis.

Table: 4.2: Outlying cases in the wind speed data from six stations over the west and east coast of the Auckland Region.

| **Wind Speed** | **With Outlying Cases** | **Without Outlying Cases** |
|---|---|---|
| N | 42734 | 42636 |
| Mean | 4.357 | 4.327 |
| Median | 3.800 | 3.800 |
| Std. Deviation | 2.729 | 2.657 |
| Minimum | .00 | .00 |
| Maximum | 22.60 | 15.20 |

Normality of the frequency distribution and independence of the cases are extremely important assumptions for statistical analysis. In addition to other assumptions the choice of statistical method primarily depends on whether a distribution is normal and independent (Table 4.3). The Kolmogorov-Smirnov test and Q-Q plots of expected and observed values were used to check the normality of the distributions. Although none of the frequency distributions could satisfy the stringent K-S test (Table 4.3), but inspection of normal probability plots (not shown here) and frequency distribution plots (histograms) (Figure 4.1) of the six meteorological variables shows that except for wind speed and relative humidity, the rest of the meteorological variables were reasonably normally distributed (Figure 4.1).

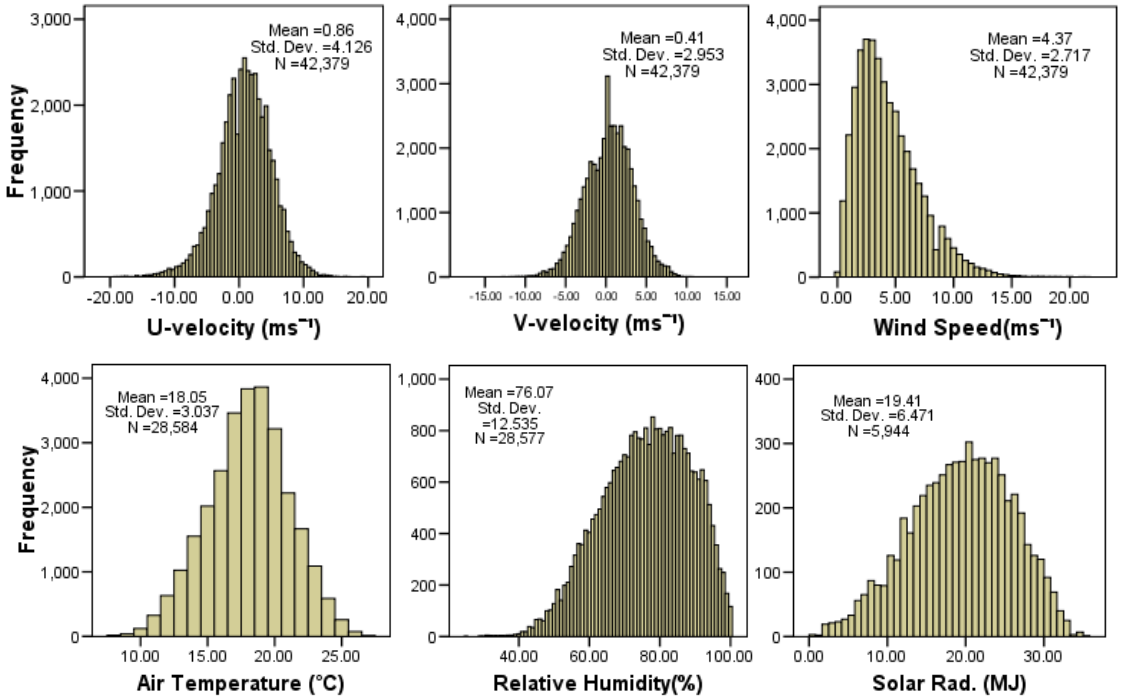


Figure 4.1: Frequency distribution plots (histograms) of 6 meteorological variables for the summer months of 2006 and 2007.

Figure 4.1 shows that the wind speed distribution is positively skewed and peaked which means that most of the cases have low values, whereas the frequency distribution of relative humidity is negatively skewed which means most of the cases have higher values. The frequency distributions of solar radiation and air temperature are normally distributed. Wind direction is a vector quantity and therefore, can be broken down into west-east (u) and south-north (v) components. Although both u and v components are normally distributed, both frequency distributions are peaked with a non-normal kurtosis. Air temperature also has a similar peak. The frequency distributions with non-normal kurtosis generally result in underestimation of the variance.

Table 4.3: Tests of normality of six meteorological variables for 10 months of summer period of 2006 and 2007.

| Meteorological Variable | Kolmogorov-Smirnov[a] | | |
|---|---|---|---|
| | Statistic | df | Sig. |
| u velocity (m $s^{-1}$) | .034 | 28222 | .000 |
| v velocity (m $s^{-1}$) | .028 | 28222 | .000 |
| Wind speed (m $s^{-1}$) | .085 | 28222 | .000 |
| Air temperature (°C) | .045 | 28222 | .000 |
| Solar radiation (MJ $m^{-2}$ $day^{-1}$) | .29 | 5944 | .000 |
| Relative humidity (%) | .050 | 28222 | .000 |

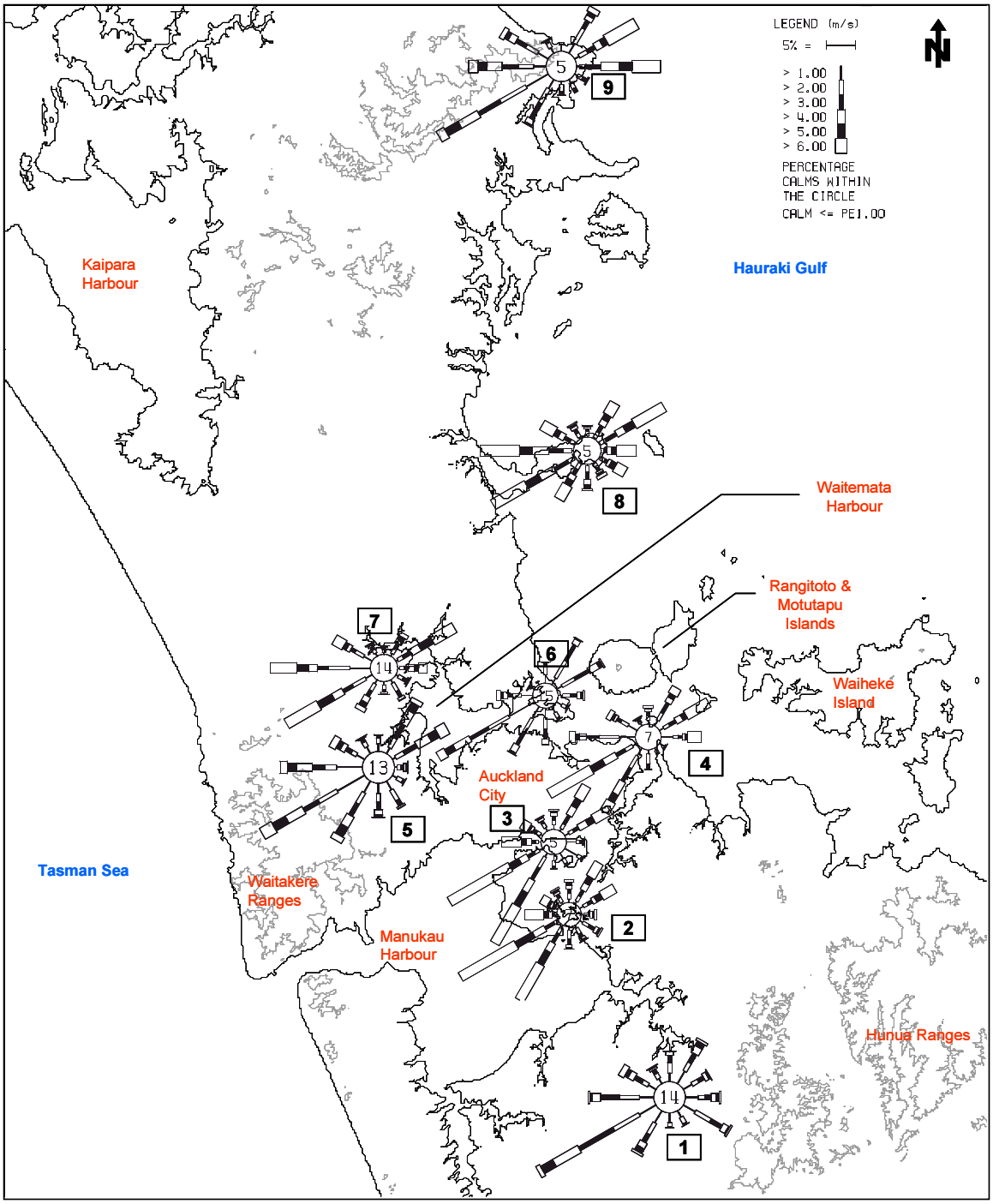


Figure 4.2: The average 24 hour wind roses at 9 stations for the 10 summer months of 2006 and 2007. The numbers in the center of the wind roses indicate percent of calm periods. Stations names 1: Pukekohe, 2: Auckland Airport, 3: Mangere, 4: Musick Point. 5: Henderson, 6: North Shore, 7: Whenuapai, 8: Whangaparaoa, 9: Leigh.

Lack of normality in wind speed and relative humidity prohibited the application of parametric statistical methods. Therefore, transformation was applied to both of these distributions so that more powerful parametric methods such as t-test, regression and ANOVA could be used for statistical analysis. Wind speed was positively skewed while relative humidity distribution was negatively skewed, so that before using these data in statistical analysis, the square root and inverse square root data transformation proposed by Tabachnick & Fidell (2001) were applied to wind speed and relative humidity distributions. After transformation, distributions appear to be reasonably normally distributed. Also, the Q-Q plots showed a fairly reasonable straight line that indicates normality of the frequency distribution.

## 4.3 Local Meteorology of the Auckland Region

### 4.3.1 Wind Field

New Zealand is in the pathway of eastward moving weather systems. The prevailing winds in the North Island are south-westerlies, although, north-easterlies are also quite common (Figure 4.2). The two years of summer data show that winds from west and southwest accounted for 46% of the time, whereas north-easterly and easterly winds accounted for only 28% of the time. Northerly and southerly winds are relatively less common, and each accounted for 13% of the summer time. Wind speed was high during the south-westerly and north-easterly flow (Figure 4.2). The average wind speed during south-westerly or north-easterly winds was above 4.5 m $s^{-1}$, while during southerly and northerly winds, the average wind speed was up to 3 m $s^{-1}$. The strongest winds (>20 m $s^{-1}$) were also observed during south-westerly and north-easterly wind flow. The hourly average wind speed (Figure 4.3a) was higher at both stations on the west coast (Auckland Airport and Mangere) and one station on the east coast (Whangaparaoa), while the average wind speed was the lowest at North Shore where the frequencies of the calms was the highest (15%). The meteorological stations that are close to the coast, for example Whangaparaoa, Auckland Airport, Mangere and Musick Point, recorded higher wind speeds, while inland stations show relatively lower wind speeds. At Mangere, the hourly average wind speed exceeded 7 m $s^{-1}$ during afternoon hours.

### 4.3.2 Temperature

The mean and median surface air temperature during the 10 summer months at four out of six coastal monitoring stations was 18°C with an average standard deviation of 3.0°C, whereas the minimum and maximum temperatures were 7.50°C and 27.10°C respectively. The near-surface air temperature data for North Shore and Musick Point were not available for this period and therefore could not be analysed. The average hourly mean air temperature was high during the afternoon hours (>20°C), while during morning hours (between 0400 to 0600 NZST) it was the lowest (Figure 4.3b).

### 4.3.3 Solar Radiation

The net all wave radiation available is the sum of net shortwave and net long wave radiation. This available energy is then converted in sensible, latent and ground heat fluxes that eventually changes air and surface temperature. The average statistics from 21 stations (list of stations attached as Appendix 4A) in the Auckland region shows that the mean daily total solar radiation during the summer months was 19.41 MJ $m^{-2}$ $day^{-1}$. The minimum daily solar radiation during this period was 0.40 MJ $m^{-2}$ $day^{-1}$, which indicates some overcast conditions while the maximum reached up to 35.42 MJ $m^{-2}$ $day^{-1}$. The box plots (Figure 4.3c) show the total average daily radiation flux at 21 stations. The highest average total solar radiation was recorded at Penrose (median: 21.79 MJ $m^{-2}$ $day^{-1}$).

### 4.3.4 Moisture

The average relative humidity (RH) for the monitoring period was 76%. Due to the overall maritime environment and coastal location of the sensors, the variation in RH at these stations was not significant. The highest daily average relative humidity was observed at Whangaparaoa (78%), while it was lowest at Mangere (73%). Air temperature and relative humidity have an inverse relationship. When air temperature increases the capacity of air to hold water also increases, which in turn reduces the relative humidity. This explains why there is a dip in the relative humidity plots during afternoon hours (Figure 4.3d).

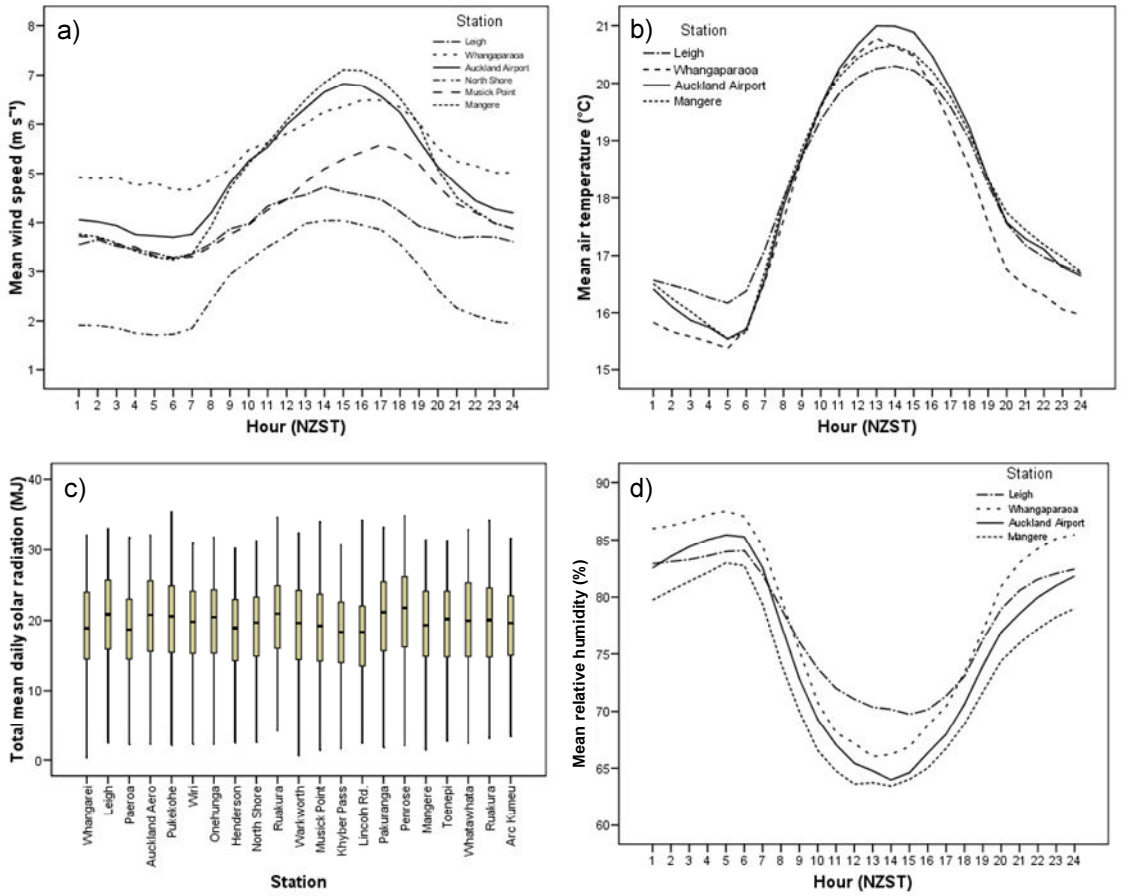


Figure 4.3: Mean line and box plots for the 10 month summer period of 2006 and 2007 for: a) hourly average 10 m wind speed at 6 monitoring stations, b) hourly average near-surface air temperature at 6 monitoring stations, c) average total daily solar radiation at 21 sites in the Auckland region, and d) hourly average near-surface relative humidity at 6 monitoring stations.

## 4.4 Identification of Sea Breeze and Non-sea Breeze Days

Many techniques have been devised for the identification of the sea breeze circulation. Most of these techniques use relation between wind vector and land-sea temperature differential to identify occurrence of sea breezes (Mathews 1982; McKendry & Roulet 1994). However, due to strong local effects such as coastline shape, topography, physical orientation, size and geography of the land mass, the technique developed for one location quite often does not work well for the other location (McPherson 1970; Miller et al. 2003; Simpson 1994). Auckland is a unique peninsula shape narrow isthmus. Observational studies in the Auckland region and other parts of the world show that in a geographic situation such as this, the sea breeze occurs on both sides of the peninsula. Therefore, to identify sea breeze days, a filter was designed based on the assumption that a summer day would be classified as a sea breeze day when onshore

flow was observed over both east and west coasts of the Auckland region. To apply the sea breeze filter, data from six coastal stations were obtained. Two of these stations were selected from west of the Auckland City (Auckland Aero and Mangere) that are in close proximity to Manukau Harbour. The remaining four stations were selected from the east coast, namely Whangaparaoa, Leigh, North Shore and Musick Point. Although Auckland Airport and Mangere are not the ideal stations to represent westerly sea breezes, meteorological data were not available from any other location close to west coast. Therefore, data from Auckland Airport and Mangere were considered to represent the west coast and hereinafter will be referred to as west coast stations. If four or more meteorological stations (at least 2 on each coast) recorded an onshore wind during afternoon hours, the day was flagged as a sea breeze day. On the other hand, if during afternoon hours all the six stations observed either westerly or easterly wind flow, the day was identified as non-sea breeze day. The sea breeze filter is defined as follows:

a) Strong sea breeze days: the wind at the 2 west coast stations had positive u velocity, while the wind at all 4 stations on the east coast had negative u velocity.
b) Weak sea breeze days: the wind at the 2 west coast stations had positive u velocity, while the wind at least 2 of 4 stations on the east coast had negative u velocity.
c) No sea breeze days: surface wind at 6 stations located on both the east and west coasts had either positive u or negative u velocity.
d) Not clear: winds at 2 stations on the west coast had positive u velocity, while wind on the east coast had negative u velocity at only one station.

Table 4.4: Data clusters obtained after application of the sea breeze filter.

| **Sea breeze status** | **Number of days** | **Percentage** |
|---|---|---|
| Non-sea breeze days | 183 | 62.5 |
| Weak sea breeze days | 27 | 9.2 |
| Strong sea breeze days | 31 | 10.6 |
| Not clear | 52 | 17.7 |
| Total | 293 | 100 |

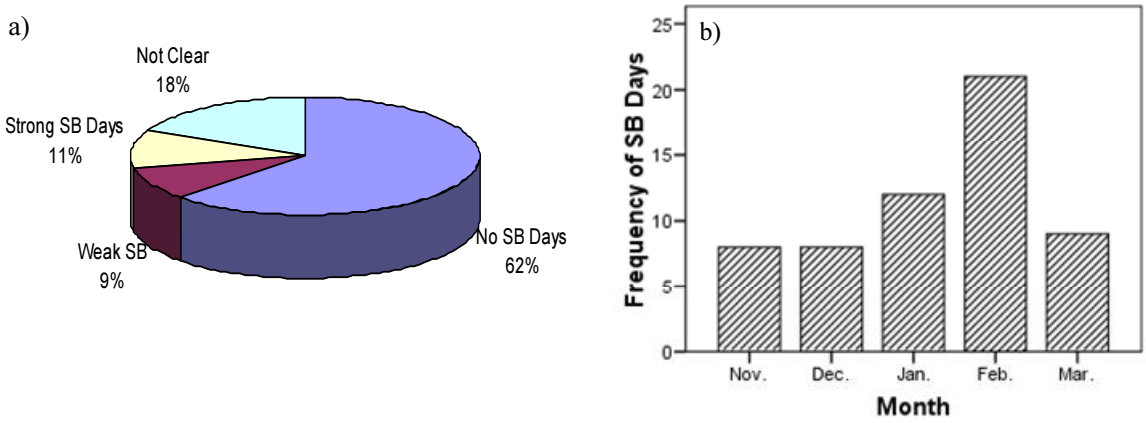


Figure 4.4: a) Percentage breakdown of sea breeze and non-sea breeze days, b) frequency of sea breeze days over 10 months of the summer period of 2006 and 2007. SB =sea breeze.

The application of the sea breeze filter resulted in four clusters from the 10 months of daily data for 2006 and 2007. Table 4.4 shows the details of these four data clusters. Non-sea breeze days accounted for a total of 62% of the ten month period, while sea breeze days (both strong and weak) accounted for nearly 20% of the total summer time, which is consistent with the previous sea breeze work in the Auckland region (McGill 1987). Only sea breeze (strong and weak) and non-sea breeze days were used for further analysis, and summer days identified as 'not clear' were removed from the dataset. This means that out of 241 summer days, the sea breeze occurred on 58 days only (both weak and strong) and the rest of the183 days were identified as non-sea breeze days. Most of these sea breeze days occurred during the months of January and February, while the frequency of sea breeze days was lowest in November and December (Figure 4.4b). Table 4.5 presents hourly daytime average statistics of the three meteorological variables (wind speed, temperature and relative humidity) for the entire diurnal cycle and for sea breeze and non-sea breeze events, whereas the fourth meteorological variable (solar radiation) is the average of the total daily incoming solar flux. The difference between sea breeze and non-sea breeze days is indicative of the basic characteristics of this mesoscale circulation. The average wind speed during sea breeze days was around 45% less than average wind speed on non-sea breeze days. The same is true for the maximum wind speed during sea breeze and non-sea breeze days. The mean and median difference of total daily solar flux between sea breeze and non-sea breeze days is up to 3.0 MJ. Although the maximum solar radiation is the same during sea breeze and non-sea breeze days i.e., 35.42 MJ $m^{-2}$ $day^{-1}$, the minimum solar flux during sea breeze days was 4.2 MJ $m^{-2}$ $day^{-1}$, while it was only 0.40 $m^{-2}$ $day^{-1}$,

during non-sea breeze days. The minimum air temperature was also 4.0°C higher on sea breeze days than non-sea breeze days. It is evident from the solar radiation and temperature statistics that during sea breeze days the land surface received more solar radiation and thus more surface heating that resulted in warmer days. The increased surface heating significantly reduced relative humidity (Table 4.5). During an onshore moist inflow of marine air mass the moisture levels are expected to increase. However, due to Auckland's maritime environment, a significant increase in moisture during a sea breeze is unlikely. This is also consistent with other work done on the sea breeze in the Auckland region (McGill 1987).

Table 4.5: Daytime 1100 to 1800 hours statistics for wind speed, air temperature, relative humidity and total solar radiation over six stations on the east and west coasts of the Auckland region. SB =sea breeze.

| SB status | | Mean total daily solar radiation (MJ) | Wind speed (m $s^{-1}$) | Air temperature (°C) | Relative humidity (%) |
|---|---|---|---|---|---|
| **SB day** | Mean | 21.6 | 3.5 | 21.3 | 64.4 |
| | Median | 21.8 | 3.1 | 21.7 | 65.0 |
| | Std. dev. | 5.3 | 1.6 | 2.3 | 10.0 |
| | Minimum | 4.2 | 0.0 | 14.0 | 25.0 |
| | Maximum | 35.4 | 8.3 | 26.2 | 100.0 |
| **Non-SB day** | Mean | 18.3 | 6.2 | 19.8 | 69.3 |
| | Median | 18.7 | 5.9 | 20.0 | 68.0 |
| | Std. dev. | 6.5 | 2.8 | 2.6 | 13.2 |
| | Minimum | 0.4 | 0.0 | 10.0 | 31.0 |
| | Maximum | 35.4 | 22.6 | 27.1 | 100.0 |

A comparison of basic meteorological characteristics during sea breeze and non-sea breeze days reflects typical conditions necessary for the development of sea breezes. The surface wind speeds on sea breeze days were lower than non-sea breeze days. During afternoon hours, the mean hourly solar radiation and air temperatures were also higher on sea breeze days that subsequently decreased near surface relative humidity (Figure 4.5). Additionally the average synoptic wind speed (at 800-850 hPa) was 5.1 m $s^{-1}$ on sea breeze days, which is less than half the average synoptic wind speeds on non-sea breeze days.

Data from the National Centers for Environmental Prediction (NCEP) show that on most of the sea breeze days there was a high over the North Island, which suggests generally clear sky conditions over Auckland. This is supported by the solar flux data

from 21 stations (Figure 4.6) around the Auckland region that reported higher insolation on sea breeze days at all the monitoring stations. The upper air data analysis suggests that on more than 65% of sea breeze days the synoptic wind speed between 850 and 800 hPa was less than 6.0 m $s^{-1}$.

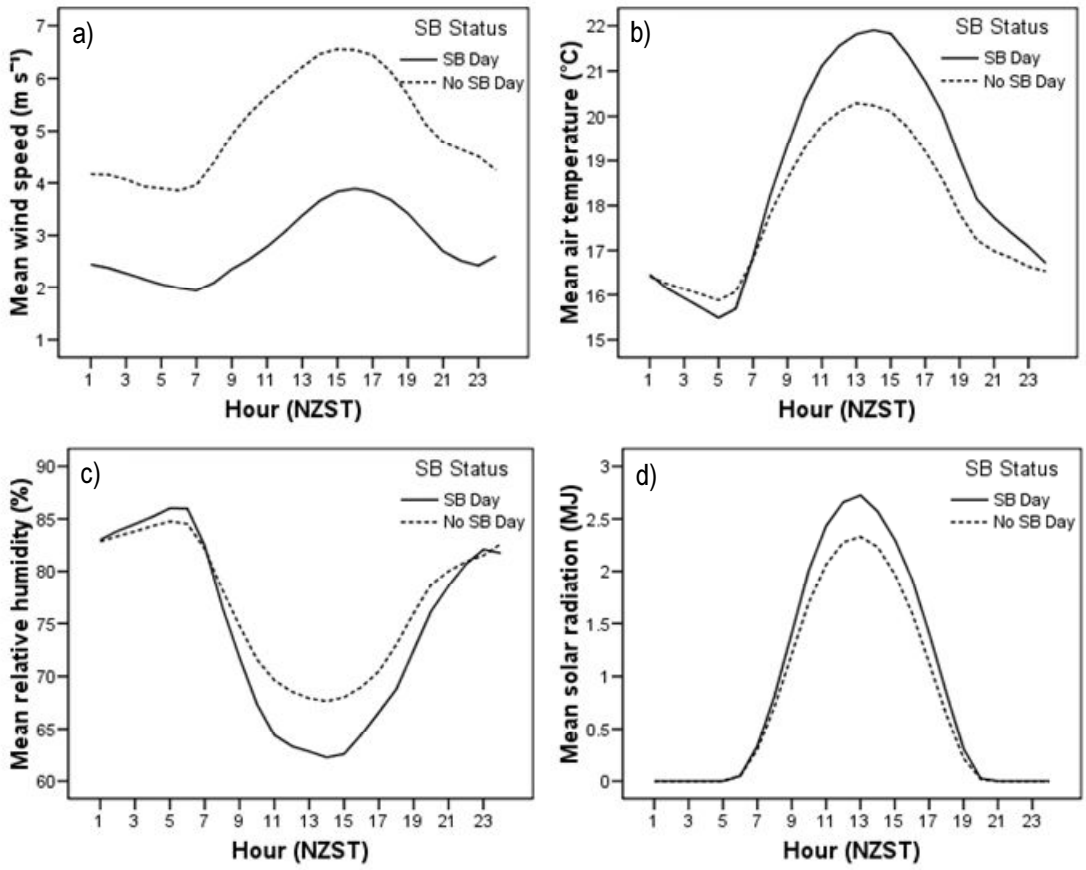


Figure 4.5: Hourly averages during sea breeze and non-sea breeze days at six stations over the west and east coasts of the Auckland region for 10 months summer period of 2006 and 2007.

During non-sea breeze days the prevailing winds were influenced by the large-scale pressure gradient and local topographical features, whereas on sea breeze days the local/small scale pressure gradient dominated the region's meteorology. A comparison of the data from east and west coast stations showed that wind speed was higher over the west coast stations during both sea breeze and non-sea breeze days. At night time, the wind speed over both west coast stations was low on sea breeze days. During day time, sea breezes were much stronger over the west coast, whereas at night the thermal gradient reversed and the offshore wind (land breeze) was generated. The offshore land breezes on the east coast stations were stronger than land breezes to west coast stations. This primarily indicates the effect of synoptic wind forcing. Due to prevailing south-

westerlies the night time offshore north-easterly land breezes at the west coast stations were quite weak, whereas the same prevailing south-westerlies increased the magnitude of land breezes on the east coast.

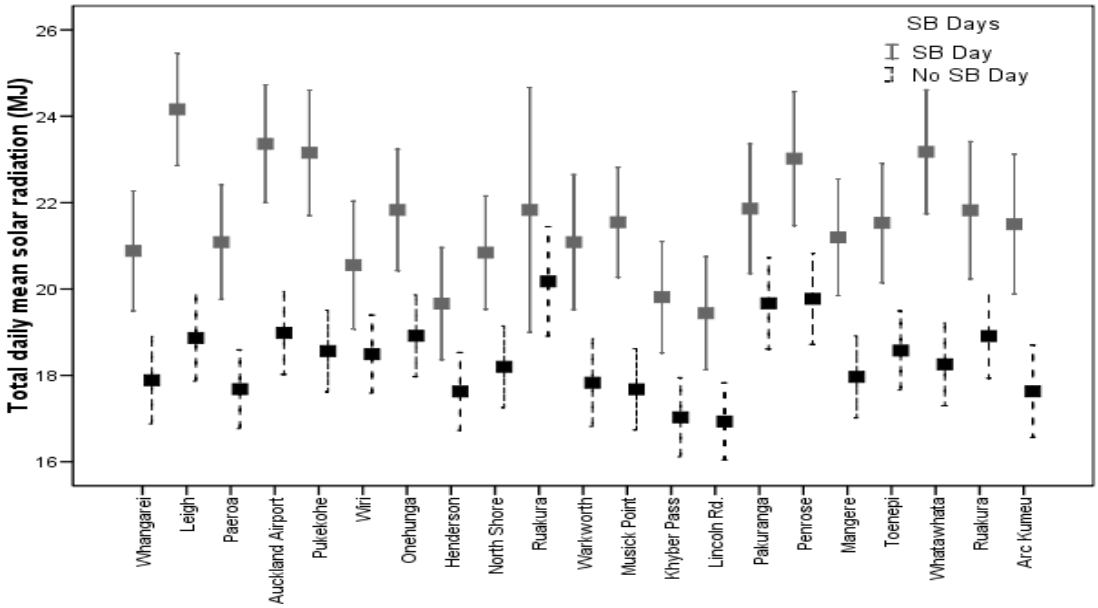


Figure 4.6: Error bar plot of 95% confidence interval for average total daily solar radiation flux from 21 monitoring stations in the Auckland region for 10 months summer period of 2006 and 2007.

To test the differences between sea breeze and non-sea breeze days, a t-test has been applied to wind speed, air temperature, relative humidity and solar radiation. Since our interest is testing the difference in these variables during sea breeze events, for the first three parameters the t-test was applied to daytime only that is from 1100 to 1800 NZST. For solar radiation, however, total daily solar radiation was calculated for the entire monitoring period. The results are presented in Table 4.6. The Levene test showed un-equal variances between sea breeze and non-sea breeze days ($p(\text{significant}) < 0.05$), so that the test for un-equal variance has been used.

The t-test is highly significant (asymptotic significance, 2 tailed < 0.05) for all the four meteorological parameters, which means that wind speed, air temperature, solar radiation and relative humidity significantly vary between sea breeze and non-sea breeze days. Table 4.6 shows lower mean wind speed, higher mean near-surface temperature and solar radiation on sea breeze days.

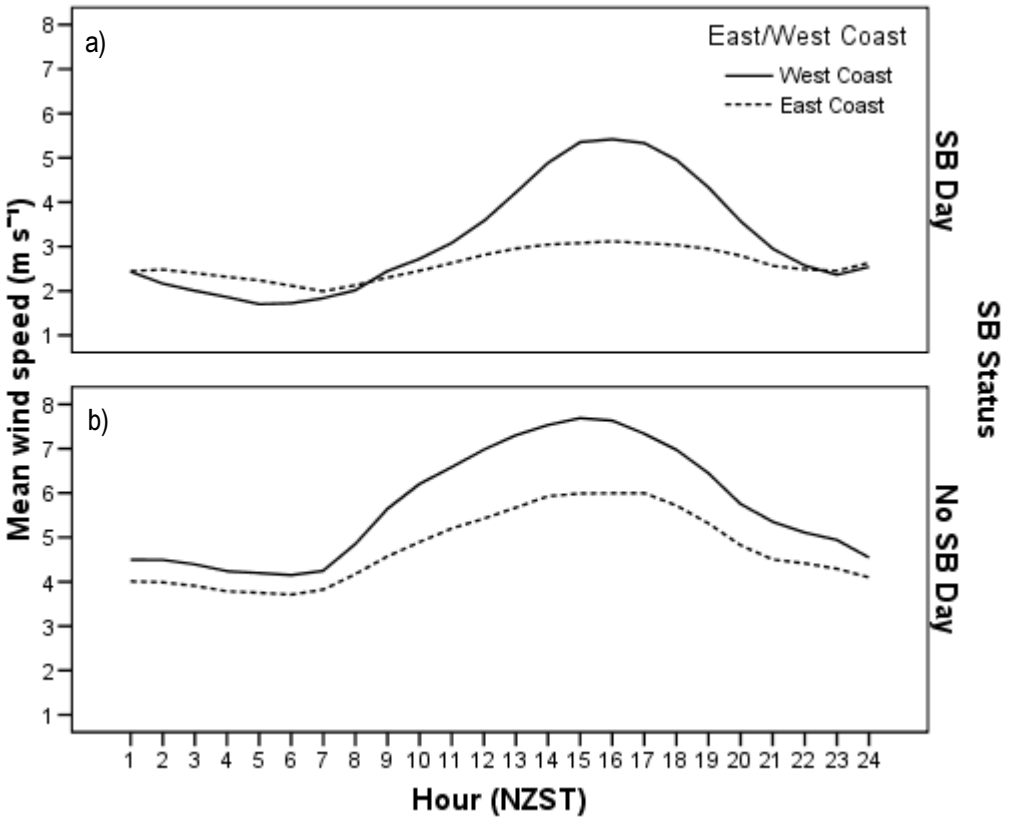


Figure 4.7: Mean wind speed during sea breeze and non-sea breeze days over two stations on the west coast and four stations on the east coast for 10 months summer period of 2006 and 2007.

The difference between sea breeze and non-sea breeze days has been assessed by the $\eta^2$ method that calculates the magnitude of the difference in meteorological variables (wind speed, temperature and relative humidity) between sea breeze and non-sea breeze days. The guideline proposed by Cohen (1988) described threshold values of 0.01 as a small effect, 0.06 as a moderate effect and 0.14 as a large effect.

$$\eta^2 = \frac{t^2}{\left[t^2 + \left(N_1 + N_2 - 2\right)\right]}$$

Where t = t-test statistic

$N_1$ = number of cases in group one

$N_2$ = number of cases in group two

Table 4.6: Independent two sample t-test for difference in meteorological variables between sea breeze and non-sea breeze days.

| Equal variances not assumed | Levene's test for equality of variances | | t-test for equality of means | | | | | | |
|---|---|---|---|---|---|---|---|---|---|
| | F | Sig. | t | Df | Sig. (2-tailed) | Mean diff. | Std. error diff. | Effect size | |
| | | | | | | | | Eta Sq. | Size |
| Wind speed ($m\ s^{-1}$) | 383.5 | .00 | -68.4 | 7914.9 | .000 | -.6169 | .0090 | 0.25 | L |
| Air temperature (°C) | 20.1 | .00 | 24.9 | 4249.7 | .000 | 1.416 | .0568 | 0.06 | M |
| Solar radiation (MJ) | 49.7 | .00 | -16.9 | 2302.7 | .000 | 3.259 | .19285 | 0.10 | M |
| Relative humidity (%) | 437.2 | .00 | 20.4 | 5795.0 | .000 | .4962 | .0244 | 0.04 | S |

The large $\eta^2$ of wind speed (0.25) indicates a large difference in wind speed between sea breeze and non-sea breeze days. The mean wind speed statistics shows that during sea breeze days, the wind speed was as low as 50% of that on non-sea breeze days. The $\eta^2$ statistic for air temperature and solar radiation suggest a moderate effect. The mean values for both air temperature and solar radiation indicates that the land surface received more radiative flux during sea breeze days that is subsequently reflected in relatively high surface and air temperatures.

## 4.5 Sea Breeze Structure and Dynamics

### 4.5.1 Surface Winds at the West Coast Stations

The dominant prevailing winds in the Auckland region are south-westerlies (Figure 4.2). During non-sea breeze days, irrespective of the time of day, the two west coast stations (Auckland Airport and Mangere) show dominant wind flow from southwest or northeast. However, during sea breeze days, the situation was more complex and shows specific features of the sea and land breeze regimes. An important feature of the diurnal wind field is the high frequency of south-westerly winds over the Auckland area, while during night time the reversal of the local pressure gradient resulted in offshore land breezes from northeast to southeast (Figure 4.8). Despite the fact that north-easterlies are quite common, the contour plots do not show any easterly winds during daytime on sea breeze days. This is probably due to the strength of the westerly sea breezes that did

not allow easterlies to reach Manukau Harbour. The contour plots also show a very low frequency of northerly and north-westerly winds throughout the diurnal cycle. Therefore, surface wind direction most of the time remained restricted between south-westerlies and easterly winds at these two stations. As a result, the typical diurnal rotation of sea and land breezes is not clearly evident in the contour plots of the two west coast stations. Studies of the diurnal rotation of sea and land breezes (Alpert & Kusuda 1984; Kusuda & Alpert 1983; Neumann 1977; Simpson 1995) have suggested that the diurnal rotation of sea and land breezes depends on a suitable combination of the Coriolis force, and the mesoscale and large scale pressure gradients. This balance is quite often disturbed due to variations in the pressure gradient caused by the terrain than may result in a shift in the wind direction of the local sea breeze. On the basis of various observational and modelling studies, Simpson (1995) concluded that topographical influences can often be responsible for variations in the expected rotation of the sea and land breezes. It also appears that in the Auckland case topographic features and local pressure gradients have a significant effect. The deviation of actual wind direction from the theoretical rotation of wind has been studied in greater detail by employing idealized modelling technique in Chapter 6 and Chapter 7.

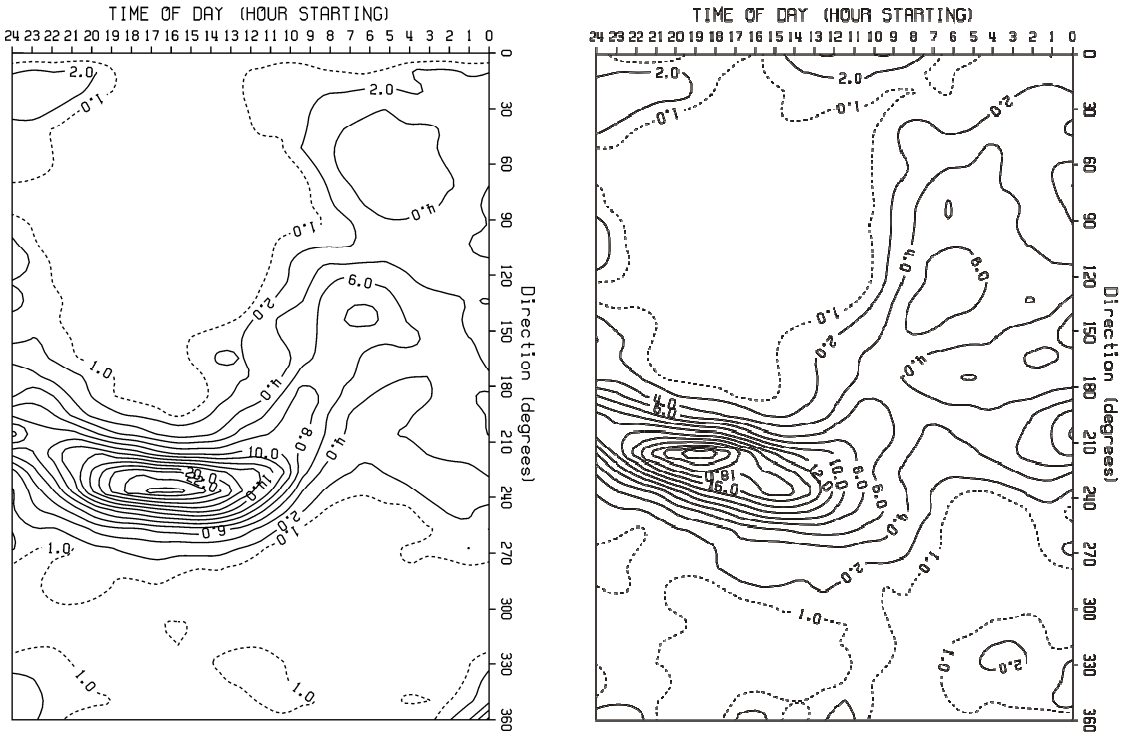


a) Auckland Airport b) Mangere

Figure 4.8: Frequency contour plots of the winds over the diurnal cycle on 58 sea breeze days for two stations on the west coast. The dashed contours indicates wind frequency <= 1 m $s^{-1}$.

The rate of rotation of surface winds was weak during daytime, especially in the afternoon hours, whereas during night time the wind shift was quite strong. This can be explained by the findings of Neumann (1977) that if the wind results from a combination of the mesoscale and large-scale pressure gradient, the wind points in the same direction (either onshore or offshore) and the rate of rotation is reduced. However, if they are in the opposite direction, the rate of rotation is enhanced. During daytime the higher frequency of prevailing south-westerlies, together with south-westerly to westerly sea breezes, reduced the rate of wind rotation, whereas during night time the mesoscale pressure gradient reversed and north-easterly land breezes were in the opposite direction to the prevailing south-westerlies that eventually increased the rotation rate.

### 4.5.2 Surface Winds on the East Coast of the Auckland Region

The contour plots of wind direction frequency for the east coast stations provide more detailed information on the sea and land breeze wind patterns. All the four stations show higher frequencies of north-easterly to easterly sea breezes from late morning until evening, whereas at night-time due to reversal of the mesoscale pressure gradient, the offshore south-westerly winds were recorded at all the four monitoring stations. The night time south-westerly land breezes were enhanced by the prevailing south-westerlies and therefore lasted for a longer time. Unlike the west coast stations the rate of rotation of surface wind direction was higher during daytime but lower at night time due to the higher frequency of prevailing south-westerly flow, which is consistent with the findings of Neumann (1977) and Simpson (1995). Unlike the west coast, the diurnal rotation of the land-sea breeze over the east coast is evident in the frequency contour plots (Figure 4.9). The frequency of the north-westerly and the south-easterly winds was low and primarily indicates the transition between sea and land breeze regimes and a higher rotation rate during morning and evening hours of the day which is consistent with previous work on the diurnal rotation of land-sea breezes (Alpert & Kusuda 1984; Kusuda & Alpert 1983; Neumann 1977; Simpson 1995).

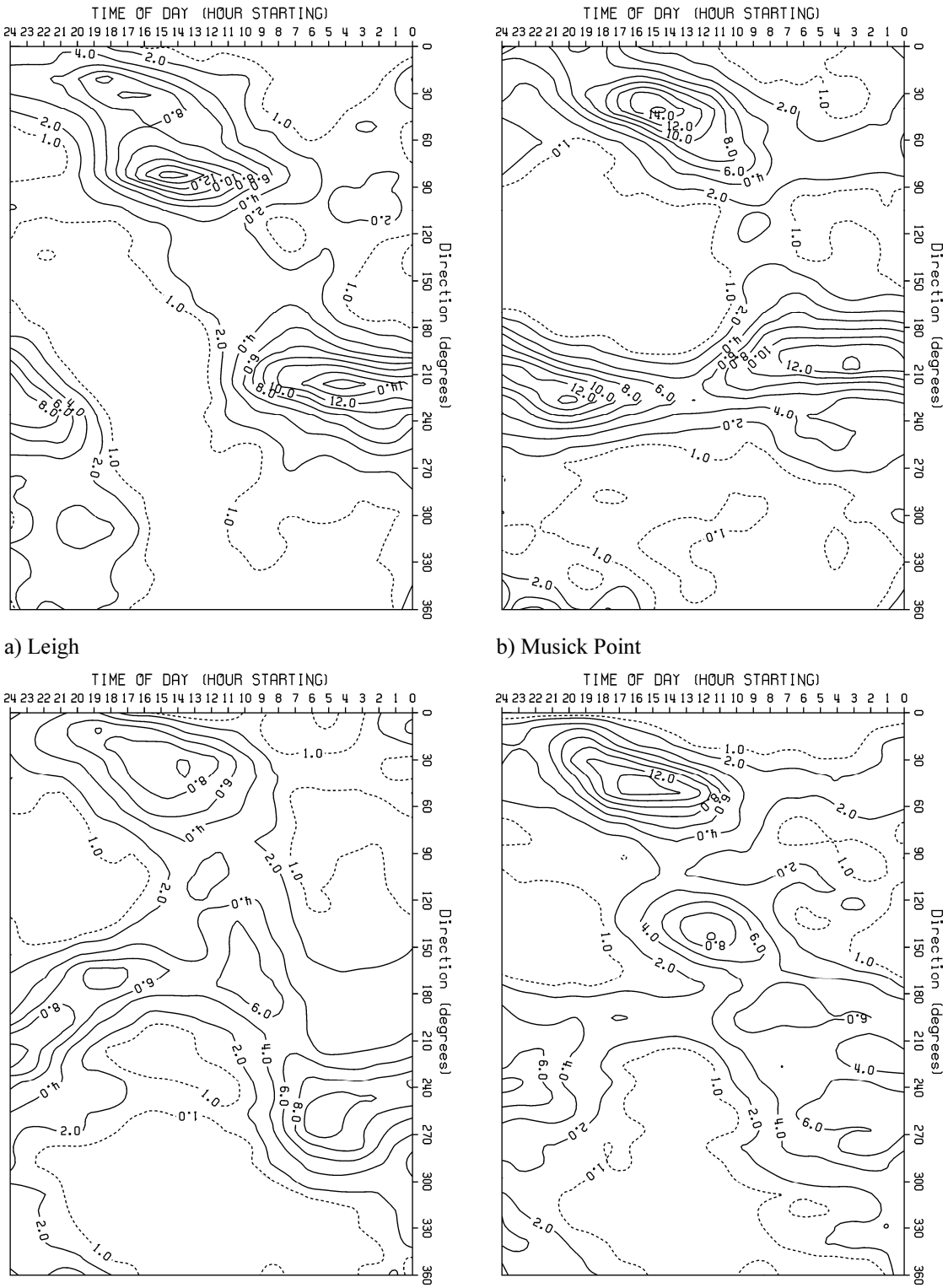


a) Leigh

b) Musick Point

c) North Shore

d) Whangaparaoa

Figure 4.9: Frequency contour plots of the wind direction frequency by time of day on 58 sea breeze days for four stations on the east coast. The dashed contours indicates wind frequency <= 1 m $s^{-1}$.

### 4.5.3 Convective Internal Boundary Layer (CIBL)

When the cold dense and moist marine air mass moves over warm land surface, it can produce a shallow convective internal boundary layer (CIBL) that grows in depth with the square root of distance from the shore (Stull 2003). The CIBLs are known for their role in degradation of the air quality of coastal urban areas by fumigation and trapping of air pollutants in the surface layer. The determination of the height of the CIBL is therefore an important component of pollutant dispersion studies in coastal areas (Luhar et al. 1998). The mixed layer height can be approximated in a number of ways. One way to derive CIBL height is by obtaining vertical profiles of turbulent kinetic energy (TKE). The top of the CIBL is approximated at a height when TKE is becomes smaller than 0.03 $m^2 s^{-2}$ (Arritt 1987; Liu et al. 2001). In slab models, the height of the CIBL is defined as the height at which temperature gradient values return to the background over-sea values. Another more commonly used method is the base of the elevated inversion layer on the potential temperature profile (Fast & Zhong 1998; Liu et al. 2001; Zhong & Takle 1992). Therefore, the top of the CIBL can be defined as the height where the vertical potential temperature gradient first become larger than 0.0025 $K m^{-1}$ (Fast & Zhong 1998). Examination of the potential temperature profile has also been used to determine the top of CIBL. Vertical profile data of temperature, wind speed and wind direction were obtained from Whenuapai station. Out of 58 sea breeze days, the 1200 NZST upper air data were available for only 6 days. The vertical profiles of potential temperature for the six days are presented in Figure 4.11. Although the resolution of the vertical profile is quite low, and in some cases the temperature data for the lowest level also does not match with the near-surface air temperature from surface observations, they still provide an assessment of the thermodynamic structure of the atmosphere on six sea breeze days. The vertical structure of wind field is quite complex over Auckland during sea breeze events. Waitemata Harbour is located approximately 2 to 3 kilometre southeast and east of Whenuapai station. Due to this terrain feature, the early morning winds during relatively weak synoptic winds always indicate a westerly offshore component. In the morning hours south-easterly bay breezes blow from Waitemata Harbour and in the afternoon hours a mature sea breeze either from the west or the east coast (depending upon the strength and direction of the large scale winds) arrives at the station. The arrival of the sea breeze front from either coast is indicated by a significant drop in the air temperature and increase in the

humidity. The time series of ambient air and dew point temperature from Whenuapai are plotted for the six days to indentify the arrival of sea breeze front by analysing reduction in air temperature and increase in moisture (dew point temperature) (Figure 4.10). These plots indicate a momentary temperature drop and increase in humidity on most of the sea breeze days. On 29th March 2006, the arrival of sea breeze front is not very apparent and there was a gradual drop in near-surface air temperature after 1300 hours. On most of the days the sea breeze front arrived after 1300 hours. This means the changes in the vertical thermodynamic structure of the lower atmosphere associated with mature sea breezes from the west and the east coast mainly occurred after 1300 hours. The observed surface temperatures during south-westerly wind flow were lower than easterly wind flow. The minimum dew point depression (and thus low temperature and higher humidity) was observed on 23rd March 2006 at 1600 hours under westerly sea breeze conditions (Figure 4.10d). This means that the marine air mass from the west coast on this day was colder and has more moisture content compared to east coast sea breezes. The potential temperature profile for 1200 hours (Figure 4.11) shows the thermal structure of the lower atmosphere that indicates a super adiabatic layer in the first 100-200 m above ground level on all the six sea breeze days. The mixed layer heights were calculated using the potential temperature method provided by Fast & Zhong (1998) and presented in Table 4.7. Figure 4.10 suggests that except for 19th March 2006, the mature sea breezes arrived after 1300 hours. Before that time due to convergence between the south-easterly bay breeze from Waitemata Harbour and the air over land a mixed layer rapidly developed. The height of the mixed layer on the 5 days ranged between 471 to 1524 m.

Table 4.7: Mixed layer height (m) at 1200 hours on six selected sea breeze days.

| **Mixed layer at 1200 hours** | **6th Feb 2006** | **19th Mar 2006** | **22nd Mar 2006** | **23rd Mar 2006** | **29th Mar 2006** | **23rd Feb 2007** |
|---|---|---|---|---|---|---|
| Height (m) | 971 | 370 | 798 | 849 | 471 | 1524 |

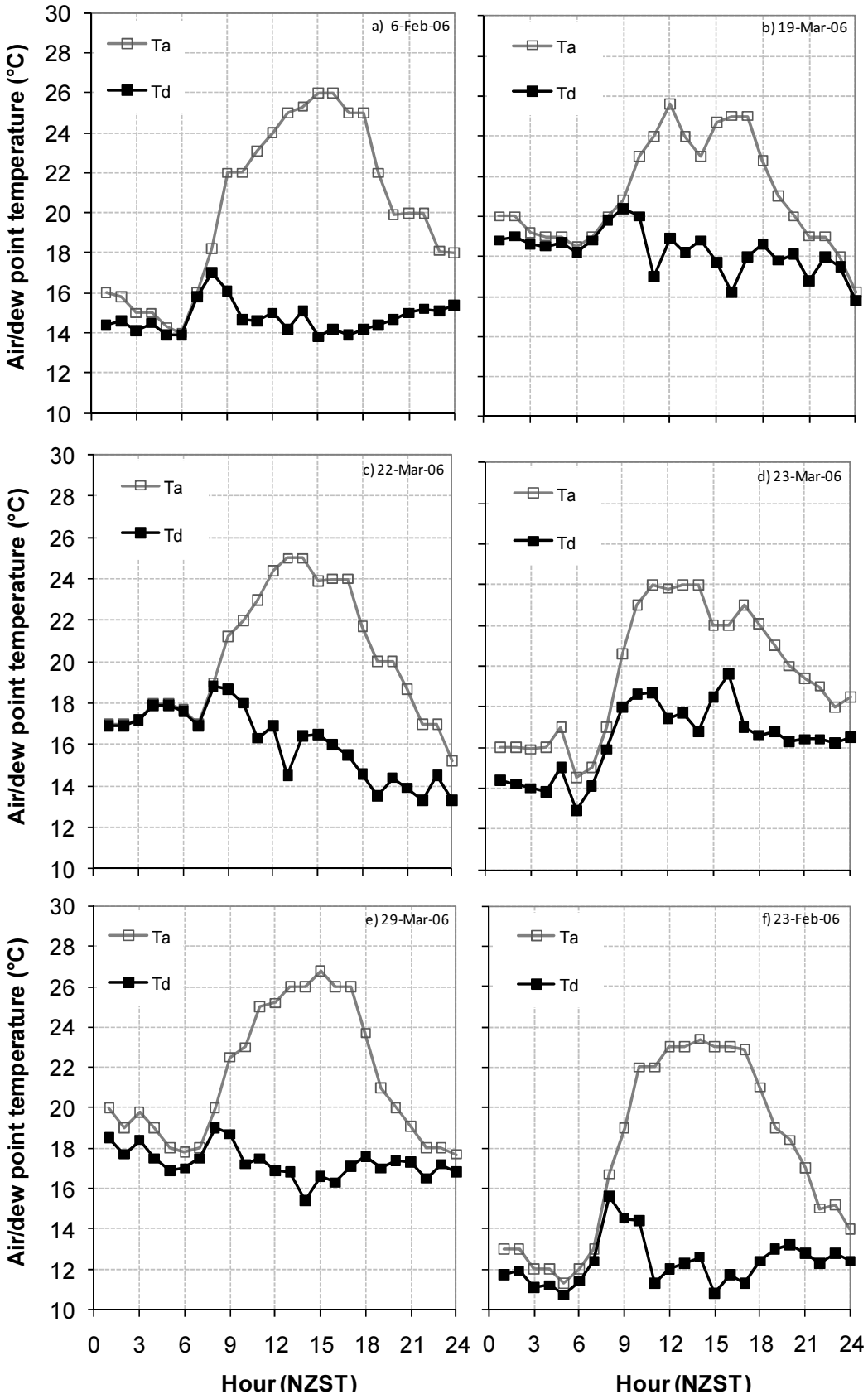


Figurer 4.10: Time series plot of ambient air (Ta) and dew point (Td) on six selected days from Whenuapai.

The time series plot of air and dew point temperature difference (Figure 4.10) suggests that on 19th March, the sea breeze front arrived at Whenuapai at around 1200 hours under north-easterly gradient wind conditions. With this early arrival, the height of the mixed layer was reduced to less than 400 m. The near-surface temperature reached its maximum between 1400 and 1500 hours, so that a much higher CIBL can be expected in the afternoon hours. Unfortunately, vertical soundings for mid to late morning and afternoon hours are not available, so that the temporal evolution and maximum observed height of the CIBL during the diurnal cycle cannot be properly assessed. The spatial evolution of the CIBL also cannot be investigated at this stage because of unavailability of reliable vertical sounding from other stations for these days.

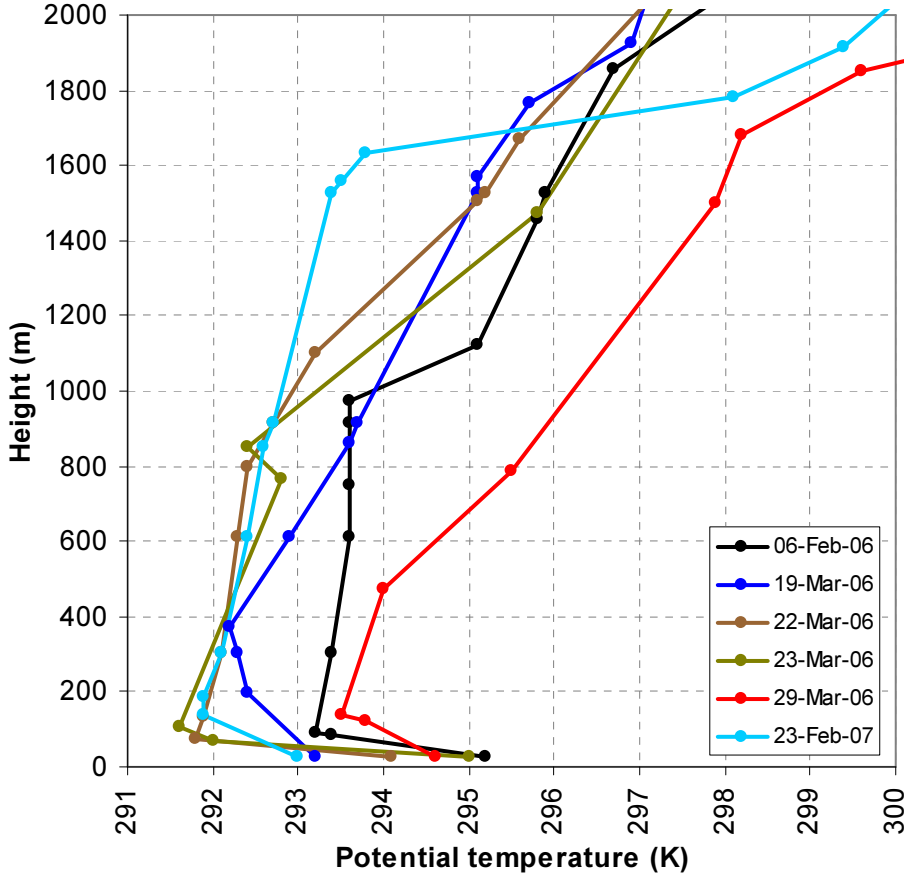


Figure 4.11: Vertical profiles of potential temperature between 1100 to 1200 hours for 6 selected days from the Whenuapai station.

### 4.5.4 Sea Breezes under Different Gradient Wind Conditions

The large scale winds can have a significant effect on the development and evolution of sea and land-breeze circulations. Various studies have shown a profound effect of the

speed and direction of the gradient wind on the development, onset, cessation, strength and structure of sea breezes (Bechtold et al. 1991; Estoque 1962; Pearson et al. 1983; Walsh 1974; Zhong & Takle 1993). Gradient winds are also the main determinant of the location and strength of the sea breeze convergence zone, which is considered an important control with respect to the air pollution meteorology of a region. Adams (1997) and Miller et al. (2003) categorized sea breezes into four different types based on the direction of the gradient wind. In this section, the effect of gradient winds on the sea breeze system in the Auckland region is studied. The data from Whenuapai station was used for gradient wind analysis. Whenuapai station was selected because of its location, which is not far from the Auckland City, and availability of relatively better quality surface and vertical sounding data. Due to the proximity of the Waitemata Harbour, Whenuapai is dominated by small scale south-easterly bay breezes during morning hours. By noon, on most sea breeze days the station was dominated by a combination of south-easterlies or mature easterly sea breezes from the east coast. The westerly sea breeze normally arrived in the afternoon hours and eliminated the bay breeze from the Waitemata Harbour and pushed easterly sea breezes towards the east coast.

To determine the gradient winds, sounding data from Whenuapai for 1200 hours were obtained and average wind speed and wind direction was calculated for the atmospheric pressure level between 850 and 800 hPa. The resulting winds were assumed to be unaffected by the sea breeze circulation and represent gradient winds. For analysis purposes, the synoptic wind direction (0-360 degrees) was split into 8 dominant wind direction categories, namely northeast, east, southeast, south, southwest, west, northwest and north. Each synoptic wind sector represents 45 degrees. Figure 4.12 shows that most of the sea breezes occur during south-easterly, southerly and northerly gradient winds when the synoptic wind speed was <= 6 m $s^{-1}$. The frequency of sea breeze days was the lowest during the north-easterly and south-westerly gradient winds that are the dominant winds in the Auckland region. However, the neighbouring easterly and westerly synoptic wind sectors have a high number of sea breeze days. This is partly due to the categorization of the synoptic wind direction and partly due to inhibition of mesoscale circulations under strong prevailing south-westerly or north-easterly wind conditions. Both the northeast and southwest wind sectors together have

only eight days of sea breezes. During these eight days the gradient wind speed was quite low (<4 m $s^{-1}$). Under these weak gradient winds, the vector sum on either coast was not strong enough to flush the whole region with one way flow so that sea breezes developed on both east and west coasts. These results are slightly different from the findings of McGill (1987) that suggest a higher number of sea breeze days during easterly and north-westerly gradients winds conditions. There are two possible reasons for this, one is the sea breeze filter applied in this analysis and second, the calculation of average gradient wind direction. McGill took average of 0600 hours and 1200 hours winds at 900 hPa as mean gradient winds, while in this analysis the gradient wind direction is calculated as average wind direction between 850 and 800 hPa at 1200 hours. It appears that due to the lower level, the gradient winds calculated by McGill were affected by the sea breeze circulation.

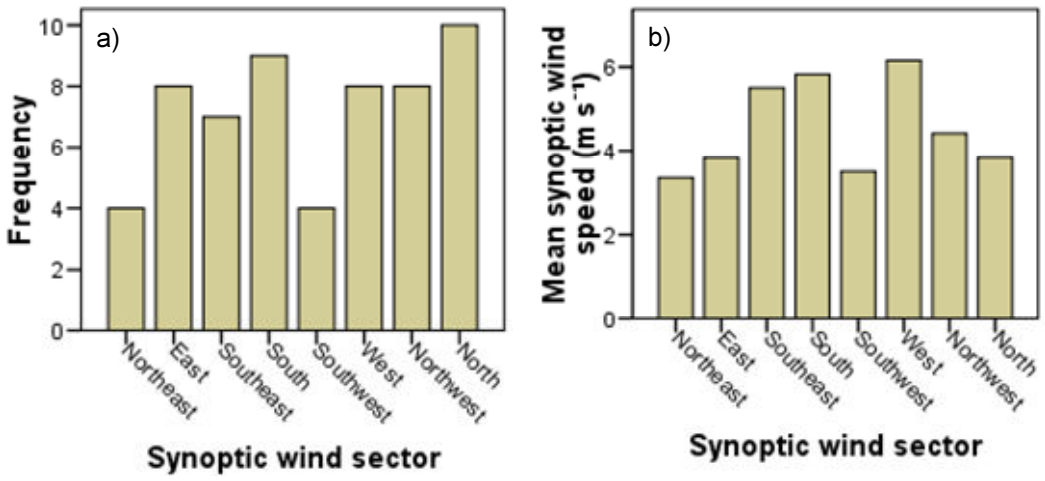


Figure 4.12: Frequency and mean strength of the synoptic wind speed at 850 hPa at 1200 hours during sea breeze days under different synoptic wind conditions.

### 4.5.5 Effect of Gradient Winds on the Diurnal Rotation of the Sea Breeze

The frequency contour plots of wind flow at Whenuapai under different gradient wind conditions show strong impact of large-scale winds on the thermally induced circulation from the harbours and the major coasts of the Auckland region (Figure 4.13). The contour plots also exhibit the signature of various topographical and geographical features in the wind field such as effect of two harbours during the day and effect of drainage winds at night time.

One important feature of the wind field at Whenuapai was consistent south-easterly flow during morning hours of the day. The higher frequency of south-easterly flow is primarily due to the onset of bay breeze from Waitemata Harbour which is in close proximity of the AWS at Whenuapai. The second important feature of the diurnal wind field at Whenuapai during the sea breeze days was the consistent occurrence of westerly land breeze from late evening to morning. The cold air drainage from Waitakere Ranges that are located to the west of the station may also have some contribution to the high frequency of the night-time westerly flow.

Under coast-normal northeast and easterly gradient winds conditions (Figure 4.13a and 4.13c), the frequency of north-easterly sea breeze was high during the day, while under southwest and westerly gradient wind conditions (Figure 4.13b and 4.13d), south-westerly/westerly sea breezes were dominant. An onshore gradient flow generally enhances the inland penetration and duration of the sea breezes (Pearson et al. 1983; Simpson 1977; Stull 2003). The wind field during coast-parallel gradient wind conditions (4.13e and 4.13f) was more complex and can be explained in terms of balance of large scale pressure gradient and low lever frictional flow (Adams 1997; Miller et al. 2003; Zhong & Takle 1993). Under northerly gradient flow, the frequency plots exhibit higher frequency of north-easterly winds during day time which is consistent with the theory that suggest enhancement of easterly sea breeze under gradient winds with strong north/northwest component. In case of southerly gradient wind conditions, the westerly sea breeze component was stronger during the day which is again consistent with the theory. The remaining two coast-sub-parallel gradient wind directions (4.13g and 4.13h) exhibit even more complex and challenging situation. Under south-easterly gradient flow (Figure 4.13g), the frequency of north-easterly winds was higher, while south-easterly gradient wind should enhance westerly sea breezes, similar to this the frequency of daytime westerly winds was higher under north-westerly gradient flow while north-westerly gradient flow should enhance easterly sea breezes. The important fact is that effect of gradient winds that are sub-parallel to the land mass (northerly and southerly gradient winds) was consistent with the theory, but effect of coast-parallel gradient winds on sea breeze was inconsistent with the theory. There could be many reasons for this; one is clustering method used to bifurcate sea breeze days in to eight different quadrants; second, probably lack of

precision in selecting the gradient wind for each sea breeze day and third and probably most important is the topography, local meteorology and position of the instrument itself. The behaviour of local winds under south-easterly and north-westerly gradient wind conditions has been further addressed in the modelling study. The frequency contour plots show more clear diurnal rotation of thermally-induced winds under gradient winds with strong easterly or northerly component (e.g. 4.13a, 4.13c, 4.13e, and 4.13g), while wind rotation under gradient winds with strong westerly and southerly component, was obscure or simply did not occur.

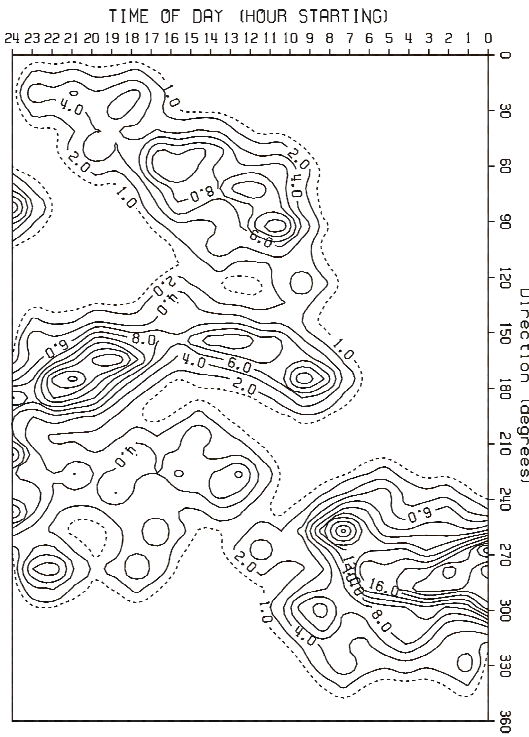


a) Sea breezes under northeast gradient wind

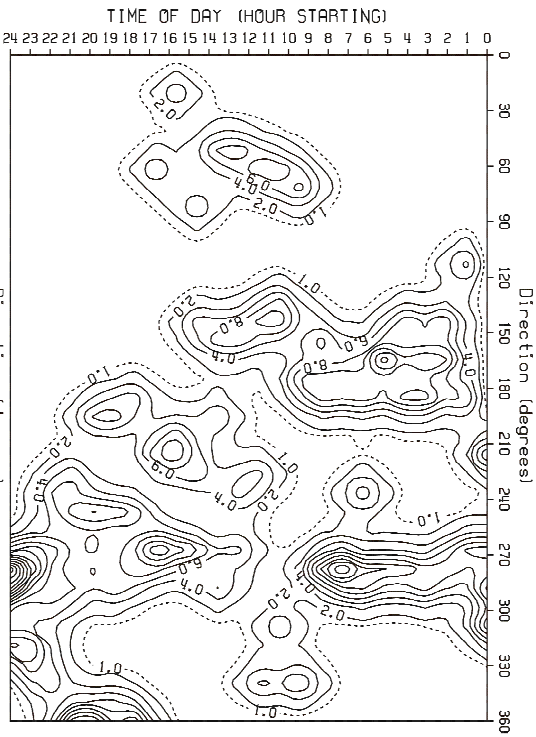


b) Sea breezes under southwest gradient wind

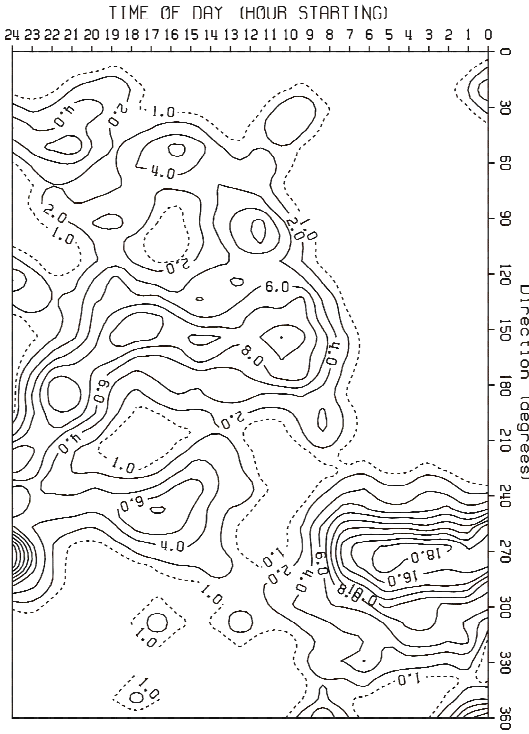


c) Sea breezes under easterly gradient wind

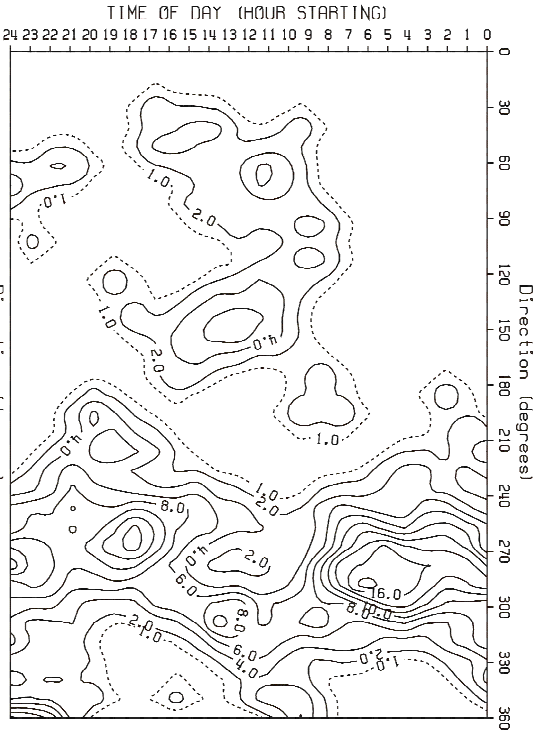


d) Sea breezes under westerly gradient winds

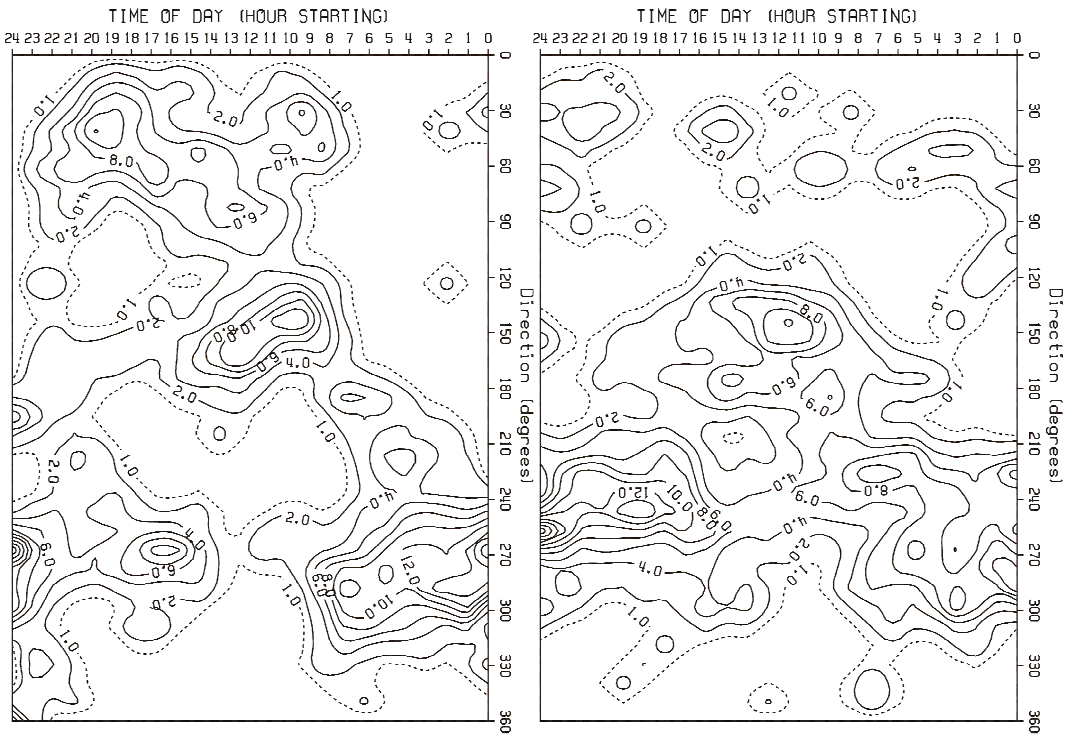


e) Sea breezes under northerly gradient wind




f) Sea breezes under southerly gradient wind

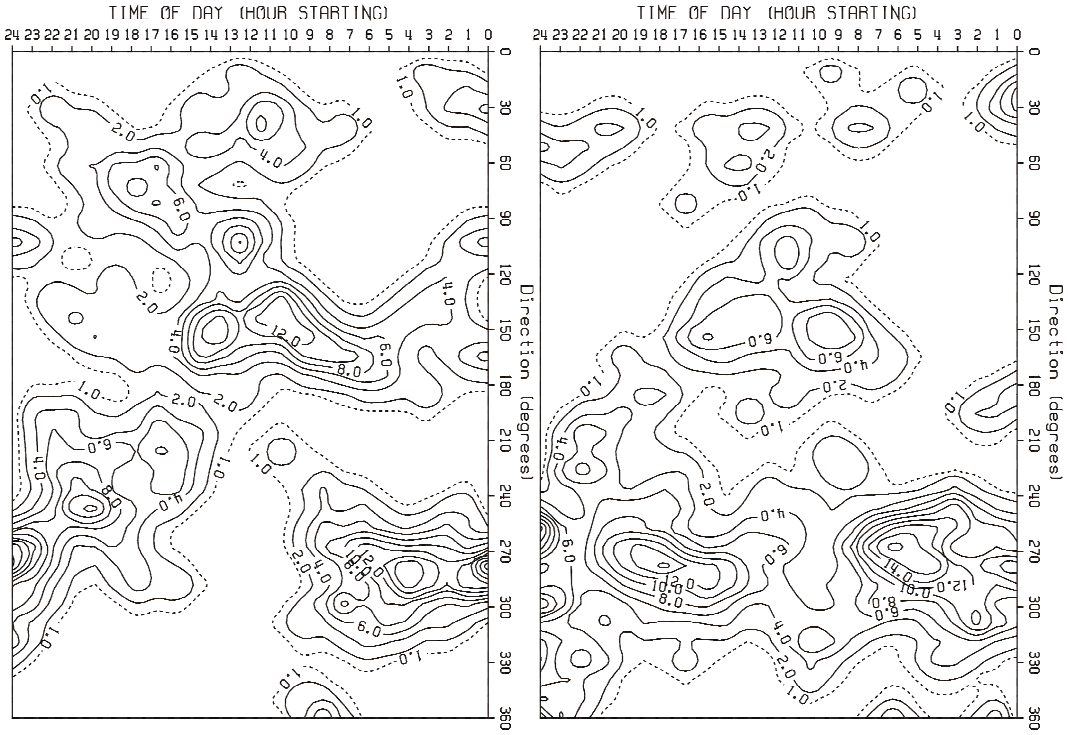


g) Sea breezes under southeast gradient wind




h) Sea breezes under northwest gradient wind

Figure 4.13: Percent frequency contour plots of sea breeze days under different gradient wind conditions at Whenuapai.

### 4.5.6 Sea Breeze Convergence Zones (SBCZ)

Previous studies on the Auckland region (McGill 1987; McKendry 1992; Revell 1978) showed that strength and position of the sea breeze convergence zones (SBCZs) are strongly influenced by gradient winds. In this section, sea breeze convergence zones (SBCZs) are qualitatively assessed. The wind data for a typical sea breeze day (18 March 2006) were obtained from 27 monitoring stations in and around the Auckland region. However, the plots in Figure 4.14 have been reduced for brevity. Figure 4.14 shows evolution of the SBCZs over the Auckland region under north-westerly gradient wind conditions. On 18$^{th}$ March 2006, a strong high was over New Zealand giving a north-westerly to northerly gradient flow over the Auckland region. The offshore land breezes were prolonged until 0600 hours (Figure 4.14a). By 0900 hours the bay breeze commenced around the Waitemata and Manukau harbours and further north of the Auckland region (Figure 4.14b). Weak convergence zones started developing near the Waitemata Harbour and eastern side of Auckland City due to interaction between these bay breezes and the air mass over land. By 1100 hours, mature sea breezes from the Hauraki Gulf and Tasman Sea also commenced. With northerly gradient winds, the sea breeze convergence zone at the Auckland seaport was pushed to the southwest of the city, close to Manukau Harbour. By 1200 hours, the west coast sea breeze moved over Auckland Airport pushing the SBCZ towards the middle of Auckland City and southeast of Manukau Harbour towards Pukekohe. Two SBCZ were also developed north of the Auckland region between Kaipara Harbour and Warkworth (further east of Kaipara Harbour). The sea breeze over both coasts intensified during the afternoon hours. At this time, four convergence lines could be clearly identified. One was to further north of the Auckland region, and the second convergence zone was formed around Waitemata Harbour due to interaction of sea breezes from the east coast and Waitemata Harbour with the sea breezes from the west coast and/or prefrontal air mass over land. A third SBCZ was formed over Auckland City due to interaction between westerly sea breezes from Manukau Harbour and easterly sea breezes from Hauraki Gulf. A fourth SBCZ was formed to the southeast and south of Manukau Harbour due to interaction of westerly sea breeze enhanced wind flow from Manukau Harbour and the with the air mass over land and/or easterly sea breezes. Although westerly sea breezes became stronger during the afternoon hours, a relatively weak northerly gradient wind flow did not allow sea breezes from the west coast to push the SBCZs

offshore along the east coast. After 1800 hours, with weakening sea breezes, the SBCZ started to collapse and by 2400 hours under northerly gradient winds, the surface winds showed northerly to north-easterly winds over the region. Due to prevailing northerly/north-easterly winds, land breezes over the east coast either did not generate at all or were very weak.

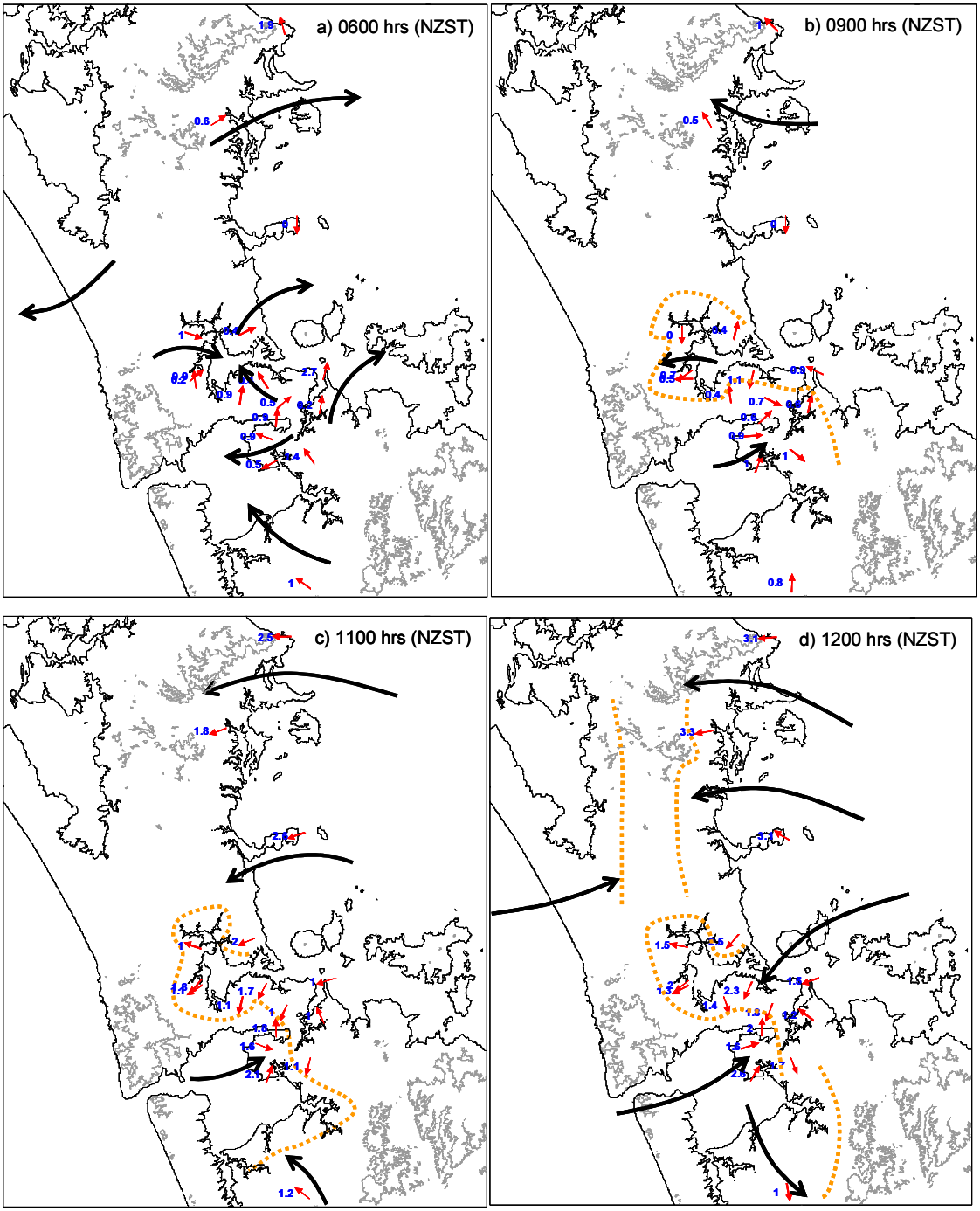

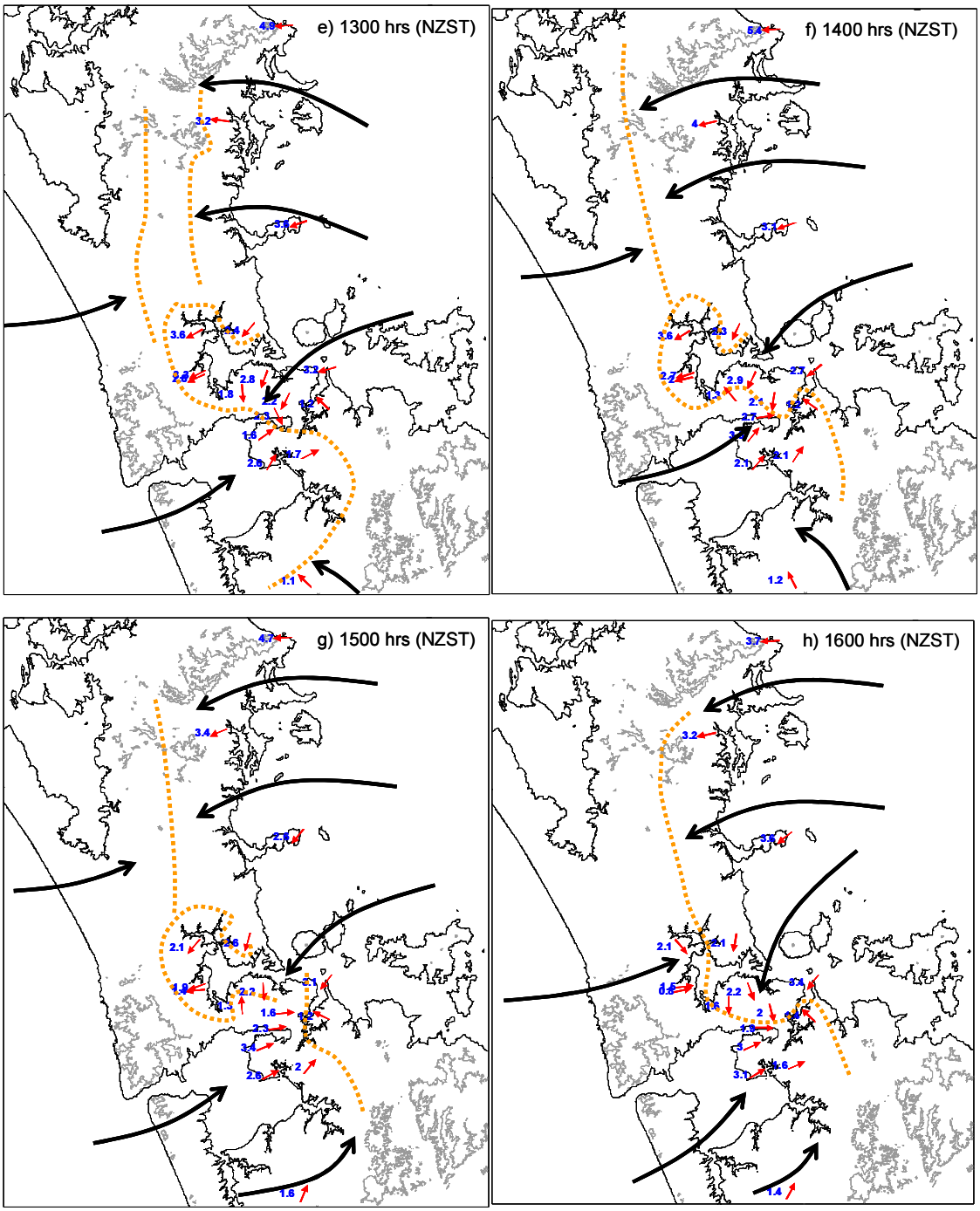
e) 1300 hrs (NZST)
f) 1400 hrs (NZST)
g) 1500 hrs (NZST)
h) 1600 hrs (NZST)

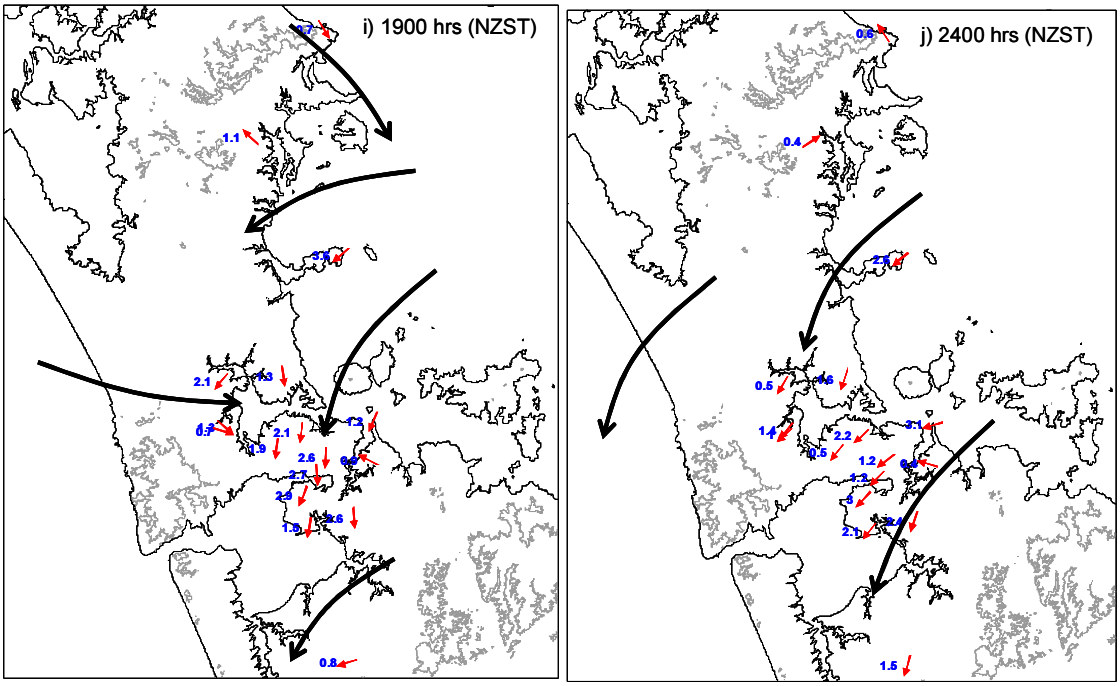


Figure 4.14: Surface wind field and sea breeze convergence zones from 0600 hours to 2400 hours on 18th March 2006. The red wind vectors show wind direction from individual stations, while the large black arrows indicate the average wind flow pattern over the area. The wind speed is given in blue colour.

### 4.5.7 Effect of Gradient Winds on the Sea Breeze Circulation

The sea breeze circulation cell is generally considered a closed system in which a shallow layer of marine air begins flowing towards the land, converging with the air mass over land and creating a region of upward vertical air currents. A seaward flow develops aloft above the upper boundary of the marine air, creating a shear zone where the flow changes direction from landward to seaward with descending air currents over the ocean, thus completing the circulation (Finkele 1995; Tijm et al. 1999). However, several authors (Banta et al. 1998; Estoque 1962) report either the complete absence of the return flow or its insufficiency at counterbalancing the low level onshore flow. The gradient winds play an important role in determining the shape and shore-relative location of the sea breeze circulation cell. Profiles of wind data on selected sea breeze days for eight dominant gradient wind directions (north, northeast, east, southeast, south, southwest, west and northwest) were obtained from Whenuapai station. Due to unavailability of even reasonably complete data for 1200 hours, it was decided to use 0900 hours vertical profiles of wind data. This means that only bay breezes would have been captured in the sounding.

Figure 4.15 shows south-easterlies to easterly near surface winds on at least five days. The strong easterly signal was due to bay breezes from Waitemata harbour or sea breezes from the east coast. The weak low level northwest wind on 19th November 2007 was more like a remnant of the land breeze. The near surface air temperature on this day at most of the stations was less than 17°C, which is almost the same as sea surface temperature for the month of November around this part of the North Island. The thermal gradient was not reversed and therefore the land breeze prolonged. On 19th Feb 2007, the low level south-westerlies under a southerly gradient flow showed a transition from a land to a slightly delayed sea breeze. The wind profile for the westerly gradient wind is an ideal example of the profound effect that a gradient wind can have over mesoscale winds. On 12th February 2006, the strong westerly gradient wind did not allow the onset of an easterly sea breeze at this station at any time of the day. Various studies (Finkele 1995; Mizuma 1995) have observed this particular characteristic of the sea breeze under relatively strong synoptic flow. The 7th February (southwest gradient wind) and 18th March (northwest gradient wind) fall under case 2 (see chapter 3 for detail) when gradient winds were opposite to the sea breeze inflow current. These types of sea breezes are preceded by calm conditions. The surface wind data from various stations over the east coast and close to Whenuapai show a very weak wind (<=1.0 m $s^{-1}$) in the early morning hours on 18th March 2006. However, on 7th February, the surface wind speed ranges between 1.0 to 3.0 m $s^{-1}$.

The depth of the south-easterly bay breeze varied but remained under 350 m above ground level. Except for 18th March 2006, the vertical wind vectors do not show any well developed return flow, although on most of the days a clear wind shear is visible above the shallow marine layer that indicates the top of the sea breeze gravity current and presence of the return flow. It is possible that in the morning hours the mesoscale pressure gradient was not strong enough to complete the circulation. The absence of a clear return flow with wind shear above the sea breeze flow also suggests a helical shape of the sea breeze circulation cell. However, observational data were not available to examine this aspect. On 18th March, the return flow merged with the gradient winds above the shallow marine layer of air. The estimated depth of the return flow above the sea breeze current is between 300 to 600 m.

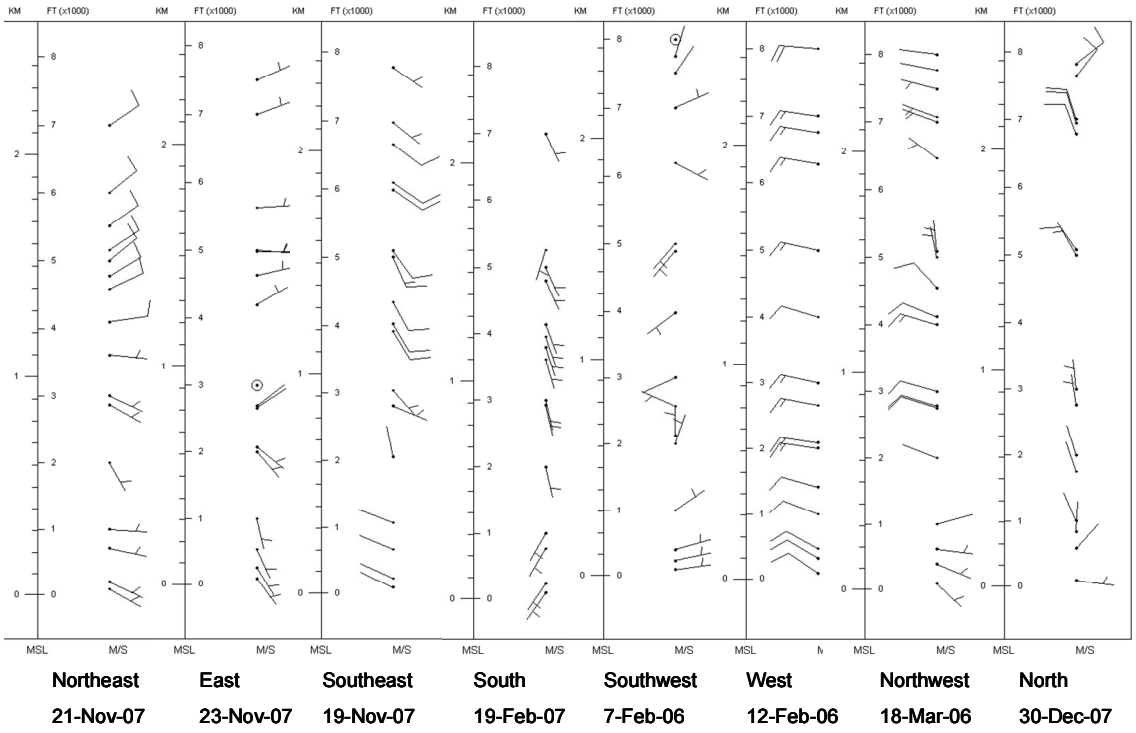


Figure 4.15: Vertical wind profiles of eight selected sea breeze days from Whenuapai station at 0900 hours. The wind arrow head points in the direction the wind is moving. A half barb represents a wind speed of 2 m $s^{-1}$ and a full barb represents 4 m $s^{-1}$. A circle + dot indicates calm condition (wind speed < 1 $ms^{-1}$).

## 4.6 Higher Pollution Levels on a Sea Breeze Day: A Case Study

### 4.6.1 The High $NO_x$ Concentration on 22nd March 2006

The aim of this case study is to examine any relationship between high pollution episodes and sea breeze events. The sea breeze day selected for this purpose is one of the high $NO_x$ pollution days in Auckland City, when $NO_x$ levels at some of the downtown area (e.g. Khyber Pass) exceeded National Environmental Standards throughout the day. Some other observational sites in Auckland City also observed high $NO_x$ levels. Figure 4.17 shows hourly $NO_x$ concentration at 8 sites on 22nd March 2006. The locations of the observational sites are indicated in Figure 4.16. By and large, the eight monitoring stations show a typical urban pattern of pollutant concentrations that is heavily affected by transport and industrial activities (Figure 4.17). During the morning and evening time the $NO_x$ concentrations were high due to peak hour traffic; between these two peaks and at night-time the concentrations were low. However, at least two stations (Khyber Pass and Queen Street) observed higher $NO_x$ concentrations during the day. At Queen Street, $NO_x$ concentrations exceeded 100 μg $m^{-3}$ at around

1200 hours, while at Khyber Pass $NO_x$ concentrations exceeded 400 μg $m^{-3}$ at around 1400 hours. The time series plot shows 3 distinct spatial patterns in the $NO_x$ concentrations. The first pattern shows very low $NO_x$ concentrations at three stations (Glen Eden, Kingsland and Musick Point). The second spatial pattern shows moderate $NO_x$ levels at four stations (Henderson, Penrose, Queen Street and Takapuna), although $NO_x$ concentrations were still less than the National Environmental Standards. The third pattern comprised of only one station (Khyber Pass) where NOx level exceeded the National Environmental Standards from morning (0700 hours) to almost midnight (2300 hours).

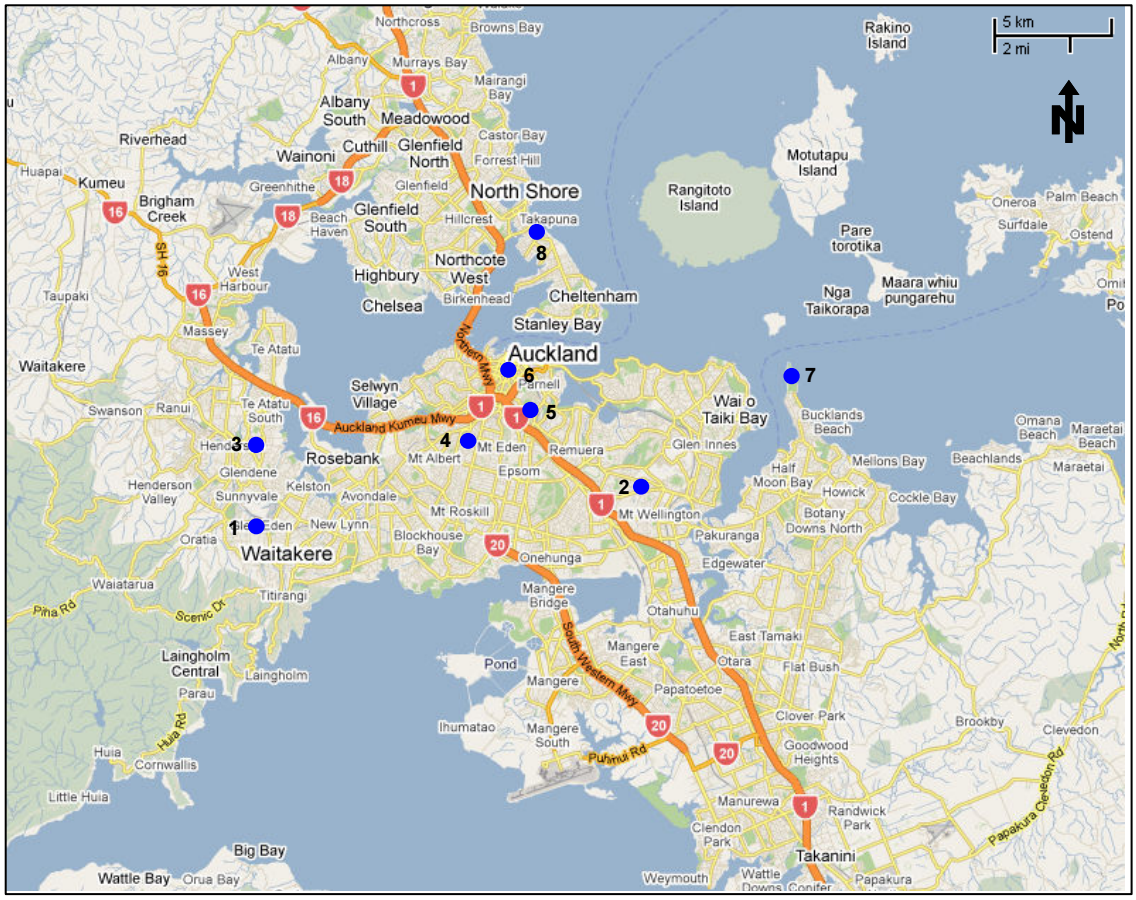


Figure 4.16: Map of selected Auckland region with eight locations of eight pollution monitoring sites used in the case study, these are 1: Glen Eden, 2: Penrose, 3: Henderson (Lincoln Road), 4: Kingsland, 5: Khyber Pass, 6: Queen Street, 7: Musick Point, 8: Takapuna. The map used in this figure is extracted from Google Maps.

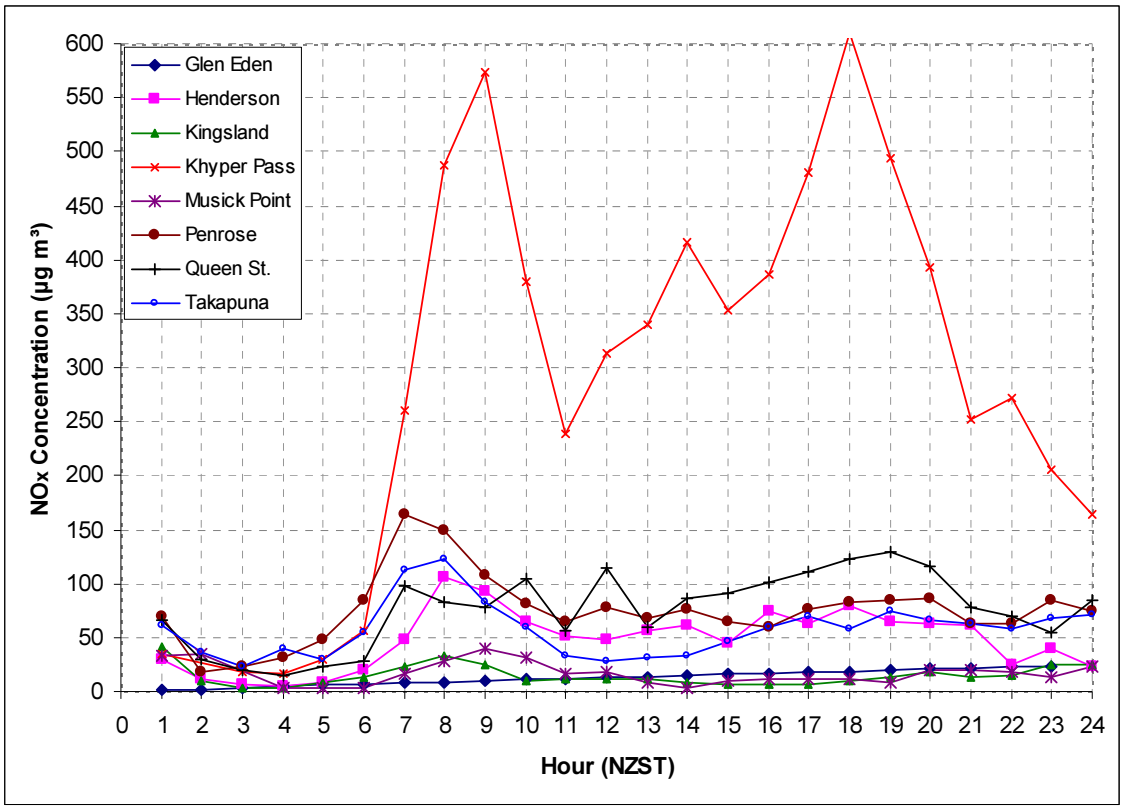


Figure 4.17: Hourly $NO_x$ concentration at 8 stations in the Auckland City area on 22nd March 2006.

Surface winds, and temperature data from more than 25 observational sites within and around Auckland, and vertical profiles of temperature and wind from Whenuapai and Auckland Airport have been utilized to examine the high pollution event on 22nd March 2006. The geopotential height charts for 850 hPa shows that on 22nd March 2006, New Zealand was surrounded by two higher pressure systems and two low pressure systems creating a 'col' like synoptic conditions over New Zealand (Figure 4.18a). The high pressure systems were to the west and east of New Zealand, while low pressure systems were sitting to the north and south of the country. A low pressure trough from the north was extended to the south over the North Island, giving weak south-east gradient flow over the Auckland region during day time (Figure 4.18a). However, the sounding data from Whenuapai at 1200 hours shows north-easterly gradient flow over the region, although the prevailing winds near surface (1000 hPa) were south-easterlies in both NCEP data and sounding data from Whenuapai. The difference in wind direction at 850 hPa is probably due to doming of boundary layer over urban Auckland at midday.

During the afternoon hours, a broad band of stratocumulus was oriented in a north-south direction over the land during day time between 1200 hours to 1500 hours (Figure 18b). Another small band of scattered stratocumulus was centred to the north of Kaipara Harbour in the middle of the land mass.

The average sea surface temperature during March in this region is around 19.0°C. The near surface air temperature exceeded 22°C over most of the stations on the same afternoon. Considering the fact that the temperature probes are giving screen temperature at around 2 m above ground, it is expected that the land surface temperature would be higher than near-surface temperature. The temperature gradient between land and sea was therefore enough to produce a thermally forced circulation.

**a) Geopotential height at 850 hPa, 22-Mar 2006**

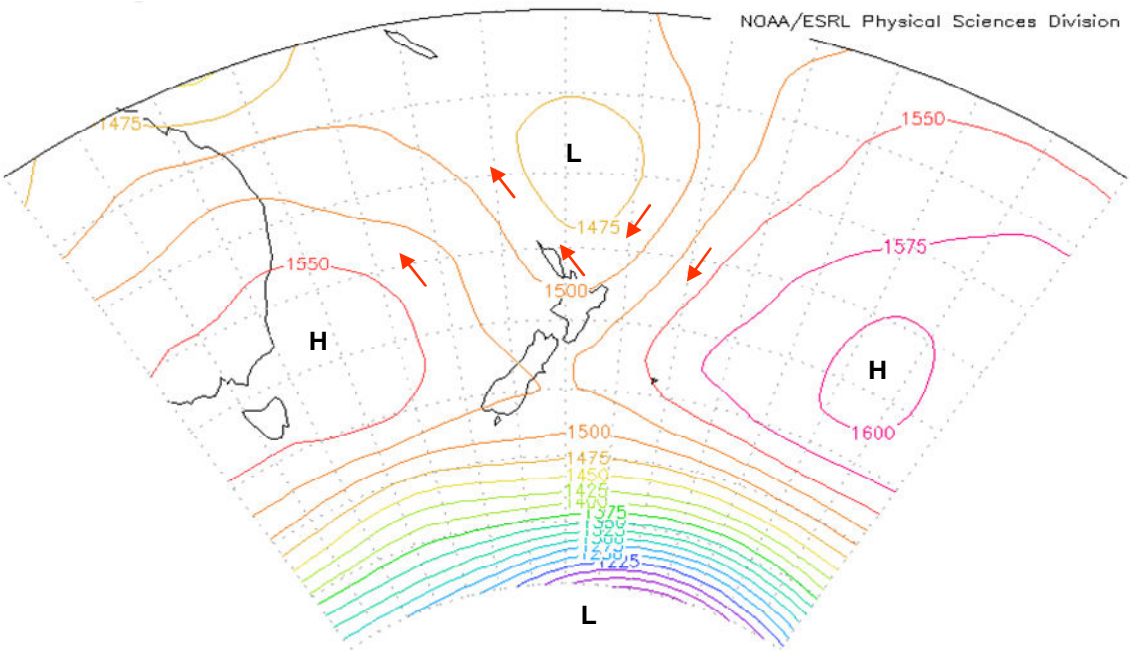

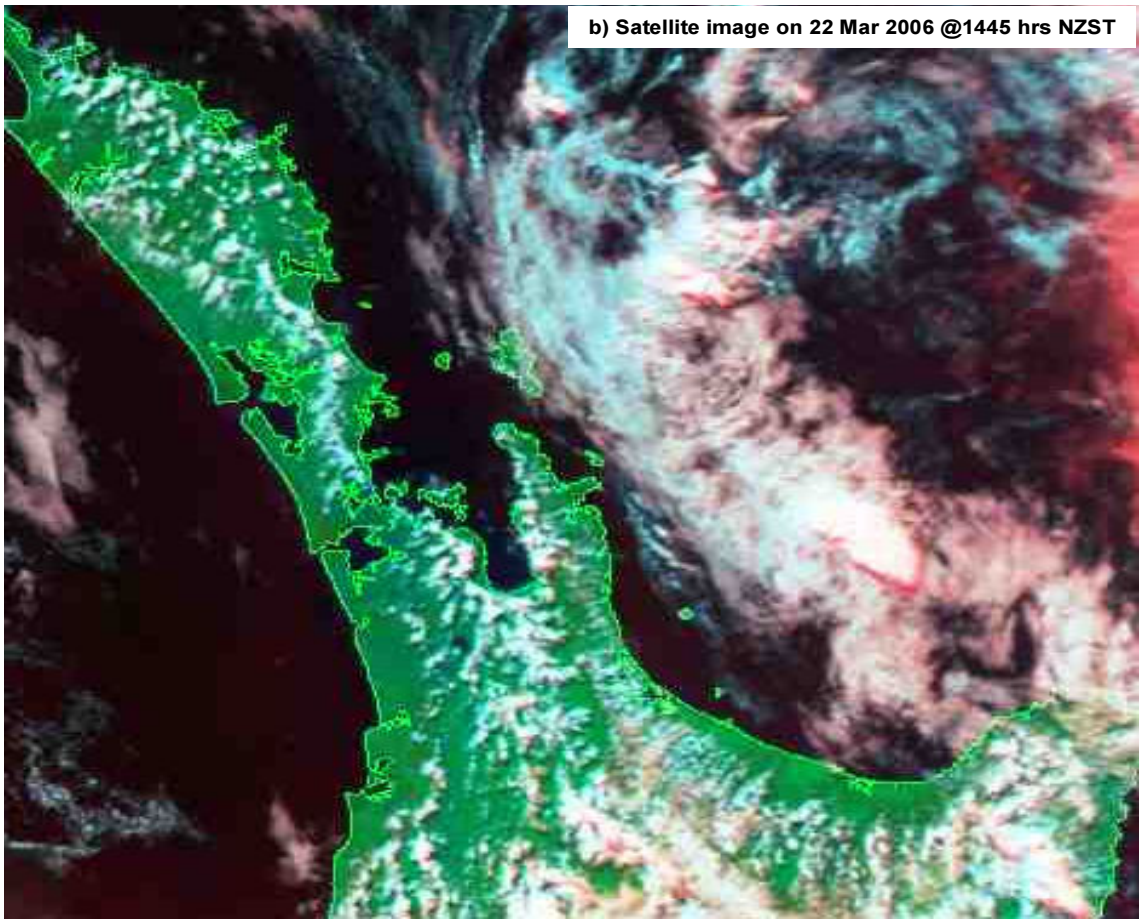


Figure 4.18: Synoptic situation over North Island on 22nd March 2006. a) NCEP reanalysis average geopotential height at 850 hPa; red arrows show the synoptic wind direction (NOAA Research 2009), and b) NOAA AVHRR satellite image for 22nd March 2006 at 1445 NZST (Landcare Research 2009).

### 4.6.2 Surface Wind Analysis

In the early morning hours, except for Musick Point, a weak land breeze was observed over both coasts, and along Waitemata and Manukau harbours. The bay breeze started at around 0700 hours. During morning hours, the southerly component of the surface wind was strong. These relatively strong surface winds were probably the result of prevailing winds, coupled with south-easterly bay breezes from the Waitemata Harbour. However, with the onset of mature sea breezes from the Hauraki Gulf and Tasman Sea (after 1100 hours), the effect gradient wind veering appears to be reduced due to the increased local thermally-induced pressure gradient. Although the sea breeze occurred on both sides of the isthmus, the westerly sea breeze was much stronger than its easterly counterpart. Analysis of the data from more than 25 stations suggests that the convergence zones started forming after 0900 hours, mostly along the land-sea

interfaces. By noon, the convergence line ran through the middle of Auckland City. Later in the day, strong westerly sea breezes pushed the sea breeze convergence zone further north-east to the Hauraki Gulf. The cumulus cloud line (Figure 4.18b) that formed due to uplift of the air mass due convergence over the Auckland region indicates this eastward placement of the SBCZ.

### 4.6.3 Daytime Vertical Profile on 22nd March 2006

Vertical profiles of wind, temperature and moisture from Whenuapai and Auckland Airport stations for 1200 hours show the vertical structure of the sea breezes at noon (Figure 4.19). Both stations show an onshore gravity current up to a depth of at least 300 m. At Whenuapai the direction of sea breezes was south-easterly, indicating bay breeze from Waitemata Harbour. Due to easterly gradient winds, a return flow did not generate. At Auckland Airport, which is to the west side of the Auckland isthmus, the direction of the gradient winds and return flow were the same, so that it was difficult to identify the depth of the return flow. However, an Ekman spiral is evident in the vertical wind profile at both stations. The temperature profiles from Auckland Airport and Whenuapai stations also vary significantly. Being away from large water bodies, the near-surface temperature at Whenuapai was higher than Auckland Airport. A super-adiabatic layer formed in the first 70 m AGL, and the atmosphere above the unstable layer was near neutral up to the height of around 1000 m where the mixed neutral layer was capped by a 500 m deep statically stable layer. This would have encouraged thermal convection in the mixed layer. Vertical mixing and uplift of moist air formed cumulus clouds at around 1000 m AGL. The sounding data for afternoon hours was not available, and therefore arrival of sea breeze inflow cannot be detected, however, the 1445 hours satellite image (Figure 4.18) shows a band of cloud passing over Whenuapai that resulted from the convergence between east and west coast sea breezes. At Auckland Airport, the atmosphere was more stable. Considering the atmospheric boundary layer structure at Whenuapai and Auckland Airport, the potential for recirculation of pollutants does exist. The uplifted air mass that moved to the west with the gradient winds might have descended close to the shore and thus become part of the onshore flow again. Any pollutant species that would be trapped in the convergence zone or moved aloft with the updraft may also become part of the return flow and thus recirculate in the sea breeze cell.

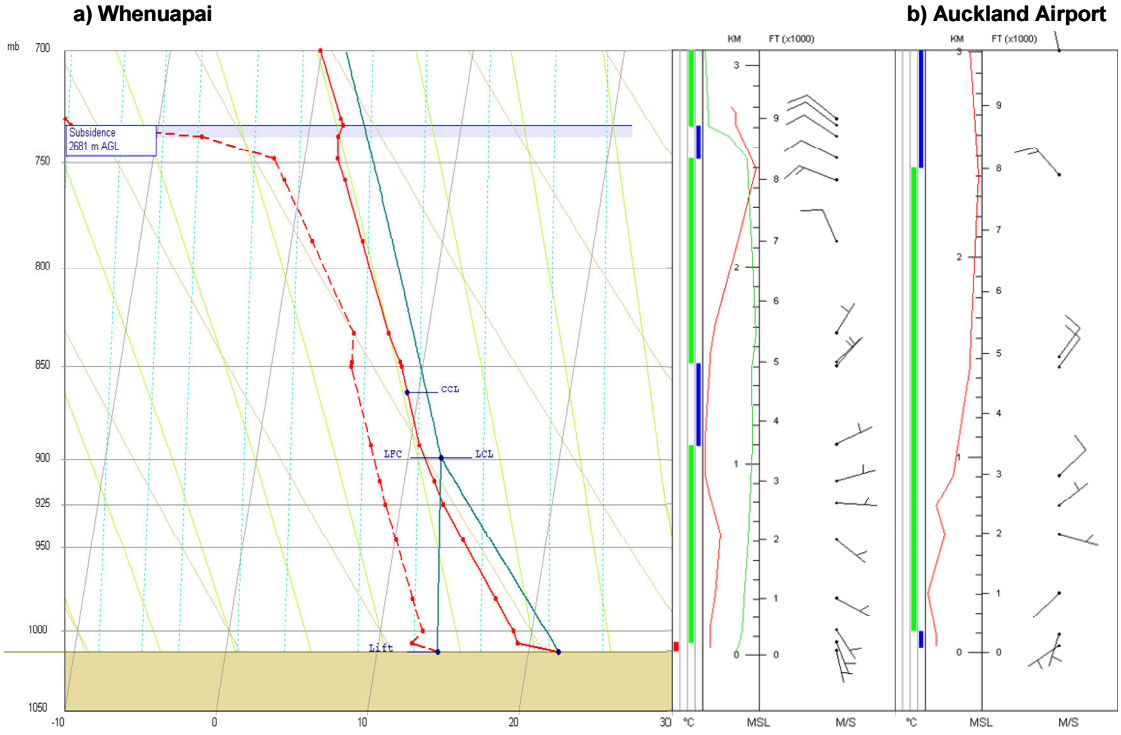


Figure 4.19: Skew-T plot of 22nd March 2006 at 1200 hours for a) Whenuapai, and b) stability bars and horizontal wind for Auckland Airport. Wind barbs represent wind speed and direction. The rounded head points in the direction of the wind while barbs represent the wind magnitude. Half barb represents 2 m $s^{-1}$ and full barb represent 4 m $s^{-1}$. The wind vector without barb indicates wind speed less than or up to 1 m $s^{-1}$. In the stability bar, a red bar indicates super adiabatic layer, green indicates conditional instability, and blue represents stable conditions. In the stability bar area, the red line represents wind speed and green line indicates relative humidity. In the thermodynamic profile, the dotted red line represents dew point temperature and the red solid line shows air temperature.

### 4.6.4 Spatial and Temporal Variations in $NO_x$ Concentration on 22nd March 2006

The surface wind field from more than 25 stations and $NO_x$ concentrations from 8 stations have been plotted over the Auckland domain to examine the spatial and temporal variations in $NO_x$ concentration from morning to evening on 22nd March 2006 (Figure 4.20). The spatial pattern of high $NO_x$ levels is very similar to the average spatial pattern of 58 sea breeze days. In the early morning hours (0600 hours) all 8 stations showed very low $NO_x$ concentration (Figure 4.20). After 0700 hours, with increased emissions from the morning traffic rush hour, $NO_x$ started building up. The south-easterly and southerly winds that carried pollutants from south of Auckland rapidly increased the pollutant concentration at Penrose, Khyber Pass, Queen Street, Takapuna and Henderson (see Figure 4.16 for site locations). Takapuna observed relatively high $NO_x$ concentrations during southerly or south-westerly flow, while

during easterly sea breezes the $NO_x$ concentrations were very low, which was presumably due to clean marine air advection from Hauraki Gulf. The Henderson station also observed higher $NO_x$ concentrations during southerly or northerly wind conditions because the urban and industrial areas are to the south and north of the station. However, during westerly winds the $NO_x$ concentration, at Henderson station were low because of less urbanized areas to the west of the Henderson station. In the evening hours the $NO_x$ levels again peaked at Khyber Pass, Queen Street, Henderson, Penrose and Takapuna (Figure 4.20f). However, except for Khyber Pass and Queen Street the $NO_x$ concentrations over the rest of the stations were lower in the evening than morning, which was due to higher wind speeds in the evening hours. The $NO_x$ concentrations in the evening hours at the two downtown stations of Khyber Pass and Queen Street were slightly higher than the morning peak, which was probably due to street canyon effects.

An important feature of $NO_x$ spatial distribution is the large difference in $NO_x$ concentration between the three central city monitoring stations. Khyber Pass observed the highest $NO_x$ concentration, although the Queen Street station which is also located in the downtown and appears to be exposed to similar traffic volume, observed almost half of the Khyber Pass $NO_x$ concentrations. The concentration of $NO_x$ at Kingsland was less than 40 $\mu g\ m^{-3}$ throughout the day. Kingsland station was located in the centre city, although slightly away from the high traffic volume of Queen Street and Khyber Pass, but it was still in close vicinity of some major roads.

The role of sea breeze dynamics in high $NO_x$ concentrations, especially in the afternoon hours, is not clear. Unfortunately, appropriate data are not available to investigate these aspects in detail. However, analysis of meteorological fields indicates an indirect effect of the sea breeze on higher $NO_x$ concentrations. For example, the data analysis of 58 sea breeze days suggests a stronger southerly surface wind component that is probably the result of convergence of bay and mature sea breezes under the high frequency southerly gradient winds. Another indirect control is the relatively low wind speed on sea breeze days that inhibited dispersion and dilution of the pollutant.

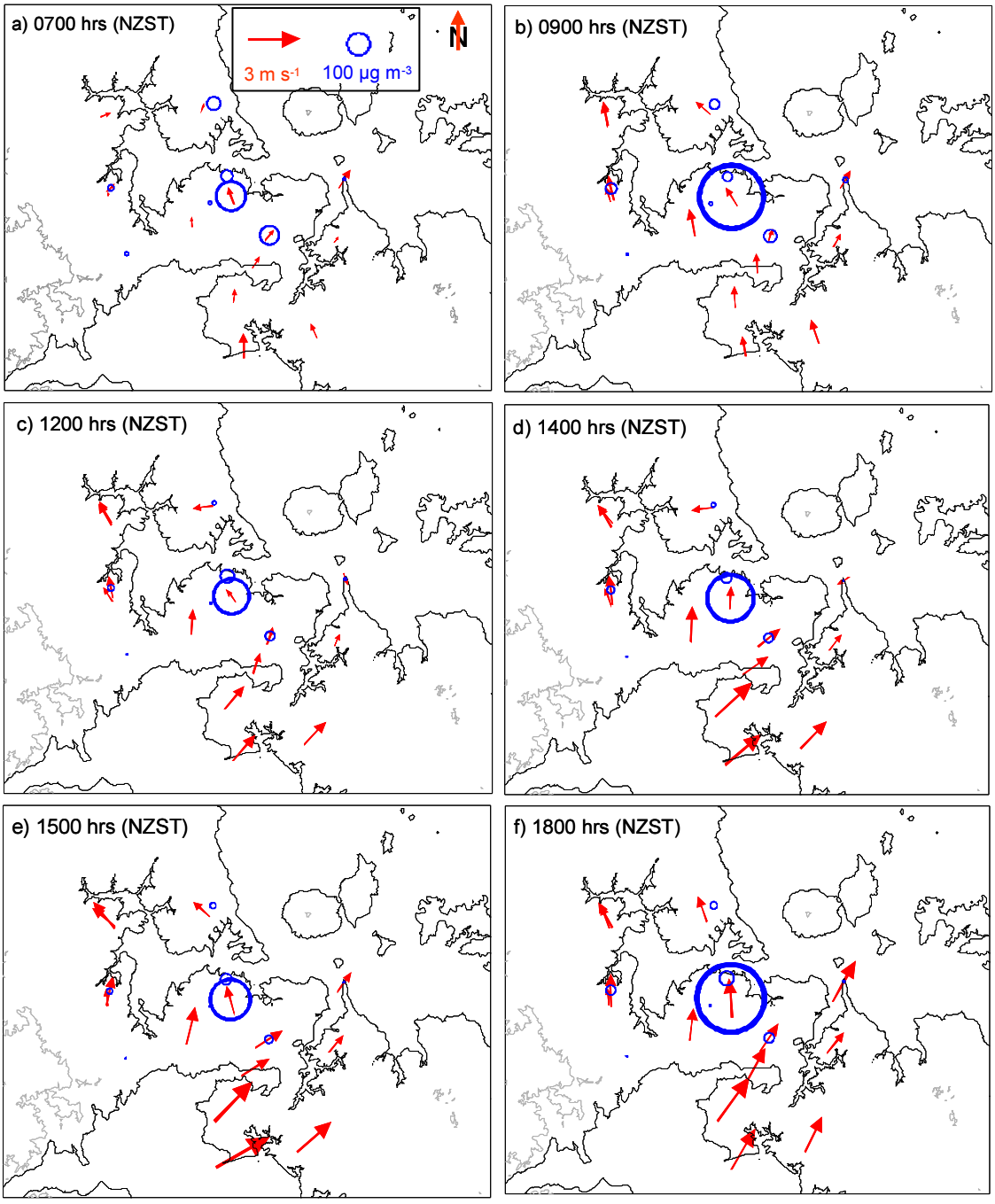


Figure 4.20: Wind field and $NO_x$ concentrations at a) 0400 hours, b) 0800 hours c) 0900 hours d) 1200 hours e) 1500 hours f) 1800 hours on 22nd March 2006. Wind vectors show the wind direction, while size of the arrow is proportional to the wind speed. The blue circles represent $NO_x$ concentration in µg m³. The size of the circle is proportional to the magnitude of the pollutant.

The convective internal boundary layer is a prominent feature of a sea breeze circulation and plays an important role in fumigation and inhibition of pollutant dispersion. The data analysis in previous sections suggests that the CIBL is generally formed after 1200 hours. If the notion of afternoon CIBL is correct then peaks in $NO_x$

concentration at Queen Street and Khyber Pass can be attributed to the formation of a CIBL. The sea breeze convergence zones (SBCZs) occur frequently during the summer period over Auckland. Ridley (1995) used a Lagrangian particle model to study pollution dispersion in SBCZs in the Auckland region. His results suggest that SBCZs limit the exchange of air between opposing circulations, while providing means of elevating near-surface pollution levels. The sea breeze convergence zones are also known for the same day and next day recirculation of pollutants. Authors in other parts of the world (Azorin-Molina et al. 2009; Liu & Chan 2002a) also linked elevated pollutant levels with convergence zones. When a sea breeze occurs on both side of the peninsula, such as 22$^{nd}$ March 2006, the SBCZ generally runs through the middle of Auckland City. Considering Ridley's findings, the higher $NO_x$ concentration can be explained in terms of inhibition of dispersion of the pollutant.

## 4.7 Summary of Results

The objective of this observational data analysis was to understand the structure and dynamics of sea breezes in the Auckland region. The interaction of sea breezes with gradient winds and their potential effect on the air quality of the region was also investigated. The summer months' data from November to March for the years 2006 and 2007 were obtained and analysed. The filter designed for identification of sea breezes extracted 20% of the total days as days when sea breezes occurred on both sides of the peninsula. The frequency of sea breezes in the two years of summer data was the highest in February and the lowest in November and December. Summary of the findings is given below:

- Westerly and south-westerly winds accounted for 46% of the total summer period, while north-easterlies accounted for 28% of the summer time. The wind direction for rest of the period was either southerly (SE & S) or northerly (NW & N).

- Near-surface wind speed during sea breeze days is much lower than wind speed on non-sea breeze days. During non-sea breeze days, average wind speed over the west coast was 5.7 m s$^{-1}$, while over the east coast stations it was 4.7 m s$^{-1}$. On sea breeze days, average wind speed over west coast stations reduced to 3.2

m $s^{-1}$, while on the east coast it was only 2.5 m $s^{-1}$. Auckland received 18% more solar radiation and the daytime average temperature at six coastal stations was also 8% (1.5°C) higher on sea breeze days.

- Bay breezes from small bodies of water, such as Waitemata Harbour and Manukau Harbour, blew from 0800 to 1100 hours, while mature sea breezes from the main bodies of water (Hauraki Gulf and Tasman Sea) overwhelmed the region from 1200 hours to late evening.

- Arrival of mature sea breeze fronts from either coast is marked by a temperature drop of up to 2.0$^{o}$C. However, there was no significant difference in moisture content, which is probably due to the overall maritime environment of the Auckland region.

- The strength and inland penetration of the sea breeze front was affected by the gradient wind flow, and the strength of the thermal gradient between land and sea. Topography also plays an important role, although with the available observational data it cannot be examined quantitatively. Consistently higher wind speeds at Auckland Airport and Mangere stations could be due to the topographic setting of Manukau Harbour and Manukau Head. Modelling techniques could be helpful in determining the topographic effect on the local meteorology.

- Most of the sea breeze days occur during weak (<=6 m $s^{-1}$) southerly or northerly gradient winds that are sub-parallel to the north-south oriented land mass. This is reasonable as during southerly or northerly gradient winds, simultaneous occurrence of sea breezes over east and west coasts is more likely due to reduced synoptic forcing over either coast.

- The gradient winds augment the local winds if both are in the same direction and weaken them if both are in opposite directions. The effect of south-easterly and north-westerly gradient winds on the sea breeze is not clear. Theoretically, north-westerly winds should enhance the easterly sea breeze and south-easterly

gradient winds should augment westerly sea breezes, but the contour plots showed the opposite behaviour.

- Over the diurnal cycle, sea breezes should rotate anticlockwise over both east and west coasts. However, the diurnal oscillation of the sea breeze was modified due to topography and synoptic wind forcing. The east coast stations show leftward rotation, while over the west coast the diurnal rotation of sea breezes could not be clearly identified. The rate of rotation of the sea-land breeze is also significantly affected by the gradient wind direction. Surface and gradient winds from the same direction slowed down the rotation rate, while a gradient wind opposite to the surface wind flow enhanced the rotation rate of the sea or land breeze.

- The mixed layer height before arrival of the mature sea breeze reached up to 1500 m. The sea breeze front generally reached at Whenuapai in the afternoon hours. In an isolated event the sea breeze front arrived earlier around 1200 hours. After arrival of the sea breeze front a CIBL of around 400 m deep was formed in the surface layer. The role of the convective internal boundary layer in trapping the pollutants close to the surface on sea breeze days could only be partly analysed on a case study basis. The spatial and temporal evolution of the CIBL and the extent of its effect could not be grasped in sufficient detail due to low vertical, temporal and spatial resolution of data. The case study of a typical sea breeze day suggests higher $NO_x$ concentrations during day time. However, due to unavailability of appropriate data, the contribution of the CIBL in increasing $NO_x$ levels could not be examined.

- The sea breeze convergence zone (SBCZ) started forming after 0900 hours, strengthened (with presumably higher vertical velocity) in the afternoon, and started to collapse after 1700 hours. The location and strength of sea breeze convergence zones (SBCZ) were affected by the gradient wind direction and surface characteristics (water bodies, higher terrain, etc.). The role of SBCZs in the air quality of the Auckland could not be quantitatively assessed due to unavailability of appropriate data.

- Wind speed and wind direction are important controls with regard to pollution dispersion in the Auckland region. Relatively low wind speed during a sea breeze episode (that may also be the result of a SBCZ) and upwind pollution sources potentially increase pollutant concentration in a particular area.

- The frequency, strength, and structure of sea breezes under different gradient wind conditions (especially northwest and southeast gradient winds) needs more detailed analysis with reliable and high resolution data, as well as using higher resolution modelling techniques. The pollutant recirculation mechanism, structure of the CIBL and sea breeze convergence zones are some important areas that require attention due to their importance with regard to pollution dispersion mechanisms in the region. For this purpose, three dimensional high resolution modelling would be worthwhile, so that mixing, entrainment and recirculation of pollutant could be better understood in a sea breeze system. The following Chapter-5, addresses these issues by employing high resolution numerical modelling techniques.

# 5. Numerical Modelling of Sea Breeze and its Effect on Pollutant Distribution in the Auckland Region

## 5.1 Introduction

The sea breeze circulation is a mesoscale phenomenon that has been extensively investigated in observational, experimental, theoretical and numerical modelling studies around the world (Atkinson 1981; Clappier et al. 2000; Kitada & Kitagawa 1990; Lu & Turco 1994; Millan et al. 2002; Simpson 1994; Zhong & Takle 1992; Zhong & Takle 1993). Nevertheless, it still fascinates researchers due to its direct impact on human life in terms of air pollution, precipitation and overall quality of life. Sea breezes are a common feature of summertime meteorology of the Auckland region (McGill 1987). Most of the observational and modelling efforts to investigate the sea breeze in the Auckland region were motivated by the important role of this mesoscale circulation in convective precipitation, and pollutant transport and dispersion (Haigh 1992; McGill 1987; McKendry 1989, 1992; Ridley 1993; Ridley 1995; Sutton 1996). However, these efforts have been hampered by the sparseness of the observational network, quality of observations, and limitations of the modelling tools. Previous studies used a variety of numerical models to investigate the sea breeze and pollution dispersion in the Auckland region, ranging from very simple box models (Wratt et al. 1990) to the mesoscale hydrostatic Colorado State University (CSU) model, and more complex Eulerian models (Sutton 1996). According to the author's knowledge, Sutton (1996) for the first time employed a non-hydrostatic Eulerian based meteorological

model (Regional Atmospheric Modelling System – 'RAMS'), to model sea breezes and pollutant dispersion. However, low resolution and errors in the RAMS code hampered confidence in the model results. Later on, Gimson (2005) employed two Eulerian models namely 'The Air Pollution Model' (TAPM), and 'California Photochemical Grid Model' (CALGRID), to investigate local flows such as the sea breeze and cold air drainage and their role in the air quality of the Auckland region. Results of Gimson's study suggest that the sea breeze convergence zone in Auckland coincides with periods of elevated ozone ($O_3$) and peaks in nitrogen dioxide ($NO_2$). However, given the coastal environment of the Auckland region and the direct impact of thermally forced flows on the most populated area of the country, a detailed investigation of the sea-land circulations and their direct and indirect effects on the air quality and local weather has not been conducted. Previous work on the sea breeze and pollutant dispersion suggests application of mesoscale, non-hydrostatic models with improved PBL and land surface parameterization. For pollution dispersion, Lagrangian and/or Eulerian approaches were recommended instead of the Gaussian or box model approach (McKendry 1989; Sutton 1996).

The main advantage of numerical modelling is its ability to simulate the atmospheric cube in four dimensions of time and space that helps investigating the three dimensional structure of the atmosphere over time, and multiple influences and interactions of the desired phenomenon with the environment. Unlike observed data, numerical modelling provides a powerful tool to estimate the meteorology and pollutant dispersion over a wide area rather than only a few points, as well as identification of the pollutant transport pathways and areas of high pollutant concentration. Nevertheless, satisfactory results cannot be achieved unless the model is able to simulate the major characteristics of the sea-land breeze phenomenon accurately. A fair agreement between modelled and observed meteorological variables is therefore crucial for both meteorological variables and pollutant dispersion mechanisms. It is therefore important that numerical models be properly evaluated with observational data before their predictions can be used with confidence (Chang & Hanna 2004). Model performance evaluation is the process of establishing the accuracy, precision and uncertainty of model simulations of the physical and chemical processes occurring in the atmosphere (ASTM Standards 2005; Chang & Hanna 2004).

Numerical modelling literature describes a variety of different statistical methods for the purpose of model evaluation. Commonly used statistical methods include estimation of bias (B), fractional bias (FB), normalized mean square error (NMSE), root mean square error (RMSE), systematic root mean square error (RMSEs), unsystematic root mean squared error (RMSEu), difference measures, correlation and fraction of data within a factor of two, mean absolute error, Pearson's correlation coefficient (r ), coefficient of determination ($r^2$) and index of agreement (IOA) (ASTM Standards 2005; Barratt 2001; Hirdman 2006; Willmott 1981).

In this chapter, two mesoscale models, the Advanced Research WRF (ARW), and TAPM, have been used to simulate the meteorology and predict pollutant dispersion over the Auckland area. WRF offers a number of options for characterizing effects of turbulence, land surface, radiation and convection parameterization. The planetary boundary layer (PBL) and land surface (LSM) parameterizations directly influence the radiation budget, diurnal cycle of near-surface air temperature, wind speed, vertical temperature gradient, temperature inversion and PBL height. Therefore, the choice of the PBL and LSM parameterization is important for both mesoscale meteorological processes and air quality modelling (Miao et al. 2006b). Results of sensitivity studies of various PBL and LSMs varies significantly. For example, Miao et al. (2006a; 2006b) concluded that sea breeze characteristics such as inland penetration and updraft and downdraft velocity are sensitive to PBL and LSMs and use of more complicated parameterization does not necessarily ensure good results. Challa et al. (2008) modelled sea breezes over the Mississippi Gulf coast to investigate the sensitivity of the mesoscale circulation to two very commonly used (especially for air quality applications), PBL schemes: the Younsei University (YSU) Scheme (which is the next generation of the MRF PBL) and the Mellor-Yamada-Janjic (Eta) Scheme. Challa et al. (2008), found that while diurnal variation in the surface wind direction was better represented by the MYJ PBL scheme, the CIBL growth across the coast was well produced by YSU parameterization. Contrary to this, Zhong et al. (2007), in their coastal environment study reported that Eta (MYJ) PBL scheme, combined with the Noah LSM and RRTM long-wave radiation scheme performed better than the MRF (YSU) scheme. For this research two PBL schemes and two LSMs were tested. A total of four simulations with different combinations of land surface and planetary boundary

layer parameterizations were run to assess the sensitivity of the mesoscale circulation to different PBL and land surface schemes (Table 5.1). The model was integrated for a period of 8 days from 18th March 25th March 2006. The choice of simulation period was based on the availability of surface and sounding data and occurrence of more than two consecutive sea breeze days. Performance evaluation of the four simulations suggested that the combination of the MYJ PBL scheme with the Noah LSM, and RRTM scheme for long-wave and Dudhia scheme for shortwave radiation better simulated the sea breeze characteristics. This is in agreement with the results of Zhong et al. (2007). Since the primary objective of this thesis is to investigate the sea breeze circulation about Auckland and its potential impact on the air quality of the region, the sensitivity analysis is outside the scope of this thesis and results of only one simulation (101cg) are presented. This simulation more accurately predicted the wind field and the thermodynamic structure of the atmosphere. However, the comparison statistics of near-surface meteorological variables for all the four simulations have been provided as Appendix 5A. Due to resource constraints, the atmospheric chemistry module of WRF (WRF-Chem) could not be employed for the purpose of pollutant dispersion. However, it was important to examine pollutant behaviour during sea breezes events, so that, as an alternative, a mesoscale pollution dispersion model TAPM was employed to conduct pollutant dispersion modelling.

## 5.2 Model Setup and Initialization

### 5.2.1 The Advanced Research WRF (ARW)

The Advanced Research WRF (ARW) modelling system is a next-generation mesoscale numerical weather prediction system developed by the National Center for Atmospheric Research (NCAR). WRF (ARW) is designed to serve both operational forecasting and atmospheric research needs (National Center for Atmospheric Research-USA 2008). As a state-of-the-art numerical modelling system, WRF is used for several research applications, such as operational weather forecasting, regional climate prediction, physics and parameterization research, atmospheric and ocean coupling, idealized and dynamical studies, air quality modelling and data assimilation (Challa et al. 2008; Michalakes et al. 2006). The WRF model is intended to be used for

a broad spectrum of applications across scales ranging from metres to thousands of kilometres (Developmental Testbed Center 2006).

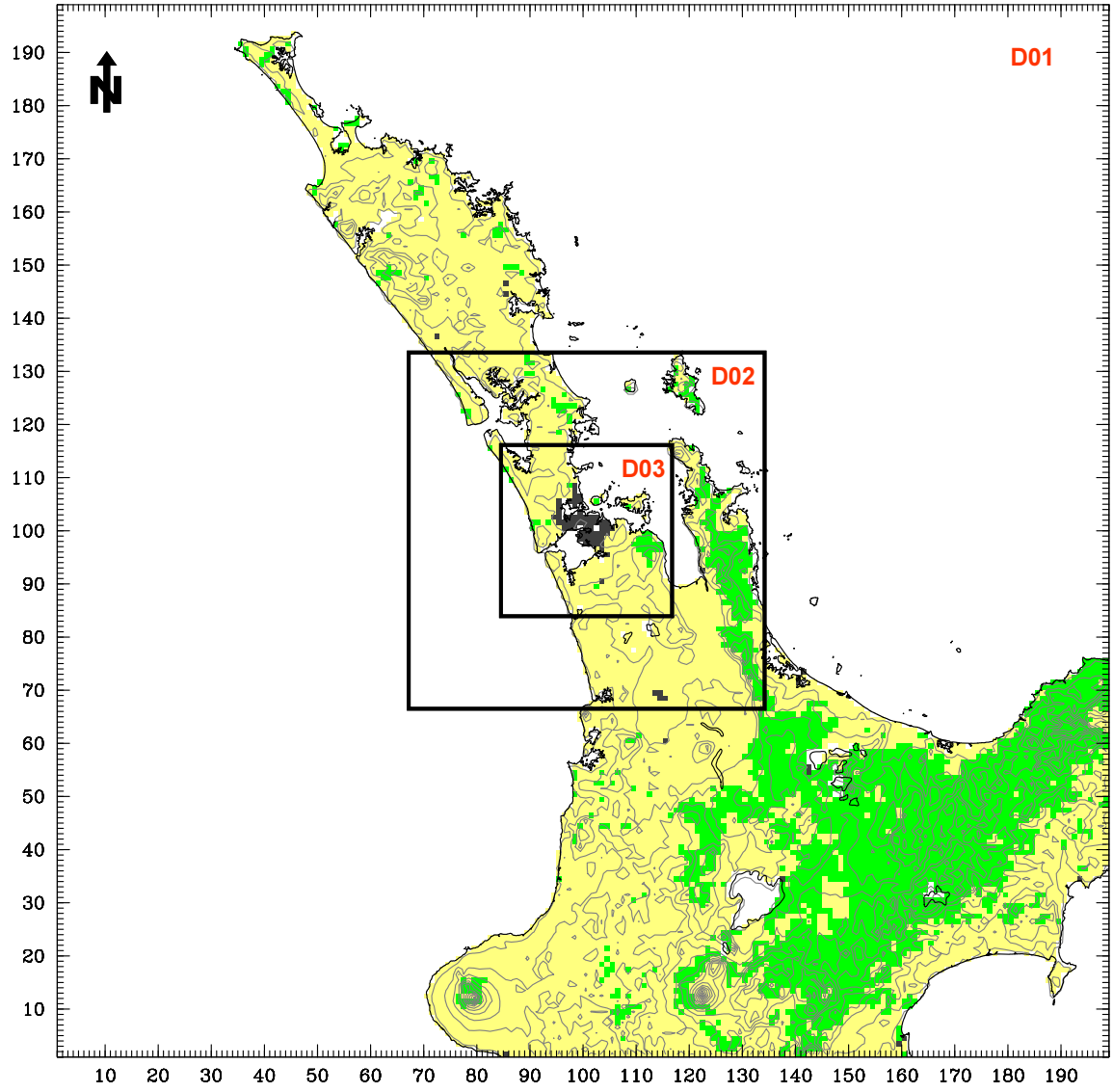


Figure 5.1: Grid configuration of WRF (ARW) simulations. Outer coarser domains D01 and D02 have resolutions of 3000 m and 1000 m, respectively, and the grid resolution of the innermost finer domain D03 is 500 m. The number of grid points in D01 and D02 are 199 x 199 each, while in the finer domain D03, the number of grid point are 197 x 197. The gray contour lines indicates topography and colour shading shows general land use characteristics of the North Island.
* White: Water; Dark gray: Urban built environment; Yellow: Pasture, cropland, grassland; Green: A mix of shrub land, grassland and mixed forest.

The model consists of fully compressible Euler non-hydrostatic equations. The prognostic variables include three-dimensional (u,v,w) wind; perturbation quantities of potential temperature, geopotential, surface pressure, turbulent kinetic energy, and scalars such as water vapour mixing ratio, cloud water, chemical species, etc. The model utilizes a terrain- following vertical coordinate (eta coordinate) system, with

Arakawa C-grid staggering used in the horizontal grid. A 2nd or 3rd order Runge-Kutta time integration is used. WRF model has several options for spatial discretization, diffusion, nesting, nudging, lateral boundary conditions, physics parameterization and map projections (Shamarock et al. 2008a).

### 5.2.2 The WRF Model Setup

The accuracy of simulating boundary layer characteristics heavily depend on representing terrain features and surface characteristics accurately. Recent studies for example Berg & Zhong (2005) and Zhong & Fast (2003) have used much finer spatial resolutions to resolve terrain and land use variations that reproduced large spatial variations in the surface winds more correctly. Given the complex coastline with a narrow landmass and rolling hill terrain, a complex sea breeze circulation was expected over the Auckland Region. These very local scale sea breeze features essentially require a very fine spatial grid resolution. Therefore, the model was setup with three nested domains namely D01, D02 and D03, with horizontal grid resolutions of 3.0, 1.0 and 0.5 km respectively (Figure 5.1). The grid ratio between D01 and D02 was 3:1, while between D02 and D03 was 2:1. The three domains consist of 199x199, 199x199 and 197x197 horizontal grid points (N-S by E-W direction), respectively. The first domain D01, covers almost the entire North Island from Wanganui in the south to the tip of the Northland in the north. The second domain (D02) covers an area from Hamilton in the south to Kaipara Harbour in the north, and also includes Coromandel Peninsula, Great Barrier Island, etc. The third domain (D03) is the area of interest and covers most of the Auckland region, including both Waitemata and Manukau Harbours. All domains have 51 vertical levels. Table 5.1 shows the PBL and land surface parameterizations used in the four simulations. The rest of the physics and dynamics options were kept constant in these simulations. Details of the parameterization schemes and dynamics options used in the four simulations are provided as Appendix 5B.

The initial and lateral boundary conditions used for all simulations were taken from the NCEP re-analysis archive data with a spatial resolution of 1° x 1° and temporal resolution of 6 hours. Topography data were used at 500 m resolution to define the lower boundary conditions. The terrain, land use and vegetation data at 30 second

spatial resolution were provided by Land Information New Zealand (LINZ) and Terralink New Zealand derived from a 25 m New Zealand digital elevation model. The simulations were conducted for eight days from 0000 NZST 18th March 2006 to 0000 NZST 26th March with model output at intervals of 30 minutes. At that time a slow moving high was centred over New Zealand at the simulation start time (see Appendix 5C). The first 12 hours were discarded as spin-up time and the remaining days were analysed.

Table 5.1: Land surface and turbulence parameterizations used in the four simulations.

| Sim. No. | Simulation Name | Surface Layer | PBL Scheme | Land Surface Scheme |
|---|---|---|---|---|
| 101cg | Eta_Noah_MYJ | Eta Similarity | Mellor-Yamada-Janjic | Noah |
| 101ch | MO_5LTD_YU | Monin-Obukhov | Yonsei Univ | 5-Layer thermal diffusion |
| 101ci | Eta_5LTD_MYJ | Eta Similarity | Mellor Yamada-Janjic | 5-Layer thermal diffusion |
| 101cj | MO_Noah_YU | Monin-Obukhov | Yonsei Univ | Noah |

## 5.3 Synoptic Conditions during the Simulation Period

During the simulation period from 18th to 25th March, a series of high and lows passed over the region. On sea breeze days, most of the time there was a high pressure cell over the North Island. Two cold fronts also passed over the North Island between 19th and 21st March 2006. The easterly moving high pressure system passed over the North Island from 18th to 20th March and 25th March 2006, while most of the time on 21st, 23rd and 24th March, the North Island was dominated by eastward moving lows. Consistent with the observational data analysis, the dominant prevailing winds during sea breeze days were north-westerlies and south-easterlies while on non-sea breeze days, the frequency of south-westerly and north-easterly flow was higher. Figure 5.2 and 5.3 show the wind speed and direction at 850 and 1000 hPa. The northerly component was stronger in the gradient winds observed from 18 to 21st March, while from 22nd to 25th March the southerly component was dominant. The sea level pressure charts for 0000 and 1200 NZST for each simulated day are provided as Appendix 5C. The synoptic situation on 22nd March was more complicated. On this day, three separate high pressure systems were centred to the southwest, south and southeast of the North

Island, while a low pressure system was centred north of the North Island, giving north-easterly flow at around 700 hPa, and easterly to southerly flow at 850 and 1000 hPa.

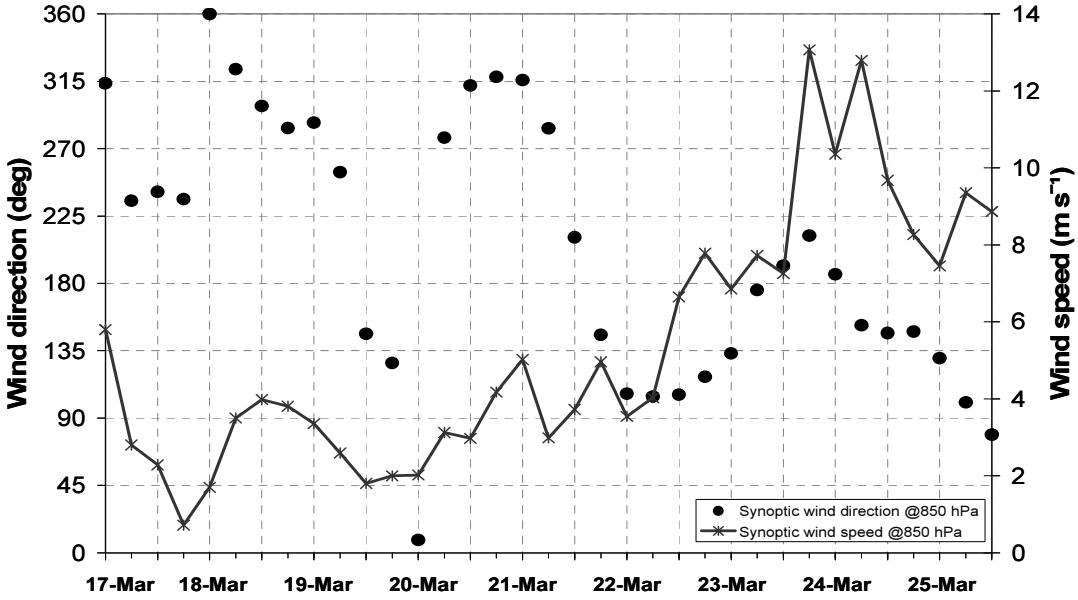


Figure 5.2: Gradient wind speed and direction at 850 hPa at Whenuapai (location 'WH' in Figure 5.2). The wind data were obtained from NCEP/NCAR re-analysis archives (NOAA Research 2009).

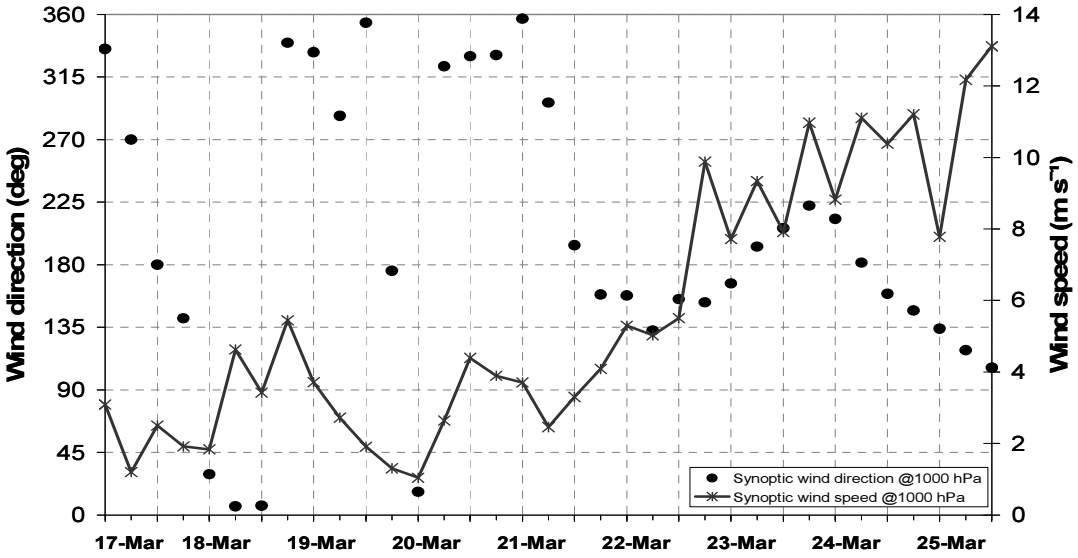


Figure 5.3: Mean sea level pressure (1000 hPa) wind speed and wind direction at Whenuapai (location 'WH' in Figure 5.2). The wind data were obtained from NCEP/NCAR re-analysis archives (NOAA Research 2009).

## 5.4 Evaluation of Model Performance

The surface observational data used for the evaluation of the model simulated meteorology were obtained from 6 sites, while the upper atmosphere data were obtained from one site within the Auckland region (Figure 5.4). To quantify the error in the near-surface meteorological properties of the model simulation, several comparison statistics are computed, including Pearson's correlation coefficient, index of agreement (IOA), root mean squared error (RMSE), systematic root mean squared error (RMSEs) and un-systematic root mean squared error (RMSEu), as presented in Table 5.2.

Table 5.2: Average comparison statistics for wind speed, u and v velocities, screen temperature and relative humidity for 6 observation sites for the 101cg simulation.

| Meteorological parameter | Wind speed ($m\ s^{-1}$) | u velocity ($m\ s^{-1}$) | v velocity ($m\ s^{-1}$) | Screen temperature (°C) | Relative humidity (%) |
|---|---|---|---|---|---|
| Mean Observed | 2.7 | -0.2 | 0.8 | 19.3 | 77.6 |
| Mean Modelled | 3.6 | -0.6 | 1.6 | 18.3 | 79.1 |
| Min. Observed | 0 | -12.4 | -4.9 | 12.7 | 43.9 |
| Min. Modelled | 0 | -13.4 | -4.4 | 11.8 | 45.3 |
| Max. Observed | 12.4 | 8.1 | 8.1 | 28.4 | 100 |
| Max. Modelled | 13.9 | 7.6 | 11.6 | 23.7 | 100 |
| Std. Observed | 1.8 | 2.3 | 2.1 | 2.4 | 13.0 |
| Std. Modelled | 2.4 | 2.9 | 2.8 | 1.9 | 10.0 |
| Corr. Coeff. | 0.81 | 0.83 | 0.79 | 0.77 | 0.70 |
| IOA | 0.83 | 0.89 | 0.85 | 0.83 | 0.83 |
| RMSE | 1.73 | 1.69 | 1.86 | 1.89 | 9.43 |
| RMSEs | 1.06 | 0.63 | 0.85 | 1.57 | 6.65 |
| RMSEu | 1.35 | 1.56 | 1.65 | 1.00 | 6.46 |

*Max: Maximum; Min: Minimum; Std: Standard deviation; Corr. Coeff.: Pearson's correlation coefficient; IOA: Index of agreement; RMSE: Root mean squared error; RMSEs: Systematic root mean squared error; RMSEu: Unsystematic root mean squared error.

Pearson's correlation coefficient describes the co-linearity between observed and predicted values. The index of agreement is a dimensionless quantity and determines the degree to which observed values were accurately predicted by the modelled values. Similar to coefficient of determination, the value of IOA lies between 0 and 1, where 0 means no agreement between observed and predicted values and 1 corresponds to perfect agreement (Hirdman 2006; Nitis et al. 2005). An IOA value greater than 0.50 is considered as acceptable agreement between observed and predicted values (Hurley 2000; Hurley et al. 2002).

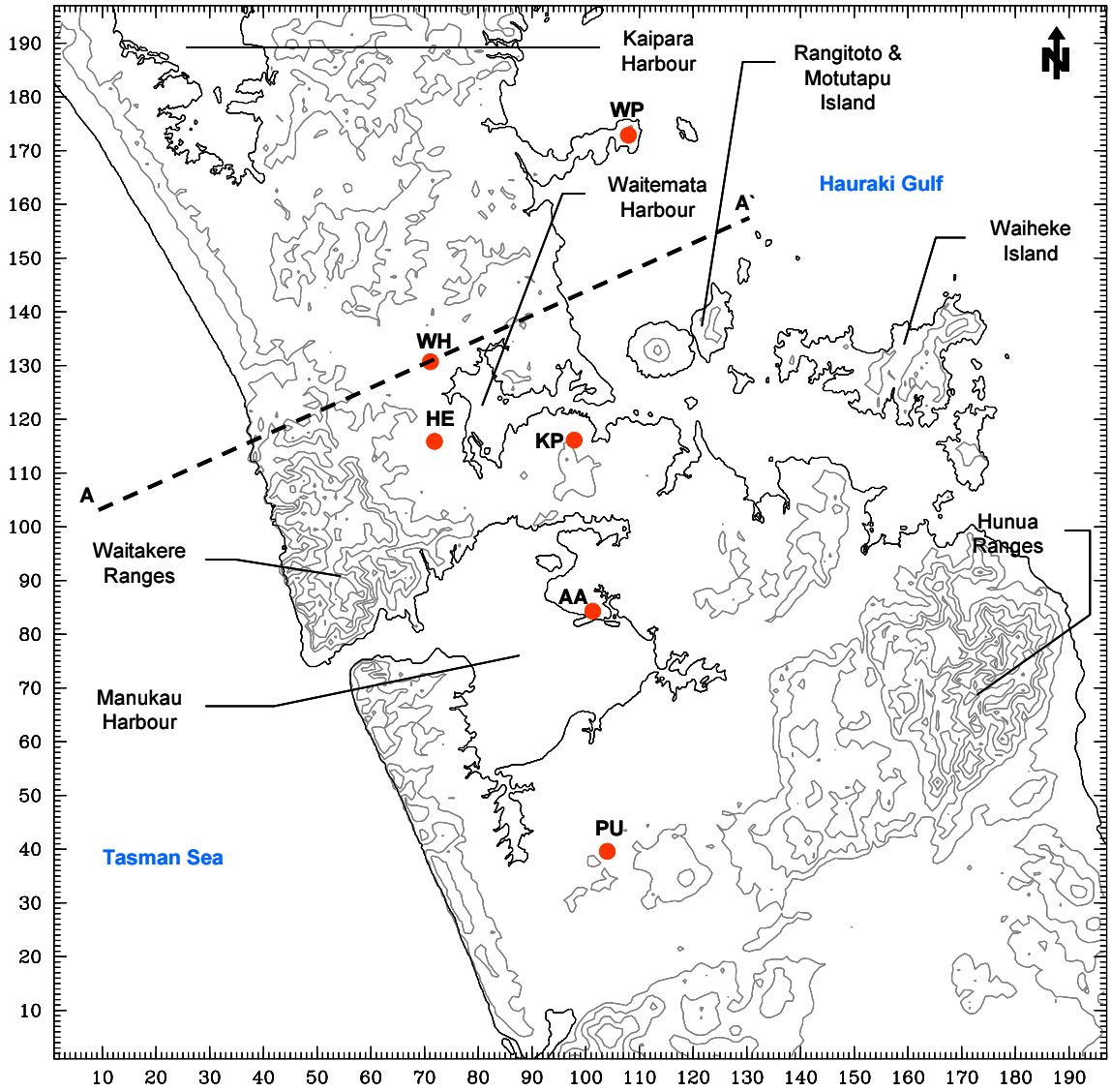


Figure 5.4: Map of the Auckland region from grid domain D03 with 500 m resolution. Red dots indicate the AWS locations of point measurements. The dashed thick black line AA` indicates the location and extent of the vertical cross-section that passes through Whenuapai (WH) station. * WP: Whangaparaoa, WH: Whenuapai, HE: Henderson (Lincoln Road), KP: Khyber Pass, AA: Auckland Airport, PU: Pukekohe.

The root mean squared error (RMSE) represents the average error produced by the model. The RMSE is further decomposed into systematic root mean squared error (RMSEs) and unsystematic root mean squared error (RMSEu). The RMSEs indicates the bias in a particular model that is caused by consistent misrepresentation of local properties, such as topography and land cover, or physical mechanisms, such as planetary boundary layer height or energy fluxes etc. However, unsystematic root mean squared error (RMSEu) shows the random variation between observed and predicted values caused by uncertainties in model initial and boundary conditions, or

uncertainties in the observations (Hirdman 2006; Nitis et al. 2005; Zhong et al. 2007). The equations of error and agreement measures used in this chapter are provided as Appendix 5D.

Table 5.2, shows the combined statistics of the data from six sites that represent urban, sub-urban and downtown locations within the Auckland region. WRF showed excellent skill in predicting basic meteorological properties at the surface level with a high correlation coefficient (>= 0.77), a large index of agreement (>=0.83) and RMSE lower than the respective observed standard deviations. The combined statistics of mean and standard deviation from 6 sites are comparable between modelled and observed variables which means that the model has successfully captured the temporal and spatial variations in the observed data. The standard deviation of modelled data for wind speed, and u and v velocity was higher than the respective observed standard deviation, while it was lower for 2 m air temperature and relative humidity. This shows higher variation in the predicted winds and lower variance in predicted near-surface temperature and relative humidity compared to observed data, which is also evident from minimum and maximum statistics. The error statistics of RMSEs were lower than RMSEu statistics for wind speed, and u and v velocity, but it was higher for 2 m near-surface temperature and relative humidity. The higher unsystematic error in wind is probably due to uncertainty in initial boundary conditions or quality of observational data (Zhong et al. 2007). Index of agreement and error statistics of individual sites are consistent with the combined statistics for u and v velocity, and for most of the sites for wind speed (except Khyber Pass and Pukekohe) (Figure 5.5). The RMSEs for wind speed was slightly higher than RMSEu at Khyber Pass and Pukekohe. Both of these sites are distinct in their location. The Khyber Pass site is located in the downtown area in the heavily urban built environment, while Pukekohe is a rural site situated south of Auckland. Slightly higher RMSEs for wind speed is probably due higher surface roughness in the densely built area at Khyber Pass and the sheltering effect of trees and nearby structures at Pukekohe. The RMSEs for 2 m air temperature was significantly higher than RMSEu at suburban and rural sites, but over urban Auckland (for example, Auckland Airport, Henderson, and Khyber Pass) the IOA and the systematic and unsystematic components of RMSE were almost the same.

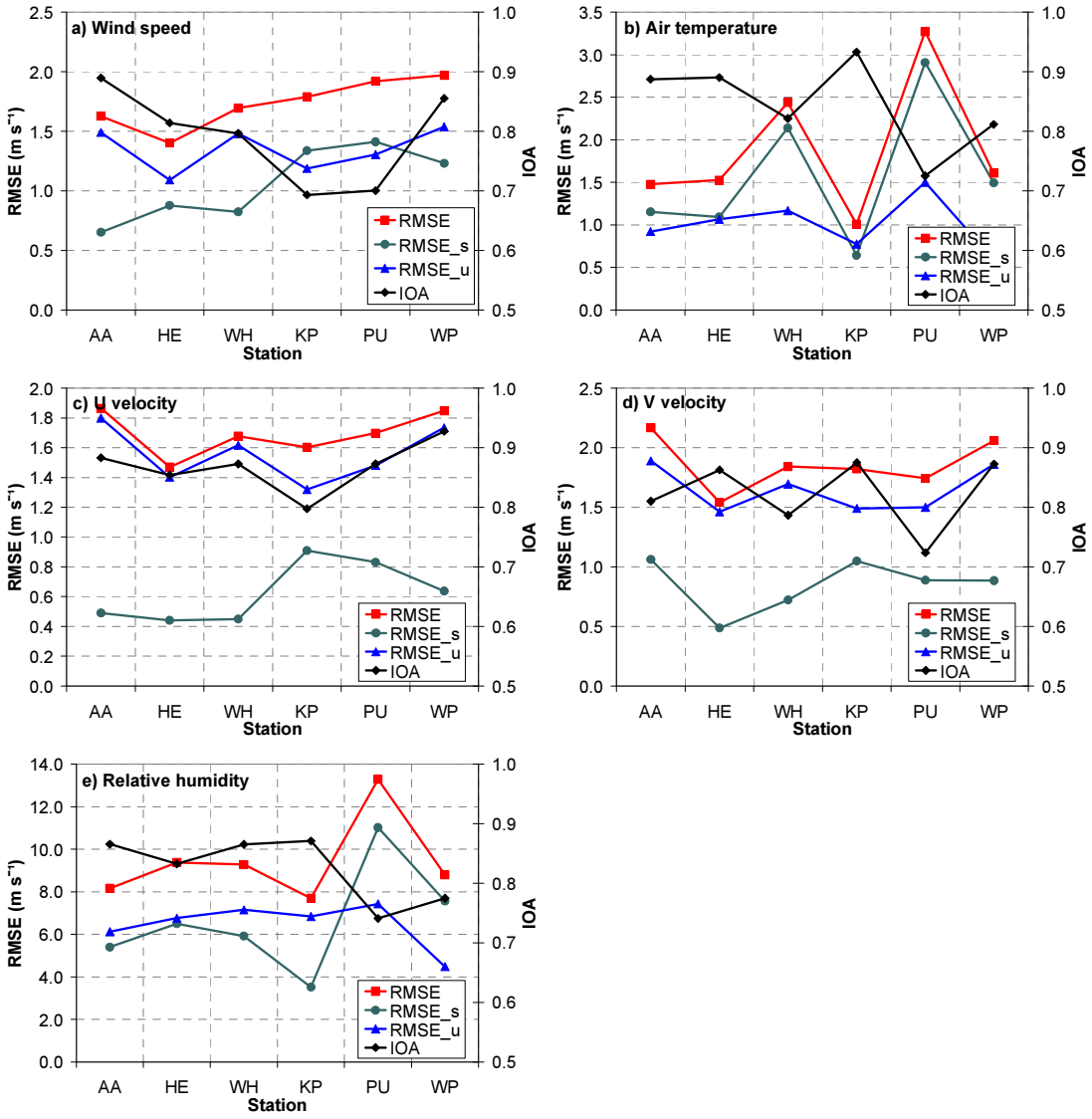


Figure 5.5: Line plot of root mean square (RMSE), systematic root mean square (RMSE_s), unsystematic root mean square (RMSE_u), and index of agreement (IOA) for wind speed, u velocity, v velocity, 2-m air temperature and relative humidity at six sites in the Auckland region. AA: Auckland Airport; HE: Henderson; WH: Whenuapai; KP: Khyber Pass; PU: Pukekohe; WP: Whangaparaoa.

The higher RMSEs for 2 m air temperature and relative humidity at suburban and rural sites indicates consistent misclassification of topography and land use such as vegetation, soil moisture and soil temperature by the Noah land surface scheme, whereas urban characteristics were better represented by Noah scheme. Given the complexity and heterogeneity of the region, this misclassification by the model is perhaps not surprising. A partial comparison of soil temperature and soil moisture (not shown here) revealed that at suburban and rural sites such as Pukekohe the model over predicted soil moisture by up to 30% and under-predicted soil temperature by up to 1.5

°C, while at urban stations such as Auckland Airport, the predicted soil temperature and soil moisture were in good agreement with the observed data. Except for Henderson, WRF showed a cold bias over the diurnal cycle at the remaining five stations. The bias was smaller over heavily urbanized areas such as Khyber Pass and Auckland Airport, which is also indicated by a higher index of agreement (~0.90) and correlation coefficient (~0.80), and a lower RMSE. This shows that land surface properties for urban areas are well represented in the Noah land-surface scheme, whereas in the less urbanized area, the heterogeneity of surface characteristics was masked by the dominant vegetation type (Chen 2007; Shamarock et al. 2008a). This is also consistent with the higher systematic error (RMSEs) in the near-surface 2 m temperature field. Variations in relative humidity are simply a response to changes in the air temperature and therefore not discussed any further. Figure 5.6 shows scatter plots of predicted and observed 2 m temperature, 10 m wind, u and v velocity and relative humidity. The consistent vertical stripe-like pattern in 2 m temperature (Figure 5.6a), and 10 m wind speed plots (Figure 5.6b) are due to data rounding by the data loggers at AWS. The 2 m temperature (Figure 5.6a) shows a warm bias at Henderson, while for the remaining five stations the model generally showed a cold bias with the highest underestimation of 2 m air temperature at Pukekohe. Given the higher predicted soil moisture and low soil temperature, the cold bias in WRF predicted 2 m temperature is probably expected. The near surface 2 m temperature was best predicted at Khyber Pass which is also reflected by the highest IOA for this station. The wind speed was overestimated by the model at almost all sites. The best agreement with the observed values was at Auckland Airport and Whangaparaoa. A close examination of the wind speed at all six stations revealed that mean wind speed at these two stations (Auckland Airport and Whangaparaoa) was more than 1 m $s^{-1}$ higher (~3.4 m $s^{-1}$) than the mean wind speed at the rest of the four stations (~2.3). This indicates that the surface layer scheme in the WRF model could not predict near-surface winds for low wind speed sites with good accuracy. The higher frequency of negative u velocity and positive v velocity indicates higher south-westerly winds during the simulation period, which is consistent with the observed data.

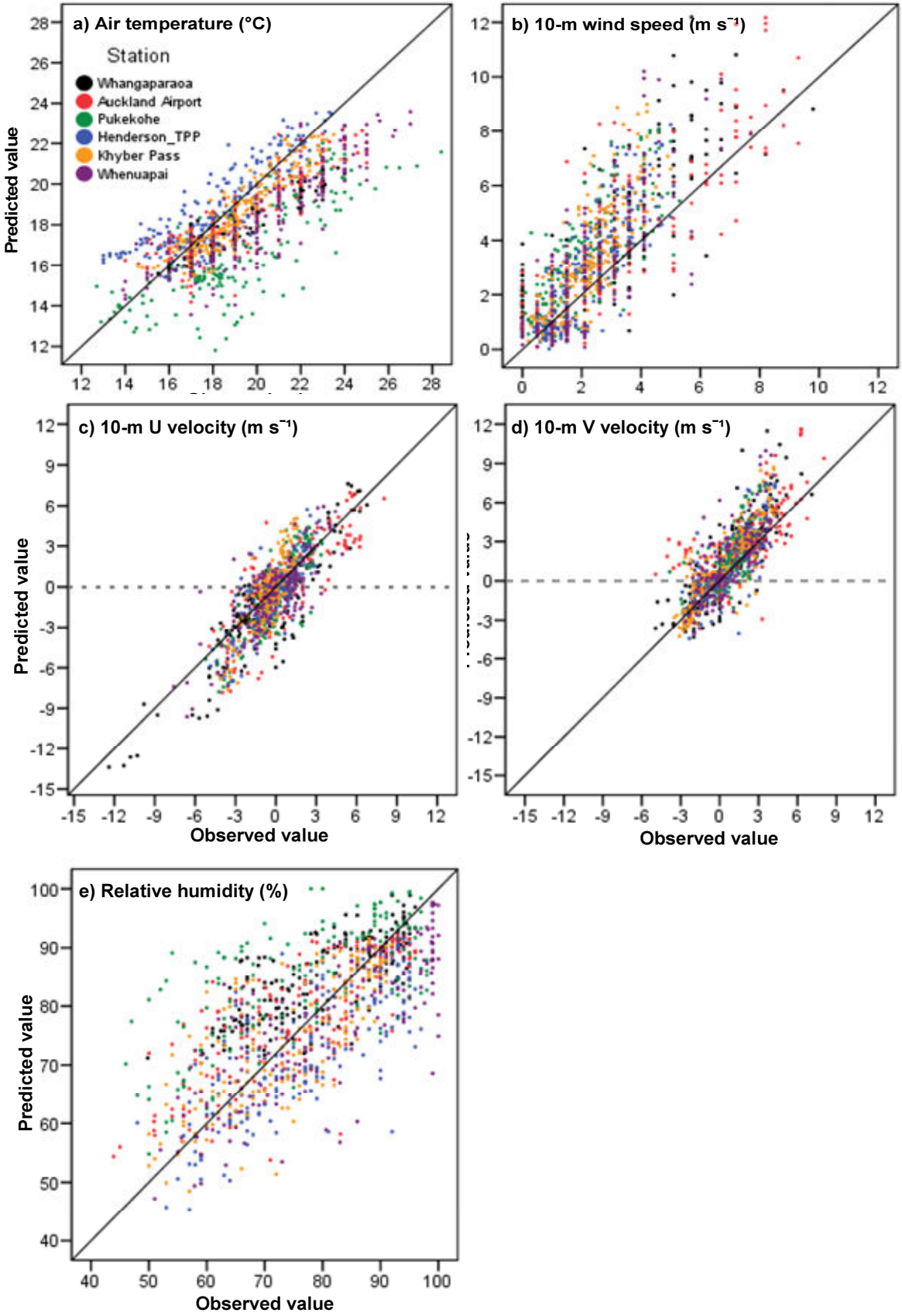


Figure 5.6: Scatter plots of observed and predicted 2-m air temperature, 10 m wind speed, u and v velocity and relative humidity for 6 locations in Auckland area (see Figure 5.4 for site location).

In summary, the model showed higher skill and a fair agreement with the observed near-surface temperature, wind speed and direction, which are crucial to understanding the onset, structure and dynamics of the sea breeze of the region and to give confidence in the model results.

## 5.5 Surface Winds

The time series plots of observed and predicted wind speed and wind direction show distinct features of the sea-land breeze, as well as the effect of large scale winds and topographic forcing in deflection of the thermally forced circulation. During days with north-westerly gradient winds both the observed and predicted surface winds showed a stronger northerly component, while on days with south-easterly gradient flow the southerly component in the surface winds was stronger. From 22$^{nd}$ to 25$^{th}$ March 2006, gradient wind flow for most of the time was south to southeast. The effect of gradient winds is also evident in the time series plot of surface winds from the 6 stations on the simulated days (Figure 5.7). An important feature of the surface winds at midnight on 23$^{rd}$ to 24$^{th}$ March was consistent south-westerly flow at all the six stations that was due to strong gradient winds that were blowing from southeast to southwest direction. The stronger south-easterly gradient flow on 24$^{th}$ and 25$^{th}$ March 2006 (Figure 5.3) did not allow the onset of the sea breeze on both sides of the peninsula. WRF largely overestimated surface wind speed, especially on 24$^{th}$ March. On these two non-sea breeze days, irrespective of the location and orientation, all the six stations showed a similar wind pattern with a strong southerly to south-easterly wind flow. By the evening of 25$^{th}$ March, the eastward migration of the high pressure system gave a strong north-easterly gradient wind flow over the region. This feature is also reflected in the surface wind plots of all the six observational sites in Figure 5.7. The surface winds during the 8 day-long simulation period are discussed below for every observational site separately.

### 5.5.1 Auckland Airport

Auckland Airport is in close proximity of Manukau Harbour and heavily influenced by both local and large scale winds. During sea breeze days, wind over Auckland Airport showed a dominant clockwise rotation. The daytime higher frequency of westerlies

indicates occurrence of bay breezes and mature sea breeze, while at night-time frequency of the north-easterly land breeze was also higher. The WRF model could not predict north-easterly winds accurately on the evening of 21st March, when due to dominant northwest gradient flow, land breezes started early.

### 5.5.2 Henderson and Whenuapai

Waitemata Harbour and the Waitakere Ranges are in close proximity to Henderson and Whenuapai. The wind field from these two stations reflects the influence of these topographic features. Waitemata Harbour is located to the east and southeast and Waitakere to the west of these stations. The wind field from 18th to 21st March at these two stations showed a high frequency of the daytime north-easterly sea breeze and night time westerly land breeze. However, the rotation of wind direction at both of these stations was more obscure. The consistent higher frequency of westerly winds from midnight to early morning indicates coupling of cold air drainage from the Waitakere Ranges with the land breeze. From 23rd to 25th March surface winds were not much different from Auckland Airport confirming the strong effect of the gradient winds on the thermally induced flow. However, on 23rd March (0000 – 0600 hours) the model incorrectly predicted an observed south-westerly land breeze as a south-easterly wind at Whenuapai.

### 5.5.3 Khyber Pass

The situation at Khyber Pass was even more complex, with Waitemata Harbour to the north-northwest, Hauraki Gulf to the east-northeast and Manukau Harbour to the southwest of the station. The downtown location and urban built environment also posed a significant challenge to WRF to predict the wind field accurately. This is also reflected in the comparison statistics (Figure 5.5) where IOA for wind speed and west-east U-velocity was the lowest of all stations, although an IOA >=0.70 is still considered a reasonably good agreement between predicted and observed values. During northerly gradient winds, both observed and predicted data showed a higher frequency of northerly winds over the diurnal cycle.

### 5.5.4 Pukekohe

Pukekohe is located to the south of Manukau Harbour, with the Hunua Ranges to the east and the west coast to the west of the station. The observed data from Pukekohe were not available from 0900 hours 20th March to 1300 hours 21st March 2006, and therefore not included in the analysis. The important features of the wind field at Pukekohe includes, the morning bay breezes from Manukau Harbour, afternoon southerly and south-westerly flow from the west coast and further south of Pukekohe, and night time easterly flow (cold air drainage) from the nearby Hunua Ranges. Unlike Auckland Airport, surface winds rotated anticlockwise at Pukekohe during weak north-westerly and north-easterly gradient flow.

### 5.5.5 Whangaparaoa

Whangaparaoa, is a narrow peninsula extended eastward into the Hauraki Gulf on the east coast. WRF at this location predicted a complete anticlockwise rotation during sea breeze days under northerly gradient wind. However, this anticlockwise rotation is not evident in observational data on most of the sea breeze days. In the morning hours of 19th and 20th March (0000 to 0600 NZST) WRF failed to predict calms in the observed data.

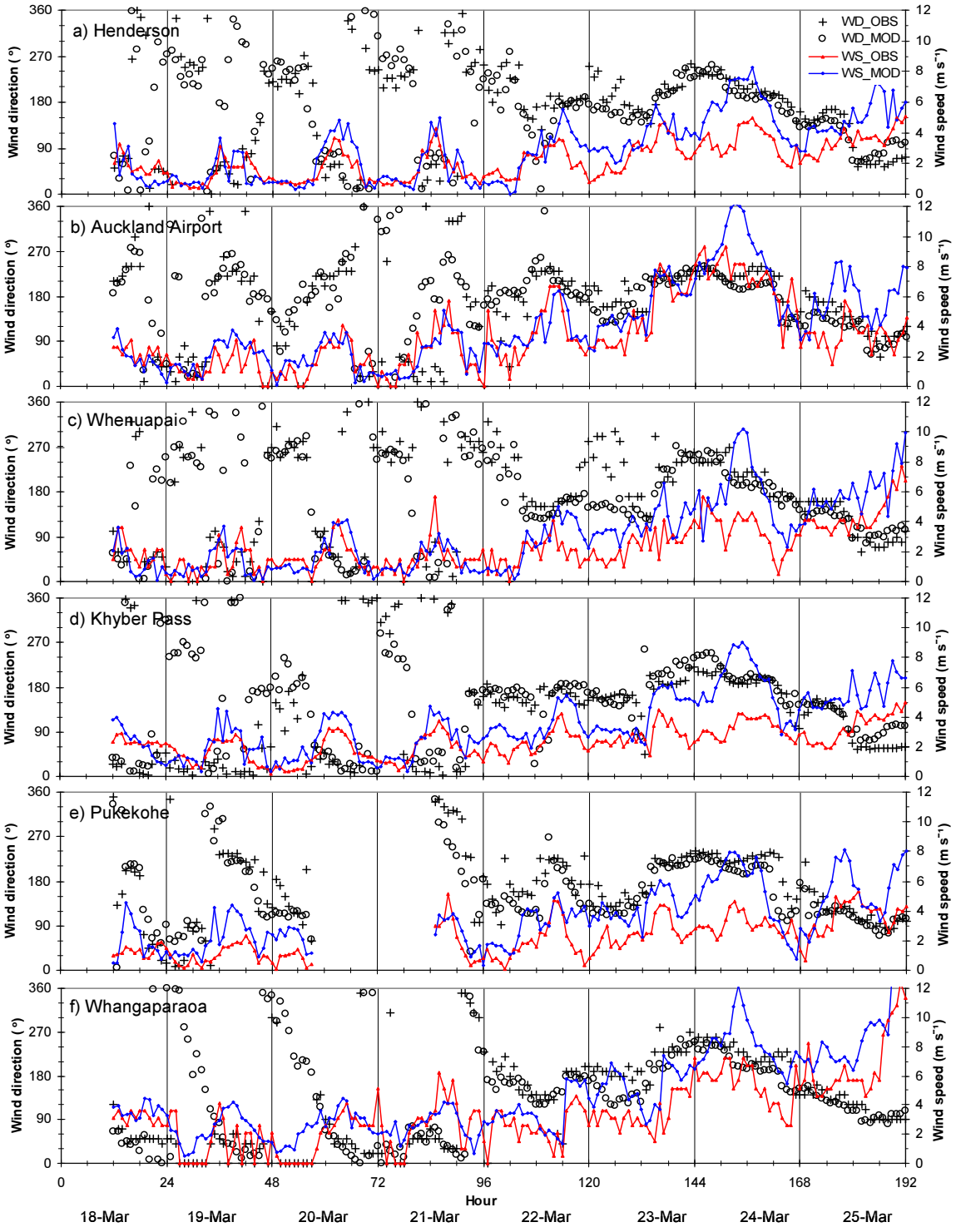


Figure 5.7: Plots of observed and predicted surface (10 m) wind speed and wind direction from 6 stations in the Auckland region. See Figure 5.4 for site locations.

### 5.5.6 Onset and Cessation of Sea Breeze

Analysis of hourly 10 m wind plots (not shown here) for the simulation period suggests onset of bay breezes occurs at around 0900 hours along the harbour coastlines and higher terrain over the east and the west coasts, while onshore flow of mature sea breezes was initiated around 1000 hours over both east and west coasts. The predicted sea breeze generally weakened after 1600 hours, although timing is subject to the direction and strength of the gradient wind. Under northerly gradient winds, the easterly sea breeze lasts longer, while under southerly gradient flow cessation of the westerly sea breeze is delayed.

## 5.6 Sea Breeze Convergence Zones

Sea breeze convergence zones occur frequently over the Auckland region on sea breeze days and, due partly to their ability to modify the boundary layer structure, sea breeze convergence zones are given significant importance in air quality literature. For this reason, most of the studies in the Auckland region also specifically discussed this distinct aspect of sea breeze circulation (McGill 1987; McKendry 1989,1992; Sutton 1996). Figure 5.8 shows the 10 m wind field and vertical velocity at around 500 m (agl) at 1500 hours for three sea breeze and one non-sea breeze days. The model predicted SBCZs on all the simulated sea breeze days, but on the non-sea breeze day of 24$^{th}$ March, strong southerly and south-westerly gradient flow did not allow the onset of the sea breeze and subsequent SBCZs. The convergence zones were stronger on 21$^{st}$ and 22$^{nd}$ March, which is also evident from relatively high magnitude upward vertical velocities (Figure 5.8b and 5.8c) and turbulent kinetic energy (TKE) (Figure 5.9b). On the non-sea breeze day of 24$^{th}$ March, although the magnitude of the vertical velocity was relatively small, but due to strong horizontal winds, TKE was the highest for most of the day (Figure 5.9d). Variation in the strength of the SBCZs was due partly to synoptic conditions, as well as the intensity of surface heat fluxes. On 19$^{th}$ and 21$^{st}$ March, the gradient winds were blowing from northwest, while on 22$^{nd}$ the gradient flow was from the southeast. The coast-parallel gradient flow on the three sea breeze days helped landward advection of warm air.

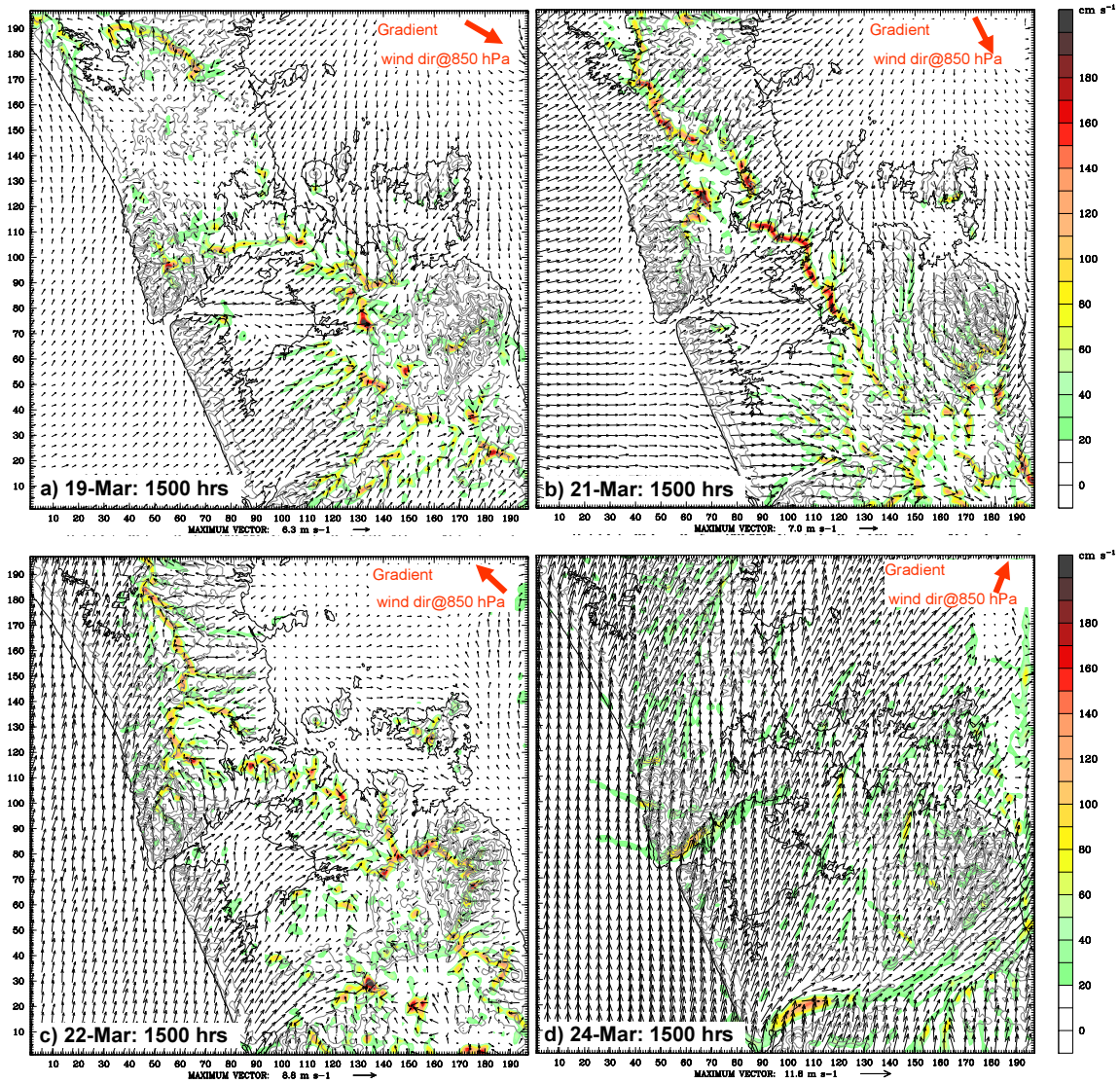


Figure 5.8: Horizontal cross-sections of 10 m wind and vertical velocity at 500 m above ground level at 1500 hours on three sea breeze and one non-sea-breeze days. In the inset in the top right corner of each plot, the red arrow indicates gradient wind direction at 850 hPa in the afternoon hours.

The temporal evolution of the predicted SBCZs was dominated by the two thermally induced local wind systems: a) bay breezes from Kaipara, Waitemata and Manukau Harbours, and b) mature sea breezes from the east and/or the west coast. During morning and early afternoon hours, convergence lines were formed due to the interaction between bay breezes and air over land or sea breezes from either coast. In the afternoon (1500 hours and later) stronger sea breezes from both coasts merged most of the localized convergence lines into a few, but more intensified, SBCZs. The intense upward and downward motion in and along the SBCZs would probably mix the pollutants emitted in the surface layer. The position of the SBCZ is strongly affected by

the topography and synoptic wind conditions (McKendry 1989,1992; Sutton 1996). On 19th and 21st March, the gradient winds were from the northwest (parallel to the land mass). After balancing the large scale pressure gradient with the mesoscale thermal gradient and friction coefficient, the resultant predicted sea breeze on the east coast intensified (Adams 1997; Miller et al. 2003; Zhong & Takle 1993), and the SBCZ on both of these days was formed in the middle of the land mass. The strong southerly component on 22nd March strengthened the south-westerly sea breeze that eventually pushed the SBCZ to the east coast of the Auckland region.

Synoptic conditions and the thermal gradient are not the only factors that affected occurrence of SBCZs. In reality, topography, surface characteristics and land use also appear to significantly influence the position and strength of the SBCZ (Mahrer & Pielke 1977; Miao et al. 2003; Nitis et al. 2005). For example, on all three sea breeze days that are presented here, the easterly and westerly sea breeze front propagated inland and the SBCZs were centred over the middle of the heavily urbanized Auckland City area, which is due partly to its geographical and topographical setting, as well as the urban heat island effect that generated intense sea breezes on both sides of the isthmus. In the same way, convergence of the westerly sea breeze to the lee side of the Waitakere Ranges resulted in a terrain-induced SBCZ. These topographical influences on the sea breeze circulation are discussed in greater detail in Chapter 7.

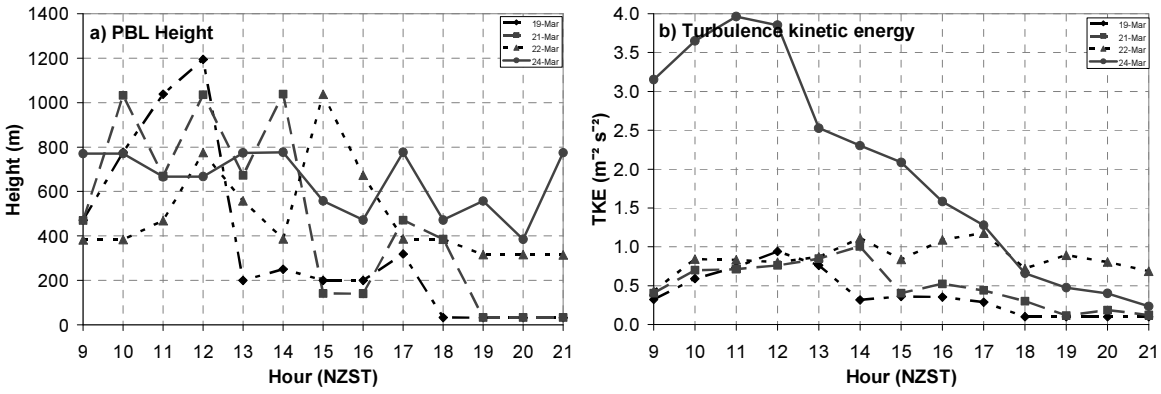

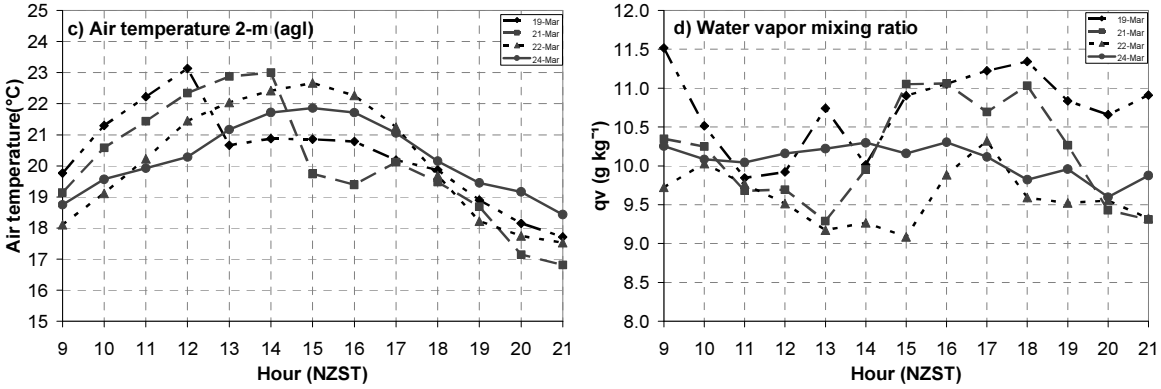


Figure 5.9: Time series plots of predicted boundary layer height, turbulence kinetic energy, 2 m air temperature, and water vapour mixing ratio at Whenuapai (shown as 'WH' in Figure 5.4).

## 5.7 Boundary Layer Structure and Evolution

The vertical structure of the boundary layer, especially the mixed layer height and its evolution, are important aspects of the structure of a mesoscale phenomenon, such as the sea breeze. The daytime sounding data for 1200 NZST from Whenuapai station was compared with the simulated potential temperature, water vapour mixing ratio, wind speed and wind direction for 19$^{th}$, 21$^{st}$, 22$^{nd}$ and 24$^{th}$ March 2006. The height of the mixed layer was determined as the base of the elevated inversion, along with a reasonable gradient in water vapour mixing ratio. To examine the vertical structure of the sea breeze and evolution of the mixed layer under sea breeze conditions, predicted vertical profiles for 1500 hours and 2000 hours are plotted along with 1200 hour profiles. The results of the comparison are shown in Figure 5.10.

In general, the model successfully captured the basic features of the boundary layer, although the predicted mixed layer has a small cold bias in the vertical. Zhong et al. (2007) reported a consistent underestimation of mixed layer height using the Eta (MYJ) scheme that coincides with a general cold bias and high moisture content in the boundary layer. However, in the Auckland case, although the predicted mixed layer depth is in good agreement with the observed one, no consistent patterns were found. For example, on 21$^{st}$ and 22$^{nd}$ March the predicted mixed layer height was in excellent agreement with the observed mixed layer height with a small cold bias, but on 19$^{th}$ March WRF over-predicted the mixed layer height by almost 100%, while on the non-sea breeze day of 24$^{th}$ March, WRF underestimated mixed layer height by 100 m. The

vertical distribution of moisture was also quite variable. On 21st March, the 1200 hour vertical profile showed significant under-prediction of wind speed up to a height of 1200 m. During day time on 21st March, a cold front was approaching the North Island, and the stronger observed winds were probably attributed to this cold front. However, the WRF model failed to capture this feature accurately and thus under-predicted wind speed. On 19th March, the model over-estimated mixed layer height and near-surface wind speed and under-estimated moisture levels, which means that the simulated atmosphere was drier and windier, resulting in a mixed layer twice (800 m) the height of the observed mixed layer. The last day (24th March) presented in Figure 5.10, was a non-sea breeze day. The vertical structure at noon was quite different from the three sea breeze days. The mean sea level synoptic charts showed an eastward moving low pressure system with a cold front to the southeast of the North Island (see Appendix 5E), giving consistent strong southerly to south-easterly flow to the region. This meteorological situation was not favourable for the onset of a mesoscale circulation, such as a sea breeze, but perfect for a cyclone-induced low level jet. Both observed and predicted wind speed profiles showed this low level jet. However, WRF significantly overestimated wind speed in the first one kilometre of the atmosphere. Above that level, predicted winds were almost in perfect agreement with the observed wind speed. The model showed a strong cold bias in the layer between 500 to 1200 m above ground and the mixed layer height was also underestimated, although the predicted temperature profile up to 400 m was in very good agreement with the observed data. The moisture content was also consistent with the vertical thermal structure of the atmosphere.

Once a landward sea breeze flow was generated, a sea breeze return flow usually developed aloft above the marine inflow layer of air. This return flow is required for a closed circulation to accomplish mass conservation. Analysis of the thermodynamic structure of the boundary layer on three sea breeze days suggests complete absence of a closed circulation. The vertical cross section of potential temperature, horizontal wind vector and vertical velocity at 1500 NZST indicates a clear, sea breeze inflow on all three simulated sea breeze days, but the return flow was either not generated at all or it was very weak and deflected by the gradient winds and mesoscale PGF. Several authors have reported the absence or inability of return flow to counterbalance the onshore sea breeze flow and associated it with the gradient wind strength and direction

and complex inland topography (Banta et al. 1993; Estoque 1962; Finkele 1995; Mizuma 1995).

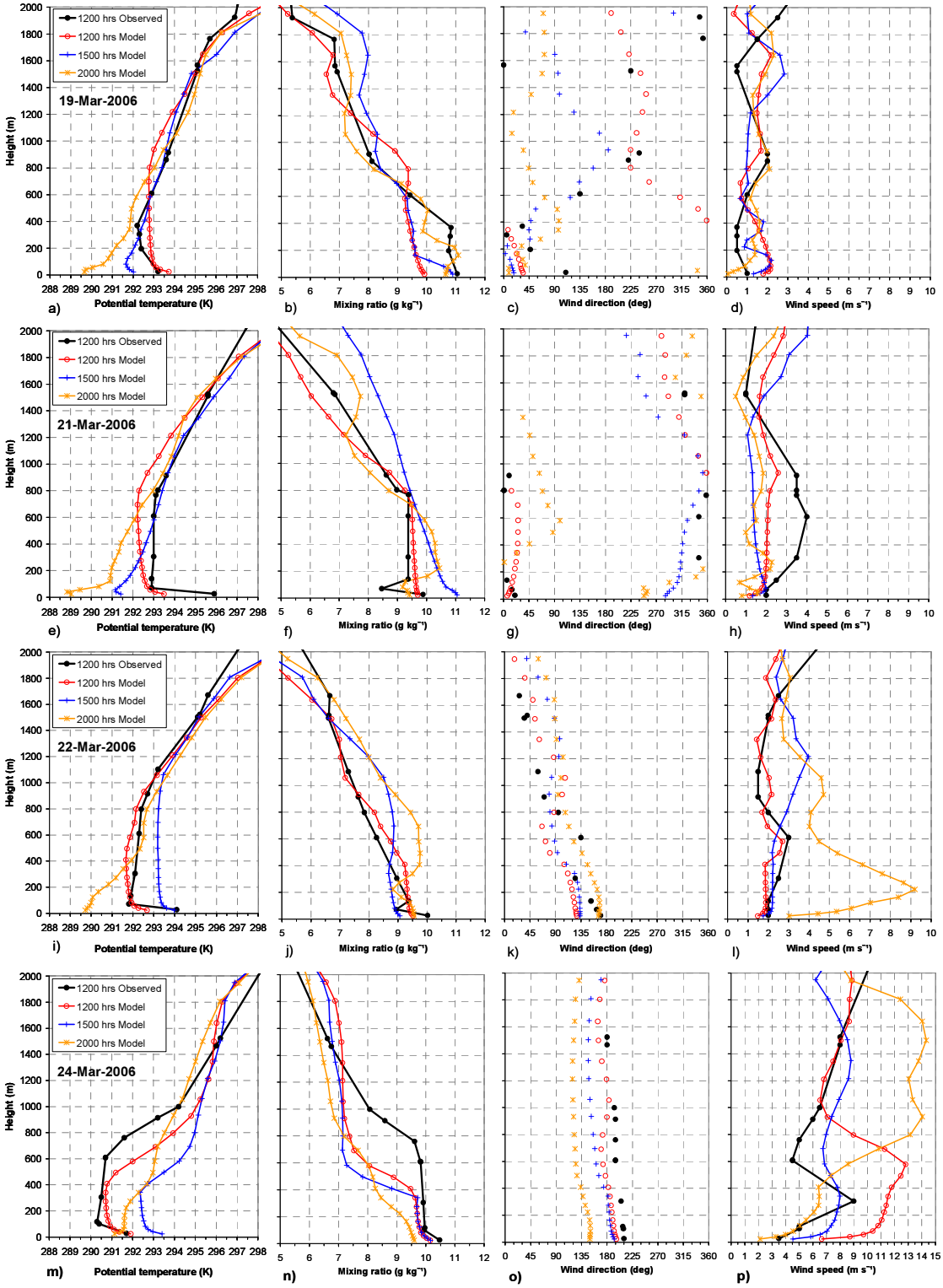


Figure 5.10: Observed and WRF predicted vertical profiles of potential temperature, water vapour mixing ratio, wind direction and wind speed from Whenuapai (AWS location 'WH' in Figure 5.4) on three sea breeze days (19th, 21st, 22nd March) and one non-sea breeze day (24th March 2006) for 1200 hours. Predicted vertical profiles for 1500 and 2000 hours are also plotted.

The vertical velocities (especially downdrafts) over the sea were negligible during afternoon hours, indicating the incomplete circulation, while overland vertical velocities were higher due to convection or convergence between relatively cool marine air and warm land air. The highest vertical velocities were predicted in sea breeze convergence zones (Figure 5.11b), where thermodynamic and kinematic fronts occur at the same place (Atkins et al. 1995; Miller et al. 2003). The intense convection in and along convergence zones would give the boundary layer a domelike shape which is significant from an air pollution perspective (Liu & Chan 2002b).

On two of the sea breeze days, 19$^{th}$ and 21$^{st}$ March, the gradient winds had a strong north-westerly component, while on 22$^{nd}$ March gradient wind direction was southeast, and on the non-sea breeze day of 24$^{th}$ March the gradient winds were from a south to southwest direction. The variation in the direction of the sea breeze inflow on the three sea breeze days indicates the phase change due to diurnal directional rotation. For example, on 19$^{th}$ March wind flow over the west coast became southerly after turning leftward, while the east coast was receiving northerly winds (Figure 5.11a). On 21$^{st}$ March, the situation was slightly different, as over the west coast sea breeze inflow was still normal to the coast, while over the east coast it had already turned leftward giving northerly/north-easterly flow to the east coast (Figure 5.11b). On 22$^{nd}$ March the westerly sea breeze rotated first, while the east coast was still getting onshore sea breeze flow normal to the coast (Figure 5.11c). The depth of the sea breeze inflow layer on the three sea breeze days varied from 200 to 600 m, while predicted depth of the return flow was between 300 to 400 m. On the non-sea breeze day of 24$^{th}$ March, the thermal structure of the lower atmosphere over land and sea was clearly different from the sea-breeze day profile, as strong south-westerly prevailing winds that overwhelmed the region suppressed convection and did not allow the thermally-induced circulation to develop.

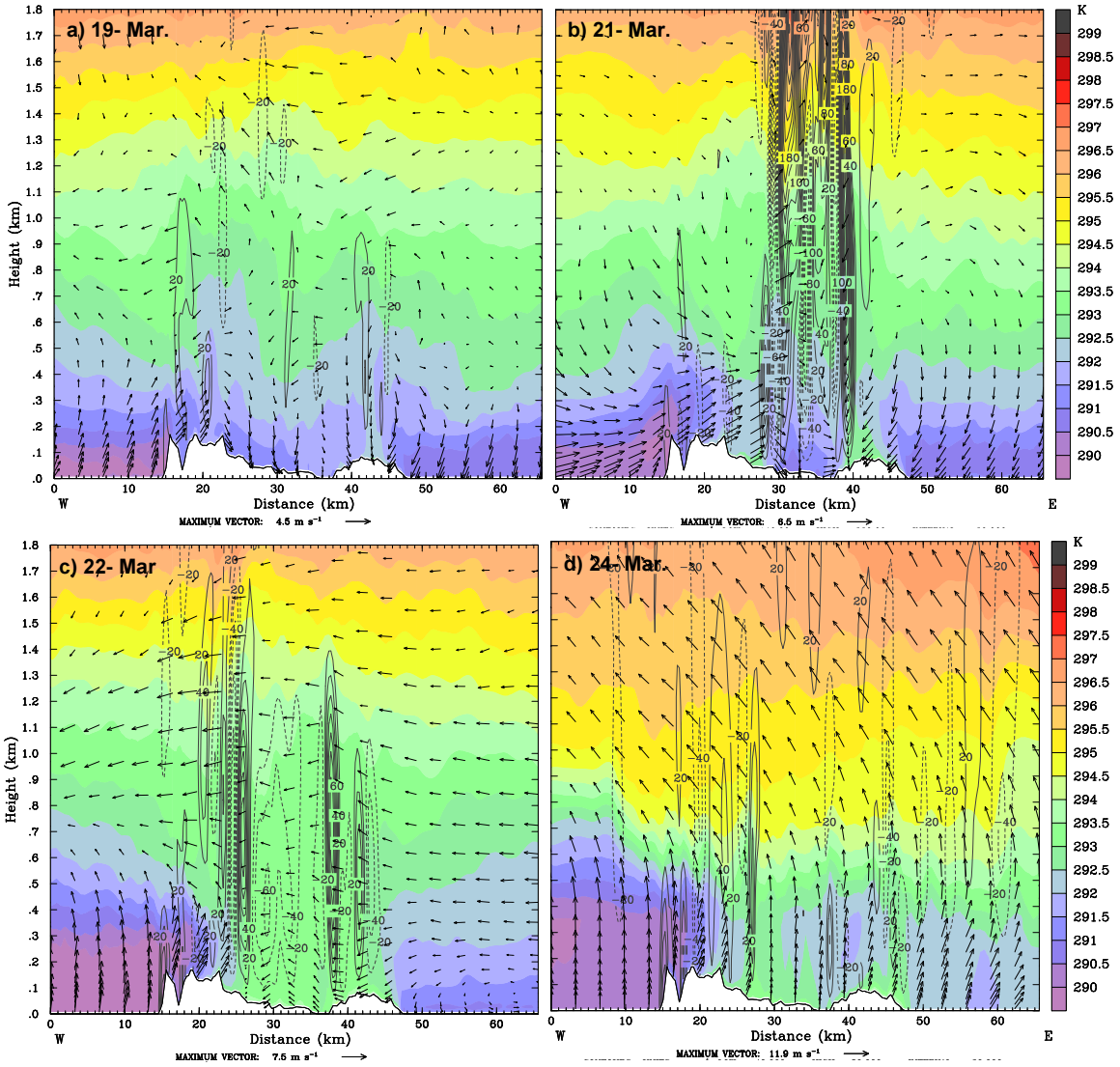


Figure 5.11: Vertical cross sections of WRF predicted horizontal wind vector, vertical velocity in black contours (solid line indicates positive and dashed line indicates negative vertical velocity) in m $s^{-1}$, and potential temperature (colour shaded) in K for 1500 NZST. The vertical cross section drawn from location AA` in Figure 5.4.

### 5.7.1 The Convective Internal Boundary Layer (CIBL)

The convective internal boundary layer (CIBL) was predicted over Auckland with varying depth and inland extent on all three sea breeze days. Figure 5.12 shows the temporal evolution of the thermodynamic structure of the boundary layer at Whenuapai. On 19$^{th}$ March, the westerly sea breeze from the west coast arrived at Whenuapai at around 1300 hours (Figure 5.12a) and was marked by a drop in air temperature and increase in moisture (Figure 5.9). The height of the CIBL varied from 150 to 400 m during afternoon hours (1300 to 1600 NZST), which is consistent with

the idealized modelling results of four gradient wind conditions (Chapter 6) that predicted a CIBL depth in the range of 200 to 400 m in depth. On 21st March, the mature sea breeze from the west coast was delayed up to 2 hours and arrived at Whenuapai at 1500 NZST. The inflow of cold, dense marine air mass from the Tasman Sea resulted in an increase in moisture content up to 2 g $kg^{-1}$ and a temperature drop of up to 3.0 °C (Figures 5.9). Consequently, the mixed layer collapsed leading to formation of a shallow convective internal boundary layer (CIBL) less than 200 m deep. The CIBL was also formed on the weak sea breeze day of 22nd March around 1400 NZST. However, due to relatively high gradient winds and low horizontal thermal gradient, the arrival of the easterly sea breeze at Whenuapai could not be clearly identified. At 1400 hours, the reduction in the predicted boundary layer height from 800 m to 400 m and nominal increase in near surface vapour mixing ratio (Figure 5.9) marked the arrival of a weak sea breeze. However, the 2 m near-surface temperature slightly increased. A detailed analysis of 10 m surface winds and time-height cross sections of wind revealed that the afternoon wind flow at Whenuapai on 22nd March was the sum vector of relatively colder marine air flow from Waitemata Harbour that was also enhanced by the easterly sea breeze and gradient wind enhanced south-easterly flow. Although continuous inflow of relatively cold air formed CIBL up to 400 m deep, soon the strong southerly flow took over and afternoon surface heating increased convection that merged the CIBL with the actual PBL at around 1500 hours (Figure 5.12). The day time thermal structure of the lower atmosphere was different on the non-sea breeze day of 24th March 2006. Under strong southerly/south-easterly winds the PBL height remained between 400 to 600 m for most of the daytime.

### 5.7.2 Residual Layer

In the evening hours, with the reduction in surface heat fluxes, the atmosphere started stabilizing, and by 2000 hours the vertical profile of potential temperature shows a multi-layer thermal structure in the lower atmosphere (Figure 5.10). The residual layer which is important in air pollution applications is predicted to be around 100 m above ground. The potential temperature profiles of the four simulated days (Figure 5.10) show the depth of the residual layer between 100 to 300 m. An important feature of the night-time meteorology are the nocturnal jets that occur due to decoupling of the colder surface layer of air from the relatively warm layer above it. WRF model successfully

predicted the nocturnal jet at 2000 hours on 22nd March 2006 (Figure 5.10) when predicted wind speed at 200 m above ground reached 9 m $s^{-1}$.

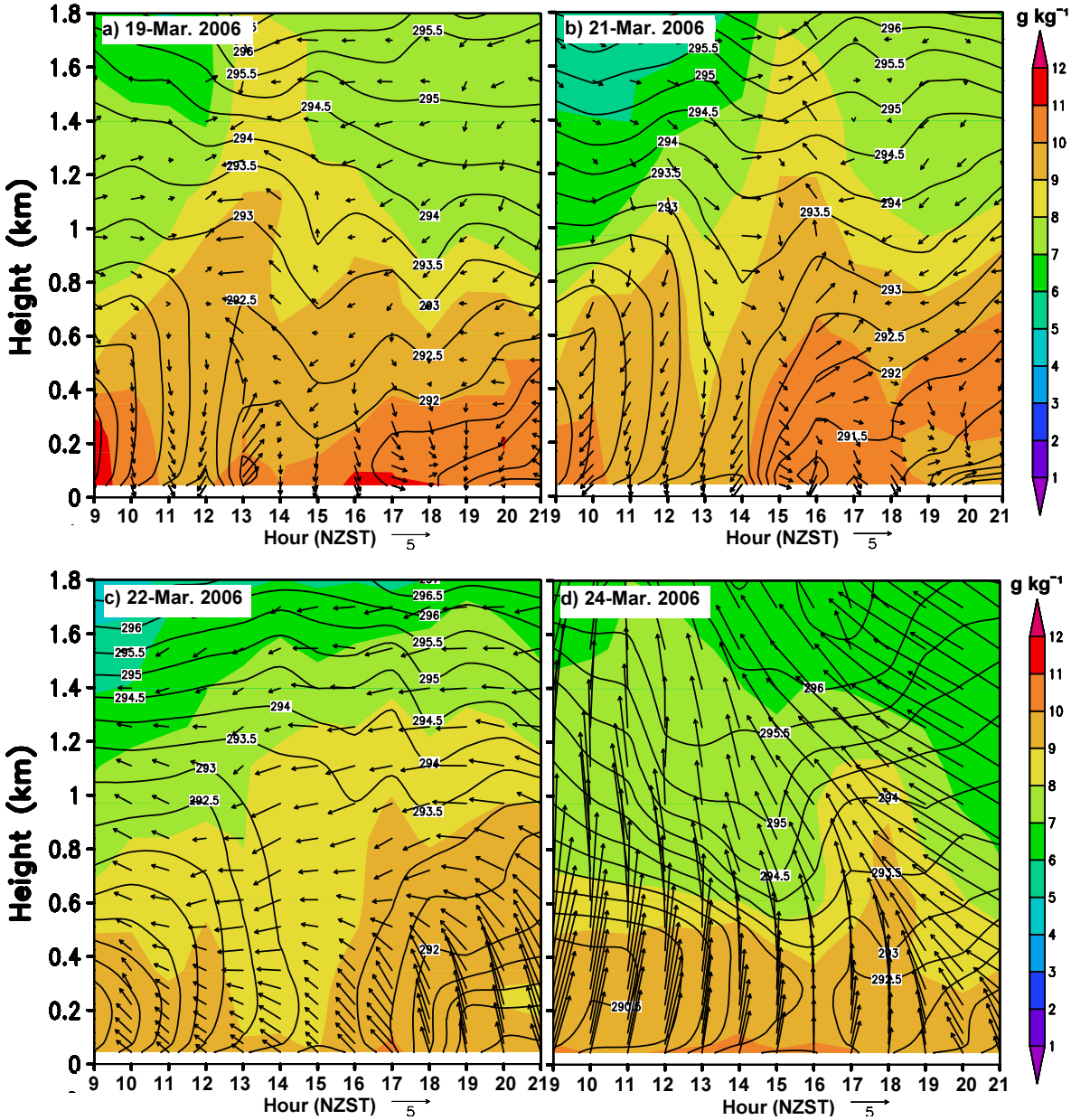


Figure 5.12: Time-height vertical cross sections of WRF predicted horizontal wind (vectors), potential temperature (contours) and water vapour mixing ratio (colour shaded) from 0900 to 2100 hours for three sea breeze days and one non-sea-breeze day.

## 5.8 Pollution Dispersion Modelling

The main objective of the pollution dispersion modelling presented in this section is not to assess the magnitude of pollutant concentrations in the region, but to examine how the sea breeze phenomenon is likely to affect the dispersion of pollutants in the Auckland region, and when and where pollutant concentrations are likely to be higher during a sea breeze circulation.

### 5.8.1 The Air Pollution Model (TAPM)

The Air Pollution Model (TAPM) is a PC-based mesoscale, incompressible, nestable, prognostic and optionally non-hydrostatic meteorological and air pollution model developed by Australia's Commonwealth Scientific and Industrial Research Organization (CSIRO). The model utilizes a synoptic meteorology input dataset supplied by the Australian Bureau of Meteorology and derived from the Limited Area Prediction System (LAPS) analysis data (Puri et al. 1998), although it can also optionally assimilate local wind observations (Hurley 2005b). TAPM uses global input databases of terrain height, vegetation and land-use with a horizontal resolution of 30 seconds (approximately 1 km) while the sea surface temperature is derived from Rand's global long-term monthly means at a resolution of 100 km (Hurley 2005b; Zawar-Reza et al. 2005a).

TAPM solves the incompressible hydrostatic and optionally non-hydrostatic continuity equations of atmospheric flow, thermodynamics, moisture conservation, turbulence and dispersion to resolve both meteorology and pollutant concentrations (Hurley et al. 2005; Luhar & Hurley 2003). It includes parameterizations for cloud/rain/snow micro-physical processes, turbulence closure, urban/vegetative canopy and soil, and radiative fluxes (Hurley 2005a). For a detailed account of technical descriptions and parameterizations, see Hurley (2005a,b; 2005). The air pollution component of TAPM uses Eulerian-based prognostic equations with an optional Lagrangian particle mode. The pollution component utilizes the predicted meteorological fields from the meteorological component of TAPM to resolve atmospheric chemistry and pollutant dispersion (Hurley 1994; Luhar & Hurley 2003). However, due to the assumption of incompressibility and non-hydrostatic effects that only reach 5000 m (above that level

meteorological variables are smoothed to minimize wave reflection from the model top), TAPM can not accurately represent deep atmospheric motions. Therefore, TAPM is not suitable to model meteorology under strong gradient flow conditions that lead to deep vertical motion (Zawar-Reza et al. 2005a).

TAPM has been successfully applied in Auckland, Christchurch, Timaru, Wellington, Nelson and some other urban and suburban parts of New Zealand (e.g. Gimson et al. 2005; Gimson 2005; Heydenrych 2002; Hirdman 2006; Wilson & Zawar-Reza 2006; Zawar-Reza et al. 2005a; Zawar-Reza et al. 2005b). The meteorological component of TAPM is capable of predicting local scale flows such as sea breezes and terrain-induced circulations, and successfully simulating mesoscale phenomena under various atmospheric conditions (e.g. Luhar & Hurley 2004; Luhar et al. 1998).

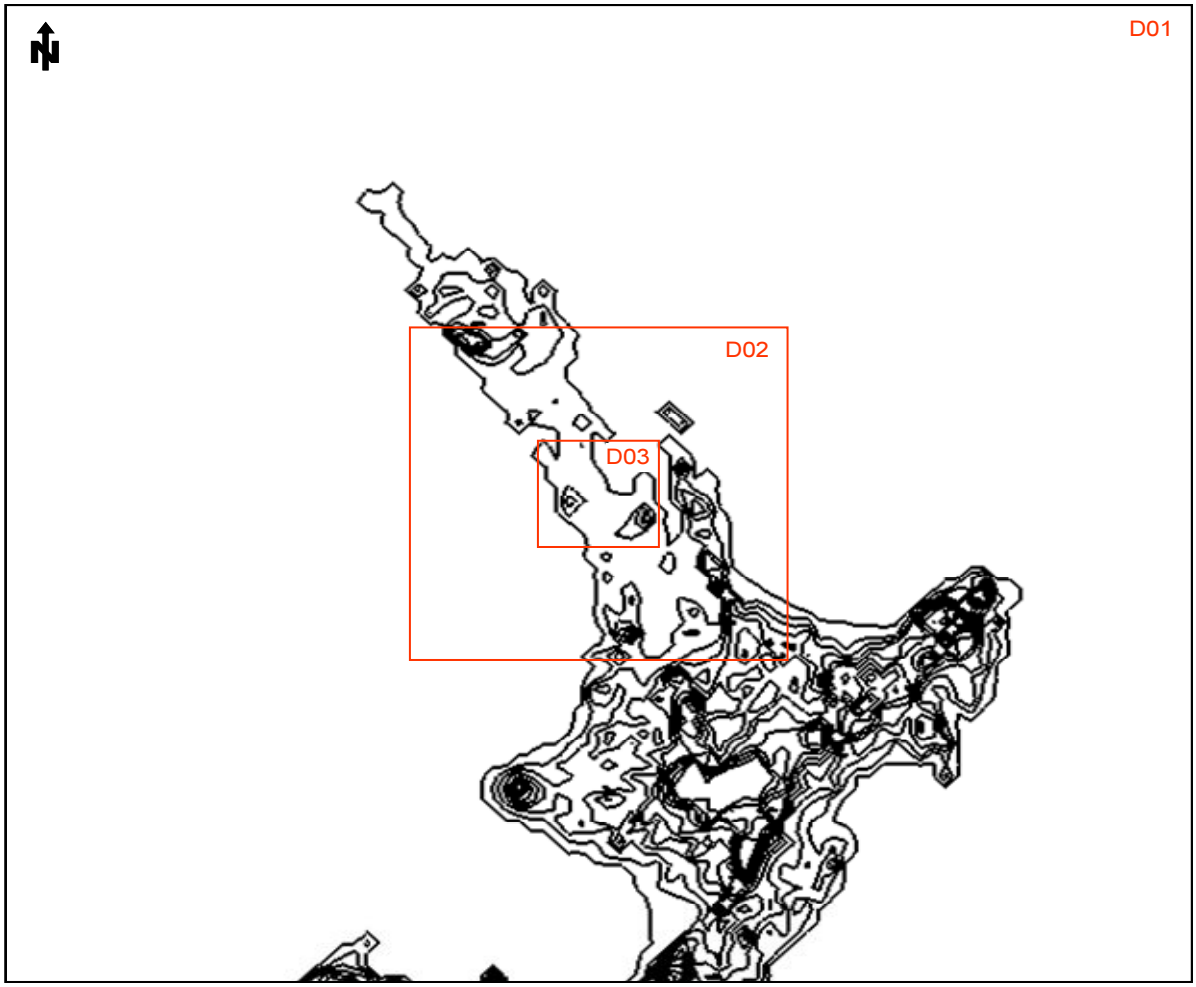


Figure 5.13: Grid configuration of the TAPM simulation. Outer domains D01 and D02 have resolutions of 10000 m and 3000 m, respectively; the grid resolution of the innermost finer domain D03 is 1000 m. The number of grid points in the x and y dimensions are 98 x 98 for all grid domains.

### 5.8.2 Model Setup

TAPM version 3.0 was run for the same eight days period as WRF and includes 5 sea breeze days (18th to 22nd March) and 3 non-sea breeze days (23rd to 25th March). Given the complexity of terrain, it was intended to run highest resolution grid with 500 m spatial resolution, however, TAPM was unstable at this high resolution and it was decided to settle for 1000 m instead of 500 m spatial grid spacing. The model was therefore configured with three nested grids of 50 x 50 x 35 points with grid spacing of 10000, 3000, and 1000 m for meteorology(Figure 5.13), and 197 x 197 x 35 points at 2500, 750 and 250 m for pollution grids. The sea surface temperature and deep soil temperature were increased by 0.5 °C to keep the model consistent with WRF and the real sea surface temperature for the month of March near the North Island. For terrain, land use and vegetation, 30 second data from USGS were used. The model was run in standard mode without data assimilation. Two simulations were run, one with an area source covering a rectangle of 15 x 10 km over the main section of Auckland city and 5 point sources around Auckland (Figure 5.14). The detailed setup of the TAPM model used here is given in Table 5.3.

Table 5.3: Meteorological and pollution grid setup of the TAPM simulations.

| **Grid centre coordinates** | **Latitude = -36.93998° Longitude=174.78°** | | |
|---|---|---|---|
| | Grid 1 | Grid 2 | Grid 3 |
| **Meteorological model setup** | | | |
| Grid spacing (m) | 10000 | 3000 | 1000 |
| Grid points (in X and Y direction) | 98 | 98 | 98 |
| Vertical levels | 35 | 35 | 35 |
| Soil temperature (K) | 292.0 | | |
| Sea surface temperature (K) | 292.0 | | |
| Soil moisture $m^3$ $m^{-3}$ | 0.15 | | |
| **Pollution model set up** | | | |
| Grid spacing (m) | 2500 | 750 | 250 |
| Grid points (in X and Y direction) | 115 x 155 | 115 x 155 | 115 x 155 |
| Area source (m) | 15000 x 10000 | | |
| Area source emissions | 50 g $s^{-1}$ continuous in time (Figure 5.14) | | |
| Points sources | a) Auckland Airport, b) Penrose, c) Henderson, c) Khyber Pass, e) Papakura (Figure 5.14) | | |
| Point source emissions | 50 g $s^{-1}$ from each point source continuous in time. | | |
| Source representation | Lagrangian grid for near-source and Eulerian grid for distant source | | |

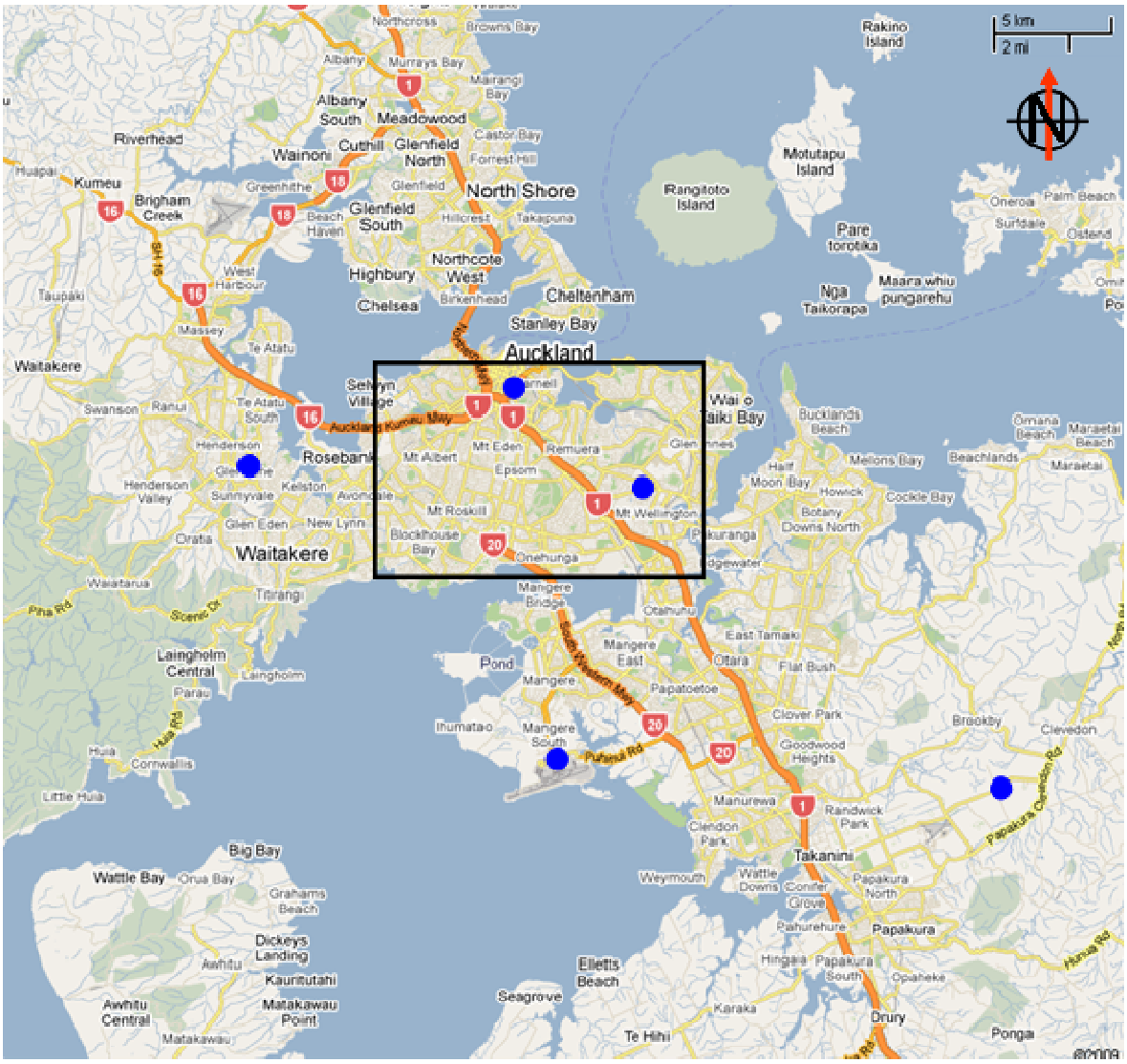


Figure 5.14: Map of the study area. Black rectangle indicates the area source and blue dots indicate point sources. Emission from the area source was 50 g $s^{-1}$ continuous in time and 50 g $s^{-1}$ from each point source, continuous in time.

### 5.8.3 Model Performance Evaluation

The model evaluation was performed for the basic near-surface meteorological variables, namely wind speed, u velocity, v velocity, screen temperature and relative humidity. The model data were extracted from six locations (same as WRF) within the Auckland region and compared with the corresponding observational data. The locations of the AWS used for comparison are indicated in Figure 5.4. The average comparison statistics of these six sites are presented in Table 5.4. Overall, TAPM showed good skill in reproducing the surface meteorology during the eight sea breeze and non-sea breeze days. Except for wind speed that has IOA < 0.80, for the remaining four meteorological variables the IOA was equal to or above 0.80, while Pearson's

correlation coefficient was consistently above 0.70. The average statistics show that, in general, TAPM underestimated both wind speed and near-surface temperature, while on average the predicted near-surface atmosphere was 5% more humid than the observed one. The root mean squared error (RMSE) for all the five surface meteorological variables was lower than the observed standard deviation which reflects relatively small error in the model predictions. Similar to the WRF simulation, RMSEs was lower than RMSEu for wind speed, u and v velocity and it was higher for near-surface temperature and relative humidity. This random error can probably be attributed to uncertainty in initial boundary conditions. On the other hand, the RMSEs was slightly higher for near-surface temperature which was probably attributed to misclassification of land surface characteristics (Zhong et al. 2007). The primary reason for this misclassification could be terrain resolution. The index of agreement for all the five TAPM predicted meteorological variables was smaller than WRF predicted surface meteorology. However, except for screen temperature and relative humidity, the error statistics (RMSE, RMSEs, RMSEu) were higher in the WRF predicted surface winds.

Table 5.4: Comparison statistics for wind speed, u and v velocities, screen temperature and relative humidity for 6 observation sites.

| Meteorological Parameter | Wind speed ($m\ s^{-1}$) | u velocity ($m\ s^{-1}$) | v velocity ($m\ s^{-1}$) | Screen temperature ($^{\circ}C$) | Relative humidity (%) |
|---|---|---|---|---|---|
| Mean Observed | 2.70 | -0.2 | 0.8 | 19.30 | 77.6 |
| Mean Modelled | 2.34 | -0.41 | 0.70 | 18.25 | 82.22 |
| Min. Observed | 0.0 | -12.4 | -4.9 | 12.7 | 43.9 |
| Min. Modelled | 0.0 | -8.3 | -3.5 | 11.3 | 54.2 |
| Max. Observed | 12.4 | 8.1 | 8.1 | 28.4 | 100.0 |
| Max. Modelled | 8.3 | 4.5 | 6.7 | 22.2 | 99.7 |
| Std. Observed | 1.80 | 2.30 | 2.10 | 2.40 | 13.00 |
| Std Modelled | 1.26 | 1.76 | 1.80 | 1.82 | 10.10 |
| Corr. Coeff. | 0.69 | 0.74 | 0.75 | 0.80 | 0.72 |
| IOA | 0.76 | 0.82 | 0.83 | 0.80 | 0.80 |
| RMSE | 1.35 | 1.51 | 1.39 | 2.03 | 10.23 |
| RMSEs | 0.95 | 0.88 | 0.63 | 1.69 | 7.47 |
| RMSEu | 0.89 | 1.14 | 1.15 | 1.10 | 6.94 |

### 5.8.4 Effect of the Sea Breeze on Pollutant Dispersion

The pollution component of TAPM was provided with five arbitrary point sources with an emission rate of 50 g $s^{-1}$. Locations of these point sources are provided in Figure 5.14. TAPM was configured to mix the tracer in the first ground level only.

Appropriate utility was not available to analyse vertical dispersion of the pollutant; therefore, recirculation of the tracer in the vertically rotated sea breeze cell could not be assessed. Although However, horizontal advection and dispersion of the tracer near the surface is examined during three sea breeze and one non-sea breeze days. Figure 5.15 shows advection and transport of the tracer released at 1500 hours from five different locations within the Auckland region. On 19$^{th}$ March 2006, the tracer was trapped in the sea breeze convergence zone that ran through middle of the Auckland City. Figure 5.16 shows parcel trajectories released at 1500 NZST, on the four selected days and indicate advection of air mass towards the convergence area. Under weak northwest gradient winds, TAPM predicted a relatively stronger sea breeze. The resulting SBCZ was thus displaced eastward, but still the horizontal dispersion of the tracer was relatively small and concentrated close to the emission point and/or eastern parts of Auckland City. Although 21$^{st}$ March was similar to 19$^{th}$ March, the wind speed under the northwest gradient wind was slightly higher which advected the tracer southward. The tracer on this day was relatively more dispersed and diffused. TAPM predicted relatively higher concentrations of the tracer on 22$^{nd}$ March, which is consistent with the observed data. The gradient wind flow on this day was easterly to south-easterly, giving a strong southerly component to the predicted surface winds. Under the strong influence of the gradient wind, the predicted sea breeze convergence zones were first predicted in the middle of the land mass but then with increasing strength of the easterly sea breeze, the SBCZs migrated westward. The higher tracer levels were thus predicted along the Manukau Harbour and further west and northwest of Auckland. The higher predicted concentration of tracer on 22$^{nd}$ March appears to be due to the recirculation of tracer under sea-land wind reversal which is an important mechanism that is associated with the sea breeze and is known for increasing pollution levels. Pollutants emitted in the morning hours in the surface layer may be partially advected seawards and return to the source with the well-developed sea breeze. The temporal evolution of the eight-day-long simulation (not shown here) suggests that in the early morning hours on 22$^{nd}$ March, the tracer plume was advected towards Manukau Harbour by remnants of the land breeze. This significantly increased tracer concentration over the Manukau Harbour, although soon after sunrise, bay breezes were initiated and started their journey towards the land mass (Auckland City). The tracer was also advected back to the land by these bay breezes and trapped in the

convergence zone that was predicted over the Auckland City. The non-sea breeze day of 24th March was overwhelmed by the strong southerly flow that blew the tracer northward over the Hauraki Gulf and reduced the tracer concentration to very low levels.

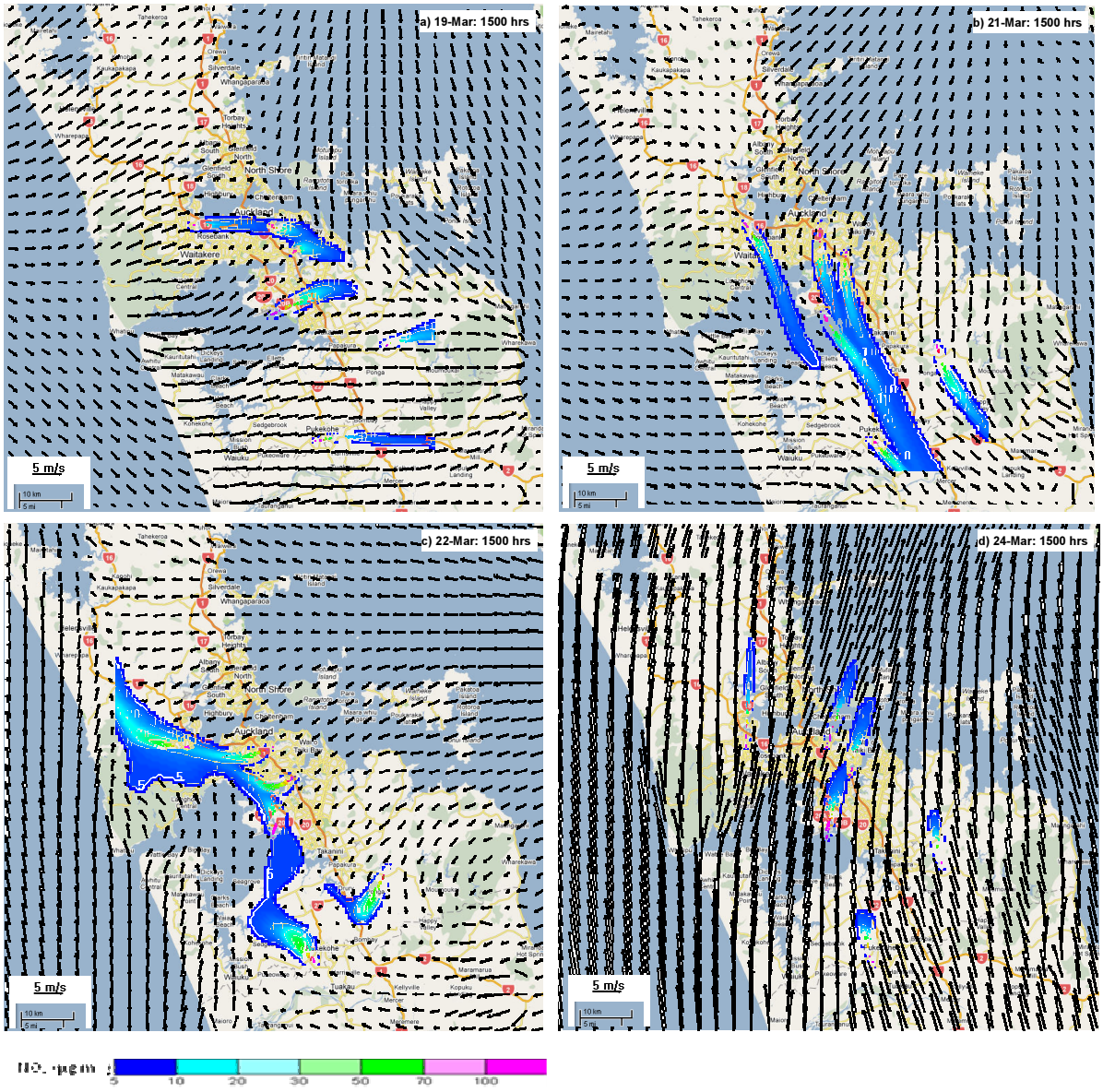


Figure 5.15: Tracer dispersion at 1500 hours on three sea breeze days (19, 21, 22nd March) and one non sea breeze day (24th March).

The maximum daily tracer dispersion on four selected days indicates the correlation between sea breeze meteorology, wind speed and effect of the gradient winds (Figure 5.17). On 19th and 21st March the prevailing winds were blowing from the northwest.

TAPM predicted the highest concentration of tracer on 19th March, when strong sea breeze convergence zones formed over the region due to collision of westerly and easterly sea breezes (Figure 5.17a). TAPM predicted higher concentrations of the tracer in the centre and south Auckland, including such areas as Auckland City downtown, Otahuhu, Mangere and Pakuranga. Most of the higher tracer concentrations were predicted towards the coastline of Waitemata Harbour and Manukau Harbour. The tracer further dispersed to the northeast (Hauraki Gulf), southwest (Manukau Harbour) and southeast (towards Pukekohe) while on 21st March, the higher tracer concentrations were found to the southwest of Auckland City (over Otahuhu, Mangere, etc.) and over Manukau Harbour (Figure 5.17b).

On 22nd March, TAPM predicted a relatively high frequency of southerly winds, with a magnitude also higher than the observed winds, which considerably reduced tracer concentrations, although the higher tracer concentration was still found along a relatively weak SBCZ (Figure 5.17c). The observational data for 22nd March show relatively high concentrations of pollutants. There could be two reasons for this a) TAPM over-predicted surface wind speed so that the southerly winds dispersed the tracer very fast and, b) compared to north-western Auckland, south Auckland is densely populated and more urbanized. A light south-easterly flow was capable of dragging pollutants from south Auckland to Auckland City where higher concentrations of various pollutants, especially $NO_x$ were observed. Since we did not use real emission data or an emission inventory for this simulation, the predicted tracer values were unable to show the effect of pollutant transport from south Auckland to Auckland City. On the non-sea breeze day of 24th March, although surface winds were southerly to south-westerly, the higher magnitude of the surface winds flushed the region and did not allow the higher concentrations of the tracer to occur at any time or location.

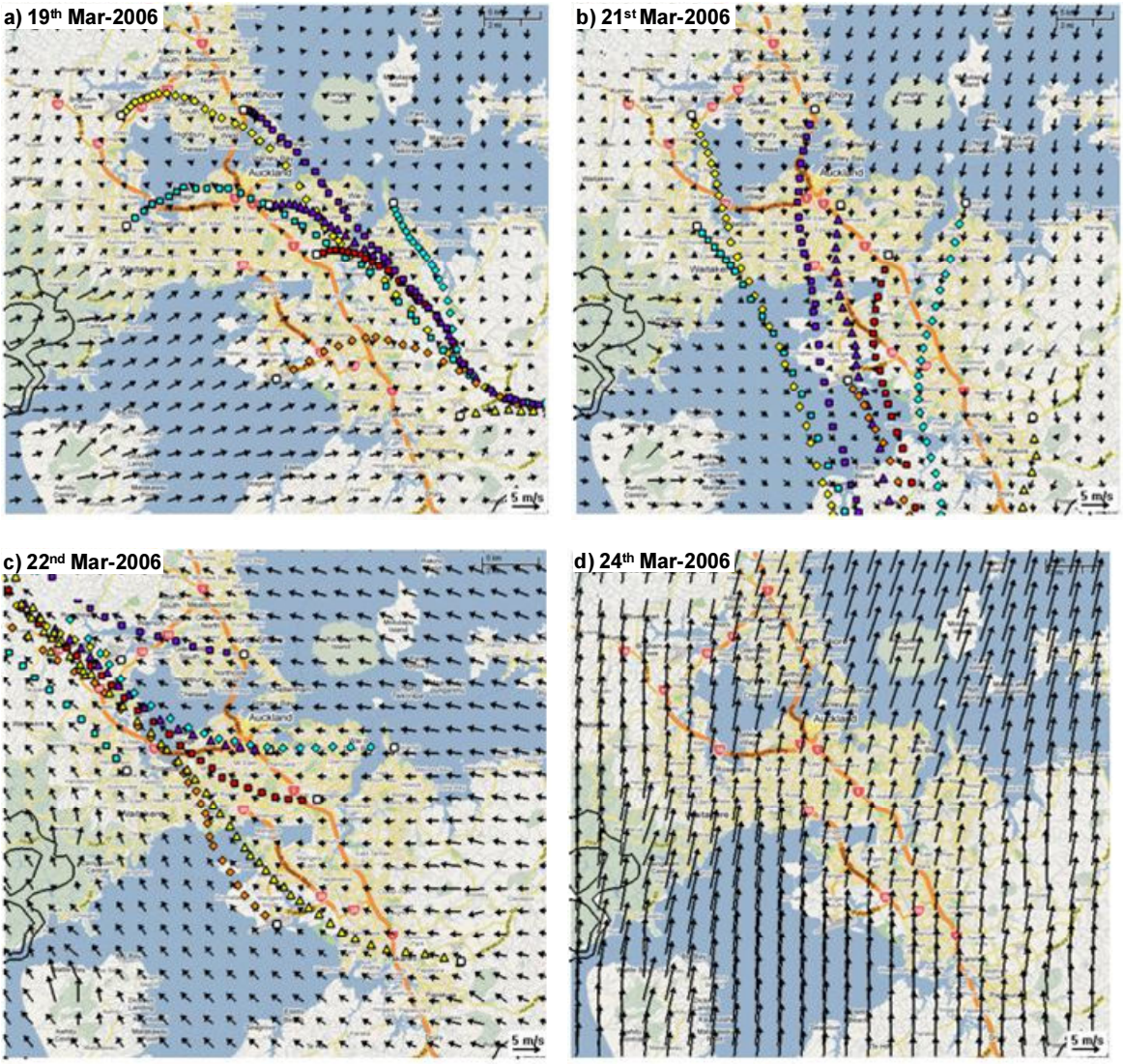


Figure 5.16: Plots of predicted parcel trajectories released at 1500 NZST from six locations on three sea breeze and one non-sea breeze days. Colour and shapes of the trajectory symbols indicates different point sources.

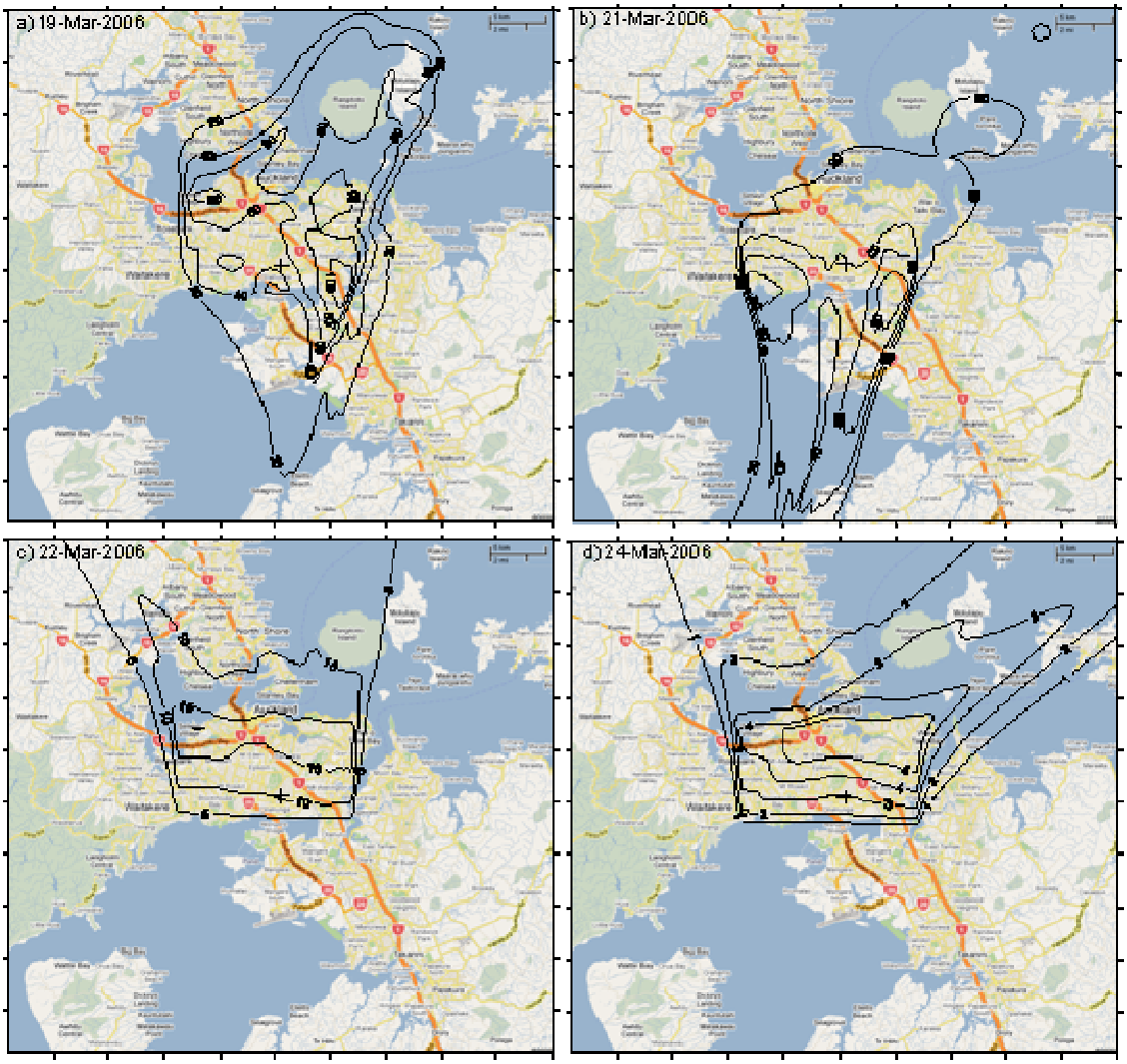


Figure 5.17: Contour plots of daily highest concentration for three sea breeze and one non-sea breeze day.

## 5.9 Summary of Results

The primary objective of this chapter was to improve our understanding of the local meteorology of the Auckland region during sea breeze events, as well as to investigate the pollution potential of the thermally forced circulation in the complex terrain of the Auckland region. Two mesoscale numerical models (WRF and TAPM) were employed for this purpose. Model evaluation of the meteorological components of both models was also conducted to establish the degree of trust in the model results.

Both WRF and TAPM models showed high skill in reproducing surface meteorology in the eight-day-long simulations, although the index of agreement for TAPM predicted wind speed was lower than the WRF predicted wind speed. The WRF model generally over-predicted surface winds, which shows the inability of the surface layer scheme to simulate low velocity winds. Additionally, except for Henderson, WRF showed a cold bias in 2 m near-surface temperature at the remaining five AWS. This cold bias in the near-surface temperature is primarily associated with the misclassification of surface characteristics by the Noah land surface model, while heat and moisture exchange coefficients supplied to Noah LSM by the PBL coupled surface layer formulation may also have indirect influence on the near surface temperature. Zhong et al. (2007) also reported consistent underestimation of temperature by the Eta PBL (MYJ) scheme and linked it with the larger latent heat flux from the model surface energy calculation, that is partially attributed to heat and moisture exchange coefficients that were supplied to the Noah LSM. At Auckland Airport, WRF could not predict north-easterly winds accurately on the evening of 21$^{st}$ March when due to dominant northwest prevailing flow, land breezes started early. On 23$^{rd}$ March between 0000 – 0600 NZST, WRF predicted an early onset of bay breezes from Waitemata harbour and incorrectly simulated the observed south-westerly land breeze as south-easterly winds. The index of agreement for wind speed and u velocity was also lower for Khyber Pass, due partly to the canyon effect. At Whangaparaoa, WRF failed to predict calms on 19$^{th}$ and 20$^{th}$ March from 000 to 0600 NZST. However, it is possible that these calms with zero wind speed are due to instrument error.

TAPM on the other hand under-predicted both surface winds and the 2 m surface temperature. The RMSEu values for wind speed, u and v-component for both WRF and TAPM were higher than the RMSEs values, which indicate a relatively high magnitude of random error in the predicted winds. However, both models showed higher RMSEs for near surface-temperature and relative humidity, which indicates misclassification of surface characteristics by the land surface scheme. In general, the WRF simulated temperature field was in better agreement with observed data, with almost the same magnitude of RMSEs and RMSEu at urban sites such as Khyber Pass, Auckland Airport and Henderson. This shows a higher skill of land surface parameterization in simulating the urban built environment, as well as better representation of urban characteristics in the model. WRF simulated vertical structure was also in good agreement with the observed vertical profile of winds and temperature at Whenuapai AWS. On 22$^{nd}$ and 24$^{th}$ March, WRF also successfully predicted two low level jets, but again overestimated wind speed.

Two distinct thermally induced circulations occurred about Auckland. The bay breezes onset at around 0900 hours from harbours and were followed by mature sea breezes from the Tasman Sea and Hauraki Gulf. The sea breezes normally decay after 1600 NZST. Although wind rotation over the west and the east coast was anticlockwise, near harbour coastlines the diurnal rotation of winds during sea breeze days was more complex. For example, at Whangaparaoa and Pukekohe predicted winds generally showed an anticlockwise rotation, while at Auckland Airport the wind rotation on sea breeze days was clockwise, which is against the general principle that is based on the balance between the pressure gradient and Coriolis force. However, rotation of thermally forced winds in the opposite direction has been observed in many other parts of the world (e.g. Kusuda & Alpert 1983; Neumann 1977,1984) and is generally caused by an imbalance between the large scale pressure gradient and the mesoscale pressure gradient force and Coriolis force. These results are consistent with the observed pattern of diurnal rotation during sea breeze days at Auckland Airport and stations located on the east coast (see Chapter 4).

The predicted easterly sea breeze inflow was stronger during north-westerly gradient flow and the consequent SBCZs were gradually pushed towards the west coast. On the other hand, the south-westerly sea breeze inflow from the west coast was stronger

during southerly gradient wind conditions and pushed the SBCZ eastward. TAPM on the other hand predicted enhanced westerly flow under a northwest gradient wind and an enhanced easterly sea breeze under south-easterly gradient flow. As a result, tracer was also dispersed accordingly.

From morning to early afternoon hours, the predicted bay breezes formed primary SBCZs along and/near the harbour coastlines that merged into a few mature SBCZs due to collision of mature east and west coast sea breezes later in the day. Bay breezes were generated at around 0900 hours along the harbour coastlines and higher terrain over the east and west coasts, while mature sea breezes onset at around 1000 hours over both east and west coasts. The sea breeze started decaying after 1600 hours, although timing was subject to the direction and strength of the gradient wind. Under northerly gradient flow, the easterly sea breeze lasts longer, while under southerly gradient flow cessation of the westerly sea breeze was delayed. The depth of the predicted sea breeze inflow layer varied from 200 to 600 m, while the depth of the return flow was approximated between 100 to 300 m.

Although WRF predicted mixed layer depth was in good agreement with the observed one, no consistent patterns were found. For example, on 19$^{th}$ March, WRF overestimated mixed layer by almost 100%, while on the non-sea breeze day of 24$^{th}$ March, WRF underestimated mixed layer height by only100 m. The convective internal boundary layer (CIBL) was formed on most of the sea breeze days and marked by collapse of the mixed layer height, a drop in near-surface air temperature and sometimes (but not always) an increase in moisture content. The depth of the CIBL varied from 150 to 400 m.

The residual layer started forming after 1800 hours at around 100 m above ground while its depth varied from 200 to 800 m. Pollutants emitted during the evening peak traffic hours could be trapped in this layer and if not advected away from the source due to gradient wind forcing, they may increase pollutant levels the following morning. This will be discussed in greater detail in Chapter 6.

The air parcel trajectories and dispersion modelling results predicted higher tracer concentration in and around convergence zones. During three sea breeze days, the model predicted high tracer concentrations at Otahuhu, Mangere, Pakuranga and the Auckland City downtown area. Under northwest gradient winds the higher pollutant concentration were predicted near the east coast, southeast and southwest of Auckland, while under southerly gradient winds, higher pollutant concentration were predicted to the west and northwest and centre of Auckland City. Recirculation due to sea-land wind reversal is more likely under relatively weak southerly wind conditions. The recirculation of pollutants may significantly increase the pollutant concentration during daytime. Under these conditions, the higher concentrations can be expected in the centre, to the west and the northwest of the City.

# 6. The Effect of Gradient Winds on the Sea Breeze Circulation

## 6.1 Introduction

It has long been long known that the direction and strength of the large scale flow affects the structure and evolution of sea breezes. Gradient winds coupled with topographic features and latitudinal position can have a significant effect on sea breeze characteristics (Miao et al. 2003,2006a; Thompson 1998; Zhong & Takle 1993). In complex terrain, such as the Auckland region, interaction of the gradient wind with an irregular coastline and undulating terrain results in complex airflows. Chapter 4 utilized data from an automated surface network of monitoring sites (meteorological and air quality) to investigate interaction of sea breeze dynamics with large scale processes, orographic features and their potential role in the air quality of the Auckland region. The observational analysis raised several underlying questions with respect to interaction between large scale processes and local scale sea breeze meteorology, such as:

- Do gradient winds have any role in the clockwise instead of anticlockwise diurnal rotation of sea breeze that are sometimes observed?
- Is the height and inland extent of the convective internal boundary layer (CIBL) affected under varying gradient wind conditions?
- How do gradient winds affect the structure of the sea breeze circulation cell especially under northwest and southeast gradient wind conditions?

- How do gradient winds affect the position and strength of the sea breeze convergence zones (SBCZ)?
- How do variations in sea breeze characteristics affect the air quality of the Auckland region?

There is a sufficient number of meteorological monitoring sites in the main urban areas of the Auckland region, but data are quite sparse around rest of the region (Gimson 2005). Most of these automated weather stations (AWS) are installed primarily to monitor the air quality in the densely populated urban areas and therefore, position of these monitoring stations is either in the middle or east of the region, but not a single AWS is located anywhere on the entire west coast of the Auckland region. The orientation, alignment and position of most of these stations are also adjusted to suit the pollutant monitoring needs. Data quality (missing and incorrect data) and temporal resolution are some added issues that hamper the detailed investigation of complex flows such as sea-land breezes. In this chapter an idealized modelling technique has been utilized to address the above questions and investigate the role of sea breeze dynamics in various pollution dispersion mechanisms under different gradient wind conditions.

## 6.2 Model Setup

Advanced Research WRF modelling system (version 3.01) was employed to examine the effect of variability in large scale winds on the sea breeze system. For a detailed description of the WRF model please see Chapter 5. Four idealized experiments were set up with four gradient wind directions, namely northeast, southeast, southwest and northwest. The southwest and northeast directions are normal to the west and east coasts of Auckland, whereas northwest and southeast directions are sub-parallel to the land mass. All the four simulations were initialized in the stable atmosphere at night time (0000 NZST) with a constant wind speed of 3.0 m $s^{-1}$ throughout the depth of the atmosphere. Table 6.1 shows the model setup for these simulations.

Table 6.1: Model setup of four idealized simulations

| **Idealized simulations** | **a) 101bx: Northeast gradient wind,**<br>**b) 101by: Northwest gradient wind,**<br>**c) 101bz: Southwest gradient wind,**<br>**d) 101ca: Southeast gradient wind.** |
|---|---|
| Initial wind speed | 3.0 m $s^{-1}$ |
| Terrain resolution | 2 minutes (approximately 4.0 km) |
| No of grids | 3 |
| Grid resolution | Grid domain 1: D01 = 3000 m,<br>Grid domain 2: D02 = 1000 m,<br>Grid domain 3: D03 = 500 m. |
| Grid points | D01 = 199; D02 = 199; D03 = 197 |
| Meteorological data | NCEP FNL re-analysis data |
| Terrain data | Land Information New Zealand (LINZ) and Terralink New Zealand |
| Land surface scheme | Noah: A unified NCEP/NCAR scheme with soil<br>temperature and moisture in four soil layers. |
| PBL scheme | Mellor Yamada-Janjic: One-dimensional<br>prognostic turbulent kinetic energy scheme with local vertical mixing |
| Explicit moisture | Lin et al. |
| Surface layer scheme | Eta similarity: based on Monin-Obukhov with Zilitinkevich<br>thermal roughness length and standard similarity functions from look-up tables<br>(National Center for Atmospheric Research-USA 2008). |
| Radiation | Dudhia scheme for shortwave radiation, Rapid radiative transfer model (RRTM) for long wave radiation. |
| Convection | Kain and Fritsch scheme on the outer grid domain, D01 only. |

The physics and dynamics options used in the four simulations were the same as 101cg (see Chapter 5 for details). To run WRF in three dimensional idealized mode with a fixed background wind field, a technique was devised so that the model could ingest user defined initial and lateral boundary conditions. Initially, NCEP FNL reanalysis meteorological data and USGS terrain data were used to prepare horizontally interpolated meteorological (met_em_*) files. Before vertical interpolation by the WRF initialization program 'real.exe', the meteorological files (met_em_*) were modified to get the desired background wind field. For this purpose, again NCEP FNL re-analysis files were used to obtain vertical profiles of pressure, geopotential, air temperature, and mean sea level pressure from a single point over the sea at the simulation start time. These profiles were then replaced with the real interpolated data in the met_em_* files in all 27 levels in three grid domains. The relative humidity was also replaced with a constant 30% value for all 27 vertical levels. For pressure and geopotential, the sea level profiles were replaced from level 2 to level 27 so that variations in the

meteorological fields due to topography could be taken into account. To ingest background winds with four different wind directions and a constant 3 m $s^{-1}$ wind speed, the west-east and north-south component of the wind in met_em_* files were replaced with the following values for each simulation separately.

Simulation with 3.0 m $s^{-1}$ northeast background wind (101bx)

West-east u velocity -2.12 m $s^{-1}$

South-north v velocity -2.12 m $s^{-1}$

Simulation with 3.0 m $s^{-1}$ northwest background wind (101by)

West-east u velocity 2.12 m $s^{-1}$

South-north v velocity -2.12 m $s^{-1}$

Simulation with 3.0 m $s^{-1}$ southwest background wind (101bz)

West-east u velocity 2.12 m $s^{-1}$

South-north v velocity 2.12 m $s^{-1}$

Simulation with 3.0 m $s^{-1}$ southeast background wind (101ca)

West-east u velocity -2.12 m $s^{-1}$

South-north v velocity 2.12 m $s^{-1}$

The modified meteorological (met_em_*) files were then processed to prepare initial and lateral boundary condition files for WRF using initialization program 'real.exe'. Once the initial and boundary condition files were successfully prepared, the WRF model was then run in real mode (em_real) for all the four simulations. Unfortunately, the initial and boundary conditions setup for constant background winds did not work properly (except for northeast gradient winds), because the geostrophic balance could not be properly achieved for the large scale winds. The primary reason for this imbalance was that the Coriolis term in the WRF model could not be kept constant in the model which consequently deflected the geostrophic wind, by rotating it to the left. The WRF model developers at NCAR (National Centre for Atmospheric Research, USA) suggested two possible solutions to fix this problem, a) change the code, and recompile the model, or b) define u_base and v_base (the base state wind) in the initial condition files (wrfinput_d0*), and then run the model with pert_coriolis (Coriolis to be

applied only on the perturbation) option. However, all this correspondence and experimentation took a long time and therefore it was decided to use slightly deflected synoptic winds of the simulations from 101bx to 101ca instead. After balancing the pressure gradient force (PGF) with the Coriolis force, the resultant gradient wind directions were as follows:

Southeast gradient wind → ESE (east of southeast); hereinafter referred to as $ESE_{gw}$
Southwest gradient wind →SSW (south of southwest); hereinafter referred to as $SSW_{gw}$.
Northwest gradient wind →WNW (west of northwest); hereinafter referred to as $WNW_{gw}$
Northeast gradient wind → NE (remained northeast wind); hereinafter referred to as $NE_{gw}$.

For brevity the subscript 'gw' has been removed from figure titles. In the analysis given below, the resultant gradient wind is referred to as the actual gradient wind. The schematic in Figure 6.1 shows the locations of the time series data extraction points and vertical cross-section (AA`) from the model results of the four simulations.

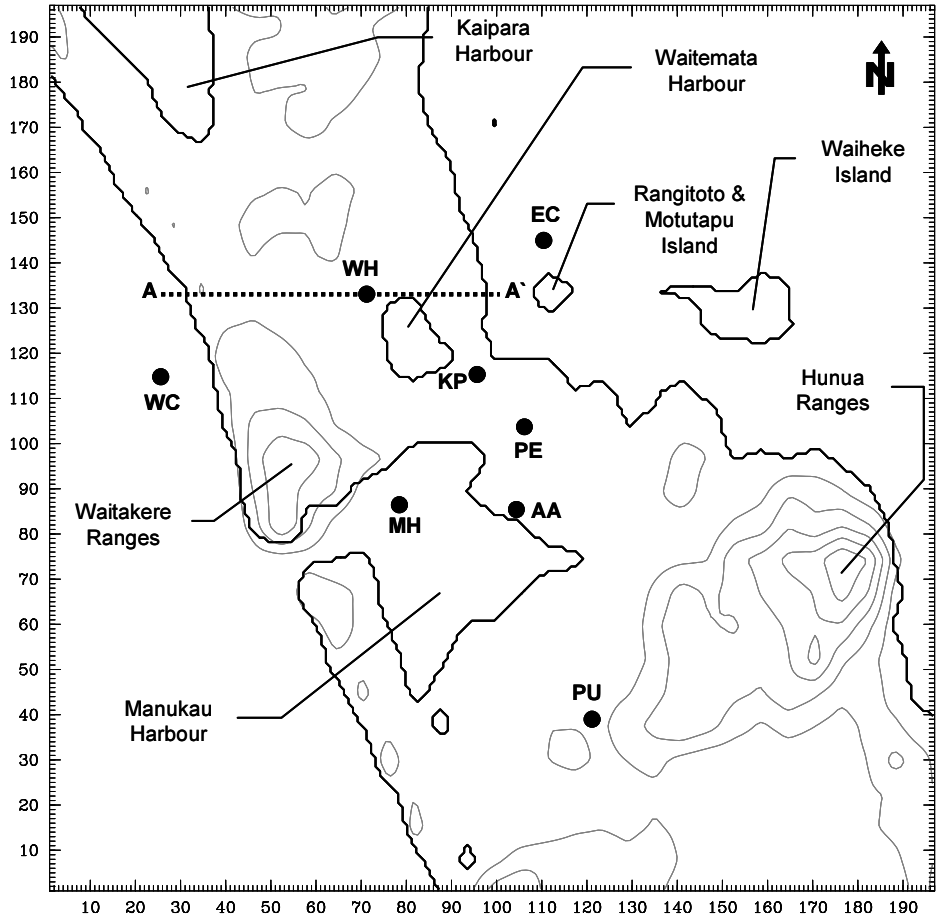


Figure 6.1: Map of the Auckland region with 4 kilometre terrain resolution. AA` : The vertical cross- section; WH: Whenuapai; EC: East coast data extraction point over Hauraki Gulf; WC: West coast data extraction point over the Tasman Sea; KP: Khyber Pass; PE: Penrose; AA: Auckland Airport; MH: Data extraction point over the Manukau Harbour; PU: Pukekohe

## 6.3 Diurnal Rotation of Sea and Land Breeze

Diurnal rotation of the sea breeze is a basic feature of sea and land breeze circulation systems. Since the sea breeze over the Auckland region occurs on both sides of the peninsula, theoretically the east and the west coast winds should rotate in an anticlockwise direction and remain in opposite directions to each other throughout the diurnal cycle. Figure 6.2 shows the diurnal cycle of 10 m winds under four gradient wind conditions at three locations (east coast, west coast and Auckland Airport). The complete anticlockwise rotation of diurnal winds was predicted on the east and west coasts only under gradient winds with a strong easterly component, which are $NE_{gw}$ and $ESE_{gw}$ (Figure 6.2a, 6.2b, 6.2j and 6.2k). Under gradient winds with a strong westerly component ($WNW_{gw}$ and $SSW_{gw}$), WRF predicted an incomplete rotation over both

coasts and the predicted surface winds moved back and forth along the respective gradient wind direction (6.2d, 6.2e, 6.2g, 6.2h). At the inland station of Auckland Airport, none of the simulations predicted a complete clockwise or anticlockwise rotation. The predicted winds rather showed a strong gradient wind effect instead (Figure 6.2c, 6.2f, 6.2i, 6.2l). Although the observed data and predicted surface winds from the real simulation (101cg) showed clockwise rotation at the Auckland Airport on 18$^{th}$ and 19$^{th}$ March (not shown here), WRF predicted a consistent back and forth movement of surface winds along the four gradient winds. An interesting feature of this incomplete rotation is that over the two coasts, winds first rotated anticlockwise for few hours and then rotated backward in a clockwise sense. However, at Auckland Airport under all four gradient wind conditions, wind first rotated clockwise and later in the day rotated backward in anticlockwise sense. This indicates the difference in the natural tendency of the wind rotation between the coasts and Auckland Airport. Over the coast, the wind tried to rotate anticlockwise, but after a few hours due to large scale wind forcing with strong westerly component they rotated backward, while at the inland station of Auckland Airport, mesoscale winds first tried to rotate clockwise but the large scale winds coupled with sea-land gradient forced them to rotate backward, as anticlockwise.

Previous work on sea-land breeze rotation characteristics found that clockwise or anticlockwise rotation and variation in rotation (incomplete rotation or no rotation) is a function of a suitable combination of the Coriolis force and pressure gradient force while the strong pressure gradient associated with mountains and/or topographical influences such as friction can often be responsible for clockwise, rather than anticlockwise rotation (Dexter 1958; Kusuda & Alpert 1983; Neumann 1977,1984; Neumann & Mahrer 1971; Orlic et al. 1988; Physick & Byron-Scott 1977; Simpson 1995; Staley 1957). Kusuda & Alpert (1983) suggested two mechanisms for a clockwise (in the Southern Hemisphere), instead of anticlockwise rotation. First is the penetration of the sea breeze into the lee region of a coastal mountain range, and second is the horizontal phase shift of some critical quantity such as temperature or pressure that is caused by the inhomogeneous characteristics of the surface boundary layer. Given the complex coastline and presence of two low elevation mountain ranges (Waitakere and Hunua) to the northwest and southeast of Auckland Airport, the above

two mechanisms appear to be responsible for the clockwise rotation at Auckland Airport. This argument is further supported by the fact that both observed data and the higher resolution (500 m) real simulation showed a complete clockwise rotation at Auckland Airport.

Neumann (1977) in his ground breaking study on sea-land breeze rotation found that if the surface and gradient winds are in the same direction, the sea or land breeze will lose its rotational characteristic. On the other hand, if surface winds and gradient winds are in opposite directions the sea breeze will be parallel to the coastline and any further rotation will be inhibited unless it is the morning or evening time of the day. To a certain extent, this explains what happens to the sea-land breeze rotation in the Auckland case where land-sea breeze rotation was hindered when the sea breeze and gradient winds were in the same direction (e.g. Figure 6.2h) and the sea breeze tends to be shore parallel when it is opposite to the gradient wind (e.g. Figure 6.2g). The rate of rotation in the four experiments was not constant over time. In almost all cases, the rotation rate was higher during morning and evening time of the day, while it was slow during afternoon and night time. This is consistent with the results of Dexter (1958) and Neumann (1977) who suggested that the interaction of the pressure gradient force, the friction force and Coriolis force with the wind vector modifies the rotation rate of the sea-land breeze system.

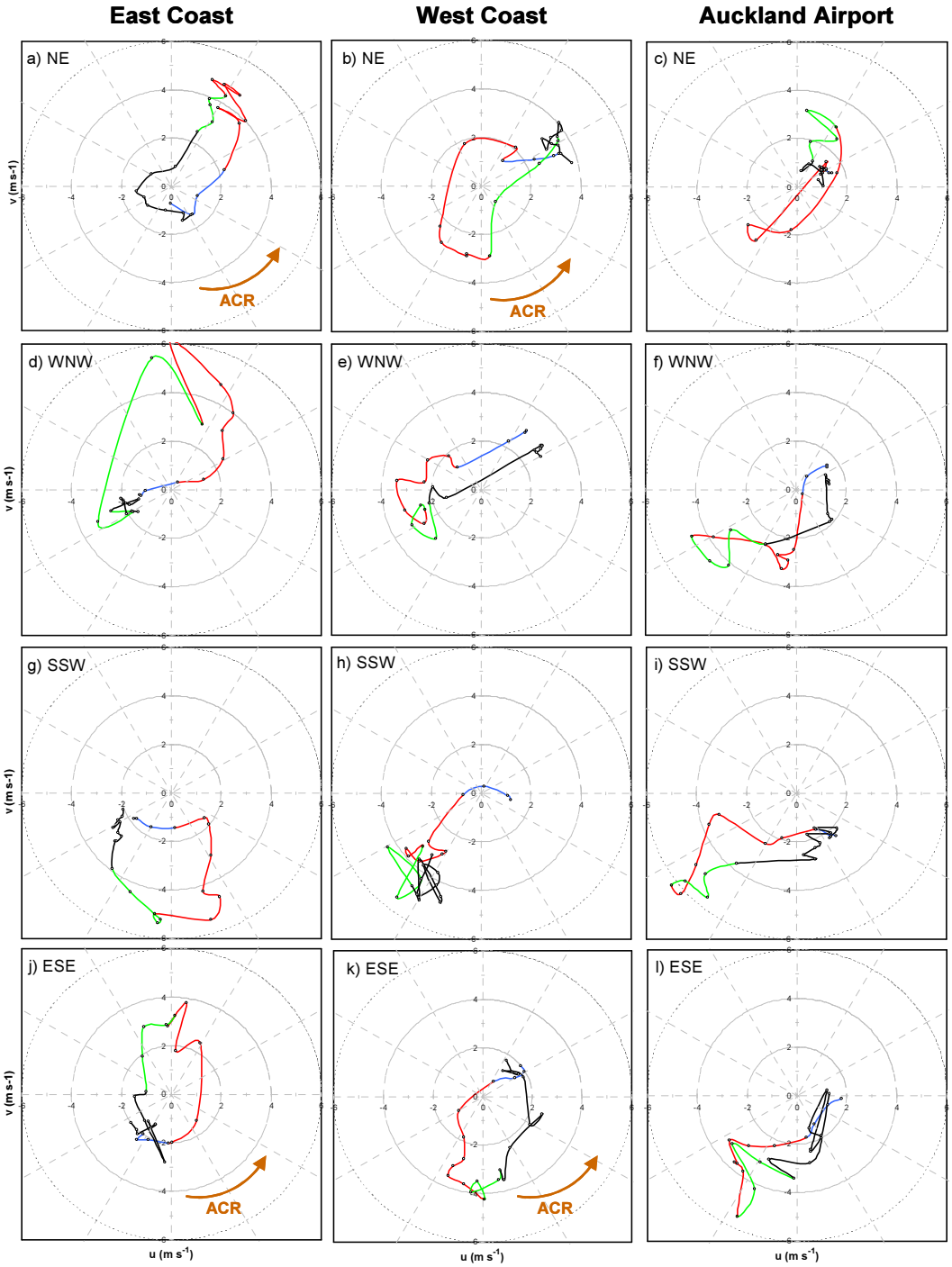


Figure 6.2: The 24 hour model predicted wind rotation 10 m above ground level from 0600 hours to 0500 hours the next morning from three locations in the Auckland region under four gradient wind conditions. Station locations are shown in Figure 6.1 (EC: East coast, WC: West coast, and AA: Auckland Airport). Blue line shows u and v from 0600 to 0900 hours, red line shows winds from 1000 to 1600 hours, green line shows wind from 1700 to 2000 hours while the rest of the time is indicated with black colour. The u and v components are reversed for easy understanding. This means data points falling in any wind quadrant of the hodograph, depicts wind direction of that quadrant. All times are NZST.

Terrain and local orographic features may affect the diurnal rotation in many ways. One feature of the terrain-induced local meteorology was the relatively higher wind

speed of the predicted westerly winds at Manukau Head. During westerly gradient wind flow the entrance to the Manukau Head provided a narrow opening to the westerly sea breeze. Following the continuity equation of conservation of momentum (Pielke 2002; Stull 2003), the model predicted relatively higher wind speeds (>= 6 m $s^{-1}$) over the Manukau Harbour during afternoon hours under $WNW_{gw}$ and $SSW_{gw}$ due to channelling of westerly winds over the Manukau Head (Figure 6.3). The predicted surface wind speed under $ESE_{gw}$ was comparable to surface winds under $WNW_{gw}$ and $SSW_{gw}$ for a few hours in the late afternoon when the predicted westerly sea breeze was strong enough to penetrate inland. Under $NE_{gw}$, however, the wind speed over Manukau Harbour was very low, especially during afternoon hours due to continuous north-easterly flow. The channelling and acceleration of wind speed over Manukau Harbour on one hand reduced the rotation rate, while on the other hand it helped in pushing the air over the land mass towards Hauraki Gulf under westerly gradient wind flow conditions. This wind acceleration is also reflected in the observational data from Auckland Airport and Mangere stations.

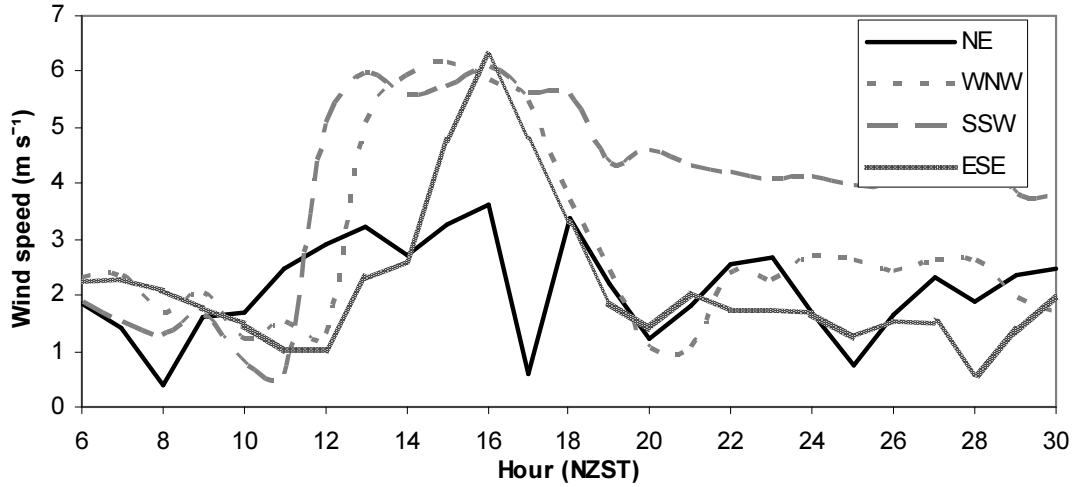


Figure 6.3: Time series of the wind speed 10 m agl over water inside Manukau Harbour (location MH: Manukau Harbour, shown in Figure 6.1) under different gradient wind regimes.

## 6.4 Convergence Zones

Sea breeze convergence zones are characterized as areas with low wind speed, higher vertical velocity and, consequently, a higher planetary boundary layer (PBL). The dome-like shape of the PBL in areas of sea breeze convergence is especially important with respect to air pollution applications (Liu & Chan 2002b). The SBCZs carry these characteristics as they migrate towards either coast. The three dimensional structure of SBCZs has been studied under the four gradient wind conditions to understand their role and interaction with pollution dispersion mechanisms. In Figure 6.4 to 6.7, the surface wind field at 10 m above ground level and vertical velocities (colour shaded) at 500 m above ground level are presented for 1000, 1200, 1500 and 1800 NZST to show the temporal and spatial evolution of the sea breeze and associated sea breeze convergence zones (SBCZs) that are predicted during daytime over the Auckland region. A SBCZ may be defined as an area where two or more thermally-induced airflows either from main bodies of water such as Tasman Sea and Hauraki Gulf or small bodies of water such as Manukau, Waitemata and Kaipara Harbour, or any combination of the above, converge to form areas of relatively low horizontal and high vertical velocities. The SBCZs are identified as areas where the vertical velocity field shows a continuous band of intense upward motion. In the four simulations, the predicted maximum updraft velocity at 500 m above ground level was of the order of 3.2 m $s^{-1}$, while the maximum downdraft velocity was 2.9 m $s^{-1}$.

### 6.4.1 Northeast Gradient Flow ($NE_{gw}$)

The $NE_{gw}$ flow is normal to the coastline either side of the Auckland. During day-time the gradient wind enhanced north-easterly sea breeze dominated the region and restricted the opposing south-westerly sea breezes to the southwest coastline. In the morning hours, WRF predicted terrain-induced convergence near higher elevation terrain of the Waitakere and Hunua Ranges (Figure 6.4a). The first convergence line was formed between 0900 to 1000 hours at the foothills west of the Waitakere Ranges near Manukau Head, due to the collision between down-slope north-easterlies and elementary south-westerly sea breezes. The second convergence line was predicted to the lee side (southwest) of the Hunua Ranges due to convergence of two north-easterly flows (to counter balance the terrain-induced low) that were split due to the mountain

range. From mid to late morning, increased convection enhanced vertical air motion, and ascending and descending thermal cells increased the PBL height over the region. The increasing thermal difference between land and sea enhanced the predicted strength and inland penetration of the sea breeze with time. Between late morning and early afternoon (1100 to 1300 hours) three more convergence lines were predicted. The first strong convergence line was formed between westerly sea breeze and gradient wind enhanced easterly sea breeze along the west coast to the north of Auckland; second to the east and south of Kaipara Harbour between a bay breeze from the Kaipara Harbour and the easterly sea breeze; and the third convergence line was predicted around the Manukau Harbour due to convergence between the bay breeze from the harbour and the easterly sea breeze (Figure 6.4b). In the afternoon hours (1400 to 1600 hours) the model predicted intense convergence between the south-westerly sea breeze and gradient wind enhanced north-easterly sea breezes. A strong SBCZ was predicted along the entire west coast, as well as around the Manukau Harbour, while the two convergence zones around Kaipara Harbour and southwest of Hunua remained intact until late afternoon (Figure 6.4c).

After 1700 hours, with the weakening thermal gradient and sea breeze rotation, the convergence zones started collapsing (Figure 6.4d). However, a weak SBCZ between west and east coast sea breezes also persisted until late evening to the south and southeast of Manukau Harbour, parallel to the land mass. The terrain-induced convergence line west of the Hunua Ranges also gradually migrated to the south due to the rotation of the thermally induced winds. After 2000 hours, stable atmospheric conditions suppressed most of the convergence in the region.

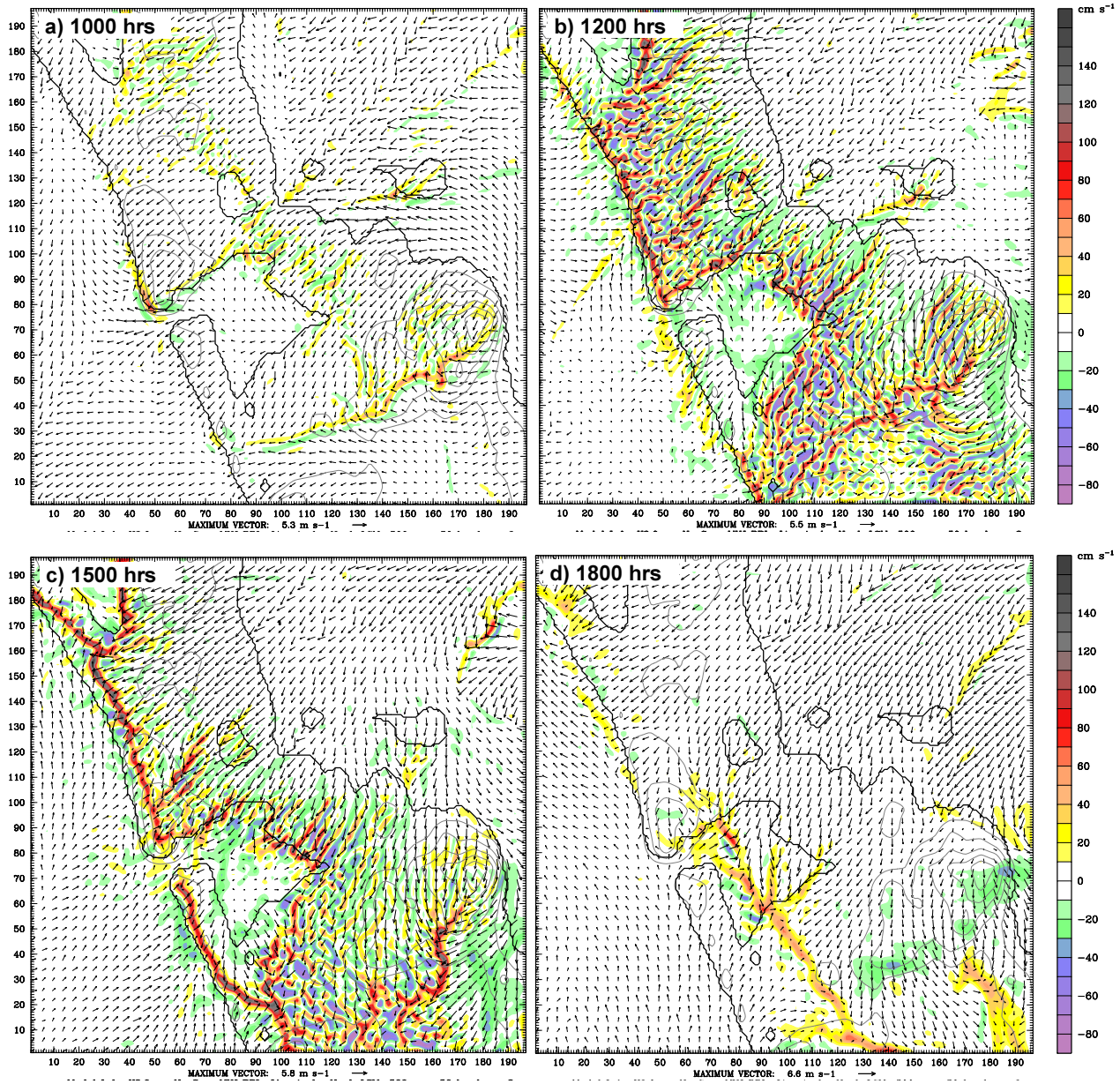


Figure 6.4: Sea breeze convergence zones over the Auckland region under $NE_{gw}$ at 1000, 1200, 1500 and 1800 NZST. Wind vectors are at 10 m above ground and vertical velocity (colour shaded) is plotted at 500 m above ground level.

### 6.4.2 West-Northwest Gradient Flow ($WNW_{gw}$)

The $WNW_{gw}$ was sub-parallel to the land mass and due to a strong westerly component, the $WNW_{gw}$ enhanced the westerly sea breeze. Although the first few convergence lines were again predicted around the higher terrain of the Waitakere and Hunua Ranges, in the mid-morning hours the eastward moving westerly sea breeze front displaced the small convergence line around the southeast side of the Waitakere Ranges and also converged with the bay breezes west of Kaipara Harbour, whereas the position of convergence line around the Hunua Ranges was attributed to the easterly

sea breeze front (Figure 6.5a). The $WNW_{gw}$ enhanced westerly sea breeze front rapidly moved inland and by 1200 hours, its horizontal extent was up to 30 km. However, the eastward movement of the westerly sea breeze was inhibited around Kaipara and Manukau Harbours due to strengthening of the SBCZs that were formed in the morning hours over the western and south-western borders of the two inland water bodies (Figure 6.5b). On the other hand, the easterly sea breeze could not penetrate inland and remained close to the east coast. The interaction between the cold, dense easterly sea breeze and warm land air resulted in strong convergence along the east coast. Near the Hunua Ranges, the inland extent of the anabatic wind-enhanced easterly sea breeze was almost three times the extent of the easterly sea breeze front over north of Auckland. The interaction of the bay breezes from Waitemata Harbour and Manukau Harbour with each other and with the mature sea breezes from the west and the east coast resulted in a ring shaped SBCZ around Waitemata Harbour. This SBCZ extended through the centre of Auckland City and also joined the terrain-induced convergence zone that was formed east of the Waitakere Ranges. Between the two sea breeze fronts, the predicted thermal cells over land resulted in a rapidly increasing PBL. The inland movement of cold marine air mass from either coast suppressed vertical motion, which resulted in stratification of the thermal structure of the atmosphere and formation of a thermal internal boundary layer over land (Figure 6.8b).

In the afternoon (1400 to 1600 hours), the eastward propagating westerly sea breeze front formed a strong SBCZ with the opposing easterly sea breeze almost along the entire length of the east coast (Figure 6.5c). The convergence line east of the Waitakere Ranges was further displaced eastward due to increasing strength and inland penetration of westerly sea breezes from both the Waitakere Ranges and the gap flow enhanced winds from Manukau Harbour. No major convergence line was predicted in a small section west of the Hunua Ranges and reflects a strong effect of terrain on the position and strength of the convergence zone. The terrain effects are discussed in greater detail in Chapter 7. After 1600 hours the SBCZs were gradually pushed eastward over the Hauraki Gulf, so that in the evening (1800 hour) only one sea breeze convergence zone was predicted on the eastern border of Auckland City. The persistence of this SBCZ can be attributed to the urban heat island effect and absence of

any significant higher terrain in this area. After 2000 hours the SBCZs had almost disappeared (Figure 6.5d).

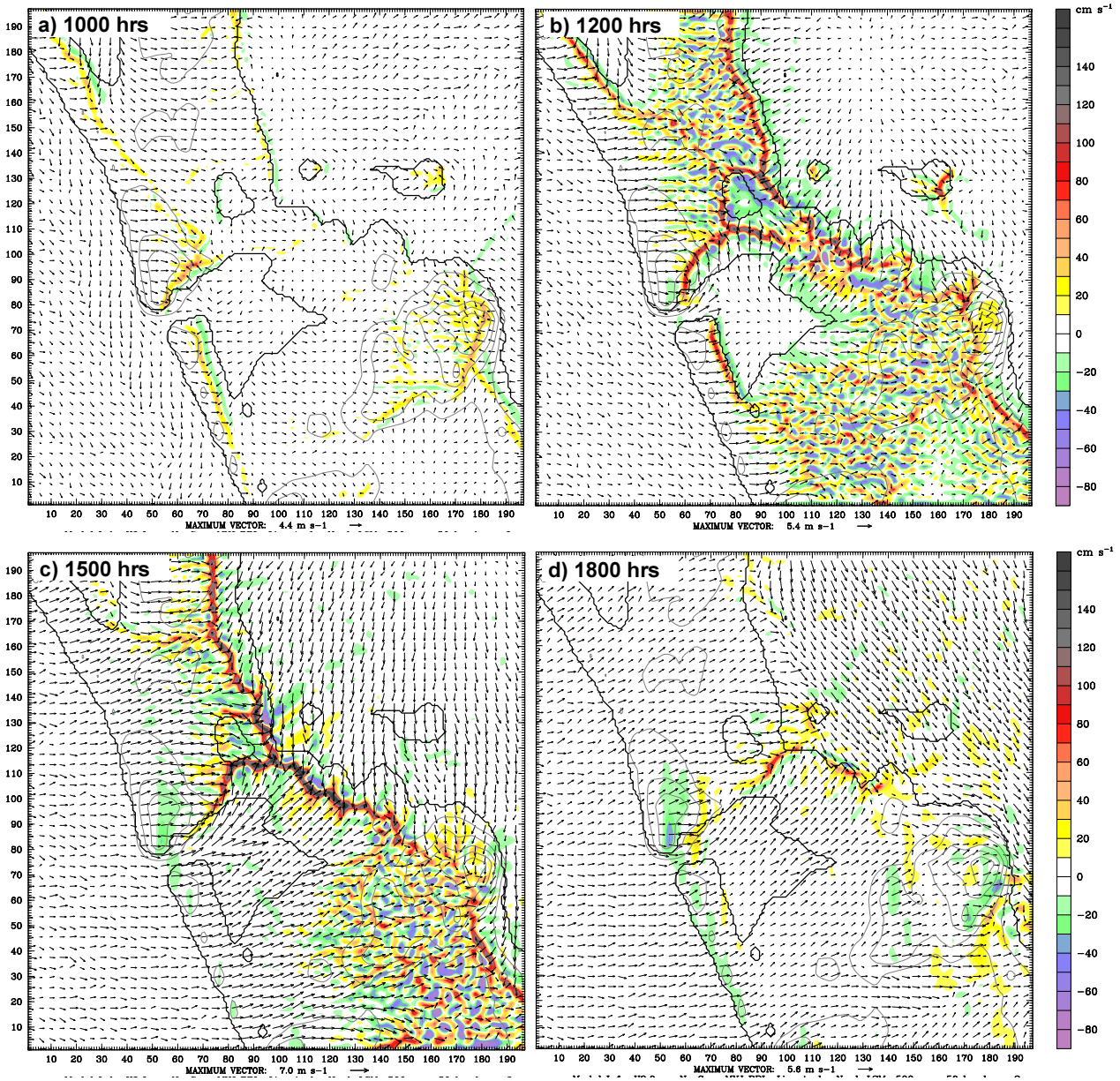


Figure 6.5: Sea breeze convergence zones over the Auckland region under $WNW_{gw}$ at 1000, 1200, 1500 and 1800 NZST. Wind vectors are at 10 m above ground and vertical velocity (colour shaded) is plotted at 500 m above ground level.

### 6.4.3 South-Southwest Gradient Flow ($SSW_{gw}$)

The $SSW_{gw}$ winds were sub-normal to the coast, in this case, the region was dominated by south-westerly prevailing winds. After sunrise, the thermal gradient between land and sea first initiated easterly onshore winds along the eastern foothills of the Hunua Ranges, which resulted in strong convergence between south-westerly gradient winds

and upslope winds enhanced easterly sea breeze (Figure 6.6a). A couple of rather weak terrain-induced convergence areas were also predicted on the eastern slopes of the Waitakere Ranges and around higher terrain southwest of Pukekohe. In the late morning to early afternoon (1100 to 1300 NZST), the inland progression of the $SSW_{gw}$ enhanced westerly sea breeze front gradually suppressed convection as it moved eastward (Figure 6.6b). The easterly sea breeze on the other hand could not penetrate inland due to the strong $SSW_{gw}$ and the resultant convergence line was predicted along the entire eastern coastline. The easterly sea breeze was strong near the Hunua Ranges due to anabatic wind effect. Another strong convergence area was predicted from east of the Waitakere Ranges to north of Waitemata Harbour due to interaction of the westerly sea breeze and bay breezes from Manukau and Waitemata Harbours.

In the late afternoon (1400 to 1600 hours), most of the Auckland region (especially north of Auckland) was overwhelmed by the $SSW_{gw}$ enhanced westerly sea breeze and the predicted SBCZs that were formed between westerly and easterly sea breezes were pushed towards the Hauraki Gulf (Figure 6.6c). Additionally, an arc of strong convergence was predicted from west to northeast of Waitemata Harbour due to a directional shear between the mature westerly sea breeze and a south-westerly bay breeze from Manukau Harbour. A similar convergence line associated with direction shear was also predicted further south of Pukekohe. The strong convection over the Hunua Ranges did not allow formation of a convergence zone. However, the convergence line over the eastern slopes of the Hunua Ranges that was formed in the late morning hours, remained intact over land. After weakening at round 1800 hours, the convergence zones disappeared by around 2000 hours (Figure 6.6d).

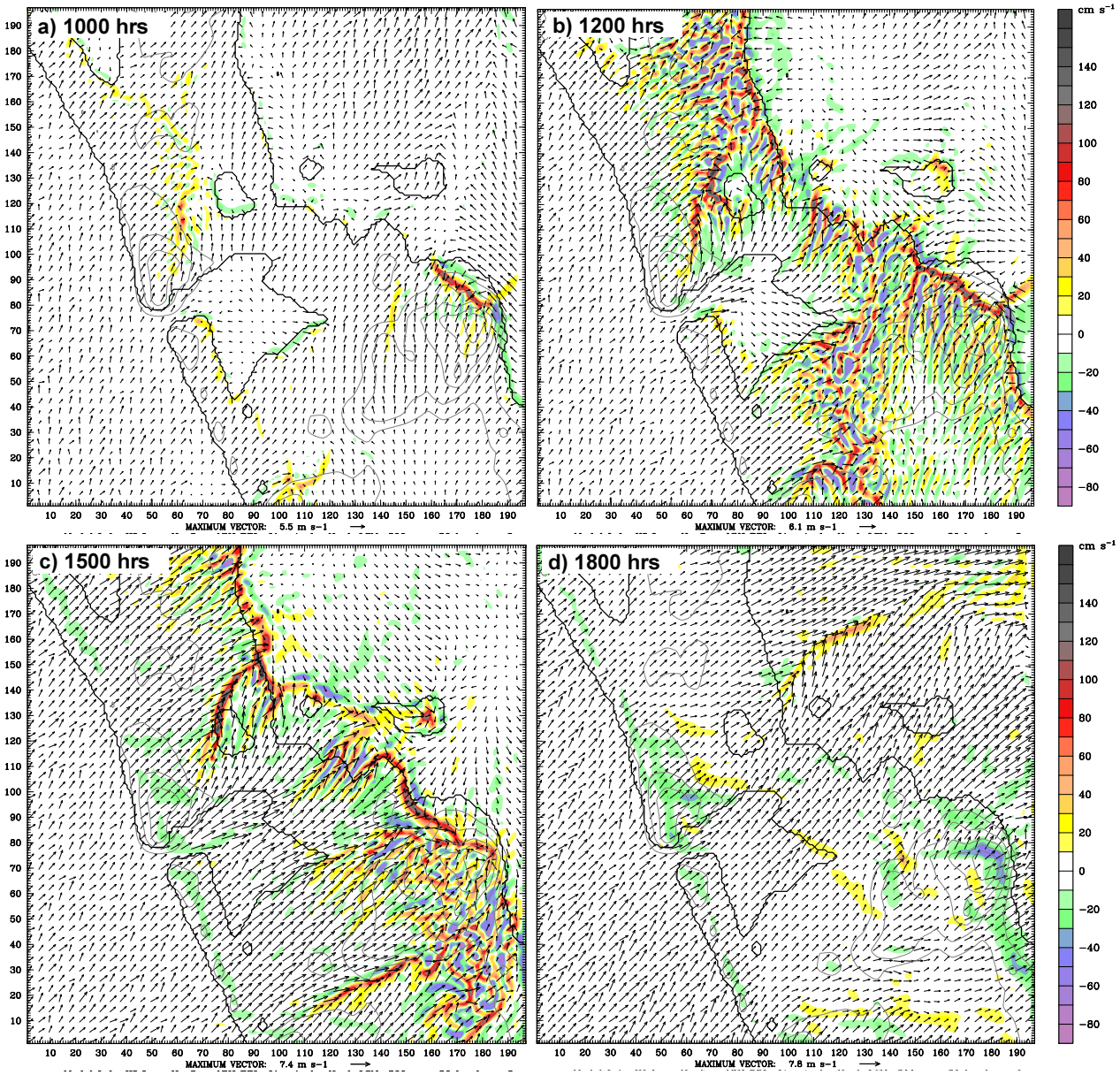


Figure 6.6: Sea breeze convergence zones over the Auckland region under $SSW_{gw}$ at 1000, 1200, 1500 and 1800 NZST. Wind vectors are at 10 m above ground and vertical velocity (colour shaded) is plotted at 500 m above ground level.

### 6.4.4 East-Southeast Gradient Flow ($ESE_{gw}$)

The $ESE_{gw}$ winds were sub-parallel to the northwest-southeast oriented Auckland region and generally enhanced easterly sea breezes. However, due to a southerly component, neither of the sea breezes (easterly or westerly) received strong inhibition or enhancement from $ESE_{gw}$. In the morning hours (0800 to 1000 NZST) convergence was predicted over the western coastline (north of Auckland) and around the Hunua Ranges (Figure 6.7a). Over the west coast, higher vertical velocities were predicted due

to the convergence between south-easterly gradient winds ($ESE_{gw}$) and the westerly sea breeze. The convergence was stronger to the west of the Waitakere ranges, where the westerly sea breeze was strong due to coupling with upslope anabatic winds. Over the Hunua Ranges, a convergence zone was predicted on the north-western slopes that was formed due to interaction between $ESE_{gw}$ and upslope anabatic wind enhanced easterly sea breeze from the Hauraki Gulf. From late morning to afternoon (1100 to 1300 hours) sea breeze fronts from both coasts propagated inland, although the inland horizontal extent of the $ESE_{gw}$ enhanced easterly sea breeze was at least twice as great as the westerly sea breeze (Figure 6.7b). Between the two fronts the daytime convection and rising and descending thermals increased PBL height to more than 1.5 km (Figure 6.8d). Similar to $WNW_{gw}$, bay breezes from the three harbours had a significant impact on the position and strength of convergence zones under $ESE_{gw}$. The extended convergence to the west of the Kaipara Harbour was attributed to interaction between the westerly sea breeze and the bay breeze from Kaipara Harbour. The predicted bay breezes from Manukau and Waitemata Harbours and the mature easterly sea breeze formed ring shaped SBCZs around their coastlines that also ran through the middle of Auckland City. In the afternoon hours (1400 to 1600 hour) the inland propagating easterly and westerly sea breezes fronts collided over the Auckland city and further north of Auckland, thus predicting a strong SBCZ. The convection in the sea breeze inflow areas (other than SBCZ) was suppressed while the more localized SBCZ (around Waitemata and Manukau Harbour) were merged with the main SBCZ that ran through from Kaipara Harbour to Papakura. This more concentrated convergence zone was positioned westward, showing the strong influence of $ESE_{gw}$. The predicted westerly and easterly sea breezes did not converge in over southern Auckland (Pukekohe and further south/southeast), although the inland extent of the sea breeze from either coast was similar to that of north of Auckland. Three major predicted convergence lines over southern Auckland were attributed to either interaction between the respective sea breeze and the land air or simply terrain effects. The convergence zones started weakening after 1700 hours due to reversal of differential heating and wind rotation. In the evening (1800 hours) only two convergence areas could be identified, one over Auckland City that persisted late in the evening due to UHI and a second convergence line predicted to the south of the Hunua Ranges, that was formed

due to higher terrain effects and the rotational characteristic of the sea breeze over both coasts. A similar convergence line was also predicted at the same time under $NE_{gw}$.

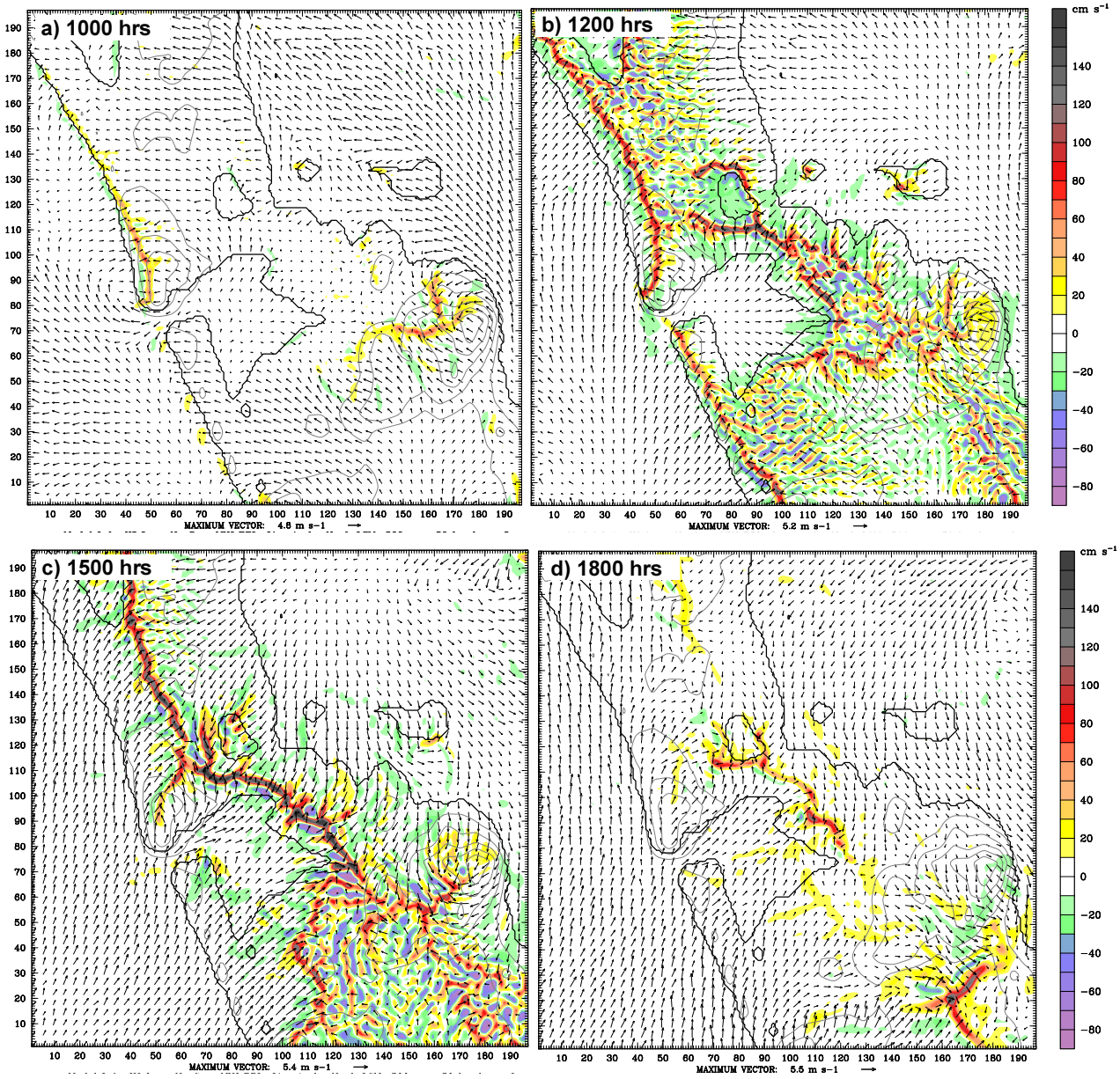


Figure 6.7: Sea breeze convergence zones over the Auckland region under $ESE_{gw}$ at 1000, 1200, 1500 and 1800 NZST. Wind vectors are at 10 m above ground and vertical velocity (colour shaded) is plotted at 500 m above ground level.

McKendry (1992) and McKendry & Revell (1991) found a mesoscale cyclonic eddy during south-easterly gradient flow in a numerical modelling study that was further verified using observational data. However, WRF did not simulate the cyclonic eddy during $ESE_{gw}$. This is probably due to lack of appropriate placement of the large scale pressure gradient in the $ESE_{gw}$ simulation.

By and large, the model results show that the position and strength of the SBCZs in the Auckland region is predominantly the result of interaction of the sea breeze inflow from the Tasman Sea and Hauraki Gulf, the three harbours (Kaipara Harbour, Waitemata Harbour and Manukau Harbour), the terrain features (Waitakere Ranges, Hunua Ranges and the Waikato river basin) and, most importantly, the strength and direction of the large scale winds. The strength of the westerly sea breeze increased under gradient winds with a strong westerly component ($WNW_{gw}$, $SSW_{gw}$). In this case, the westerly flow dominated the surface winds and reached the east coast. The SBCZs that are formed due to interaction between west and east coast sea breezes also migrated eastward. On the other hand, easterly sea breezes under $NE_{gw}$ pushed the SBCZ westward. In this case, the predicted inland penetration of the easterly sea breeze was much higher than westerly sea breezes. The gradient wind forcing under $ESE_{gw}$ was sub-parallel to the land mass, so that the effect on blocking or enhancing surface winds was reduced and convergence zones were formed nearly in the middle of the terrain. The results are generally in agreement with McGill (1987), McKendry (1992) and Sutton (1996).

Sea-land breezes are thermally-induced winds that develop due to sea-land temperature differences. Generally, a land mass width > 100 km (Miller 2003; Xian & Pielke 1991a) and a temperature gradient between 3.0 to 6.0 °C across land and sea are considered enough to generate an effective sea breeze (Comet 1999). Since sea surface temperature does not vary a lot over the diurnal cycle, it is the land surface temperature which (due to lower heat capacity) creates the thermal differential that subsequently initiates the sea-land circulation. The sea breeze strength and the sea-land temperature gradient has a linear relationship (Defant 1951; Mathews 1982), so that the higher the gradient the stronger the sea-land breeze, and vice versa. Figure 6.9, shows average predicted potential temperature difference between land (Whenuapai) and sea (Tasman Sea and Hauraki Gulf) in the first 60 m above the surface under four gradient wind conditions, while stars show the difference between predicted and observed near surface potential temperature at the Whenuapai station.

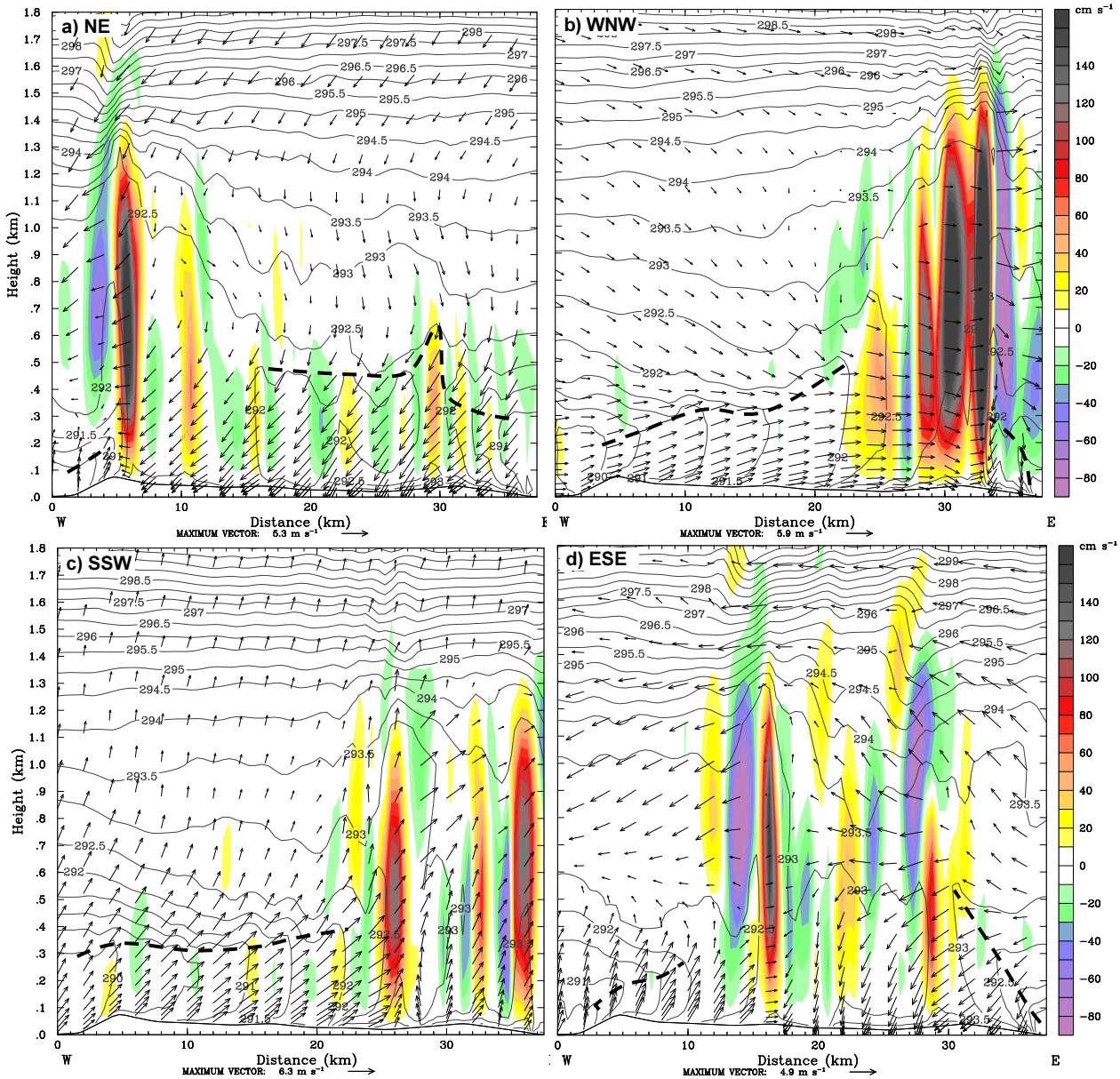


Figure 6.8: The x-z vertical cross sections of horizontal (u,v) wind vectors, vertical velocity (colour shaded) and potential temperature (contoured) for four gradient wind conditions from Whenuapai ( location AA` in Figure 6.1) at 1500 hours (NZST). The thick black dashed line represents the height of the convective internal boundary layer (CIBL).

The sounding data from Whenuapai was not averaged in the vertical due to coarse resolution and only the first level (around 2 m agl) is presented for 0900 and 2100 hours. The WRF model underestimated near-surface temperature under all four gradient wind conditions, which means smaller temperature gradients between land and sea and thus relatively weaker sea breezes.

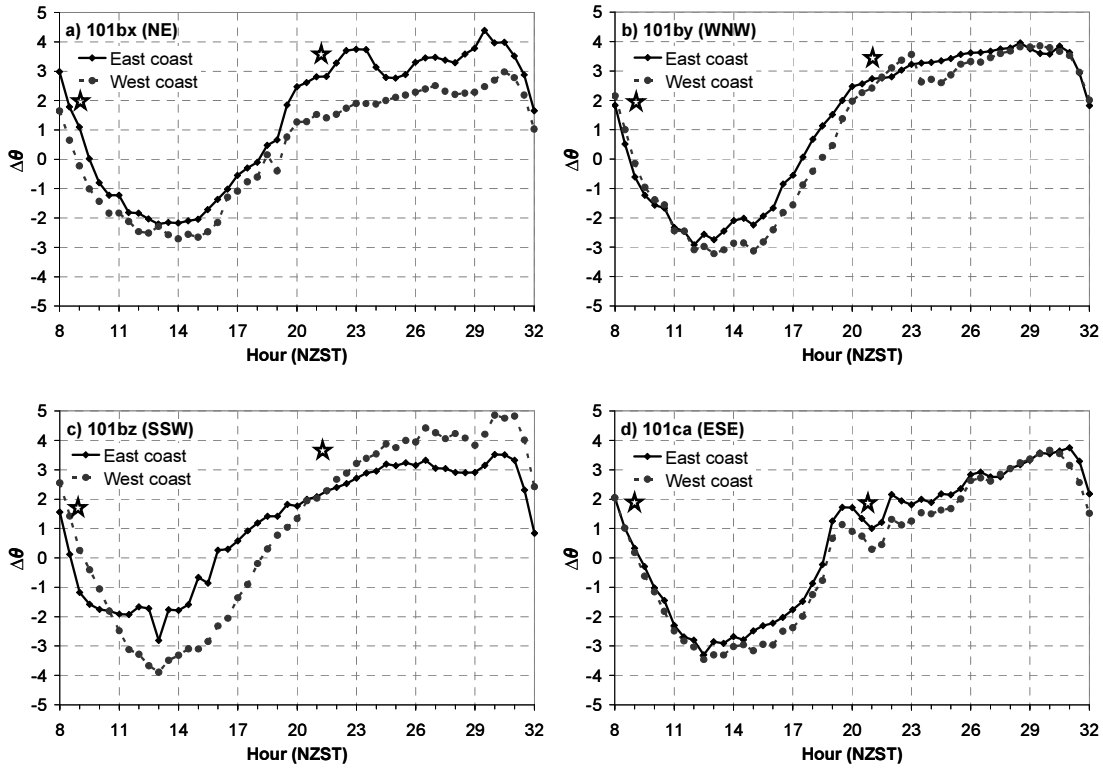


Figure 6.9: Time series plots of the average potential temperature gradient between land and sea in the first 60 m of the surface layer for the four gradient wind conditions. The potential temperature for the east and the west coast were obtained over the sea approximately 15 km from the coastline. Whereas the average potential temperature from the landward point was obtained from Whenuapai (EC: East coast, WC: West coast, WH: Whenuapai in Figure 6.1). The stars indicate observed potential temperature at around 2 m above ground at Whenuapai at 0900 and 2100 NZST.

The average potential temperature plots of the east and west coast (Figure 6.9) show a higher temperature gradient over the west coast than the east coast which means the sea surface temperature over the Tasman Sea was lower than Hauraki Gulf waters. Moreover, the predicted thermal gradient between the Tasman Sea and land was the highest under $SSW_{gw}$ during both day and night time that resulted in stronger south-westerly sea breezes. This is also in qualitative agreement with the observational data analysis (Chapter 4). The stronger sea breezes under $SSW_{gw}$ and $WNW_{gw}$ resulted in rapid inland propagation, higher vertical velocities in the sea breeze frontal zone, and a deeper PBL over the SBCZ (Figure 6.10). A higher PBL top and directional wind shear was consistently found in the SBCZs.

The vertical velocity along the sea breeze front is quite often used as a measure of intensity of the sea breeze (Bechtold et al. 1991; Pearson et al. 1983; Xian & Pielke 1991a). Previous studies show that in coastal regions with a straight coastline, an

offshore gradient wind increases the intensity (higher vertical velocities) of the sea breeze and the resulting convergence zone, whereas an onshore gradient wind weakens the sea breeze flow and results in a weak convergence by advecting cold air towards the land (Arritt 1993; Bechtold et al. 1991; Estoque 1962; Pearson et al. 1983; Xian & Pielke 1991a; Zhong & Takle 1993). However, simulation results of Zhong & Takle (1993) suggest that an onshore flow can also develop an intense convergence with strong vertical velocities in areas where inland bodies of water (river, lake, bay) exist close to the coastline. In the same way, Walsh (1974) found that an offshore flow slows down the inland penetration of the sea breeze as well as considerably reduces the magnitude. Despite certain variations, due to the peninsula shape of the Auckland region, both onshore and offshore winds come either from Hauraki Gulf or Tasman Sea. The maximum width of the land mass in the Auckland region is around 60 km, so any gradient wind parallel or sub-parallel to the landmass (especially northwest) also have marine air component. Xian & Pielke (1991a) in their study of the effects of the width of land masses on sea breezes found that a land mass extent of 100 to 150 km is suitable for the development of a sea breeze circulation and associated properties such as sea breeze head, return flow, etc.

Table 6.2: Maximum updraft and downdraft velocities at 500 m above ground and minimum 10 m horizontal wind speed in the convergence zones under four gradient wind conditions.

| Gradient wind | Updraft | | Downdraft | | Minimum 10 m horizontal wind speed in SBCZ ($m\ s^{-1}$) |
|---|---|---|---|---|---|
| | Velocity ($m\ s^{-1}$) | Time (NZST) | Velocity ($m\ s^{-1}$) | Time (NZST) | |
| $NE_{gw}$ | 2.2 | 1500 | 1.4 | 1300 | 0.5 |
| $WNW_{gw}$ | 3.1 | 1600 | 1.6 | 1500 | 1.6 |
| $SSW_{gw}$ | 2.8 | 1300 | 1.4 | 1300 | 1.6 |
| $ESE_{gw}$ | 2.6 | 1300 | 1.2 | 1300 | 0.4 |

Due to the unique geographic and orographic setting of the Auckland region, results of this study differ from the findings of straight coastline studies (e.g. Arritt 1993), but are in partial agreement with the results of complex coastline studies (e.g. Zhong & Takle 1993). The strongest positive vertical velocities were predicted under westerly gradient wind conditions ($WNW_{gw}$ and $SSW_{gw}$) that were onshore on the west coast but offshore over the east coast of the Auckland region (Table 6.2). The reason for a stronger westerly sea breeze is probably the stronger thermal gradient that increased the

mesoscale pressure gradient which is supported by the stronger 10 m wind speed of the westerly sea breeze fronts.

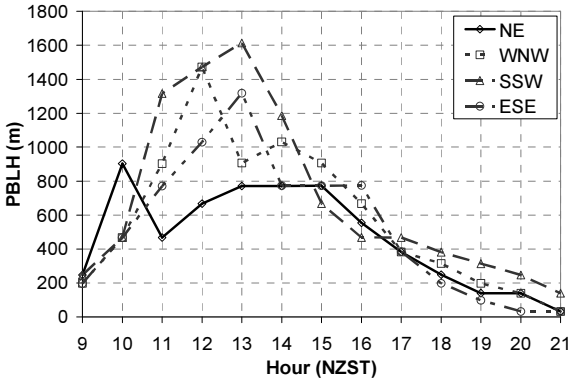


Figure 6.10: Predicted planetary boundary layer height under four gradient wind conditions between 0900 and 2100 NZST, from Whenuapai (location shown as 'WH' in Figure 6.1).

The higher predicted velocities (Table 6.2) and deep PBL (Figure 6.10) are also attributed to the location and surface characteristics. The convergence zones under westerly gradient wind conditions ($WNW_{gw}$ and $SSW_{gw}$) were predicted near the east coast, where model predicted surface temperature was more than 5°C higher than the SBCZ location near the west coast under $NE_{gw}$. This further explains that surface characteristics have a significant effect on the strength of the SBCZ. For example, in highly urbanized coastal cities, the urban heat island effect may result in stronger SBCZs that may have air quality and other local meteorological implications. These effects have been referenced by many authors, for example Pielke (1974), Bornstein (1999) and Lu & Turco (1996).

## 6.5 Vertical Structure of Sea the Breeze Circulation

The vertical structure of the onshore sea breeze circulation was modified under different gradient winds. Figure 6.8 shows variations in the sea breeze structure and inland penetration of the sea breeze front under the four gradient wind conditions. The predicted wind field shows a deeper and stronger sea breeze inflow when the gradient winds and the sea breeze were in the same direction. In the opposite case, the model predicted lower inland extent and reduced depth of the sea breeze gravity current (Table 6.3). In all the four experiments the inland movement of the sea breeze front was faster when the sea breeze was enhanced by the gradient winds. Previous studies, for example Clarke (1984), Stull (2003) and Simpson (1977) confirmed this behaviour of the sea breeze and approximated the net speed of the sea breeze front as the linear sum

of the gradient wind component perpendicular to the sea breeze front and the speed of the front in still air. The predicted sea breezes under westerly gradient wind conditions were the strongest. Simpson (1977) suggested that the inland advance of the sea breeze is governed locally by the density difference across the front. A decrease in temperature contrast between the sea breeze air and the land air would decrease the density difference. This coincides with the higher thermal gradient between the Tasman Sea and the land mass that produced a relatively stronger westerly sea breeze (Section 6.5).

Table 6.3: Sea breeze structure from an x-z cross section near Whenuapai at 1500 NZST.

| Gradient wind | Height of SB Inflow (m) | | Average wind speed of sea breeze front (m $s^{-1}$) | | Average wind speed in sea breeze inflow (m $s^{-1}$) | |
|---|---|---|---|---|---|---|
| | WSB | ESB | WSB | ESB | WSB | ESB |
| $NE_{gw}$ | 200 | 600 | 0.40 | 1.5 | 3.5 | 4.5 |
| $WNW_{gw}$ | 700 | 250 | 1.8 | 0.4 | 4.5 | 3.5 |
| $SSW_{gw}$ | 800 | 300 | 1.6 | 1.4 | 5.3 | 4 |
| $ESE_{gw}$ | 400 | 600 | 0.8 | 1.2 | 4.0 | 3.8 |

* WSB: Westerly sea breeze; ESB: Easterly sea breeze

WRF predicted a clear, well developed sea breeze under $ESE_{gw}$, on both east and west coasts of the Auckland region (Figure 6.8d). This is consistent with the observational data analysis (Chapter 4) that suggests the highest number of sea breeze days under southerly gradient winds. The return flow was modified by the gradient winds in the four experiments. If the gradient winds and the return flow were in the same direction, the return flow merged with the gradient wind flow, if both were in the opposite direction, the return flow above the shear zone was deflected completely or partially in the gradient wind direction (Figure 6.8). This deflection is controlled by a balance between the large scale PGF, mesoscale thermal PGF and the Coriolis force that is affected by surface friction (see for example, Miller et al.(2003) and Adams (1997)). The updrafts and downdrafts in the sea breeze frontal zone appear to mix most of the air within a few kilometres of horizontal distance over the land. However, mixing between sea breeze inflow and return flow is unlikely because of the density difference between cold marine sea breeze inflow and the warmer air in the return flow above the shear zone (Figure 6.8). This inhibition of air mass mixing between sea breeze inflow and return flow was also evident in the laboratory experiments conducted by Simpson & Britter (1980). The analysis of grid domain D01 and D02 (not shown here) revealed

that the simulated sea breeze circulation was not closed and the air mass in the return flow, whether moving seaward or deflected to another direction, adjusts itself slowly over the region, generally towards the gradient wind direction.

The horizontal cross-section from Whenuapai (Figure 6.8) shows the spatial evolution of the mixed layer height over land and the CIBL under the sea breeze gravity current at 1500 hours. Under the coast-parallel gradient wind conditions, the inland movement of the sea breeze front was simultaneous and slow. The horizontal extent of the mixed layer that was formed in between the two fronts due to day time processes was much larger than coast-normal gradient wind conditions. However, the CIBL that formed under $WNW_{gw}$ and $ESE_{gw}$ due to movement of cold marine layer of air over land was shallower than for $NE_{gw}$ and $SSW_{gw}$.

Depth and rate of growth of the mixed layer depends on the thermal properties of the air mass over land. Analysis of thermal profiles of the lower atmosphere at Whenuapai suggests that the evolution of the mixed layer was largely controlled by the advection processes in the four gradient wind simulations (Figure 6.11). In the morning hours (1000 NZST), the predicted mixed layer height under coast-normal gradient winds ($SSW_{gw}$ and $NE_{gw}$) was around 600 m, while under coast-parallel gradient winds ($WNW_{gw}$ and $ESE_{gw}$) the predicted mixed layer height was of the order of 200 to 400 m only. The lower depth of the mixed layer under coast-parallel gradient winds ($WNW_{gw}$ and $ESE_{gw}$) was due to advection of air over cooler land surfaces while under coast-normal gradient wind conditions ($SSW_{gw}$, $NE_{gw}$) relatively warm air was advected from the sea giving a higher depth to the evolving mixed layer in the morning hours. However, later in the day the thermal gradient reversed and the mixed layer started growing rapidly under all four gradient wind conditions and ranged between 800 to 1200 m in the early afternoon hours. The cut-off point is probably 1600 NZST, when except for $ESE_{gw}$ the predicted mixed layer height under $NE_{gw}$, $WNW_{gw}$ and $SSW_{gw}$ ranged between 400 to 600 m. The shallow depth of mixed layer (CIBL) under the three gradient wind conditions was due to inflow of the sea breeze from the west or east coast that overwhelmed the Whenuapai station. However, the situation under $ESE_{gw}$ was different, so that even at 1600 hours the mixed layer height was around 1000 m. This is mainly due to the reduced gradient wind forcing from either coast that produced

a sea breeze of more or less equal strength on both coast. The wind speed of both easterly and westerly sea breeze fronts was also relatively low (Table 6.3). The SBCZs were thus predicted almost in the middle of the land mass and ran through Whenuapai station. The higher mixed layer depth under $ESE_{gw}$ is associated with this intense SBCZ.

The predicted wind speed under the $SSW_{gw}$ enhanced sea breeze was relatively higher than other gradient wind conditions due to a stronger thermal gradient between the Tasman Sea and the land mass. The stronger south-westerly sea breeze resulted in rapid horizontal growth of CIBL. The inland extent of the CIBL was 25 km over the west coast at 1500 NZST which was the largest amongst four gradient wind conditions (Figure 6.8). In the evening (1800 NZST) the mixed layer depth under coast parallel ($WNW_{gw}$ and $ESE_{gw}$) gradient winds decreased at a greater rate than coast normal gradient winds due sharp reduction in the surface heat fluxes over land. The predicted depth of the CIBL under both coast-parallel gradient winds ($SSW_{gw}$ and $WNW_{gw}$) was less than 200 m, which may have significant implications on the air quality of the region. After 1800 hour, the cooling of the land surface reduced the convection, and stratification of the lower atmosphere gradually evolved with a residual layer developing as the result of a weakening mixed layer. In the late evening after 2000 hours, the model predicted a strong inversion in the surface layer under $NE_{gw}$, with a 200 m deep residual layer starting around 100 m above the ground. The residual layer under the three remaining gradient wind conditions formed with two hours delay at around 2200 hours. The potential temperature profiles from more urbanized locations (not shown here), for example Penrose and Khyber Pass, show a shallow mixed layer till late evening (2100 NZST) that can be attributed to an urban heat island effect.

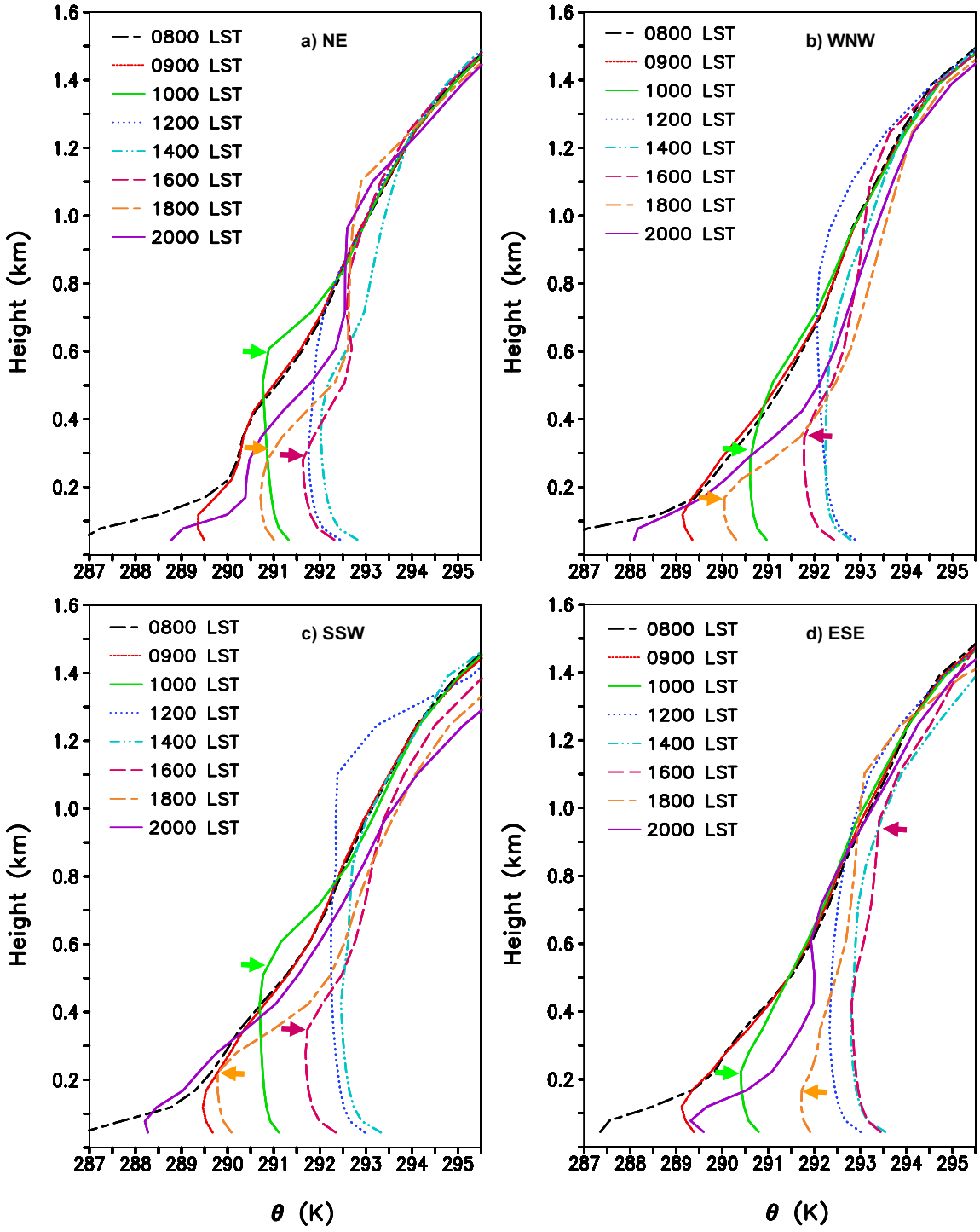


Figure 6.11: Vertical profiles of potential temperature from near Whenuapai (location 'WH' in Figure 6.1) for 0800 hours to 2000 NZST. Green arrows show height of the mixed layer at 1000 hours, magenta arrows show height of mixed layer at 1600 hours and brown arrows show mixed layer height at 1800 NZST.

## 6.6 Potential Effect of the Sea Breeze on Pollutant Dispersion

The predicted results show strong influence of gradient winds on the bay breezes from three harbours and mature sea breezes from the east and west coasts. Under gradient winds normal to either coast, bay breezes were either not initiated or they were very weak and short-lived, while the inland movement of the sea breeze from the opposite coast was inhibited. For example, under $NW_{gw}$, the inland penetration of the westerly sea breeze was limited to the west coast and the SBCZ was formed along the western coastline. A proper onset of bay breezes on three harbours and mature sea breezes over the east and west coasts was predicted under coast-parallel winds ($WNW_{gw}$ and $ESE_{gw}$). These results are in partial agreement with the observational data analysis (Chapter 4) that shows the highest number of sea breeze days during southeast and northwest gradient wind conditions. The sea breeze circulation under coast-normal gradient winds may occur only when gradient winds were very weak. The two coast-parallel gradient wind directions are therefore important with respect to the effect of the sea breeze and its associated characteristics on the air quality of the region. The predicted results of the two coast-parallel gradient winds show that during morning time (between 0600 and 0800 NZST) remnants of the land breeze may advect the pollutants emitted in the urban surface layer during morning peak traffic hours towards the Manukau and Waitemata Harbours and the Hauraki Gulf. If the gradient winds are not strong enough to advect the urban air mass further away from the small bodies of water, the polluted air may return with the bay breezes that are associated with these three water bodies. This is also in qualitative agreement with the pollution dispersion modelling and trajectory analysis in Chapter 5. The air pollution studies conducted around the world suggest that this process is especially important for photochemical pollution. The non-methane hydrocarbons (NMHCs) and oxidants such as $NO_x$ (oxides of nitrogen) that are emitted in the surface layer during morning peak traffic hours may be advected to the sea, where in relatively calm conditions, photochemical reactions take place unhindered by addition of fresh NO (nitrogen oxide). When the sea breeze develops in the late morning, the $O_3$ is transported onshore and over the urban areas that were responsible for its precursors (Cope et al. 1990; Gusten et al. 1988; Hawke et al. 1983; Hyde et al. 1978; Lalas et al. 1983; Lalas et al. 1987; Manins et al. 1992). Model results show that $SSW_{gw}$ did not allow local winds to occur till late morning, and especially early morning land breezes and bay breezes from Manukau and Waitemata

Harbour were suppressed by the strong westerly flow. Consequently, morning time peak traffic hour emissions that would be advected seawards (Hauraki Gulf) might not return to the source. On the other hand, the westerly sea breeze could not move in under $NE_{gw}$ and the SBCZs were formed along the west coast and the coastline around the Manukau Harbour. Under these conditions, although pollutant reversal is unlikely, due to near stagnant conditions in the convergence around the coastline of the Manukau Harbour, higher pollutant concentrations can be expected in these areas.

The intense vertical motion in the SBCZs in some cases is considered as a vent for surface pollutants, although their potential to increase pollution levels on the following morning has not been denied (Lu & Turco 1995). However, various studies at home and overseas considered SBCZs as areas where pollutants are trapped and the concentration increased to unacceptable levels (Azorin-Molina et al. 2009; Bornstein 1999; Liu & Chan 2002b; Liu et al. 2002; Ridley 1995; Sutton 1996). Ridley (1995) used a Lagrangian particle dispersion model to study the role of SBCZs on the air quality of the Auckland region, and suggested inhibition of mixing of air between east and west coast sea breezes in the SBCZ that resulted in increased particle concentration in the convergence area. The dispersion modelling results (Chapter 5) suggest potential advection of particles towards the convergence zones. However, due to particle dispersion setup in the first level only, vertical mixing of the tracer could not be investigated. Simulations under the four gradient wind conditions also suggest that polluted air in the shallow CIBL (averaging 400 m deep) may be advected to the SBCZ, where it may experience both horizontal and vertical wind shear. In the SBCZ the air mass would be lifted by continuity-induced upward motion and diverge over the top of the mixed layer where it is deflected southward or northward. The deflection of wind vectors during south-westerly flow was northward, while under $WNW_{gw}$ conditions the deflection was eastward. The potentially polluted air mass above the elevated boundary layer may subside in the stable return flow. Due to the strong influence of gradient winds, it is more likely that most of the subsidence would occur towards the windward direction. However, due to limited mixing between the return flow and sea breeze inflow, the polluted air mass would be dispersed and slowly advected away. If the polluted air mass is unable to move aloft and mix with the opposing sea breeze, as Ridley (1995) suggested, then pollutants would disperse slowly

in the surface layer and increase ground level pollutant concentration. The nature of pollutants may also have important implications for advection within the return flow. For example, Lyons & Olsson (1973) found that the heavier particles that subside into the top region of the inflow were then brought back to land within a time scale of a few hours. The pollutants at the top of the boundary layer may also be washed out or rained out by the convective clouds and their associated precipitation (Bornstein 1999).

A shallow convective internal boundary layer with low wind speed can significantly increase pollution levels through fumigation and inhibition of vertical mixing. The CIBL depth slightly varies between coast-normal and coat-parallel gradient winds. In general, the predicted CIBL depth under coast-parallel gradient winds ($ESE_{gw}$ and $WNW_{gw}$) was either the same or lower than coast-normal (sub-parallel) gradient winds. This means that urban areas of the Auckland region are potentially more vulnerable during a sea breeze event under coast-parallel gradient winds. There were small variations in the CIBL depth between westerly and easterly sea breezes, but wind magnitude was the highest under $SSW_{gw}$. The higher pollution levels are therefore unlikely under westerly sea breeze conditions for two reasons. First, the westerly winds are clean because of low population density and less anthropogenic activities towards the west coast, and second, they are stronger than easterly, southerly or northerly flow. The strong and clean westerly air mass will replace or push the polluted air over land towards the east coast and despite a relatively low CIBL the strong westerly sea breezes would probably advect the polluted urban air mass towards the Hauraki Gulf.

In summary, the modelling study of sea breeze dynamics under four gradient wind conditions suggests that given the specific local meteorological and orographic features of the region, the highest potential of increased pollution levels during a sea breeze event is associated with the shore parallel north-westerly, and especially south-easterly to southerly, gradient wind conditions. These results are also consistent with the dispersion modelling in Chapter 5. Recirculation of pollutants in the vertical sea breeze circulation cell is unlikely in the Auckland region, especially under prevailing south-westerly and north-easterly gradient wind conditions. However, the heavier particles may return to the land because of the effects of the gravitational force. The same day mechanism of morning time land-sea transition is not quite apparent under westerly and

strong north-easterly gradient wind flow. However, during southerly/south-easterly, north-westerly or weak north-easterly gradient winds, pollutant emitted during the peak morning traffic hour may return to land. The higher concentration of pollutants in the CIBL is also possible only when both depth and wind speed within the CIBL is low. The pollution concentration is more likely to increase during southerly gradient wind conditions. This is consistent with the observational analysis result (Chapter 4). However, a comprehensive in situ observational study and three dimensional pollutant dispersion modelling is essentially required to confirm the results of the idealized modelling studies.

## 6.7 Summary of Results

The interaction of large scale winds with the mesoscale sea breeze system results in important modifications in sea breeze characteristics, such as the sea breeze circulation cell, sea breeze convergence zones (SBCZs) and convective internal boundary layer (CIBL) that are capable of affecting the air quality of coastal urban areas. Four experiments were designed to investigate the effect of gradient wind conditions on the sea breeze system, with a particular emphasis on those characteristics of the sea breeze that are associated with the air quality of the coastal regions. Two of the simulations were run with a constant coast-parallel gradient wind direction (southeast and northwest) and the remaining two were run with constant coast-normal background winds (southwest and northeast). However, due to the intricacies associated with three dimensional idealized modelling with WRF, the final gradient winds were slightly deflected leftward (due to the Coriolis effect) from the desired gradient wind direction. The resultant final gradient wind directions were therefore northeast ($NE_{gw}$), east of southeast ($ESE_{gw}$), south of southwest ($SSW_{gw}$) and west of northwest ($WNW_{gw}$). Despite this variation in the gradient wind direction, the four idealized simulation results showed important features, of the sea breeze system in and around the Auckland region. Amongst these features probably formation of the convective internal boundary layer (CIBL) and SBCZs are the most important characteristics of the sea breeze system with regard to air quality applications. The SBCZs may contribute to increase ground level concentration due to stagnant conditions and may also transport pollutants in the upper layers of the atmosphere while trapping and fumigation of pollutants in the shallow mixed CIBL may increase the near surface pollutant concentrations (Abbs &

Physick 1992; Barbato 1975; Liu et al. 2001; Luhar et al. 1998; Lyons et al. 1981; Zhong & Takle 1992). Luhar & Hurley (2004) found spots of high pollutant concentration in the Kwinana (Western Australia) coastal fumigation study that resulted from fumigation in CIBL. Recirculation of pollutants within the sea breeze, and offshore and onshore wind transition during the morning is also considered important with respect to increased concentration of pollutants (especially photochemical species) during the day (Cope et al. 1990; Hawke et al. 1983; Hyde et al. 1978; Lyons & Olsson 1973; Manins et al. 1992; Stull 2003). Contribution of the residual layer to trapping pollutants and increasing the pollutant concentration on the following morning has also been investigated in the air quality literature (e.g. Lu & Turco 1994; Lu & Turco 1995; Lu & Turco 1996). This chapter investigated these sea breeze characteristics and their potential role in affecting the air quality of the Auckland region under four different gradient wind conditions.

The diurnal rotation of the thermally induced flow is an important feature of the sea breeze system and reflects the reversal of the temperature gradient over the diurnal cycle. In ideal conditions, the rotation of winds in the southern hemisphere should be anticlockwise. Due to diurnal wind reversal, the sea-land breeze rotation may contribute to recirculation of pollutants. Results of the analysis of four experiments show that anticlockwise rotation is more likely to occur over both the east and the west coast under gradient winds with a strong easterly component. Under gradient winds with a strong westerly component, the rotation was incomplete and winds had a tendency to move back and forth along the gradient wind direction. Over land this diurnal rotation was strongly affected due to topographical effects. At Auckland Airport none of the four simulations show anticlockwise simulation. The rotation over Auckland Airport was also incomplete, with back and forth movement along the gradient wind direction. An important difference between Auckland Airport and the east and west coasts is that at the former site wind has a tendency of clockwise instead of anticlockwise rotation. From an air quality perspective this means that a complete rotation of land-sea breezes is more likely to occur under coast-parallel south-easterly gradient winds and coast normal north-easterly gradient winds. This is in general agreement with the observation data analysis (Chapter 4) and dispersion modelling

results (Chapter 5) that suggest high pollution levels under southerly gradient wind conditions.

In the Auckland region, SBCZs have frequently been observed and simulated by many authors (for example, McGill 1987; McKendry 1989,1992; McKendry & Revell 1991; Ridley 1992; Ridley 1995; Sutton 1996; Sutton 1992). The results of the four simulations suggest that under $SSW_{gw}$ and $NE_{gw}$ the SBCZs were predicted either close to the east or west coast, while under gradient winds with a strong northwest or southeast component ($WNW_{gw}$ and $ESE_{gw}$) the convergence zones were initially predicted on both sides of the peninsula and then seem to migrate inland with increasing strength of the sea breezes. The convergence lines were also predicted around the edge of three harbours under both $WNW_{gw}$ and $ESE_{gw}$. In either case, the major and stronger SBCZs run through Auckland City and most of the urban areas. In addition to the gradient wind, the higher terrain of the Waitakere and Hunua Ranges play an important role in modification of the wind field and the position and strength of SBCZs. Under all the four gradient wind conditions, the first two convergence zones were predicted around the Waitakere and Hunua Ranges. Later in the day, more convergence lines were predicted around Manukau Harbour, Waitemata Harbour, Kaipara Harbour, over the west coast, the east coast and south of Pukekohe. The location, strength and migration of these convergence zones were relative to the mesoscale pressure gradient and gradient wind direction. Results of the four simulations are in general agreement with the previous work (McKendry 1992; Sutton 1996) that suggested that the strength and location of the SBCZs is strongly affected by the gradient wind speed, direction and topography. This study further suggests that surface characteristics (vegetation, soil type) and resulting change in the surface temperature and soil moisture may also affect the strength of the convergence zones. In the air quality literature, SBCZs have been associated with the air quality of the coastal urban regions. Pollutants advected to the convergence zone may increase concentration of pollutants in the surface layer and/or be uplifted due to higher vertical velocity, where again they either become part of the return flow and return to the source (in case of a closed circulation) or disperse within the gradient flow. In case of intense SBCZs (large vertical velocities) the top end of the mixed layer in the convergence zone would cross the stable layer and pollutants might disperse above the boundary layer (Lu &

Turco 1994; Lu & Turco 1995; Lu & Turco 1996). In the complex terrain of the Auckland region, recirculation especially under south-westerly and north-easterly gradient wind conditions is unlikely, but under coast parallel north-westerly and south-easterly gradient winds, pollutant concentration in the surface layer may exceed acceptable levels in the convergence areas. Analysis of the thermodynamic structure of the lower atmosphere does not support the argument that pollutants uplifted in the convergence zone will recirculate the same day with the onshore sea breeze. If pollutants from the peak evening traffic hours were trapped in the convergence zone, they may move aloft and reside in the residual layer and may increase pollutant concentration the next morning after breakup of the night time inversion. However, dispersion modelling in Chapter 5 could not examine this aspect because the pollutant dispersion was set up for the single level only. However, considering higher magnitude of the prevailing winds and the narrow land mass of the Auckland region, the following day pollution appears to be unlikely. As for the Auckland region, this is still an important area and needs intensive observational data analysis coupled with three dimensional dispersion modelling.

The four simulations consistently predicted CIBL over the Auckland area during the sea breeze inflow from either coast, but the depth and inland extent of the CIBL depends on many factors, such as gradient wind direction, position of the convergence zone and wind speed of the respective inland moving sea breeze front. In general the CIBL depth was shallower (200 – 400 m) under coast-parallel gradient wind conditions while the inland extent of the CIBL was greater under south-westerly gradient winds, mainly due to the relatively high wind speed of the westerly sea breeze front under $SSW_{gw}$. The inversion over the top of the CIBL acts as a cap that inhibits vertical mixing of pollutants that are emitted near the surface, while pollutants that are emitted in the inversion layer above CIBL are fumigated (Luhar & Hurley 2004; Luhar et al. 1998). Pollution levels, therefore, may also raise under south-westerly and north-easterly gradient wind conditions. However, considering the fact that first westerly wind flow is generally clean and second, the predicted wind speed in the sea breeze inflow under $SSW_{gw}$ was relatively high, the potential for higher pollution levels under $SSW_{gw}$ is less than $NE_{gw}$ conditions. On the other hand the mixed layer depth under coast-parallel ($WNW_{gw}$ and $ESE_{gw}$) gradient winds was the lowest in the evening (1800

hour), which may increase pollutant concentrations at night. Considering the narrow land mass of the Auckland region and presence of relatively high prevailing winds, the next day pollution mechanism is probably unlikely in the Auckland area.

The terrain features in the Hauraki Gulf, such as Rangitoto and Motutapo Islands, Waiheke Island, Panui Island, and the Coromandel Peninsula, generate their own sea breeze systems. Due to proximity of these islands to the Auckland region, the variation in the thermal/pressure gradient caused by these small scale sea breeze systems over the Hauraki Gulf may contribute towards relatively weak sea breeze flow from the east coast. This feature has been partially discussed in Chapter 7, but a complete analysis of the effects of islands in the Hauraki Gulf on the sea breeze system in the Auckland region is out of the scope of this thesis.

# 7. The Effect of Topography on the Sea Breeze

## 7.1 Introduction

Terrain height and spatial variation of land surface characteristics are important controls of any local and/or mesoscale meteorological phenomena such as the sea-land breeze circulation. The effect of coastal topography on sea breeze structure has been investigated by many authors (e.g. Arritt 1993; Melas et al. 1998; Miao et al. 2003; Nitis et al. 2005; Zhong & Takle 1993). Orography has crucial importance for both local and large scale meteorological processes due to its ability to modify the mesoscale pressure field (Buzzi et al. 1998). Hills and coastal mountains affect the initiation and development of the sea breeze. It is therefore imperative that the effect of topography be studied in greater detail in observational and modelling studies (Nitis et al. 2005). Typically, modelling studies that considered the effect of topography on the sea breeze were based on two dimensional hydrostatic models (Abbs & Physick 1992; Tijm et al. 1999). However, only a few studies are available examining topographical influences on the sea breeze using non-hydrostatic three dimensional numerical modelling approaches with realistic topography (e.g. Lu & Turco 1995; Miao et al. 2003). In this chapter, the effects of topography (higher terrain) on the initiation, strength and cessation of the sea breeze over the Auckland region are investigated by utilizing idealized three dimensional modelling techniques.

## 7.2 Model Setup

To examine the topographical influence on the sea breeze circulation, Advanced Research WRF (ARW) modelling system version 3.01 was employed in three dimensional idealized mode. Two simulations namely '101bv' and '101bw' were run with the same physics, initial and lateral boundary conditions, but with different topography. The first simulation (101bv) was initialized at midnight with real terrain and 500 m meteorological grid spacing (for the highest resolution grid) and 2 minute (approximately 4 kilometres) terrain resolution. The second simulation (101bw) was also initialized at midnight, but with zero terrain elevation. The water bodies and surface characteristics (vegetation type, soil type, etc.) were not changed within all grid domains. Except for terrain and background wind, the rest of the model physics, dynamics and domain configuration were the same as real 101cg simulation and idealized simulation from 101bx to 101ca (please see Chapter 5 for detail). The model setup for the two simulations is described in Table 7.1.

Table 7.1: Model setup of the two idealized simulations

| **Idealized Simulations** | **101bv: Simulation with 2-minutes (approximately 4000 m) terrain resolution.** |
|---|---|
| | 101bw: Simulation with flat terrain |
| Vegetation, land use and surface characteristics | 2-minute (approximately 4000 m) resolution |
| Background wind | 0 |
| No of Grids | 3 |
| Grid resolution (m) | D01: 3000 m; D02: 1000 m; D03: 500 m |
| Grid points | D01: 199; D02: 199; D03: 197 |
| Surface layer scheme | Eta similarity |
| Land surface scheme | Noah |
| PBL scheme | Mellor-Yamada & Janjic |
| Microphysics | Lin et. al. |
| *Vertical levels* | 51 |

To initialize both simulations with zero background winds and to additionally remove topography from the flat terrain simulation (101bw), the pre-processed meteorological files were modified. Initially NCEP FNL re-analysis meteorological data and USGS terrain data were used to prepare horizontally interpolated meteorological (met_em_*)

files. Before vertical interpolation by the WRF initialization program 'real.exe', the meteorological files (met_em_*) were modified to provide the desired background wind field and topography. For this purpose, the vertical profiles of pressure, geopotential, air temperature and two dimensional field of mean sea level pressure were extracted from a point over seal level from NCEP FNL re-analysis data at the simulation's start time. These data were replaced with the respective fields in met_em_* files, although vertical level K=1 was left unchanged in 101bv to take into account the topographical variations over land.

In the model setup of the flat terrain simulation (101bw), the first K level for the three dimensional fields of pressure and geopotential height were replaced with the mean sea level pressure of 101325 Pa and 0 m geopotential height respectively. The two dimensional mean seal level pressure (PMSL) field in the met_em_* files was also replaced with a constant seal level pressure of 101325 Pa. To ingest zero background winds in simulations, the west-east and north-south components of wind in the met_em_* files were replaced with zero '0'. To remove terrain for the flat terrain (101bw) setup, data in the five terrain related fields (HGT_M, HGT_U, HGT_V, SOILHGT, SLOPECAT) were replaced with '0' in all three model domains of the flat terrain simulation (101bw). The schematic in Figure 7.1 shows locations of the data extraction points, area blocks and vertical cross-sections from the model results for grid domains D02 and D03.

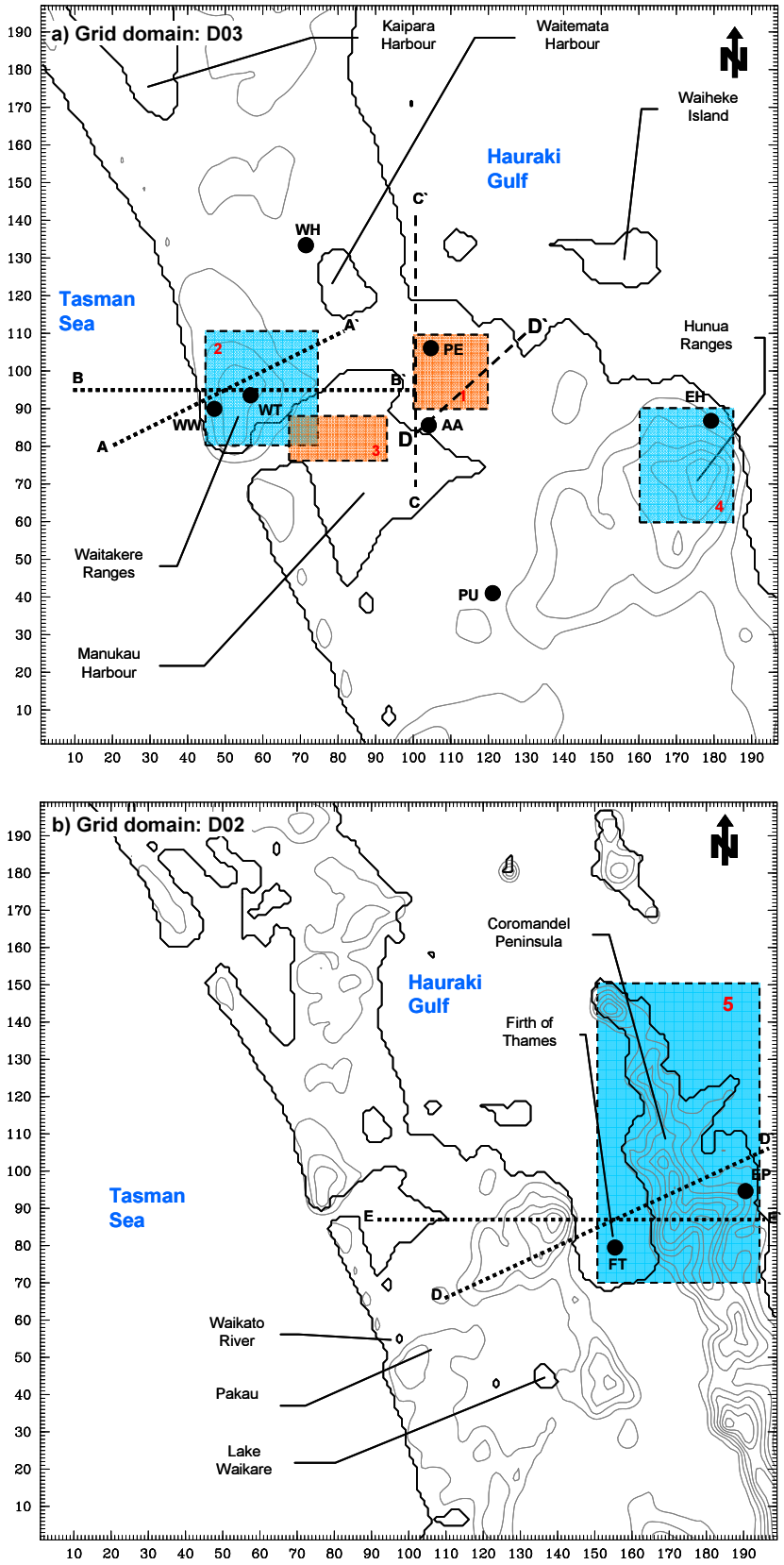


Figure 7.1: Map of the Auckland region for a) Grid domain D03 with horizontal resolution of 500 m. Terrain and land surface properties were smoothed at 4000 m resolution. Thick black dashed lines indicate locations of cross-sections used in the analysis. Boxes with black dotted outline show areas where average or maximum quantities were calculated. The red digits in the boxes indicate the number of the block area. The black dots with two letter code indicate points where data has been extracted from and used in the analysis. The gray contour lines indicate elevated terrain. b) Same as 7.1a but for grid domain D02 with horizontal grid resolution of 1000 m. * WH: Whenuapai; WW: West of Waitakere Ranges, WT: Top of Waitakere Ranges; PE: Penrose; AA: Auckland Airport; PU: Pukekohe; EH: East of Hunua Ranges; EP: East of Coromandel Peninsula (Ranges); FT: Firth of Thames.

## 7.3 Evolution of the Sea Breeze

The irregular coastline and complex sea-land interactions between three major harbours and higher terrain of the Waitakere, Hunua and Coromandel Ranges in the Auckland area offer a significant challenge to investigate a mesoscale meteorological phenomenon such as the sea breeze. Analysis of two idealized simulations (101bv: real terrain; and 101bw: flat terrain) was able to extract some of the topographical effects on sea-land breeze structure and dynamics. Comparison of the real and flat terrain simulations showed that higher terrain resulted in early onset of the predicted sea breeze, triggered by upslope anabatic winds (Figure 7.2) around the Waitakere Ranges and east of the Hunua and Coromandel Ranges. Over the western slopes of the Waitakere Ranges, the upslope flow triggered an early onset of the sea breezes around 0900 hours, while over flat terrain the sea breezes were initiated around 1100 hours. Although in reality the western slopes of the Waitakere Ranges would be shadowed due to the azimuth angle of the morning sun, the real terrain simulation still predicted relatively higher sensible heat flux around the Waitakere Ranges which is probably due to relatively coarser terrain resolution (4 km). The higher terrain of the Hunua and Coromandel Ranges also triggered an early onset of the sea breeze at 0800 hours and 0900 hours respectively, while the flat terrain simulation (101bw) showed initiation of the sea breeze one hour later. These results are consistent with the findings of Chapter 6 that suggest early onset of sea breeze near Waitakere, Hunua and Coromandel ranges. In the morning hours the wind speed over the Firth of Thames near the Hunua Ranges (not shown here) was up to 2 m $s^{-1}$ higher (between 3.5 to 4.5 m $s^{-1}$) than the flat terrain, which is attributed to the higher terrain, of the Hunua and Coromandel Ranges that provides relatively strong southerly to south-easterly surface flow over the Firth of Thames.

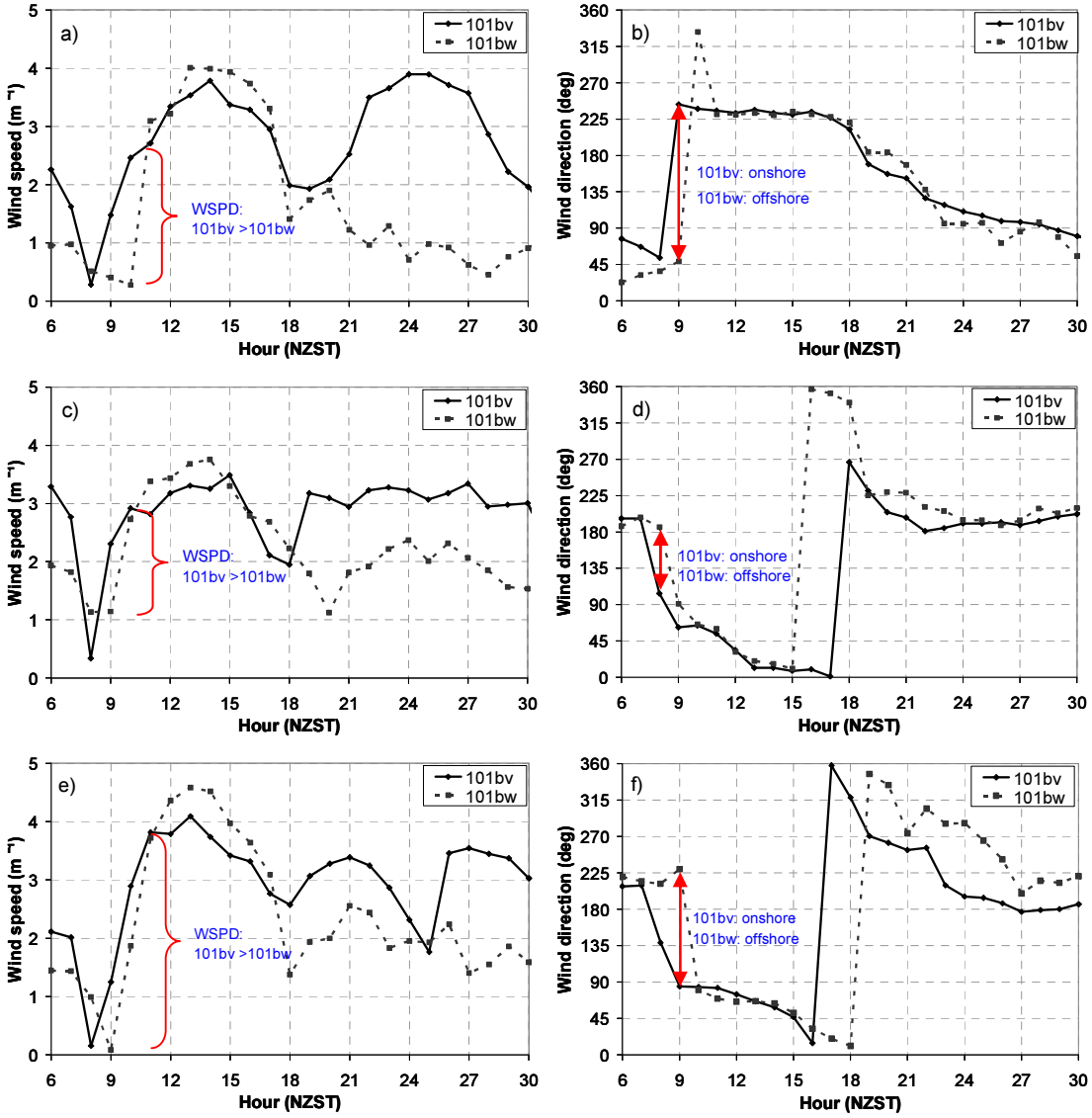


Figure 7.2: Time series plots of wind speed and wind direction from the foothills west of the Waitakere Ranges (top), east of the Hunua Ranges (middle) and east of Coromandel Peninsula (bottom), shown as points WW and EH in Figure 7.1a and point EP in Figure 7.1b, respectively.

In the morning hours, the real terrain simulation predicted slightly higher wind speed on the seaward side of the three ranges that was due to upslope anabatic winds coupled to the sea breezes. Later in the day, from 1200 to 1600 hours, the wind speed over the flat terrain was slightly higher than the real terrain simulation. A possible reason of this modification in the wind speed appears to be terrain height and surface temperature. Although higher terrain acted as a catalyst to early onset of the sea breeze, once the sea breeze developed, the same higher terrain also acted as a barrier. This mountain blocking effect has been investigated by numerous two and three dimensional numerical studies (e.g. Lu & Turco 1994; Lu & Turco 1995; Nitis et al. 2005;

Ookouchi et al. 1978). During the afternoon hours the predicted near-surface (2 m) air temperature over flat terrain was approximately 2.0°C higher than real terrain (Figure 7.3). Another important reason for lower wind speed compared to flat terrain is the terrain-induced convergence of airflow over the lee side (landward side) of the Waitakere and Hunua Ranges due to differences in the pressure field caused by the higher terrain. The sea breeze in both simulations weakened after 1600 hours. At night time the real terrain simulation predicted relatively strong winds (compared to flat terrain) in the vicinity of the three mountain ranges, especially over the seaward slopes (Figure 7.2 and Figure 7.4) that are mainly associated with the cold air drainage from the elevated terrain. This is further discussed in Section 7.3.2.

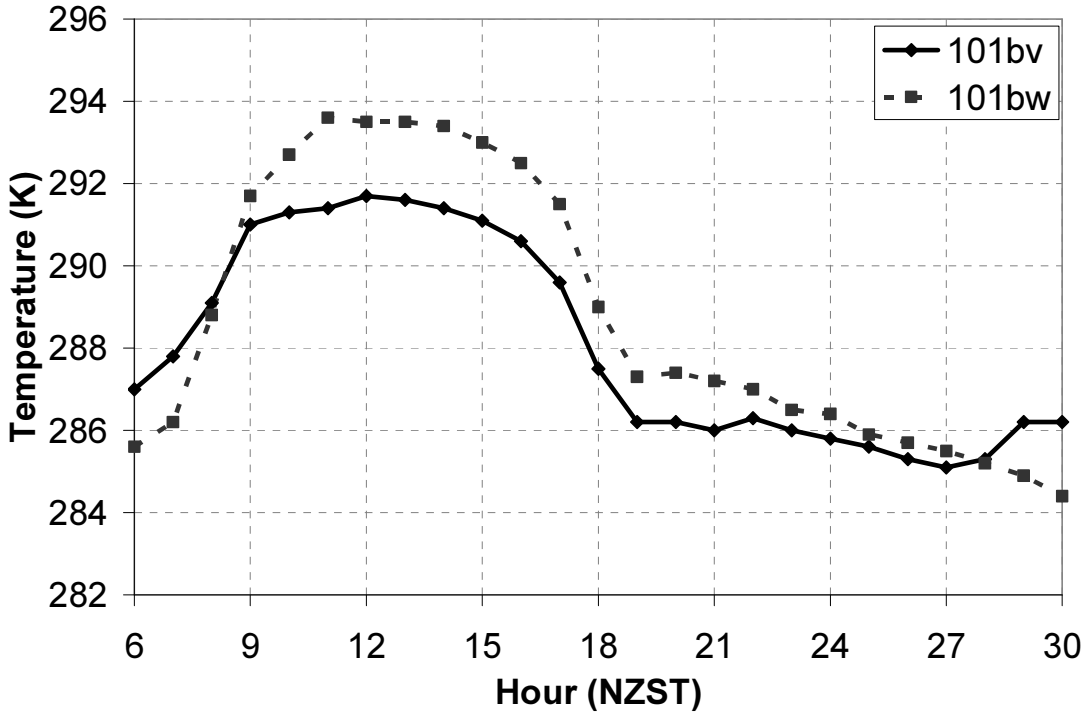


Figure 7.3: Surface temperature 2 m above ground from the location near the top of the Waitakere Ranges, shown as point WT in Figure 7.1a.

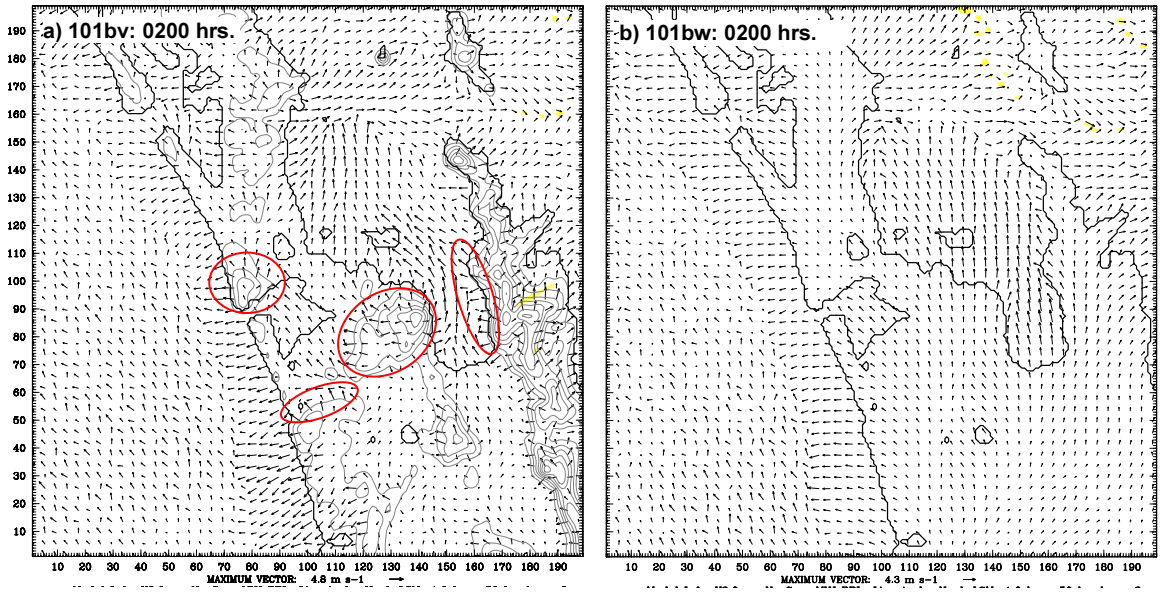


Figure 7.4: Wind field plots of a) real and b) flat terrain simulation at 0200 NZST.

### 7.3.1 Diurnal Rotation of Winds

In general, both simulations showed a diurnal anti-clockwise rotation of sea breezes over the main east and west coasts (Figure 7.2 b, d and f). The surface wind field plots (not shown here) also indicate the modification in the surface flows resulting from the combined effect of topography and the diurnal wind rotation over land. An important feature of the diurnal rotation of thermally induced flow is a difference of rotation rate between the east and west coasts. Over the west coast the wind rotation was much slower than the east coast. This variation in the rotation rate has also been noticed with limited evidence in the observational data analysis (Chapter 4) and real simulation 101cg (Chapter 5). From various studies around the world it is established that rate of rotation of sea-land breezes is not constant over the diurnal cycle. For example, it is higher during morning and evening and slower in the afternoon and at night (Dexter 1958; Kusuda & Alpert 1983; Neumann 1977,1984; Simpson 1995). Neumann (1977) suggested that interaction of the mesoscale pressure gradient and friction force with the Coriolis force is responsible for variation in the rate of wind turning. In the Auckland case, the difference in thermal gradient between land and sea over the west and east coasts is probably one important factor responsible for different rates of rotation.

During night-time, the interaction of drainage flows with mesoscale thermal forcing (diurnal rotation) modifies the wind field in the vicinity of elevated terrains. Over the west coast, the westerly sea breeze became a southerly wind in the evening hours after rotating leftward. The areas of higher wind speed were therefore predicted to the north and on the north-eastern slopes of the Waitakere Ranges. The same is true for the higher terrain of the Waikato River southwest of Pukekohe. On the other hand, the easterly sea breeze became a northerly wind in the evening, and therefore stronger winds were predicted to the south and southeast of the Hunua Ranges. The location, of the areas of higher wind speed changed with time as the wind rotated to balance the Coriolis force and mesoscale pressure gradient forces.

The theoretical anticlockwise rotation was largely affected further inland by the landscape and surface characteristics, such as the three harbours. The surface (10 m) wind hodographs of the real terrain, flat terrain and observed wind from the Auckland Airport and Penrose stations (Figure 7.5) show the effect of surface and synoptic forcing on the diurnal circulation of the sea-land breeze. The wind field at Auckland Airport, which is in close proximity to Manukau Harbour, was largely affected by local and large scale wind. On 18$^{th}$ and 19$^{th}$ March the mean sea level isobar plots showed north-easterly to north-westerly flow over the North Island. The hodographs of the observed surface wind showed clockwise rotation at the Auckland Airport (Figure 7.5c), which is consistent with observational data analysis (Chapter 4) that shows a higher frequency of complete and/or partial clockwise wind rotations at the Auckland Airport during sea breeze days. At Penrose, observed winds were variable (Figure 7.5d), although a northerly component during both day and night time was strong. The idealized simulations 101bv and 101bw were initialized with zero background winds and therefore did not have synoptic wind forcing. Unlike observed winds and wind rotation over east and west coast sites, both real terrain (101bv) and flat terrain (101bw) simulations predicted strong south-westerly flow for most of the diurnal period at Auckland Airport. These results are consistent with the observational data analysis (Chapter 4) and results of Chapter 6 that suggest stronger south-westerly flow due to a stronger thermal gradient between the Tasman Sea and the land surface.

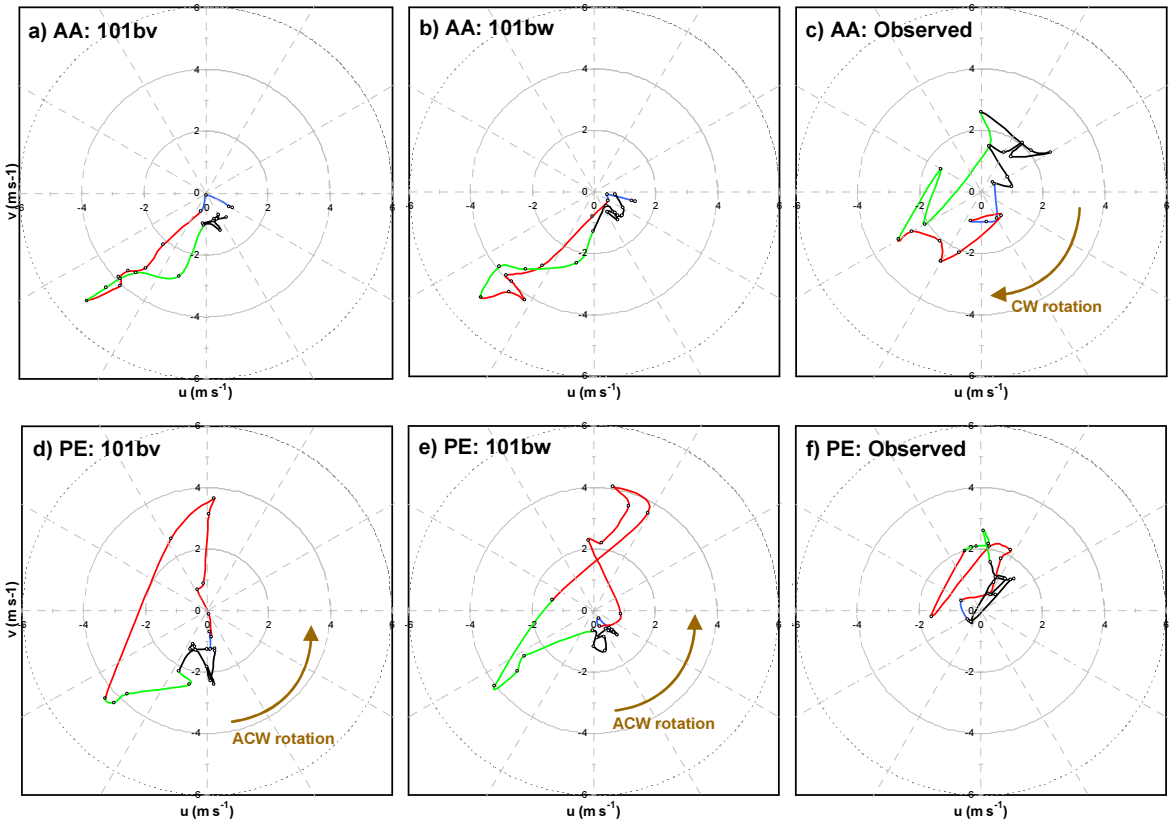


Figure 7.5: Hodographs of surface (10 m) predicted winds from 0600 to 0500 hours next morning at Auckland Airport (AA) and Penrose (PE) for real terrain (101bv) and flat terrain (101bw) simulations shown as point 'AA' and 'PE' in Figure 7.1a respectively. Blue line shows u and v from 0600 to 0900 hours, red line shows winds from 1000 to 1600 hours, green line shows winds from 1700 to 2000 hours while the rest of the time is indicated with black colour. The u and v components are reversed for easy understanding. This means data points falling in any wind quadrant of the hodograph, depicts wind direction of quadrant. All times are NZST.

At Penrose station both simulations (101bv and 101bw) predicted anticlockwise rotation over the diurnal cycle, which is not in good agreement with the observed wind direction data from Penrose (Figure 7.5f). The hodograph of the observed 10 m, wind data for 18$^{th}$ March shows strong northerly component which is due to a north-westerly gradient flow over the region. The rate of rotation also significantly varies between the two simulations. Although both simulations (101bv and 101bw) show a complete anticlockwise diurnal cycle over both coasts, over inland areas the diurnal rotation was modified by the surface characteristics. This indicates that in addition to topographic height and synoptic forcing the inland bodies of water such as Manukau and Waitemata Harbours has a strong effect on the diurnal rotation of thermally induced local winds.

### 7.3.2 Sensible Heat Flux

The thermally induced onshore flow is a function of differential heating between land and sea which is mainly driven by the sensible heat flux. Previous studies show that the distribution of sensible heat flux is a critical factor in the onset and development of the mesoscale sea breeze circulation (Miao et al. 2003; Segal & Arritt 1992). The magnitude of the sensible heat flux is greatly affected by surface characteristics, for example, vegetation cover, soil type, soil moisture and terrain height (Miao et al. 2003; Physick 1980; Yan & Anthes 1988). An onshore flow is attributed to reduced latent heat flux and enhanced sensible heat flux over land. Therefore, areas of well developed and stronger sea breeze correspond to areas of higher sensible heat flux (Rouse & Bello 1985; Rouse et al. 1987). Comparison of the sensible heat flux distribution of grid domain D02 of the real and flat terrain simulations (101bv and 101bw) revealed important information with regard to the influence of topography on the onset, strength and inland propagation of the sea breeze front (Figure 7.6). The eastern slopes of the Hunua and Coromandel Ranges warmed up relatively rapidly with the incoming solar radiation from the morning sun (0900 – 1100 hours). The magnitude of the sensible heat flux at the Waitakere Ranges during morning hours was much lower than the Hunua and Coromandel Ranges but slightly higher than the surrounding low elevation terrain with some hot spots starting to develop over the slopes. The differential heating coupled with the upslope wind flow therefore led to a relatively strong onshore flow in the morning hours, which is also evident from the surface wind time series plot (Figure 7.2). The higher predicted sensible heat flux over the eastern slopes of the Hunua and Coromandel Ranges was primarily due to the azimuth angle of the sun. In the morning hours, the west side of the Waitakere Ranges would be in the shadow and it is not expected to heat up at the same rate as the eastern slope. However, the higher predicted sensible heat flux to the west of the Waitakere Ranges that triggered the early onset of the westerly sea breeze was probably due to lower terrain resolution.

In the afternoon hours, in the real terrain simulation the magnitude of sensible heat flux over the slopes of the three ranges was larger than the surrounding low elevation terrain, as well as the flat terrain simulation. However, the real terrain simulation predicted slightly lower wind speeds over the three ranges than the flat terrain simulation, which means despite higher sensible heat flux and upslope wind

enhancement the net wind speed was reduced over the seaward side of the ranges. The possible explanation of this behaviour of the onshore winds is the convergence between upslope winds from opposite directions, the coastline shape (Baker et al. 2001; MetEd 2008; Purdom 1976) and mountain blocking effect (Millan et al. 2000).

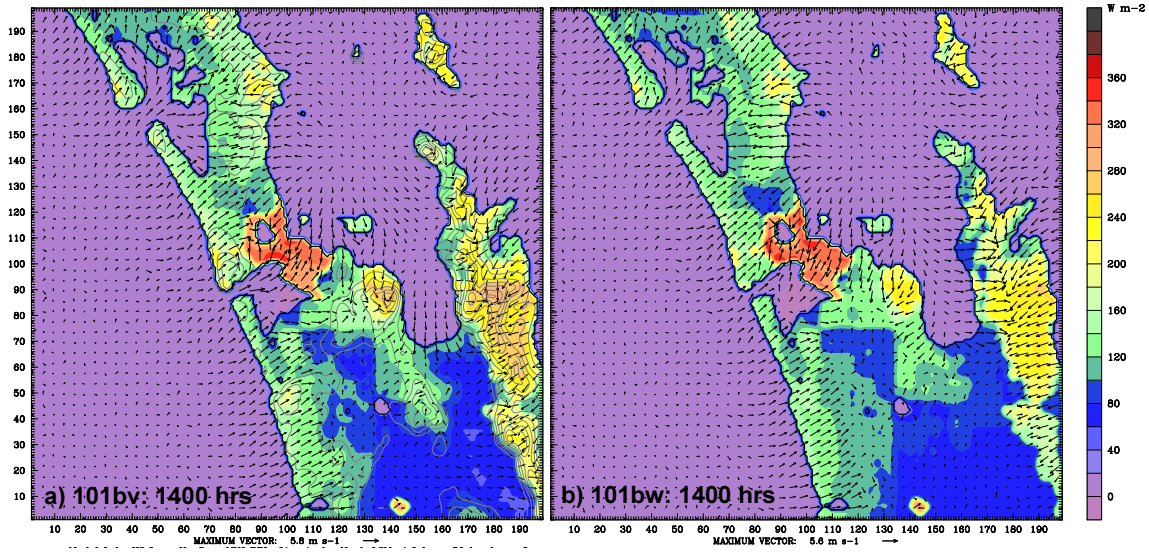


Figure 7.6: Sensible heat flux over the Auckland region at 1400 NZST in grid domain D02 of the idealized simulations of a) real terrain and b) flat terrain.

The predicted sensible heat flux over the main Auckland city area was lower than the eastern slopes of the Hunua and Coromandel Ranges in the morning hours, but by 1200 hours the magnitude of the sensible heat flux in the heavily urbanized Auckland city exceeded the rest of the Auckland region (Figure 7.6). This is reflected by development of an intense sea breeze circulation over the city domain. The time series plot of maximum wind speed over Auckland City suggests that the wind magnitude predicted by the flat terrain simulation was 1 m $s^{-1}$ higher than real terrain, while in the evening hours and at night time the flat terrain predicted wind magnitude was lower than the real terrain simulation (Figure 7.7). This indicates that removal of physical barriers helped in increasing sea breeze strength in the afternoon, while after sunset the drainage winds from the Waitakere and Hunua Ranges contributed to relatively strong winds.

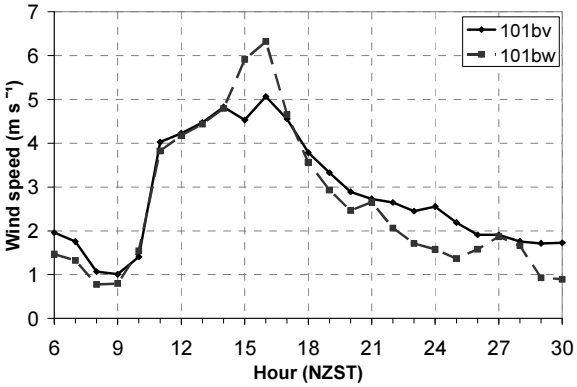


Figure 7.7: Time series plot of the maximum wind speed over Auckland City (10 x 10 km area), shown as area block 1 in Figure 7.1a.

### 7.3.3 Effect of the Gap Flow at Manukau Harbour

The entrance of Manukau Harbour to the Tasman Sea, with higher terrain on both sides, provides a narrow opening to the westerly winds. In the literature, the wind flow, in this type of topographic setting is known as a mountain-gap wind, jet effect wind, canyon wind or simply gap flow (Lin 2007). The wind across the barrier can develop into a strong wind due to the pressure gradient across the barrier (Lin 2007). Following the continuity equation of mass conservation (Pielke 2002; Stull 2003), the real terrain simulation (101bv) predicted a higher wind speed than the flat terrain simulation (101bw) over the Manukau Harbour during afternoon hours (Figure 7.8), which may have some effect on the wind regime over Auckland City, as discussed in the following section.

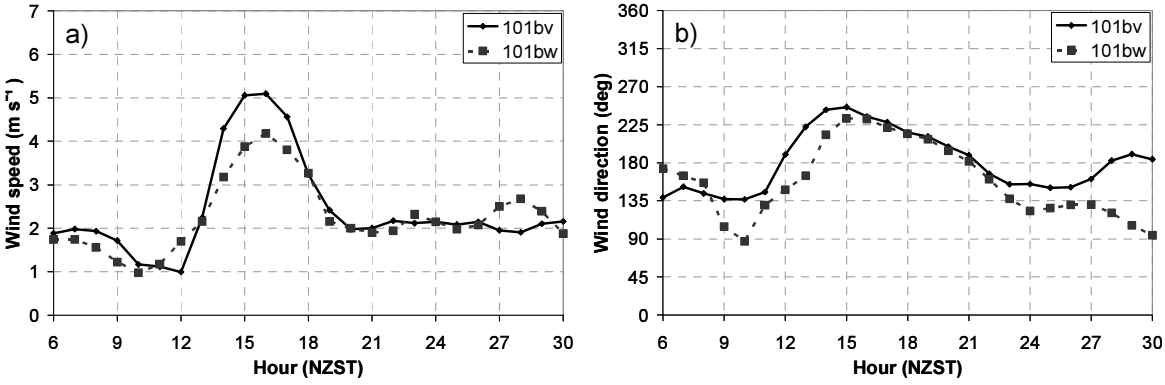


Figure 7.8: Time series plot of wind speed and wind direction of the predicted surface (10 m) winds averaged over an area of 78 km$^2$ over Manukau Harbour, shown as orange colour area block 3 in Figure 7.1a.

## 7.4 Position and Strength of Convergence Zones

The inland propagation of the sea breeze front forms convergence between a cold and moist marine air mass and the warm air over land. The position of the convergence zone is quite often used to identify the frontal edge of the sea breeze. The horizontal winds ahead of the sea breeze front are nearly calm, but the vertical velocities are significantly higher in convergence zones (Miao et al. 2003; Millan et al. 2000). Previous studies suggest that terrain height and coastline shape play an important role in the formation, strength and position of convergence zones (Miao et al. 2003; Varvayanni et al. 1993). A comparison of grid domain D02 of the two (101bv and 101bw) simulations revealed important features with regard to the role of topography in the onset, strength and inland propagation of the sea breeze front (Figure 7.9). In the absence of any synoptic wind forcing, the sea and bay breezes were solely dominated by surface processes. Analysis of the real and flat terrain simulation results suggest that upslope flow over the three main ranges (Waitakere, Hunua and Coromandel) triggers convergence in the morning hours, with the first three areas of convergence predicted between 0900 and 1000 hours over the higher terrain. Although areas of relatively weak vertical velocities (with the same spatial and temporal configuration) were also found (indicating weak convergence) in the flat terrain simulation, which was mainly due to coastline shape. Studies have shown that the coastline shape may either enhance or reduce convergence and vertical motion along the sea breeze front (Abbs 1986; Baker et al. 2001; Purdom 1976). The sea breeze tends to diverge over a concave coastline and converge over a convex coastline (MetEd 2008). This is also evident in Figure 7.10 that shows the comparable magnitude of maximum vertical velocities from real and flat terrain simulations over the three ranges. This further explains that convergence over these ranges was not only terrain induced, as the coastline shape also contributed to the strength of the convergence zones. This is also reflected in Figure 7.9a and 7.9b that shows convergence in the morning hours around higher terrain and convex coastline in both real and flat terrain simulations, although the flat terrain simulation predicted slightly weaker and relatively diffused convergence compared to the real terrain simulation. In the absence of any synoptic influence, the westerly sea breeze was stronger than the easterly sea breeze, which was due to a greater thermal differential between land and sea over the west coast. The convergence lines were also formed around the three harbours during the morning hours due to interaction of bay

breezes from the three harbours with the warm inland air. In the afternoon hours, the inland propagation of the sea breeze fronts from the main coasts overwhelmed the bay breezes. The bay breeze induced convergence lines merged with the main sea breeze convergence zones that were formed due to collision between mature east and west coast sea breezes. These SBCZs gradually migrated eastward due to a relatively strong westerly sea breeze. Another feature of the particular topographic setting of the Auckland region is the combined effect of the higher terrain of the Waitakere Ranges and the large inland water body of Manukau Harbour on Auckland City. The real terrain simulation predicted higher wind speeds (discussed in Section 7.3.3) over Manukau Harbour that increased the strength of the westerly sea breeze front. Therefore, the predicted SBCZ over Auckland City migrated further eastward. However, the effect of gap flow was gradually reduced over southern Auckland.

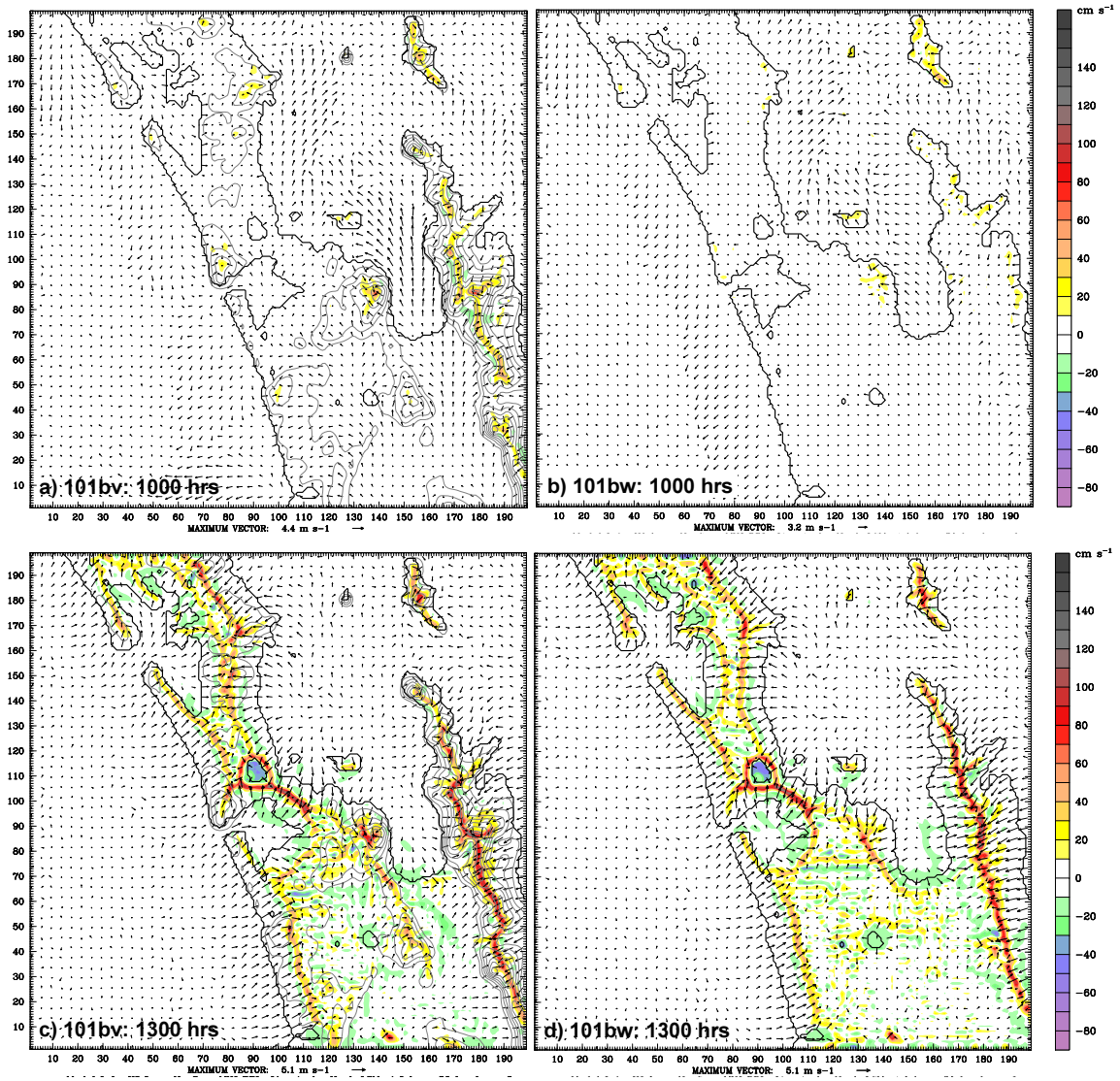

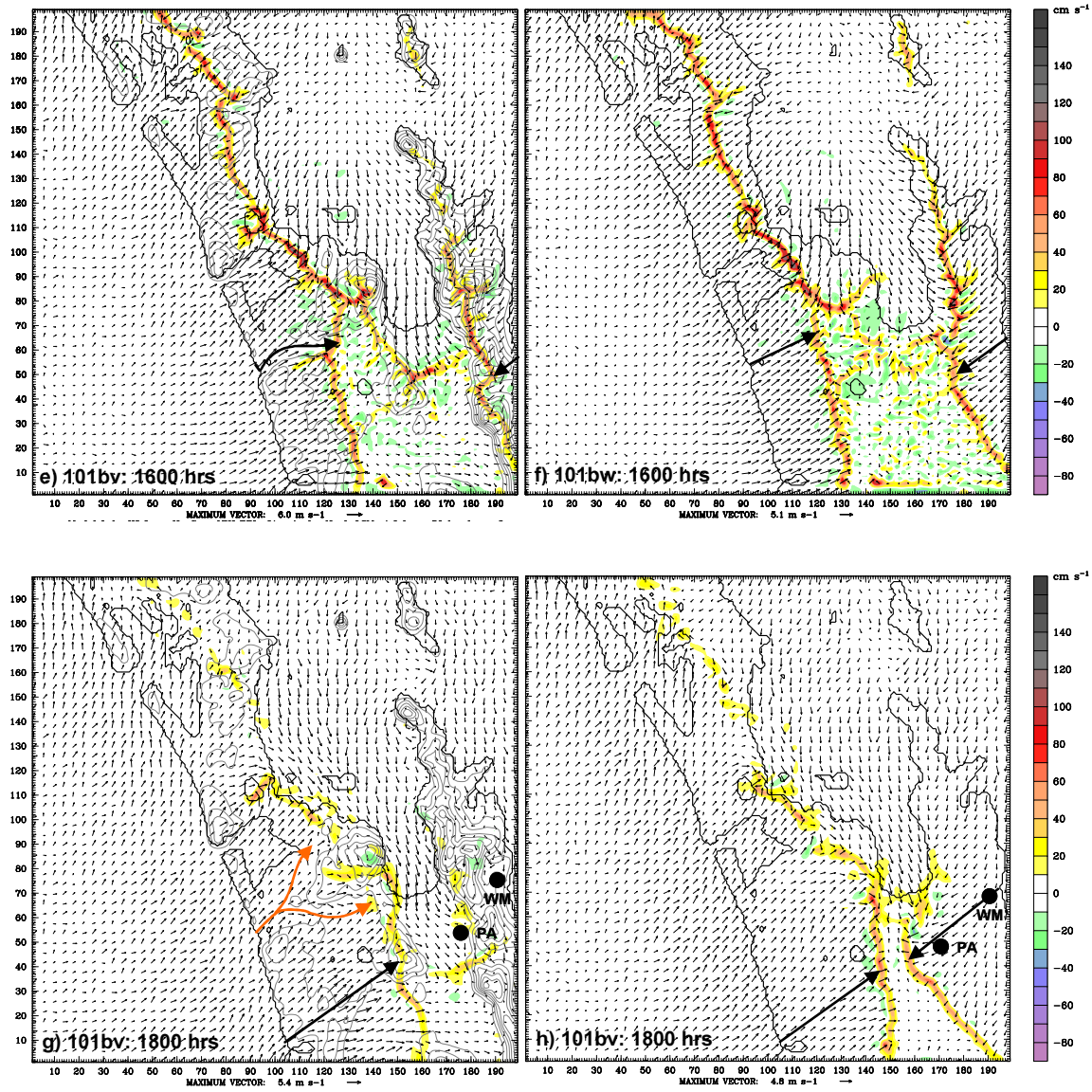


Figure 7.9: Maps of the wind field 10 m above ground level and vertical velocities (colour shaded) approximately 500 m above ground level. Panels to the left (a,c,e,g) are 1000, 1300, 1600 and 1800 NZST plots from real terrain simulation (101bv), while panels to the right (b,d,f,h) are plots from the flat terrain simulation (101bw) for the same times. Large thick black and orange arrows indicate the inland extent and path of the sea breeze fronts. * WM: Whangamata, PA: Paeroa.

Figure (7.10d) shows relatively high upward vertical velocities over Auckland City due to strong convergence between north-easterly and south-westerly sea breezes. Both simulations predicted intense sea breezes driven by the strong sensible heat flux, especially over Auckland City (>300 W $m^{-2}$) which was primarily attributed to the urban heat island effect. The magnitude of the vertical velocities was higher in the flat terrain simulation during afternoon hours, which is probably due to removal of the blocking effect of the uneven terrain. This is further supported by slightly higher

horizontal winds predicted by the flat terrain simulation in the afternoon hours of the day.

Over Coromandel Peninsula, due to the narrow width of the land mass, the convergence line that was formed in the middle of the land mass remained intact during the day and weakened in the evening. A more distinct terrain effect can be observed further south of Coromandel Peninsula (near Whangamata and Paeroa). In the afternoon hours, the predicted convergence line over the Coromandel Ranges in the real terrain simulation was extended further south over the higher terrain near Whangamata. The sea breeze front reached the top of the higher terrain but did not propagated further inland due to the blocking effect of the elevated terrain, as well as the upslope anabatic flow from the opposite (landward) side of the range, while the sea breeze front in the flat terrain simulation continued moving inland. By 1800 hours the flat terrain simulation predicted a sea breeze front penetrating approximately 50 km inland, while over the real terrain the easterly sea breeze front could not move further inland and died later in the evening when winds rotated northward due to gradual reversal of the thermal gradient between land and sea.

Another terrain-induced convergence line was formed over the higher terrain to the south of the Hunua Ranges and ran through east of Lake Waikari. The other leg of this convergence line also joins the convergence line over Coromandel Ranges. This convergence line is mainly related to sea breeze inflow from the Firth of Thames. The higher terrain east of Lake Waikari, and the Hunua and Coromandel Ranges caused intensification of the sea breeze in this region. This convergence line remained intact throughout the day until it was dissipated after 1700 hours. Over the west coast, the higher terrain (< 250 m asl) of Pakau, Pukeotahinga and Putataka, south and southwest of the Waikato River valley modified the surface winds. The inland propagation of the sea breeze front and the position of the convergence zone were also affected due to the higher terrain. The mouth of the Waikato River (near Port Waikato) forms an orographic setting similar to a coastal valley. The sea breeze fronts tend to extend further inland rapidly along coastal valleys and remain close to the coast if they encounter coastal mountain ranges (Millan et al. 2000). The strong wind flow of the westerly sea breeze moves inland faster along the Waikato River valley with higher

terrain of Pakau to the south and Hunua to the northeast than the flat terrain simulation. The inland extent of the front with terrain was 10 to 20 km more than the flat terrain simulation, although pressure variation due to the hilly terrain also slightly turned the westerly sea breeze southward.

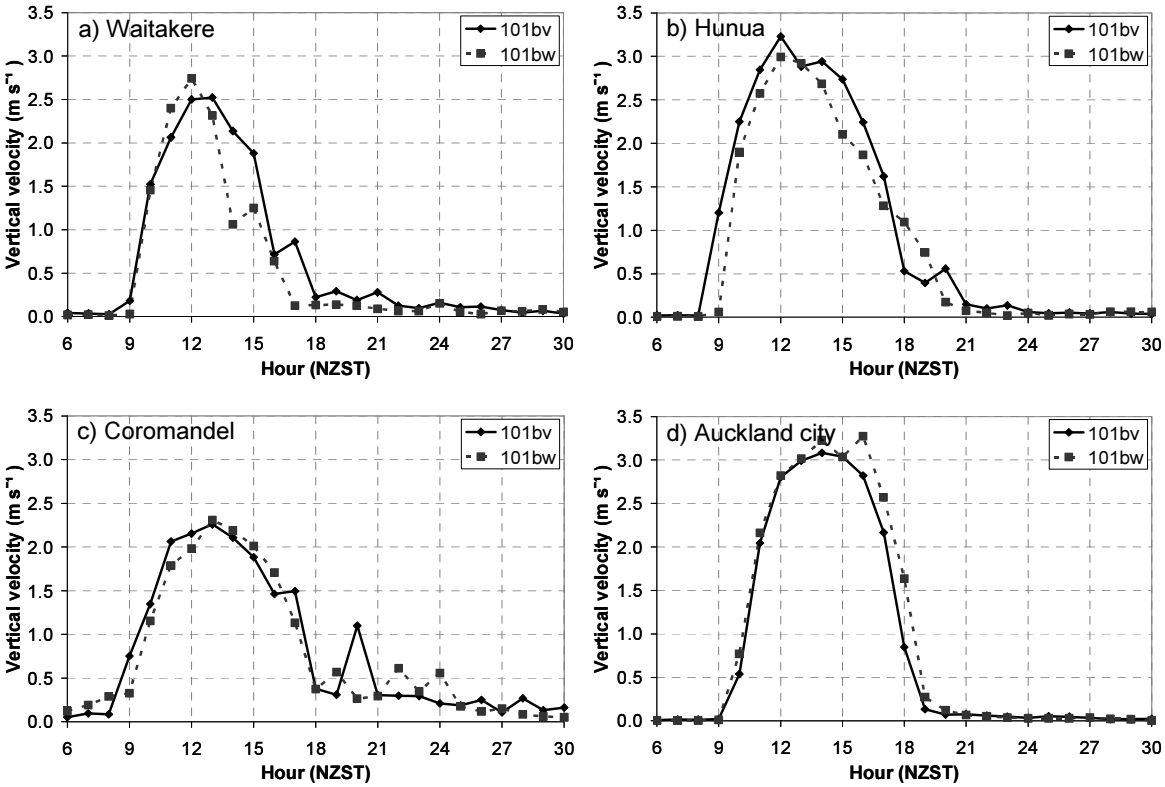


Figure 7.10: Time series plots of maximum upward vertical velocities over a) Waitakere Ranges from area block 2 shown in Figure 7.1a, b) Hunua Ranges from area block 4 shown in Figure 7.1a, c) Coromandel Peninsula from area block 5 shown in Figure 7.1b, and d) Auckland city from area block 1, shown in Figure 7.1a. The solid black line represent predicted vertical velocity with actual terrain, while the dotted black line shows vertical velocity predicted by the flat terrain simulation (101bw).

## 7.5 Sea Breeze Circulation

The interaction of the thermally induced sea-land breeze and coastal mountains has significant implications for the thermodynamic structure of the boundary layer. Coastal mountains affect sea breezes in many ways, for example the mountain upslope flows coupled to onshore sea breezes produce a more intense sea breeze circulation. However, mountains also act as a barrier to the inland propagation of the sea breeze (Mahrer & Pielke 1977; Ookouchi et al. 1978). Lu & Turco (1994) found that the dynamics of the upslope winds coupled with the sea breeze circulation is strongly affected by the vertical temperature profile of the atmosphere, the size and height of the

mountain and the distance of the coastal mountain from the coast, while Millan et al. (2002) suggested that land surface characteristics of the mountains are also important controls that affect development of upslope wind coupled sea breeze circulations. The resulting sea breeze circulation affects the transport and dispersion of air pollutants by contributing to either venting or increasing pollutant species in the coastal urban areas (Lu & Turco 1994; Lu & Turco 1995). Vertical cross-sections were obtained from the real (101bv) and flat terrain (101bw) simulations to examine the recirculation mechanism and topographical influence in the vicinity of the Waitakere and Hunua Ranges (Figures 7.11, 7.12, and 7.13).

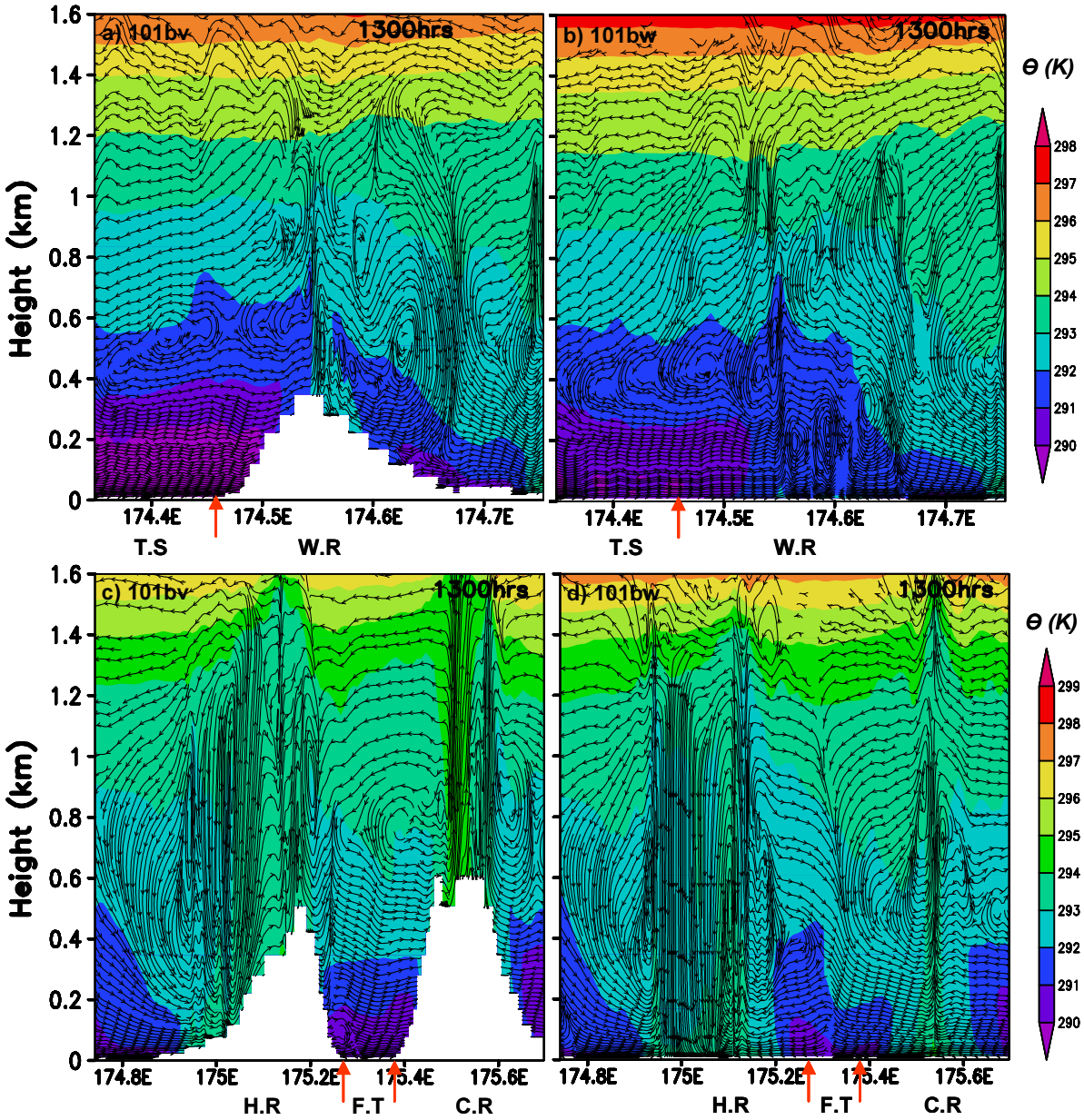

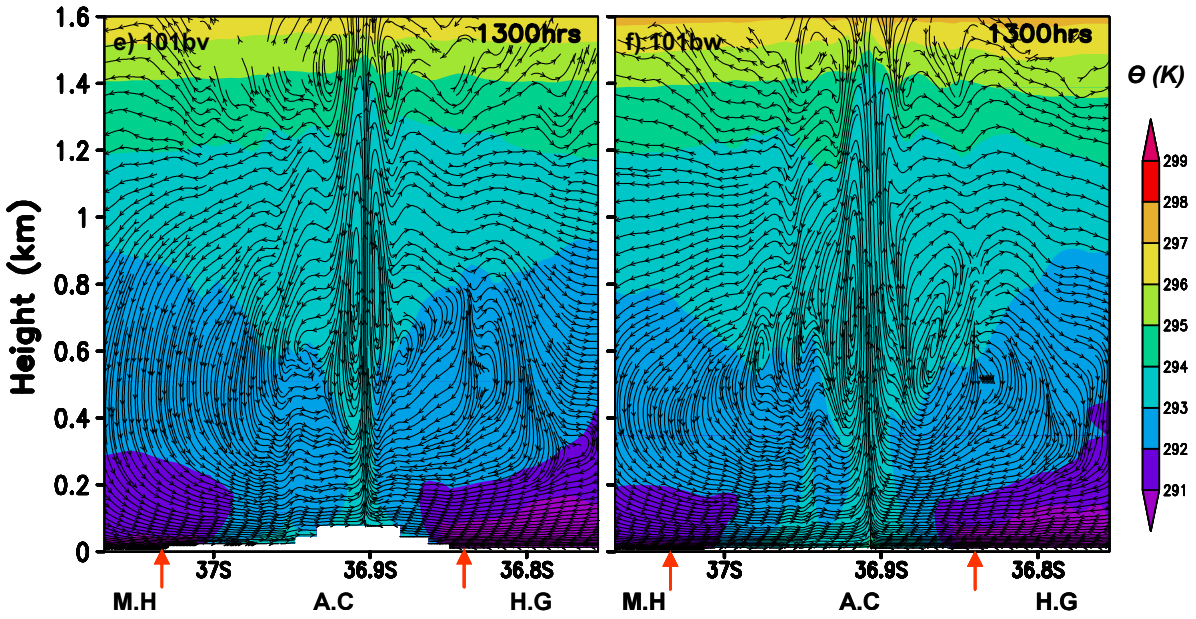


Figure 7.11: Vertical cross-sections of streamlines of horizontal and vertical velocity (m $s^{-1}$) and potential temperature (colour shaded) at 1300 NZST. The panels on the left were obtained from the real terrain simulation and the panels on the right were obtained from the flat terrain simulation. The top two panels (a and b) were derived for the Waitakere Ranges from location BB` in Figure 7.1a, the middle two panels (c and d), were derived for the Hunua and Coromandel Ranges from location EE` in Figure 7.1b, and the bottom two panels (e and f), were derived for Auckland City from location CC` in Figure 7.1a. The stream lines for Waitakere and Hunua and Coromandel Ranges (top and middle panels) were calculated for the u and w velocity, while for Auckland City (bottom panels) streamlines were calculated for v and w velocity. The vertical velocity is adjusted by a factor of 3.0 to improve the appearance vertical component. Orange arrows indicate the interface between land and water. The east-west extent of plot 'a' and 'b' is 45 km, 'c' and 'd' is 106 km, while north-south extent of plot 'e' and 'f' is 35 km.
* T.S: Tasman sea; W.R: Waitakere ranges; H.R: Hunua ranges; C.R: Coromandel ranges; F.T: Firth of Thames; M.H: Manukau Harbour; A.C: Auckland City; and H.G: Hauraki Gulf.

The vertical cross-sections from the Hunua Ranges have been combined with Coromandel Peninsula due to proximity and the large influence of the Hunua and Coromandel Ranges on each other. In addition, a Y-Z cross-section is also plotted over Auckland City to examine the circulation and any effect of the elevated topography of the three ranges on the dynamic and thermal structure of the boundary layer over Auckland City. The vertical cross-section for the Waitakere Ranges and Auckland City have been drawn from grid domain D03 (500 m resolution), while for Hunua and Coromandel Ranges, the vertical cross-sections were obtained from grid domain D02 (1000 m resolution).

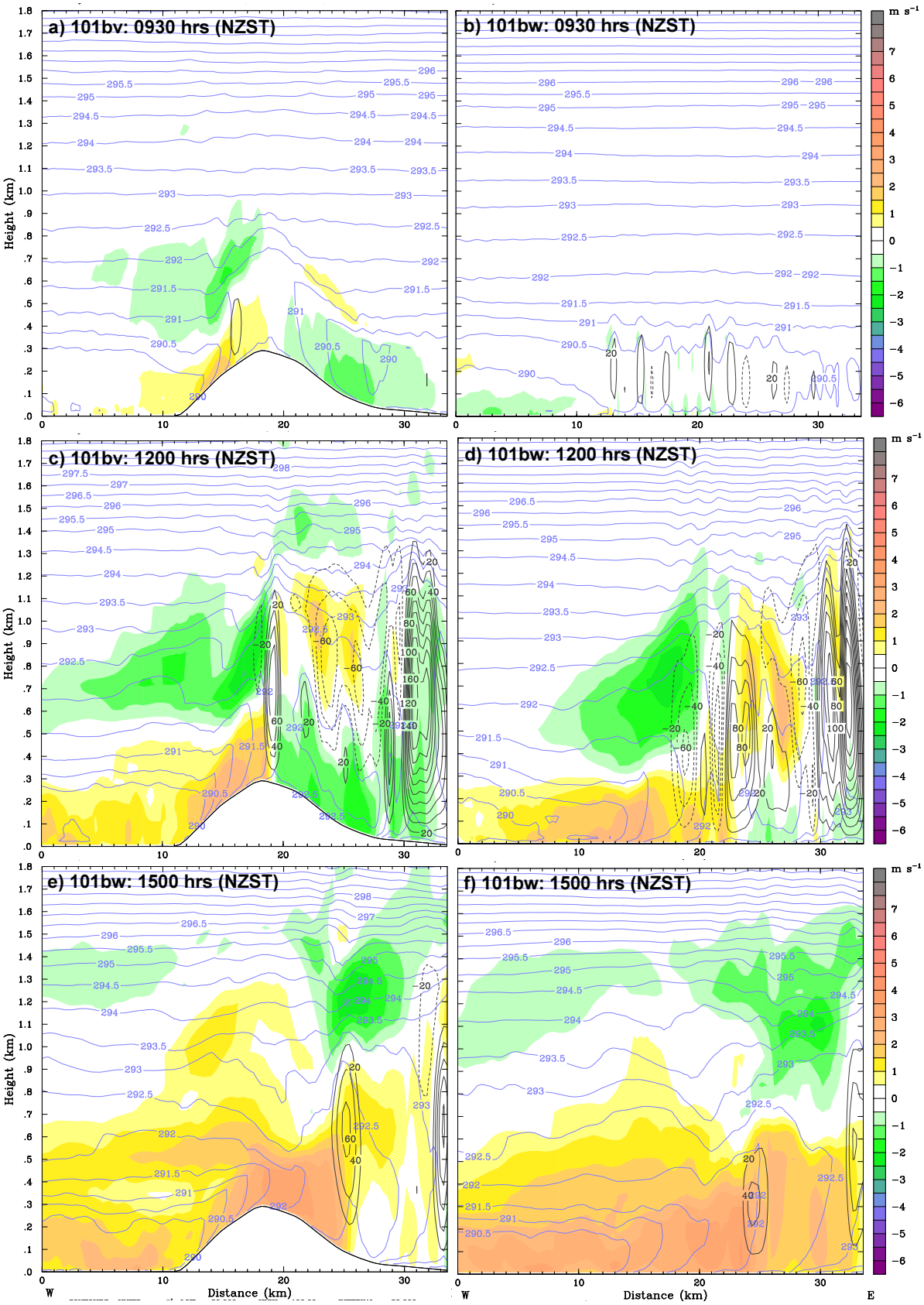


Figure 7.12: Vertical cross-sections (AA` in Figure 7.1a) of the u velocity (m $s^{-1}$) colour shaded, potential temperature (K) as blue contour lines and vertical velocity (cm $s^{-1}$) as black contour lines over the Waitakere Ranges for 0930, 1200 and 1500 NZST. Panels on the left were obtained from the real terrain simulation (101bv) and panels on the right were obtained from the flat terrain simulation (101bw).

### 7.5.1 Waitakere Ranges

In the morning, the mixed layer expands, and rapidly increasing sensible heat flux over higher terrain of the Waitakere Ranges resulted in the early onset of an anabatic wind coupled sea breeze that gradually accelerated with time. The higher terrain and bay-breeze from the Manukau Harbour also developed a relatively strong upslope flow on the easterly (landward) slopes of the Waitakere Ranges that offered a significant barrier to the onshore sea breezes from the Tasman Sea (Figure 7.12c). During the day, sea breeze and mountain up-slope flow combined as a coupled circulation. The cold and moist marine air warmed over the slopes of the Waitakere Ranges and rose into the inversion above the mountain top and created a return flow offshore in the inversion layer. Later in the day (after 1200 hours) as the thermal gradient between land and sea further increased, the westerly sea breeze flow overcomes the opposing easterly wind (Figure 7.12e). Also, the sea breeze front predicted by the flat terrain simulation was 4 to 6 km ahead of the real terrain simulation.

Due to orographic lifting the predicted mixed layer depth over the Waitakere Ranges was higher in the real terrain simulation in the morning hours. However, with the increase in solar flux, convection initiated and the mixed layer height in the flat terrain simulation rapidly increased. In the afternoon hours, the flat terrain simulation predicted near surface (2 m) air temperature was 2 °C degree higher than for the real terrain, which apparently compensated for the topographic lifting of the real terrain simulation (Figure 7.3). The predicted depth of the terrain-induced sea breeze density current, sea breeze head and the return flow was 100 – 300 m higher than the flat terrain simulation (101bw). The depth of the sea breeze current predicted by the real terrain simulation varied from 200 m (in the morning) to 1000 m (in the afternoon), whereas the top of the sea breeze head was in the range of 900 to 1400 m. The depth of the return flow layer ranged from 200 to 500 m. For most of the time, a shallow shear zone with wind speeds less than 1 m $s^{-1}$ also formed between the onshore sea breeze flow and offshore return flow. The vertical streamline cross-sections (Figure 7.11a and 7.11b) showed rotors similar to Kelvin-Helmholtz Billows (KHB) in this shear zone. The KHB's are formed along the upper boundary of the inland marine air mass and cause mixing between the cold and moist marine air mass and relatively warm return flow (Chiba et al. 1999; Miller et al. 2003).

The upslope flow from the seaward side is clean due to absence of any anthropogenic activity. However, over the eastern (landward) side of the Waitakere Ranges, the easterly see breeze would carry loads of pollutants from Auckland City and western Auckland when it reaches the foothills of the Waitakere Ranges. The upslope flow would carry the pollutants above the top of the Waitakere Ranges and inject these pollutants either directly into the inversion layer or in case of strong convergence over the mountain where mixed layer forced through the inversion layer, thus venting pollutants directly into the free atmosphere above the boundary layer top. This venting of pollutant due to terrain induced upslope flows is known as a mountain chimney effect (Fast & Zhong 1998; Lu & Turco 1994; Lu & Turco 1995). If the pollutant was inserted into the inversion layer over the mountain top it would become part of the return flow and be transported towards the east coast. An elevated pollution layer can thus be generated over the Auckland area. Considering the low elevation of Waitakere Ranges, most probably the pollutants would be dispersed in the return flow (Lu & Turco 1994). However, both of the idealized simulations (101bv and 101bw) were run with zero background winds and the simulation with real or idealized background winds (real simulation:101cg, in Chapter 5 or idealized simulations with constant background winds 101bx to 101ca in Chapter 6) did not show this type of organized circulation. The return flow in the simulations with background winds was more diffused and dispersed, and therefore, recirculation of pollutants by the return flow of the easterly sea breeze is unlikely, unless the gradient wind flow is very weak. However, if it happens the possibility of recirculation of pollutants under easterly sea breeze conditions does exist, especially heavier particles such as $PM_{10}$ (Lyons & Olsson 1973).

### 7.5.2 Hunua and Coromandel Ranges

The topographic features of the Hunua and Coromandel Ranges exhibit complex wind flows during a sea breeze event. The most important feature of this topographic setting is two small but simultaneous circulations over the Hunua Ranges, Coromandel Peninsula and the Firth of Thames (Figure 7.13). The two steep sections of terrain on both sides of the Firth of Thames create a valley setting, with the valley floor comprised of water. In this setting, the wind field behaviour was similar to mountain –

valley winds (Figure 7.11 and 7.13). The anabatic flow started in the morning hours over the heated slopes of the Hunua and Coromandel Ranges creating divergence over the Firth of Thames. Due to this divergence over the sea, the return flow over both the Hunua and Coromandel Ranges was stronger, as the air mass from both ranges subsided over the Firth of Thames to again become part of the anabatic flow of either the Hunua or Coromandel Ranges. Similar to the Waitakere Ranges, in the morning hours when solar flux was weak, the greater mixed layer depth predicted by the real terrain simulation was attributed to orographic lifting. In the afternoon, although the higher surface temperature of the flat terrain simulation compensated for the elevated terrain effect, for most of the day, the terrain-induced elevated mixed layer was 200 to 400 m higher than the flat terrain mixed layer height. The sea breeze circulation on the seaward side (Hauraki Gulf) of the Coromandel Ranges was also quite evident. The potential temperature contours and u velocity indicate the structure of the sea breeze fronts over both sides of the Hunua and Coromandel Ranges (Figure 7.13). The strong updrafts and downdrafts over the hills led to intense mixing of the basic meteorological properties, such as temperature, momentum and moisture. Pollutants being emitted in the vicinity, for example at Pukekohe, may be diluted by the deep circulation on a sea breeze day (Figure 7.11 and 7.13).

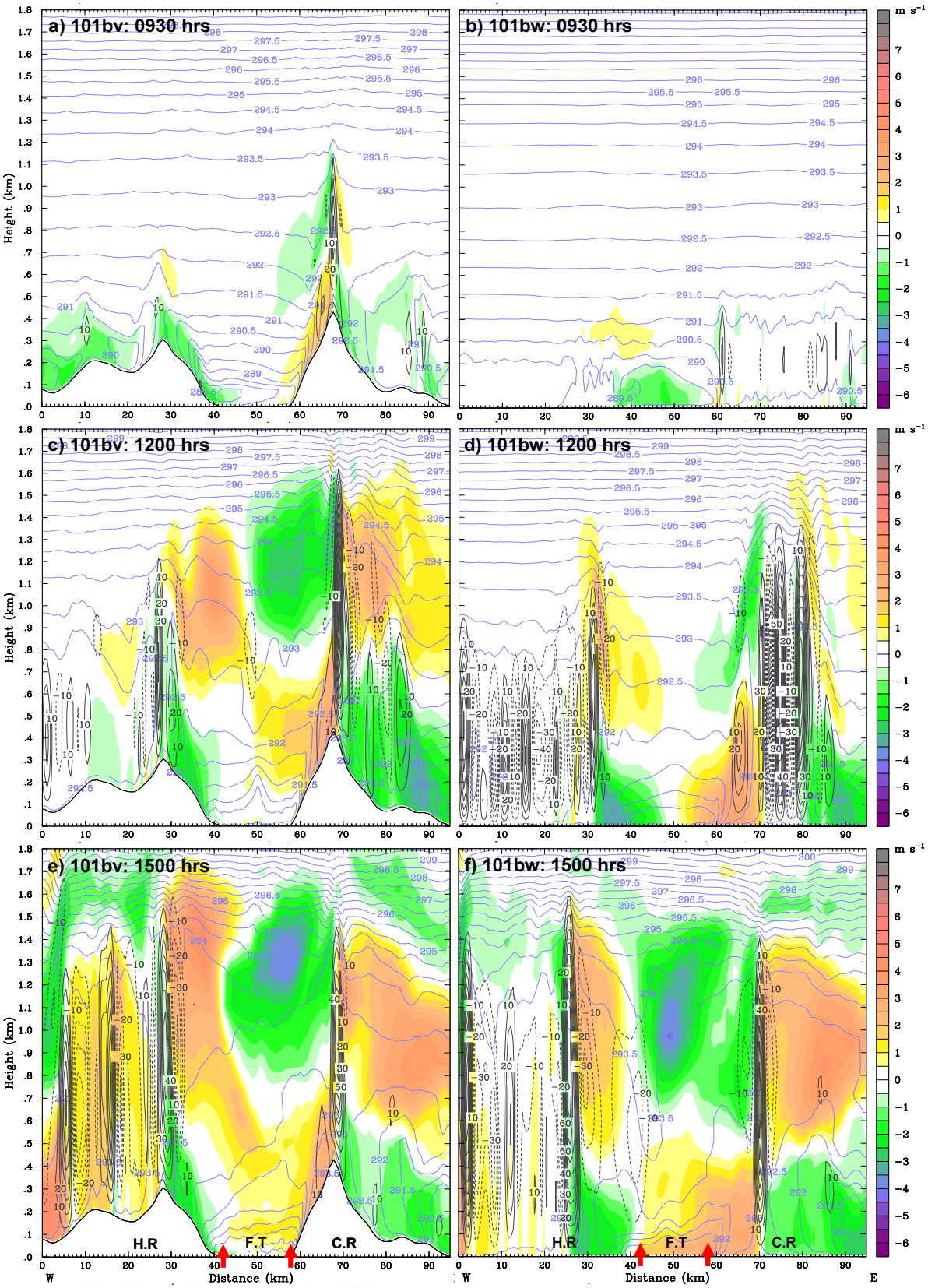


Figure 7.13: Same as 7.12, but for the Hunua and Coromandel Ranges from location DD` in Figure 7.1b. Red arrows in the two bottom plots indicate points of interface between land and water. * H.R: Hunua Ranges, F.T: Firth of Thames, C.R: Coromandel Ranges.

Most of the highly urbanized areas are located to the north, northwest and west of the Hunua Ranges. An obvious question is whether the higher terrain of the Coromandel and especially Hunua Ranges has any impact on the air quality of the region. The peak elevation of model terrain at Hunua and Coromandel is around 600 m. Lu & Turco (1994) in their numerical modelling study assessed the effect of mountain elevation on sea-land breeze circulation and suggested that low elevation terrain such as the Hunua Ranges (~500 m) showed a relatively small effect on the sea breeze, but the sea breeze circulation was still able to control the pollutant transport. During daytime under coast-parallel north-westerly and westerly prevailing winds the deflected/enhanced sea breeze from the east or west coast may advect pollutants towards Hunua. The upslope winds then transport pollutants to the top of the ranges where the polluted air mass may be advected back in the return flow. Results in Chapter 6 suggest that direction of the return flow strongly depends on the gradient wind direction and strength.

### 7.5.3 Auckland City

The north-south vertical cross section through Auckland City shows a strong convergence between westerly and easterly sea breezes over the middle of the city. The two circulation cells extend to both Manukau Harbour and Hauraki Gulf (Figure 7.11e and 7.11f). Due to absence of any significant higher terrain, there were no major differences in the vertical structure of the circulation in real and flat terrain simulations, except that the thermal structure of the surface layer was slightly modified in the real terrain simulation. The time – height cross-section of potential temperature, moisture and wind vectors from Penrose station (Figure 7.14) shows strong convergence from mid-morning to afternoon hours (1000 – 1400 hours) that runs through the centre of the city with no significant variation in moisture, wind speed and direction. The mixed layer height under real terrain simulation (101bv) was up to 200 m higher than the flat terrain simulation (101bw). In the early afternoon hours both simulations were predicting northerly winds. At around 1500 hours, the convergence zone predicted by the flat terrain simulation moved westward giving north-easterly flow at Penrose that resulted in slight reduction in moisture content. At 1600 hours, the westerly sea breeze front moved in and the gap flow enhanced westerly sea breeze (especially in the real terrain simulation), pushed the SBCZ eastward and overwhelmed the Penrose station. The inflow of westerly sea breeze changed the thermal structure of the boundary layer

over Penrose and a shallow 200 m deep CIBL was formed in the cold and moist marine westerly airflow. In the flat terrain simulation, the inflow of westerly sea breeze was delayed for one hour, the mixed layer therefore collapsed around 1700 hours. There were no significant differences in the CIBL depth for both real and flat terrain simulations. Although both simulations predicted stable stratification of the boundary layer and formation of a residual layer over less urbanized (sub-urban or rural) areas after 1800 hours, due to the UHI effect a stable layer did not form over Penrose until 2100 hours.

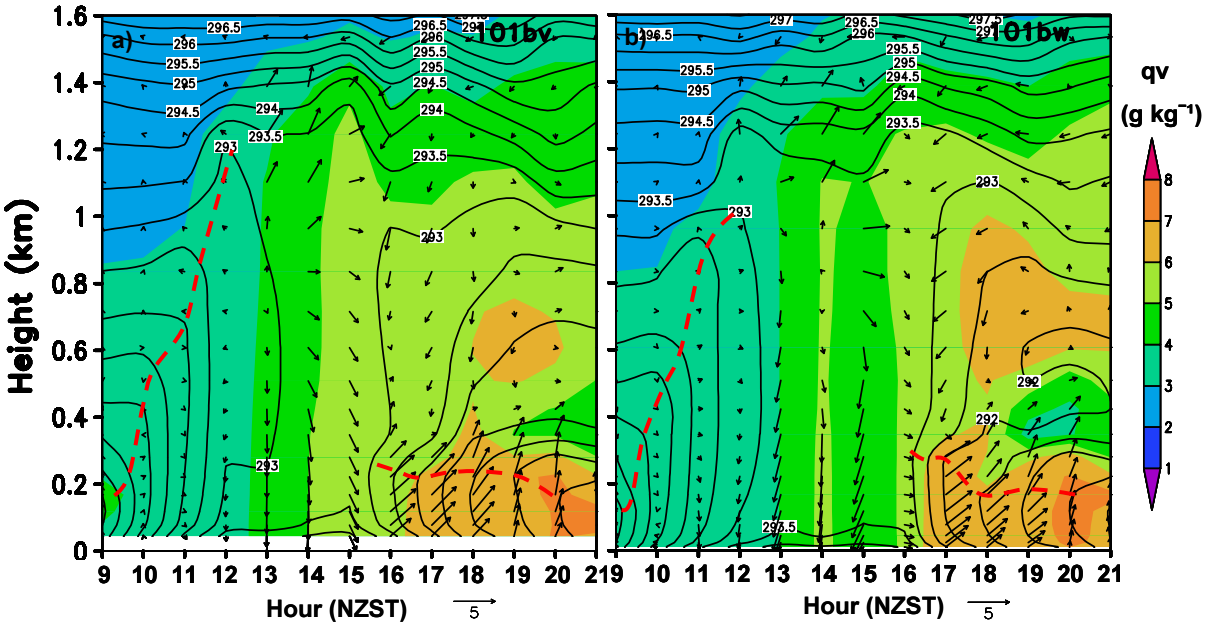


Figure 7.14: Predicted time-height cross sections of potential temperature (black contours lines), water vapour mixing ratio (colour shaded) and horizontal wind vectors (m $s^{-1}$) from Penrose for a) real terrain simulation (101bv), and, b) flat terrain simulation. The red thick dashed line indicates the temporal evolution of the mixed layer height.

The residual layer in both simulations started forming after 2100 hours at around 300 m (agl). The atmosphere was at rest at night time, but due to the effect of drainage winds from the Hunua Ranges and diurnal rotation of easterly sea breezes, the real terrain simulation predicted stronger southerly winds. The depth of this southerly flow was around 200 m at 2400 hours.

## 7.6 Summary of Results

Topography (terrain height) affects the local and mesoscale circulation due to its ability to modify the surface pressure field, creating mechanical shear and by disturbing the distribution of the sensible heat flux. Numerical modelling techniques were used to investigate the effects of topography on the sea breeze system. The Advanced Research WRF modelling system was employed to run two three dimensional (3-D) idealized simulations. For a detailed description of the WRF (ARW) modelling system please see Chapter 5. Both simulations were run using the same physics and dynamics, and without any background winds. The first simulation was run with realistic topography (101bv), while the second simulation was run with only flat terrain (zero terrain height). The two simulations were then analyzed to assess topographical influences on the sea breeze structure and dynamics. Summary of results of the analysis is given below:

- The higher terrain of the Waitakere, Hunua and Coromandel ranges attributed to early onset and early decay of the sea breeze. The onset of the sea breeze over the Hunua and Coromandel ranges were one hour earlier (0800-0900 hours) than the Waitakere Ranges. The contribution of higher terrain to sea breeze depth varies from 100 to 300 m for various properties of the sea breeze cell.
- In the morning hours, wind speed accelerated over the seaward sides of the ranges due to coupling of upslope anabatic winds and onshore sea breeze flow. Soon after, the upslope enhanced sea breeze from the west and anabatic wind from the landward sides reached the top of the ranges creating a return flow on both landward and seaward directions. The inland penetration of sea breeze front was inhibited by the blocking effect of the higher terrain of the ranges and the anabatic flow from the landward side of the ranges.
- At night time, the drainage flow from the three ranges appears to significantly affect the wind field over the region. The drainage winds not only increased the wind speed at night, but also affect the diurnal rotation of the thermally induced circulation.

- The strength of the sea breeze flow is the direct consequence of the amount of sensible heat flux and its temporal and spatial distribution over land. The higher magnitude of the sensible heat flux leads to development of stronger sea breezes and a lower magnitude results in a weaker sea breeze. In addition to latitudinal position, the important controls of sensible heat flux are surface characteristics and terrain elevation. A relatively high sensible heat flux over the higher terrain of the three ranges resulted in early onset of sea breezes. In the afternoon hours, the very high magnitude of sensible heat flux due to the urban surface characteristics of Auckland City resulted in a stronger sea breeze on both sides of the isthmus that also led to marked sea breeze convergence zones (SBCZs).
- The model predicted anticlockwise wind rotation over both the east and west coasts. However, the wind rotation over the west coast was much slower than the east coast, especially during daytime and at night. Diurnal rotation of sea breezes is the result of a combination of the mesoscale and large scale pressure gradient, and the Coriolis force, although topographical influences can often cause winds to rotate in the opposite direction (Simpson 1995). For example, Auckland Airport, which is in close proximity of the Manukau Harbour, did not show this diurnal rotation and most of the daytime winds showed a strong south-westerly component from the Manukau Harbour, whereas the predicted wind field at Penrose which is located further inland showed a complete anticlockwise rotation. Although there are no high mountains in the region the complex topography, land-water configuration and resulting local winds are capable of creating sufficient perturbation in the pressure field to cause clockwise instead of anticlockwise rotation.
- The gap flow generated due to the orographic setting of the mouth of Manukau Harbour intensified the westerly sea breeze over and along the coastline. The gap flow also helped accelerate the speed of the westerly sea breeze front.
- The convergence zones were first formed over the three ranges due to higher terrain and their convex shaped coastline (especially the Waitakere and Hunua Ranges). Before noon, the convergence lines were formed

around the three harbours due to interaction between bay breezes and the warm land air. In the afternoon hours, these convergence lines were merged with the main sea breeze convergence zones formed due to collision of west and east coast sea breezes. The intensity of the sea breeze convergence zone was the highest over relatively flat and highly urbanized Auckland City, with upward vertical velocities reaching up to 3 m $s^{-1}$ at 500 m above ground level. A few more convergence lines were formed to the south of the Auckland region and clearly indicated blocking of the easterly sea breeze front by the Coromandel and Hunua Ranges.

- The coastal valley setting of the Waikato River mouth resulted in higher inland penetration of the westerly sea breeze front that also modified the position of the SBCZ.
- The areas of stronger convergence showed a relatively complete sea breeze circulation cell. Over the three ranges and Auckland City. However, these circulation were not predicted by the real simulation (101cg: Chapter 5) and idealized simulations (101bx to 101ca) with a constant background wind from a certain wind quadrant (Chapter 6). This mean that vertically rotating cells similar to the ones predicted by 101bv and 101bw can only be expected in very low gradient wind conditions.
- The effect of the higher terrain of the Waitakere and Hunua Ranges over the Auckland region was assessed. Results of the simulation with zero background winds suggest possible recirculation over Auckland. During easterly sea breezes, pollution may move to the top of the Waitakere Ranges in the upslope enhanced easterly sea breezes, diverge into the inversion layer and become part of the return flow. If the circulation is closed or mixing occurs in between the two flows, this may increase the pollutant concentration in the urban areas, especially western Auckland and Auckland City. However, for this to happen, the synoptic flow needs to be very weak. Hunua Ranges are located to the south/southeast of Auckland City and east of Pukekohe. In this case, pollutants emitted from residential and industrial areas of Pukekohe may be advected towards the Hunua Ranges and move up with the upslope wind enhanced westerly sea breeze where they can become part of the seaward return flow. Results of streamlines at this

location indicate this circulation, as well as some mixing between westerly sea breeze inflow and eastward moving offshore return flows. The northern side of the Hunua Ranges is probably more important with respect to pollutant recirculation. In the late afternoon and evening hours the north-easterly sea breeze that deflects southward due to diurnal rotation may advect pollutants from Auckland City toward Hunua Ranges. This deflection is also evident in the particle trajectories (Chapter 5). The return flow induced by the higher terrain of Hunua may advect pollutants towards the northeast over the Hauraki Gulf. However, considering the results of Chapter 6, there is a strong possibility of deflection of return flow towards the gradient wind direction. This means that pollutant laden return flow may be advected towards Auckland City under light southerly/south-easterly gradient flow. This is in qualitative agreement with the observational data analysis that suggested higher pollutant concentrations under southerly gradient flow, but three dimensional particle dispersion modelling is required to confirm this process.

- The other possible mechanism is the trapping of pollutants in the sea breeze convergence zones. Results of Chapter 4 and 6 suggest intense convergence during coast parallel gradient wind conditions, while dispersion modelling results suggest advection of pollution towards the SBCZ where they can increase the pollutant concentration. Auckland does not have similar geographic and topographic features to Los Angles (Lu & Turco 1994; Lu & Turco 1995; Lu & Turco 1996) or Mexico basin (Fast & Zhong 1998). Therefore, the next day pollution mechanism due to pollutant trapping in the residual layer is considered unlikely.

# 8. Summary and Conclusion

## 8.1 Introduction

The sea-land breeze circulation is an important mesoscale phenomenon that is associated with coastal areas where most of the world population lives and therefore, has manifold impacts on the social, commercial and environmental aspects of human society. Although the sea-land circulation is understood as a simple case of the response of lower atmosphere to the thermal gradient between land and water, in reality it is quite a complicated phenomenon that has both internal and external interactions. In the maritime environment of the Auckland region, the sea breeze is the dominant feature of the summer time meteorology. Despite the predominant effect of sea breeze on the peninsula shaped landmass of Auckland and its potential effect on the local meteorology and air quality of the region, a general lack of interest is manifested towards this important facet of the local meteorology in the air quality literature for the Auckland region. The focus of most of the studies conducted on sea breezes has also been limited to the investigation of the sea breeze convergence zone. However, the sea breeze and associated air pollution issues have not been addressed at a broader scale. This work is an effort to fill this gap and investigate and improve our understanding of the thermally forced circulation and its potential impact on the air quality of the Auckland region. Observational data analysis and numerical modelling techniques (both real and idealized) were utilized to achieve this goal. Two years of near-surface meteorological data (2006 and 2007) from various meteorological sites within the Auckland region were obtained and analysed. The sea breeze and non-sea breeze days were identified and separated using a simple technique based on the criteria that a

summer day is a sea breeze day when onshore flow is initiated on both sides of the peninsula. Various statistical techniques were used to investigate evolution of the sea breeze and its characteristics, especially those associated with the degradation of the air quality in the region. Real and idealized modelling techniques were used to extend observational analysis to a) investigate various characteristics of the sea breeze in greater detail, b) evaluate the influence of external controls such as the gradient wind and topography on the sea breeze circulation, and c) investigate links between various sea breeze characteristics and the air pollution meteorology of the region. Two mesoscale numerical models, namely the Advanced Research WRF and 'The Air Pollution Model' (TAPM), were employed in non-hydrostatic mode for this purpose. Both models were first validated with the surface meteorology against observation data from six different stations within the Auckland region. WRF showed better skill in predicting surface meteorology than TAPM. The observed vertical profiles from Whenuapai were also in good agreement with the predicted profiles by WRF. In general WRF showed positive bias in the predicted wind speed and relative humidity and a cold bias in the near-surface 2 m temperature. TAPM on the other hand slightly under-predicted wind speed, but, the bias for 2 m temperature and relative humidity was similar to WRF. The error in the WRF predicted surface meteorology was associated with misclassification of the land surface scheme that performed well for urban characteristics, although the heterogeneity of land use (other than urban canopy), was not well represented by the land surface parameterization. A possible reason is the terrain resolution. Results of the observational and numerical modelling analysis for the sea breezes are summarized below.

## 8.2 Sea Breeze Circulation (sea breeze inflow and return flow)

Sea breezes in the Auckland region occur during the summer period from November to March on warm clear sky days under weak gradient wind conditions. Generally, the sea breeze occurs on both east and west coasts of the region. Due to its peninsula shape and northwest-southeast orientation, the wind speed during sea breeze events is up to 2 m $s^{-1}$ lower than non-sea breeze days. The wind magnitude of the westerly sea breeze is around 1 m $s^{-1}$ greater (3.2 m $s^{-1}$) than the east coast sea breeze (2.5 m $s^{-1}$). Results of observation and numerical modelling are consistent with the previous work that suggests existence of two thermal circulations in the Auckland region. The first type of

sea breeze originates from the three harbours (Manukau, Waitemata and Kaipara) and along the eastern coast line of the Hauraki Gulf in the morning hours (0800 – 0900 hours NZST) of the day and is referred to as a bay breeze. The second sea breeze originates from the Tasman Sea and larger Hauraki Gulf area in the late morning hours and is referred to as a mature sea breeze. Arrival of the mature sea breeze fronts from either coast is marked by a temperature drop of up to 2.0 $^{o}$C. However, there was no significant difference in moisture content, which is probably due to the overall maritime environment of the Auckland region. The coexistence of sea breeze system at two different scales has been observed in many parts of the world (e.g. Abbs & Physick 1992; Physick & Byron-Scott 1977). After arrival of the mature sea breeze, the bay breeze merges with it. The modelling results are consistent with the observed data and suggest the onset of the bay breeze at around 0800 hours. The sea breeze decays after 1600 hours, but the frequency and timing of the onset and decay is subject to many factors, such as sea-land thermal gradient, topography, sea-land orientation and the direction and strength of the gradient wind. The coastal mountain ranges of Waitakere and Hunua helped early onset of westerly and easterly sea breeze in their area of influence, but reduced the inland penetration speed. Relatively stronger observed wind speed at Auckland Airport and Mangere (located close to the coastline of Manukau Harbour) are due to a) local pressure variation caused by the narrow entrance of Manukau Head, b) reduced friction over the water surface, and c) divergence of winds caused by the concave shape of the eastern coastline of Manukau Harbour. Another terrain induced feature was found further south of Manukau Harbour, where the coastal valley setting of the Waikato River mouth resulted in greater inland penetration of the westerly sea breeze front that also modified the position of the SBCZs. Under northerly gradient flow, the predicted north-easterly sea breeze lasts longer, and under southerly gradient flow cessation of the westerly sea breeze was delayed. Results of observational and modelling studies suggest that most of the sea breeze days occur during weak (<=6 m $s^{-1}$) southerly or northerly gradient winds that are parallel to the northwest-southeast oriented land mass. In addition to frequency, another important aspect was the enhancement or inhibition effect of the coast parallel gradient winds on the sea breezes. Theoretically, the north-westerly gradient wind should enhance the easterly sea breeze and the south-easterly gradient wind should enhance the westerly sea breeze (Adams 1997; Miller et al. 2003; Zhong & Takle 1993), but observational data analysis

suggested an opposite behaviour. One of the objectives of numerical modelling was to investigate this issue, although the Coriolis affect could not be removed from the background wind causing a leftward deflection. Despite failure to align background winds correctly in the northwest and southeast direction, the resultant WNW and ESE gradient winds were consistent with the observed data that indicates violation of the general principle of balance between the large scale PGF and variations in Coriolis force due to frictional drag (see Chapter 2 for details). This violation was also evident in the sea breeze convergence zone study of McKendry (1992) for southeast gradient winds only.

The depth of the predicted sea breeze inflow layer varied from 200 to 600 m. The inland penetration of the sea breeze flow is directly related to the magnitude of the sensible heat over land. The higher the sensible heat flux the stronger the sea breeze. Azimuth angle, topography and surface characteristics are also important controls of the magnitude of the sensible heat flux. In the morning hours a relatively high sensible heat flux over the higher terrain of the three ranges (Waitakere, Hunua and Coromandel) resulted in early onset of the sea breeze. The thermally induced onshore sea breeze coupled with upslope anabatic winds moved over the mountain slopes and formed a seaward return flow over the top of the mountain range. A similar upslope flow and return flow was also predicted over the landward sides of the Waitakere and Hunua Ranges. The onset of the sea breeze over the Hunua and Coromandel Ranges were one hour earlier than the Waitakere Ranges, due to steep sun facing eastern slopes of the Hunua and Coromandel Ranges. However, the inland movement of the sea breeze front was inhibited due to the blocking effect of the higher coastal terrain and the anabatic flow from the landward side of the ranges. The contribution of higher terrain to sea breeze depth varies from 100 to 300 m.

## 8.3 Diurnal Rotation

Sea-land breezes rotate over the diurnal cycle due to the thermal reversal between land and sea. This is one of the basic characteristics of the sea-land breeze system and in many ways is associated with the air quality of the region. In the Southern Hemisphere, this rotation is anticlockwise. Results show a complete anticlockwise diurnal rotation at both east and west coast of the Auckland region under gradient wind conditions with a

strong easterly component. However, observed data from Auckland Airport which is located to the west of Auckland, consistently show a partial or complete clockwise rotation of the wind vector. The idealized modelling results show a partial clockwise rotation under all the four gradient wind conditions. A partial or incomplete rotation at this station was associated with a strong gradient wind effect when the wind vector moved mostly back and forth along the gradient wind direction. Simpson (1995) suggest that topographical influences can cause wind to rotate in the opposite direction by disturbing the local pressure gradient. The results of the modelling study were found to be in agreement with previous finding and suggest that the presence of a large inland water body (Manukau Harbour) and proximity of the higher terrain of the Waitakere and Hunua Ranges are responsible for the clockwise rotation of the winds at some inland stations. The rotation rate of the sea breezes also varied over the diurnal cycle and between east and west coast. The rotation rate was lower during day and night time but it was higher during the transition time of morning and evening hours of the day. Compared to the west coast, the rotation rate was significantly higher over the east coast. The gradient wind direction and speed significantly affected the rotation rate over both coasts. When surface and gradient winds were from the same direction, the rotation rate slowed down, while a gradient wind opposite to the surface wind flow enhanced the rotation rate of the sea or land breeze. The transition from land to sea breeze is important for air pollution applications. Results of dispersion modelling suggest that emissions from peak morning traffic hours may be advected towards Manukau Harbour by the remnants of the land breeze under coast-parallel gradient wind condition. These pollutants may return after a few hours with the bay breeze or mature westerly sea breeze. This process is especially favourable for photochemical pollution.

## 8.4 Mixed Layer Height

Analysis of the limited day time upper air sounding data suggests a mixed layer height of around 1500 m, while the CIBL depth was approximately 400 m. The real simulation results (Chapter 5) are consistent with the observed data. During the afternoon hours the mixed layer height was in the range of 600 to 1400 m, while CIBL depth ranged between 200 to 500 m. WRF predicted lower CIBL depth under coast-parallel gradient wind conditions (200 - 400 m) than coast-normal gradient wind

conditions (400 - 500 m). The inland extent of the CIBL was relatively high under coast-normal and especially south-westerly gradient winds. This is mainly due to a stronger thermal gradient between the Tasman Sea and the land surface. The inversion over the top of the CIBL acts as a cap that inhibits vertical mixing of pollutants that are emitted near the surface, while pollutants that are emitted in the inversion layer above the CIBL may fumigate in the surface layer (Luhar & Hurley 2004; Luhar et al. 1998). Although pollution levels may rise in the CIBL under any gradient wind condition if they were not advected offshore over the Hauraki Gulf or Tasman Sea, the case with coast-parallel gradient wind conditions is more complicated. The simultaneous inland movement of east and west coast sea breezes and their resultant convergence in the middle of highly urbanized areas makes air quality of the region more vulnerable, and the air pollutants emitted in the surface layer may increase the pollution concentration over the region to unacceptable levels. The pollution dispersion modelling results (Chapter 5), indicate this higher pollution concentration over the Auckland City and south and north of Auckland under coast parallel northwest and southerly wind flow. The observational data analysis is also consistent with the dispersion modelling results and suggests higher pollution levels under coast-parallel southerly gradient flow. In the evening hours, the surface cools faster under coast-parallel gradient winds that reduced the shallow mixed layer at a rate faster than coast-normal gradient flow cases. Assuming that wind speed is the same, this means higher pollution levels in the late evening and at night. The evening emissions can also be trapped in the evolving residual layer and may contribute to higher pollution levels in the following morning. However, Auckland does not have geographic and topographic setting such as Los Angles (Lu & Turco 1994; Lu & Turco 1995; Lu & Turco 1996) or the Mexico basin (Fast & Zhong 1998). Considering the narrow land mass of the Auckland region and presence of relatively high prevailing winds, remixing of pollutants that are stored in the residual layer, with the following morning emissions is probably unlikely in the Auckland area and only possible in very weak gradient wind conditions. This is consistent with the results of the Sutton (1996) and contrary to earlier suggestions by Ridley (1993), and Bell & Fisher (1995). However, a three dimensional pollution dispersion modelling is essentially required to confirm this.

## 8.5 Sea Breeze Circulation Cell

Results of idealized simulation of gradient flow and topographical impacts (Chapter 6 and 7) suggest that a complete sea breeze circulation cell is possible only in very weak gradient wind conditions when synoptic pressure gradient is slack. In the Auckland region, with relatively strong prevailing winds and without any significant high terrain, a closed circulation cell is highly unlikely. The return flow over the Waitakere and Hunua Ranges and above the convergence zones may carry pollutants, although its remixing in the surface layer is subject to many factors such as gradient wind direction and speed, direction of the return flow and nature (size and state) of the particles. But if it happens, higher pollution levels over Auckland City and west and south of Auckland are expected during easterly sea breeze conditions under coast-parallel northwest gradient flow. More importantly, the Auckland area (Auckland City, Northern Auckland) may experience higher pollution levels during south-westerly sea breezes under coast-parallel southerly gradient flow.

## 8.6 Sea Breeze Convergence Zones

Previous research in the Auckland region has given special importance to sea breeze convergence zones and discussed their characteristics and air quality implications over the region (see for example, McGill 1987; McKendry 1992; Ridley 1993; Ridley 1995; Sutton 1996). Results of this research are in agreement with the previous work that the strength and position of the SBCZ is influenced primarily by the gradient wind direction, terrain, thermal gradient between land and sea, and land surface characteristics. Bay breezes from the three harbours also play a significant role in the position of the SBCZ in the morning hours of the day. The SBCZs were predicted near the east coast under south-westerly gradient wind, while under north-easterly gradient winds, the SBCZs were predicted along the west coast. Under coast-parallel or sub-parallel gradient winds with a strong northwest or southeast component, the convergence zones were predicted in the middle of the peninsula when both east and west coast sea breeze fronts meet, and then migrate eastward or westward depending on the strength of the sea breeze front. In either case, the major and stronger SBCZs run through Auckland City and most of the urban areas. In addition to the gradient wind, the higher terrain of the Waitakere and Hunua Ranges plays an important role in the

modification of the wind field and the position and strength of SBCZs. Under all the four gradient wind conditions, the first three topographically induced convergence zones were predicted around the Waitakere, Hunua and Coromandel Ranges. The location, strength and migration of these convergence zones were affected by the mesoscale pressure gradient and gradient wind direction. The SBCZs have been extensively discussed in the air quality literature for their potential role in pollution transport and dispersion. The intense vertical motion in SBCZs is capable of uplifting pollutants that are trapped in the convergence zone and injecting them into the return flow. However, given the particular geography of the region, gradient winds need to be very weak to recirculate pollutants that are advected into the return flow. The dispersion modelling results (in Chapter 5), however, suggest a higher ground level pollutant concentration in the convergence zone which is due to inhibition of horizontal dispersion.

## 8.7 Conclusion

In this research, various characteristics of the sea breeze system and their potential effect on the air quality of the Auckland region have been investigated. The important sea breeze characteristics that may have air quality implications include the sea breeze circulation, sea breeze convergence zone, the mixed layer height and diurnal rotation of the thermally forced mesoscale flow. The influence of higher terrain and gradient winds on sea breeze characteristics was also investigated. Some other interactions between sea breeze and external factors, such as the effect of land cover, sea-land orientation and coastal valley environments were also looked at partially.

Sea breezes occur in the weak gradient wind conditions generally on both sides of the peninsula. The highest frequency of sea breeze days was found on coast-parallel gradient wind conditions (northwest and southeast). Wind speed during sea breeze events is generally lower than non-sea breeze days, while solar radiation and temperature are generally higher, which makes meteorological conditions favourable for degraded air quality especially for photochemical pollution. The diurnal rotation of the sea breeze system may cause an increase in pollution levels, especially in the Auckland City area by re-introduction of pollutants in the late morning that were advected away towards Manukau Harbour by remnants of the land breeze in the early

morning hours. The sea breeze convergence zone is an important dynamic feature of the mesoscale phenomenon that is quite often associated with higher air pollution levels over the region. Pollutants advected by sea breeze inflow from the east and west coasts may increase pollution levels in the sea breeze convergence zone. Given the higher upward motion and doming in the convergence zone, the uplifting of the trapped pollutants is expected. However, there was no strong evidence of recirculation, because pollutants are more likely to be dispersed in the return flow that is dominated by the gradient wind direction. At the same time, vertical mixing within the convergence zone is quite likely which would help reduce the surface concentration of pollutants. The pollutants trapped in the SBCZs will also be displaced with the migration of SBCZ. The terrain induced return flow at the Waitakere and Hunua Ranges may carry pollutants and increase ground level concentration under weak coast-parallel (northwest or southeast) gradient wind conditions. The next day pollution mechanism due to stabilizing of the mixed layer in the evening hours is considered unlikely due to presence of strong synoptic winds in the region. A shallow CIBL is consistently formed in the sea breeze inflow layer, although gradient wind direction and topography influences the depth, horizontal growth and inland extent of the CIBL. Under coast-parallel gradient wind conditions, although the horizontal growth rate of the CIBL was slow, the CIBL depth was up to 100 m less than coast-normal gradient wind condition. This means that northwest and southeast gradient wind conditions are more favourable for increased air pollution levels due to a shallower CIBL.

In summary, the sea breeze system in the Auckland region is as complicated as its coastline and topography. Large scale winds, orientation of the Peninsula and land features extensively influence the development of this thermally induced mesoscale phenomenon. Pollution levels may increase during a sea breeze event, especially under weak southerly/south-easterly gradient wind.

## 8.8 Future Research

In this research, the quality, quantity, resolution and siting of the AWS greatly hampered the observational data analysis. To confirm the results of this research and further investigate the frequency, strength and structure of sea breezes a thoughtful, intelligent and precise AWS campaign is desired for one or two summer periods. In

addition to that, to capture the vertical structure of the boundary layer and pollution dispersion during sea breeze inflow, short term SODAR or LIDAR monitoring is also desirable on at least some selected sea breeze days. The data collected from this campaign, coupled with numerical modelling (meteorological and pollution dispersion) would improve our understanding of the sea breeze structure, dynamics, and its role in the air quality of the region.

The terrain features in the Hauraki Gulf, such as Rangitoto and Motutapo Islands, Waiheke Island, Panui Island and the Coromandel Peninsula, generate their own sea breeze systems. Due to proximity of these islands to the Auckland region, the variation in thermal/pressure gradient caused by these small scale sea breeze systems in the Hauraki Gulf may have contributed towards sea breeze inflow from the east coast. A detailed analysis focusing on the effects of these land features on the local and mesoscale thermal and pressure gradient and resultant wind field needs to be undertaken.

This research did not take into account the effect of the extensive mudflats that form on the Waitemata, Manukau and Kaipara Harbour as part of the normal tidal cycle and may significantly affect the evolution, strength and magnitude of the sea breeze. Any future research on the sea breeze needs to address this issue and investigate the interaction between the tidal cycle and the thermally forced circulation in the region.

In the North Island, heat lows generally occur during the summer period over the Waikato, Bay of Plenty, Rotorua and Lake Taupo areas. Although compared to main continents of the world, these heat lows are very weak but enough to influence the sea breeze circulation in the region. The heat lows that form over the central North Island cause deflection of wind in the SBCZs over the Auckland region (McGill 1987). The effect of the heat lows has also not been accounted for in this research. Considering their association with the sea breeze phenomenon, future sea breeze studies need to address and include the effect of heat lows on sea breeze circulation over the region.

The urban heat island effect is known for the intensification of sea breezes in the urban coastal area. Numerous studies have shown that in coastal urban areas, interaction of

sea breeze circulation with urban heat island, play an important role in transport and dispersion of pollutants (Frietas et al. 2006; Lin et al. 2008; Miao 2006; Miao et al. 2006a). Although this research has partially addressed this issue, however, given the importance of the issue, a detailed study is recommended on assessing the magnitude of the urban heat island effect (UHI) in the Auckland region.

Throughout this research, the focus has been on the sea breeze and its external and internal controls. However, it is just half of the equation. It is desirable to either study the sea-land breeze as one whole system, or at least put some research effort into understanding the nocturnal part of the thermally forced flows as well.

## References:


Abbs, DJ 1986, 'Sea-breeze interactions along a concave coastline in southern Australia: Observations and numerical modelling study', *Monthly Weather Review,* vol. 114, pp. 831-48.

Abbs, DJ & Physick, WL 1992, 'Sea-breeze observations and modelling: A review', *Australian Meteorological Magazine,* vol. 41, pp. 7-19.

Adams, E 1997, 'Four ways to win the sea breeze game', in *March, 1997*. Sailing World, pp. 44-9.

Adeeb, F & Shooter, D 2003, 'Ozone concentration in the ambient air at two sites of differing elevation in Auckland, New Zealand: 1997-2001', *New Zealand Natural Sciences,* vol. 28, pp. 9-25.

Adeeb, F & Shooter, D 2004, 'Variation of surface ozone in the ambient air of Auckland, New Zealand.', *Environmental Monitoring and Assessment,* vol. 95, pp. 201-20.

Ahrens, CD 2007, *Essentials of Meteorology, An Invitation to the Atmosphere,* 8th edn, Books/Cole Thomson Learning; Australia; Pacific Grove, CA.

Alpert, P & Kusuda, M 1984, 'Anti-clockwise rotation, Eccentricity and tilt angle of the wind hodograph, Part II: An observational study', *Journal of the Atmospheric Science,* vol. 41, no. 24, pp. 3568-83.

Apel, JR 1987, *Principles of ocean physics,* 1st. edn, Academic Press, Sab Diego, Calif.

ARC 1995, *Auckland Regional policy statement*, Auckland Regional Council, Auckland. Retrieved 15-Aug, from http://www.arc.govt.nz/library/s82562_2.pdf

ARC 1997, *Ambient Air Quality : Monitoring results for the Auckland region 1964-1995.*, Auckland Regional Council., Auckland, 88, Technical Publication.

Arritt, RW 1987, 'The effect of water surface temperature on lake breezes and thermal internal boundary layers', *Boundary-Layer Meteorology,* vol. 40, pp. 101-25.

Arritt, RW 1993, 'Effects of the large-scale flow on characteristic features of the sea breeze', *Journal of Applied Meteorology,* vol. 32, pp. 116-25.

Asai, T & Mitsumoto, S 1978, 'Effects of an inclined land surface on the land and sea breeze circulation, A numerical experiment', *Journal of Meteorological Society of Japan,* vol. 56, no. 6, pp. 559-70.

ASTM Standards 2005, *Standard guide for statistical evaluation of atmospheric dispersion model performance*, American Society for Testing and Materials.

Atkins, NT & Wakimoto, RM 1997, 'Influence of synoptic-scale flow on sea breezes observed during CaPE', *Monthly Weather Review,* vol. 125, pp. 2112-30.

Atkins, NT, Wakimoto, RM & Weckwerth, TM 1995, 'Observations of the sea breeze front during CaPE, part II: Dual-doppler and aircraft analysis', *Monthly Weather Review,* vol. 123, pp. 944-69.

Atkinson, BW 1981, *Mesoscale atmospheric circulations*, Academic Press, New York, pp. 495.

Auckland Regional Council 2004a, *Auckland Air Emission Inventory*, Auckland Regional Council, Auckland.

Auckland Regional Council 2004b, *State of the Auckland region: Report 2004*, Auckland Region, Auckland, from http://www.arc.govt.nz/albany/fms/main/Documents/Plans/Reports/

Auckland Regional Council 2006a, *Auckland Air Emission Inventory: 2004*, Auckland Regional Council, Auckland, Technical Publication 292.

Auckland Regional Council 2006b, *Auckland Air Emissions Inventory:2004*, Auckland Regional Council, AQ06-01.

Auckland Regional Council 2007a, *Air quality standards and targets*, Auckland Regional Council, Auckland, from http://www.arc.govt.nz/albany/fms/main/Documents/Environment/Pollution/airfacts7.pdf

Auckland Regional Council 2007b, *State of the region's air quality*, Auckland Regional Council, Auckland, from http://www.arc.govt.nz/albany/fms/main/Documents/Environment/Pollution/airfacts4.pdf

Auckland Regional Council 2009, *Air Quality*, Auckland Regional Council, Auckland. Retrieved 29-Jul-09, from http://www.arc.govt.nz/environment/air-quality/aucklands-air-quality/standards-and-guidelines.cfm#Exceedences%20of%20the%20standard

Avissar, R, Moran, MD, Wu, G, Meroney, RN & Pielke, RA 1989, 'Operating ranges of mesoscale numerical models and meteorological wind tunnels for the simulation of sea and land breezes', *Boundary-Layer Meteorology,* vol. 50, pp. 227-75.

Azorin-Molina, C, Connell, BH & Baena-Calatrava, R 2009, 'Sea breeze convergence zones from AVHRR over the Iberian Mediterranean area and the isle of Mallorca, Spain', *Journal of Applied Meteorology and Climatology,* vol. 48, no. 10, pp. 2069-85.

Baker, RD, Lynn, BH, Boone, A, Tao, W-K & Simpson, JE 2001, 'The influence of soil moisture, coastline curvature and land-breeze circulations on sea-breeze initiated precipitation', *Journal of Hydrometeorology,* vol. 2, pp. 193-211.

Banta, RM, Oliver, LD & Levinson, DH 1993, 'Evolution of the Monterery bay sea breeze layer as observed by pulsed doppler radar', *Journal of the Atmospheric Sciences,* vol. 50, no. 24, pp. 3959-82.

Banta, RM, Senff, CJ, White, AB, McNider, RT, Valente, RJ, Mayer, SD, Alvarez, RJ, Hardesty, RM, Parrish, D & Fehsenfeld, FC 1998, 'Daytime build-up and night-time transport of urban ozone in the boundary layer during a stagnation episode', *Journal of Geophysical Research,* vol. 103, no. D17, pp. 22519-44.

Barbato, JP 1975, *The sea breeze of the Boston area and its effects on the urban atmosphere*, PhD. Thesis, Boston University Graduate School.

Barratt, R 2001, *Atmospheric dispersion modelling; An introduction to practical applications,* 1st edn, Earthscan Publications Limited, London.

Bechtold, P, Pinty, J-P & Mascart, P 1991, 'A numerical investigation of the influence of large-scale winds on sea-breeze and inland breeze type circulations', *Journal of Applied Meteorology,* vol. 30, no. 09, pp. 1268-79.

Beljaars, ACM 1994, 'The parameterization of surface fluxes in large-scale models under free convection', *Quarterly Journal of the Royal Meteorological Society,* vol. 121, pp. 255-70.

Bell, MJ & Fisher, GW 1995, *The siting of air quality monitors for photochemical pollutants in the Auckland Region - A report to the Auckland Regional Council*, National Institute of Water and Atmospheric Research Ltd., Auckland, AK95017.

Berg, LK & Zhong, S 2005, 'Sensitivity of MM5-simulated boundary layer characteristics to turbulence parameterizations', *Journal of Applied Meteorology,* vol. 44, p. 16.

Biggs, WG & Graves, ME 1962, 'A lake breeze index', *Journal of Applied Meteorology,* vol. 1, pp. 474-80.

Bornstein, R 1999, 'Urban induced convergence zones and air pollution episodes', in *International Conference on Air Quality Management*. San Jose State University, Darussalem, Brunei., p. 3, 15-19 Nov 1999.

Brasell, MR 1982, 'Photochemical Oxidant Formation in the Auckland Region', *Journal of the Clean Air Society of Australia and NZ,* vol. 16, no. 01.

Bureau of Meteorology-Australia 1977a, *Aviation meteorology* Australian Govt. Pub. Services, 1977, Canberra, Australia.

Bureau of Meteorology-Australia 1977b, *General meteorology* Canberra : Australian Govt. Pub. Services, 1977, Canberra, Australia.

Bureau of Meteorology-Australian Government 2006, *MSLP Analysis Charts, Pacific Ocean*, from http://www.bom.gov.au/nmoc/MSL/index.shtml

Buzzi, A, Tartaglione, N & Malguzzi, P 1998, 'Numerical simulations of the 1994 Pieddmont flood: Role of orography and moist processes', *Monthly Weather Review,* vol. 126, pp. 2369-83.

Challa, VS, Indracanti, J, Rabarison, MK, Patrick, C, Baham, JM, Young, J, Hughes, R, Hardy, MG, Swanier, SJ & Yerramilli, A 2008, 'A simulation study of mesoscale coastal circulations in Mississippi Gulf coast', *Atmospheric Research,* vol. 91, no. 1, pp. 9-25.

Chang, JC & Hanna, SR 2004, 'Air quality model performance evaluation', *Meteorology and Atmospheric Physics,* vol. 87, pp. 167-96.

Chen, F 2007, 'The Noah Land Surface Model in WRF', *LSM Group Meeting: NCAR*, NCAR, Boulder - Colorado, pp. 42; http://www.rap.ucar.edu/staff/feichen/LSM/LSM-tutorial.pdf.

Chiba, O 1993, 'The turbulent characteristics in the lower part of the sea breeze front in the atmospheric surface layer', *Boundary-Layer Meteorology,* vol. 65, pp. 181-95.

Chiba, O, Kobayashi, F, Naito, GI & Sassa, K 1999, 'Helicopter observations of the sea breeze over a coastal area', *Journal of Applied Meteorology,* vol. 38, pp. 481-92.

Clappier, A, Martilli, A, Grossi, P, Thunis, P & al, e 2000, 'Effect of sea breeze on air pollution in the greater Athens area. Part I: Numerical simulations and field observations', *Journal of Applied Meteorology,* vol. 39, no. 4, p. 546.

Clarke, RH 1984, 'Colliding sea-breezes and the creation of internal atmospheric bore waves: Two dimensional numerical studies', *Australian Meteorological Magazine,* vol. 32, pp. 207-26.

Clarke, RH & Arritt, R 1995, 'Numerical simulations of the effect of soil moisture and vegetation on the development of deep convection', *Journal of Applied Meteorology,* vol. 34, pp. 2029-45.

Cohen, A 1980, 'On the graphical display of the significant components in a two-way contingency table', *Communication in Statistics - Theory and Methods,* vol. 9, no. 10, pp. 1025-41.

Cohen, J 1988, *Statistical power analysis for the behavioral sciences*, Hillsdale, NJ; Erlbaum.

Comet 1999, *The New Jersey Sea Breeze and the relationship to Coastal Upwelling* COMET, 13 Aug 2008, from http://marine.rutgers.edu/cool/seabreeze/

Cope, ME, Carnovale, F & Johnson, MH 1990, 'An air quality modelling system for oxidant transport and production in the Port Phillip control region', *10th International Conference of Clean Air Society of Australia and New Zealand*, CASAZ, Auckland, pp. 165-70.

Davey, CA & Pielke, RA 2005, 'Microclimate exposures of surface-based weather stations: Implications for the assessment of long-term temperature trends', *Bulletin of the American Meteorological Society*, p. 7.

Deardorff, JW 1974, 'Three dimensional numerical study of the height and mean structure of heated boundary layer', *Boundary-Layer Meteorology,* vol. 7, pp. 81-106.

Defant, F 1951, 'Compendium of Meteorology', *American Meteorological Society*, p. 655.

Developmental Testbed Center 2006, *The Weather Research & Forecasting Model. Developmental Testbed Center*, from http://wrf-model.org/index.php

Dexter, RV 1958, 'The sea-breeze hodograph at Halifax', *Bulletin of the American Meteorological Society,* vol. 39, pp. 241-7.

Durand, PBS & Druilhet, A 1989, 'A sea-land transition observed during the COAST experiment', *Journal of the Atmospheric Sciences,* vol. 46, pp. 96-116.

Estoque, MA 1962, 'The sea breeze as a function of the prevailing synoptic situation', *Journal of the Atmospheric Sciences,* vol. 19, pp. 244-50.

Fast, JD & Zhong, S 1998, 'Meteorological factors associated with inhomogeneous ozone concentrations within the Mexico City basin', *Journal of Geophysical Research,* vol. 103, no. D15, pp. 18927-46.

Federovich, EF, Nieuwstadt, TM & Kaiser, R 2001, 'Numerical and laboratory studies of horizontally evolving convective boundary layer', *Journal of the Atmospheric Science,* vol. 58, pp. 546-60.

Finkele, KJ 1995, 'A complete sea-breeze circulation cell derived from aircraft observations', *Boundary-Layer Meteorology,* vol. 73, pp. 299-317.

Forsdyke, AG 1997, 'Meteorological factors in air pollution', *World Meteorological Organization*, no. 114. Technical Note.

Franchito, SH, Rao, VB, Stech, JL & Lorenzzetti, JA 1998, 'The effect of coastal upwelling on the sea breeze circulation of Cabo Frio, Brazil: A numerical experiment', *Ann. Geophys.,* vol. 16, pp. 866-81.

Friendly, M 2001, *Visualizing Categorical Data*, SAS Institute Inc., Cary, NC, USA.

Frietas, ED, Rozoff, CM, Cotton, WR & Dias, PLS 2006, 'Interactions of an urban heat island and sea-breeze circulations during winter over the metropolitan area of Sao Paulo, Brazil', *Boundary-Layer Meteorology,* vol. 122, pp. 43-65.

Gamo, M, Yamamoto, S & Yokoyama, O 1982, 'Airborne measurements of the free convective internal boundary layer during the sea breeze', *Journal of Meteorological Society of Japan,* vol. 60, pp. 1284-98.

Gimson, N, Xie, S, Zawar-Reza, P & Revell, M 2005, *Straight-line paths and urban airshed modelling*, National Institute of Water and Atmospheric Research, University of Canterbury, Christchurch.

Gimson, NR 2005, 'Modelling the air quality of Auckland -- A comparison between CALGRID and TAPM simulation based on observed and modelled meteorology', *Boundary-Layer Meteorology,* vol. 39, no. 3, pp. 38-46.

Gusten, H, Heinrich, G, Cvitas, T, Klasinc, L, Ruscic, B, Lalas, DP & Petrakis, M 1988, 'Photochemical formation and transport of ozone in Athens, Greece', *Atmospheric Environment (1967),* vol. 22, no. 9, pp. 1855-61.

Haigh, BM 1992, *A study of the Auckland Sea Breeze*, M.Sc. Thesis, The University of Auckland.

Hair Joseph F, J, Black, WC, Babin, BJ, Anderson, RE & Tatham, RL 2005, *Multivariate Data Analysis,* 6th edn, Pearson Prentice Hall, New Jersey 07458.

Hawke, GS, Heggie, AC & Hyde, R 1983, 'Meteorological factors controlling high ozone levels in the Sydney region', in JN Carras & GM Johnson (eds), *The Urban Atmosphere - Sydney , a case study*, CSIRO, Australia, Sydney.

Helmis, CG, Papadopoulas, KH, Asimakopoulas, DN, Kalogiros, JA & Soilemes, AT 1995, 'Influence of background flow on evolution of Saronic Gulf sea breeze', *Atmospheric Environment,* vol. 29, pp. 3689-701.

Hessell, JWD 1988, *The climate and weather of the Auckland region*, New Zealand Meteorological Service, Wellington, 115-20.

Heydenrych, C 2002, 'Validation and implementation issues of air quality meteorological models in New Zealand', *16th International Clean Air and environment conference 19-22 August 2002*, NIWA, Christchurch.

Hirdman, D 2006, *Sensitivity analysis of the mesoscale air pollution model TAPM*, Uppsala University, Sweden., Christchurch.

Hong, X-D, Leach, M & Raman, S 1995, 'A sensitivity study of convective cloud formation by vegetation forcing with different atmospheric conditions', *Journal of Applied Meteorology,* vol. 34, pp. 2008-28.

Hsu, SA 1985, 'A note on estimating the height of the convective internal boundary layer near shore', *Boundary-Layer Meteorology,* vol. 35, pp. 311-6.

Hsu, SA 1988, *Coastal Meteorology*, Academic Press., San Diego, Calif., pp.260.

Hurley, PJ 1994, 'PARTPUFF-- A Lagrangian particle/puff approach for plume dispersion modelling applications', *Journal of Applied Meteorology,* vol. 33, pp. 285-94.

Hurley, PJ 2000, 'The Kwinana coastal fumigation study: Meteorological and turbulence modelling on selected days', *Boundary-Layer Meteorology,* vol. 94, pp. 115-38.

Hurley, PJ 2005a, 'The air pollution model (TAPM) version 3. Part 1: Technical description', *CSIRO Atmospheric Research,* vol. Technical Paper No. 71.

Hurley, PJ 2005b, *The air pollution model (TAPM) Version 3; User Manual*, CSIRO Atmospheric Research, Internal Paper No. 31.

Hurley, PJ, Physick, WL & Luhar, AK 2002, 'The air pollution model (TAPM) Version 2. Part 2: Summary of some verification studies', *CSIRO Atmospheric Research,* vol. Technical Paper NO. 67.

Hurley, PJ, Physick, WL & Luhar, AK 2005, 'TAPM: a practical approach to prognostic meteorological and air pollution modelling', *Environmental Modelling & Software,* vol. 20, no. 6, pp. 737-52.

Hurnard, SM 1980, *Auckland's climate*, Ministry of Transport, Wellington, 167-1.

Hyde, R, Hawke, GS & Heggie, AC 1978, 'The transport and recirculation of photochemical smog across the Sydney basin II: At the coast', *4th International Conference of Clean Air Society Australia and New Zealand*, CASANZ, Brisbane, pp. 157-66.

Janjic, ZI 1994, 'The step-mountain eta coordinate model: further developments of the convection, viscous sublayer and turbulence closure schemes', *Monthly Weather Review,* vol. 122, pp. 927-45.

Jiang, N 2000, *Quality of the Auckland Airshed*, Ph.D. thesis Thesis, University of Auckland.

Kain, JS & Fritsch, JM 1990, 'A one-dimensional entraining/ detraining plume model and its application in convective parameterization', *Journal of atmospheric Sciences,* vol. 47, pp. 2784-802.

Kanda, M, Inoue, Y & Uno, I 2001, 'Numerical study on cloud lines over an urban street in Tokyo', *Boundary-Layer Meteorology,* vol. 98, pp. 251-73.

Kitada, T & Kitagawa, E 1990, 'Numerical analysis of the role of sea breeze fronts on air quality in coastal and inland polluted areas', *Atmospheric Environment,* vol. 24, no. 6, pp. 1545-59.

Kusuda, M & Alpert, P 1983, 'Anti-clockwise rotation of the wind hodograph, Part I: Theoretical study', *Journal of the Atmospheric Science,* vol. 40, pp. 487-99.

Lalas, DP, Asimakopoulos, DN, Deligiorgi, DG & Helmis, CG 1983, 'Sea-breeze circulation and photochemical pollution in Athens, Greece', *Atmospheric Environment (1967),* vol. 17, no. 9, pp. 1621-32.

Lalas, DP, Tombrou-Tsella, M, Petrackis, M, Asimakopoulas, DN & Helmis, CG 1987, 'An experimental study of the horizontal and vertical distribution of ozone over Athens', *Atmospheric Environment,* vol. 21, pp. 2681-93.

Landcare Research 2009, *NOAA Satellite Image Archive of New Zealand*. Retrieved 20-Dec., from http://satellite.landcareresearch.co.nz/noaa/

Lin, C-Y, Chen, F, Huang, JC, Chen, W-C, Liou, Y-A, Chen, W-N & Liu, S-C 2008, 'Urban heat island effect and its impact on boundary layer development and land-sea circulation over northern Taiwan', *Atmospheric Environment,* vol. 42, no. 22, pp. 5635-49.

Lin, Y-L 2007, *Mesoscale dynamics*, Cambridge University Press, 2007.

Lin, Y-L, Farley, RD & Orville, HD 1983, 'Bulk parameterization of the snow field in a cloud model', *Journal of Climate and Applied Meteorology,* vol. 22, pp. 1065-92.

Liu, H & Chan, JCL 2002a, 'An investigation of air-pollutant patterns under sea-land breezes during a severe air-pollution episode in Hong Kong', *Atmospheric Environment,* vol. 36, pp. 591-601.

Liu, H, Chan, JCL & Cheng, AYS 2001, 'Internal boundary layer structure under sea-breeze conditions in Hong Kong', *Atmospheric Environment,* vol. 35, no. 4, pp. 683-92.

Liu, HP & Chan, JCL 2002b, 'Boundary layer dynamics associated with a severe air-pollution episode in Hong Kong', *Atmospheric Environment,* vol. 36, no. 12, pp. 2013-25.

Liu, K-Y, Wang, Z & Hsiao, L-F 2002, 'A modeling of the sea breeze and its impacts on ozone distribution in northern Taiwan', *Environmental Modelling & Software,* vol. 17, no. 1, pp. 21-7.

Lu, R & Turco, RP 1994, 'Air pollutant transport in a coastal environment. Part I: Two-dimensional simulations of sea-breeze and mountain effects', *Journal of the Atmospheric Sciences,* vol. 51, no. 15, p. 2285.

Lu, R & Turco, RP 1995, 'Air pollutant transport in a coastal environment - II: Three-dimensional simulations over Los Angeles basin', *Atmospheric Environment,* vol. 29, no. 13, pp. 1499-518.

Lu, R & Turco, RP 1996, 'Ozone distributions over the Los Angeles basin: Three-dimensional simulations with the smog model', *Atmospheric Environment,* vol. 30, no. 24, pp. 4155-76.

Luhar, AK & Hurley, PJ 2003, 'Evaluation of TAPM, a prognostic meteorological and air pollution model, using urban and rural point-source data', *Atmospheric Environment,* vol. 37, no. 20, pp. 2795-810.

Luhar, AK & Hurley, PJ 2004, 'Application of a prognostic model TAPM to sea-breeze flows, surface concentrations, and fumigating plumes', *Environmental Modelling & Software,* vol. 19, no. 6, pp. 591-601.

Luhar, AK, Sawford, BL, Hacker, JM & Rayner, KN 1998, 'The Kwinana coastal fumigation study: II - Growth of the thermal internal boundary layer', *Boundary-Layer Meteorology,* vol. 89, pp. 385-405.

Lyons, WA 1972, 'The climatology and prediction of the Chicago lake breeze', *Journal of Applied Meteorology,* vol. 11, no. 08, pp. 1259-70.

Lyons, WA & Olsson, LE 1973, 'Detailed meso-meteorological studies of air pollution dispersion in the Chicago lake breeze', *Monthly Weather Review,* vol. 101, pp. 387-403.

Lyons, WA, Sawdey, ER, Schuh, JA, Calby, RH & Keen, CS 1981, 'An updated and expanded coastal fumigation model', *74th Annual Meeting, Air pollution control association*, Philadelphia.

Mahfouf, JF, Richard, E & Mascart, P 1987, 'The influence of soil and vegetation on the development of mesoscale circulation', *Journal of Climate and Applied Meteorology,* vol. 26, pp. 1483-95.

Mahrer, Y & Pielke, RA 1977, 'The effects of topography on sea and land breezes in a two-dimensional numerical model', *Monthly Weather Review,* vol. 105, pp. 1151-62.

Manins, PC, Hurley, PJ, Jhonson, GM & Assi, M 1992, *Predicted wind fields on possible ozone days. A contribution to the Perth Airshed photochemical study funded by SECWA, CSIRO division of atmospheric research*, CSIRO, Perth.

Mathews, JH 1982, 'The Sea-breeze - forecasting aspects', *Australian Meteorological Magazine,* vol. 30, pp. 205-9.

McGill, AJ 1987, *Sea Breeze Circulations about Auckland*, New Zealand Meteorological Service, Wellington, Scientific Report 29.

McKendry, IG 1989, 'Numerical simulation of sea breezes over the Auckland region, New Zealand - Air quality implications.', *Boundary-Layer Meteorology,* vol. 49, no. 1-2, pp. 7-22.

McKendry, IG 1992, 'Numerical simulation of sea breeze interaction over the Auckland region, New Zealand.', *New Zealand Journal of Geology and Geophysics,* vol. 35, pp. 9-20.

McKendry, IG 1996, 'A Study of the Photochemical Pollution Potential in New Zealand's Major Cities.', *NIWA Report AK96076 VSK601*.

McKendry, IG 2003, 'Applied climatology', *Progress in Physical Geography,* vol. 27, no. 4, pp. 597-606.

McKendry, IG & Revell, CG 1991, 'Mesoscale eddy development over South Auckland - A case study', *Weather and Forecasting,* vol. 7, pp. 134-42.

McKendry, IG & Roulet, N 1994, 'Sea breezes and advective effects in southwest James Bay', *Journal of Geophysical Research,* vol. 99(D1), pp. 1623-34.

McKendry, IG, Sturman, A & Owens, IF 1988, 'Interactions between local winds adn coastal sea surface temperatures near the Canterbury coast', *New Zealand Journal of Marine and Freshwater Research,* vol. 22, pp. 91-100.

McPherson, RD 1970, 'A numerical study of the effect of coastal irregularity on the sea breeze', *Journal of Applied Meteorology,* vol. 9, pp. 767-77.

Melas, D, Ziomas, I, Klemm, O & Zerefos, CS 1998, 'Anatomy of the sea-breeze circulation in Athens area under weak large-scale ambient winds', *Atmospheric Environment,* vol. 32, no. 12, pp. 2223-37.

MetEd 2008, *Thermally-forced Circulations I: Sea Breezes*. Retrieved 27-Nov, from http://www.meted.ucar.edu/mesoprim/seabreez/

Meyer, D, Zeileis, A & Hornik, K 2009, 'vcd: Visualizing categorical data. R package version 1.2-3.'. http://epub.wu-wien.ac.at, 28-Sep-09.

Miao, J 2006, *Meteorological modelling in coastal areas*, GOTEBORG University.

Miao, J, Chen, D & Wyser, K 2003, 'Impacts of topography and land degradation on the sea breeze over eastern Spain', *Meteorology and Atmospheric Physics,* vol. 84, pp. 157-70.

Miao, J, Chen, D & Wyser, K 2006a, 'Sea breeze modelling over the Swedish west coast with MM5: Sensitivity to PBL and LSM parameterizations', in *Meteorological modelling in coastal areas - local climate and air quality*, Earth Sciences Centre, GOTEBORG University A107 2006.

Miao, J, Chen, D, Wyser, K, Borne, K, Lindgren, J, Svensson, MK, Thorsson, S, Achberger, C & Almkvist, E 2006b, 'Evaluation of MM5 mesoscale model at local scale for air quality applications over the Swedish west coast: Influence of PBL and LSM parameterizations', in *Meteorological modelling in coastal areas - local climate and air quality*, Earth Sciences Centre, GOTEBORG University A107 2006.

Michalakes, J, Dudhia, J, Klemp, JB & Skamarock, WC 2006, 'Design of next-generation regional Weather Research and Forecast Model', *WRF Users Workshop, 19-Jun. 2006*, Mesoscale & Microscale Meteorological Division / NCAR, BOULDER, Colorado, p. 12.

Millan, MM, Jose Sanz, M, Salvador, R & Mantilla, E 2002, 'Atmospheric dynamics and ozone cycles related to nitrogen deposition in the western Mediterranean', *Environmental Pollution,* vol. 118, no. 2, pp. 167-86.

Millan, MM, Mantilla, E, Salvador, R, Carratala, A & Sanz, MJ 2000, 'Ozone cycles in the Western Mediterranean Basin: Interpretation of monitoring data in complex coastal terrain', *Journal of Applied Meteorology,* vol. 39, no. 4, pp. 487-508.

Miller, STK 2003, 'Synoptic-scale controls on the sea breeze of the Central New England Coast', *Weather and Forecasting,* vol. 18, pp. 236-48.

Miller, STK, Keim, BD, Talbot, RW & Mao, H 2003, 'Sea breeze: Structure, forecasting, and impacts', *Journal of Geophysical Research,* vol. 41, no. 3, p. 31.

Ministry for the Environment 2002, *Ambient air quality guidelines*, Ministry for the Environment, Wellington. Retrieved 30-Jun., from http://www.mfe.govt.nz/publications/air/ambient-air-quality-may02/ambient-guide-may02.pdf

Ministry for the Environment 2005, *Updated Users Guide to Resource Management (national environmental standards relating to clean air pollutants, dioxins and other toxics) regulations 2004 (including amendments 2005)*, Ministry for the Environment.

Mizuma, M 1995, 'General aspects of land and sea breezes in Osaka Bay and surrounding area', *Journal of Meteorological Society of Japan,* vol. 73, no. 6, pp. 1029-40.

Monin, AS & Obukhov, AM 1954, 'Basic laws of turbulent mixing in the surface layer of the atmosphere', *Contrib. Geophys. Acad. Sci. USSR,* vol. 151, pp. 163-87.

Nakane, H & Sasano, Y 1986, 'Structure of a sea-breeze front revealed by scanning Lidar observation', *Journal of Meteorological Society of Japan,* vol. 64, pp. 787-92.

National Center for Atmospheric Research-USA 2008, *Weather Research and Forecasting (ARW) Version 3 Modelling System User's Guide*, National Center for Atmospheric Research.

Neumann, J 1977, 'On the rotation rate of the direction of sea and land breezes', *Journal of the Atmospheric Sciences,* vol. 34, pp. 1913-7.

Neumann, J 1984, 'The Coriolis Force in relation to the sea and land breezes - A historical note', *Bulletin of the American Meteorological Society,* vol. 65, no. 1, pp. 24-6.

Neumann, J & Mahrer, Y 1971, 'A theoretical study of the land and sea breeze circulation', *Journal of the Atmospheric Sciences,* vol. 28, pp. 532-42.

Neumann, J & Mahrer, Y 1973, 'Evolution of a sea breeze front: A numerical study', in *Climatological Research*, vol. The Hermann Flohn 60th Birthday Volume. University of Bonn, West Germany, pp. 481-92.

Nitis, T, Kitsiou, D, Bencetic, K, Prtenjak, TM & Moussiopoulos, N 2005, 'The effects of basic flow and topography on the development of the sea breeze over a complex coastal environment', *Quarterly Journal of the Royal Meteorological Society,* vol. 131, pp. 305-27.

NIWA 2005, *Climate data and activities*, NIWA, Auckland. Retrieved 25-Nov, from http://www.niwascience.co.nz/edu/resources/climate/

NOAA 2008, *Sea Breeze*, NOAA, National Weather Service. Retrieved 10-Sep., from http://www.srh.noaa.gov/jetstream//ocean/seabreezes.htm

NOAA Research 2009, *NCEP/NCAR Reanalysis data archives*, Earth System Research Laboratory, Physical Science Division. Retrieved 15-Dec, from http://www.esrl.noaa.gov/psd/cgi-bin/DataAccess.pl?DB_dataset=NCEP+Reanalysis+Pressure+Level&DB_variable=Geopotential+height&DB_statistic=Individual+Obs&DB_tid=26034&DB_did=2&DB_vid=14

Ohashi, Y & Kida, H 2001, 'Observational results of the sea breeze with a weak wind region over the northern Osaka urban area', *Journal of Meteorological Society of Japan,* vol. 79, no. 4, pp. 949-55.

Oke, TR 1987, *Boundary layer climates,* 1st edn, London; New York: Routledge, 1987.

Oke, TR 1992, *Boundary layer climates,* 2nd edn, London; New York: Routledge, 1992, c1987.

Ookouchi, Y, Uryu, M & Sawada, R 1978, 'A numerical study of the effects of a mountain on the land and sea breeze', *Journal of Meteorological Society of Japan,* vol. 56, pp. 368-86.

Orlic, M, Penzar, B & Penzar, I 1988, 'Adriatic sea and land breezes: Clockwise versus anticlockwise rotation', *Journal of Applied Meteorology,* vol. 27, pp. 675-9.

Pearson, RA 1975, 'On the asymmetry of the land-sea breeze circulation ', *Quarterly Journal of the Royal Meteorological Society,* vol. 101, pp. 529-36.

Pearson, RA, Carboni, G & Brusasca, G 1983, 'The sea breeze with mean flow', *Quarterly Journal of the Royal Meteorological Society,* vol. 109, pp. 809-30.

Physick, WL 1980, 'Numerical experiments on the inland penetration of the sea breeze', *Quarterly Journal of the Royal Meteorological Society,* vol. 106, pp. 735-46.

Physick, WL & Abbs, DJ 1989, 'Formulation of the thermal internal boundary layer in a mesoscale model', *Boundary-Layer Meteorology,* vol. 49, pp. 99-111.

Physick, WL & Byron-Scott, RAD 1977, 'Observations of the sea breeze in the vicinity of a gulf', *Weather,* vol. 32, pp. 373-81.

Pielke, RA 1974, 'A three-dimensional numerical model of the sea breezes over south florida', *Monthly Weather Review,* vol. 102, pp. 115-39.

Pielke, RA 1984, *Mesoscale meteorological modeling*, Academic Press, New York.

Pielke, RAS 2002, *Mesoscale meteorological modeling,* 2nd edn, Academic Press, Fort Collins, Colorado.

Purdom, JFW 1976, 'Some uses of high-resolution GOES imagery in the mesoscale forecasting of covection and its behavior', *Monthly Weather Review,* vol. 104, pp. 1474-83.

Puri, K, Dietachmayer, G, Mills, G, Davidson, N, Bowen, R & Logan, L 1998, 'The BMRC limited area prediction systems, LAPS', *Australian Meteorological Magazine,* vol. 47, pp. 203-23.

Rayner, GS, Sethuraman, S & Brown, RM 1979, 'Formation and characteristics of coastal internal boundary layers during onshore flows', *Boundary-Layer Meteorology,* vol. 16, pp. 487-514.

Raynor, GS 1975, 'Studies of atmospheric diffusion from a near-shore oceanic site', *Journal of Applied Meteorology,* vol. 14, no. 6, pp. 1080-94.

Revell, CG 1978, *A note on sea breeze circulation systems*, New Zealand Meteorological Service, Wellington, Unpublished., Wellington, 03.

Ridley, RN 1992, *Sea breeze convergence and particle dispersion in a region with complex coastlines and orography*, National Institute of Water and Atmospheric Research (NIWA). Wellington.

Ridley, RN 1993, *Particle dispersion and sea breeze convergence on time scales of 1-3 days*, NIWA Atmosphere Report, Gracefield, New Zealand.

Ridley, RN 1995, 'Lagrangian particle dispersion simulations in cases of sea-breeze convergence', *Mathematical and Computer Modelling,* vol. 21, no. 9, pp. 137-42.

Rouse, W & Bello, R 1985, 'Impact of Hudson Bay on the energy balance in the Hundson Bay lowlands and potential for climatic modification', *Atmosphere and Ocean,* vol. 23, pp. 375-92.

Rouse, W, Hardill, S & PM., L 1987, 'The energy balance in the coastal environment of James Bay and Hudson Bay during the growing season', *Journal of Climatology,* vol. 7, pp. 165-79.

Rutledge, SA & Hobbs, PV 1984, 'The mesoscale and microscale structure and organization of clouds and precipitation in midlatitude cyclones. XII: A diagnostic modeling study of
precipitation development in narrow cloud-frontal rainbands', *Journal of Atmospheric Sciences,* vol. 20, pp. 2949-72.

Schumann, EH, Illenberger, WK & Goschen, WS 1991, 'Surface winds over Algoa Bay, South Africa', *South Affrican Journal of Science,* vol. 87, pp. 202-7.

Segal, M & Arritt, R 1992, 'Nonclassical mesoscale circulations caused by surface sensible heat-flux gradients', *Bulletin of the American Meteorological Society,* vol. 73, no. 10, pp. 1593-604.

Segal, M & Pielke, RA 1985, 'The effect of water temperature and synoptic winds on the development of surface flows over narrow, elongated water bodies', *Journal of Geophysical Research,* vol. 90, pp. 4907-10.

Sha, W & Kawamura, T 1991, 'A numerical study on sea/land breezes as a gravity current: Kelvin-Helmholtz Billows and inland penetration of the sea breeze front', *Journal of the Atmospheric Sciences*, pp. 1649-65.

Shamarock, WC, Klem, JB, Dudhia, J, Gill, DO, Barker, DM, Wang, W & Powers, JG 2008a, *A description of the advanced research WRF version 3*, NCAR, Boulder, Colorado, USA, NCAR/TN-468+STR.

Shamarock, WC, Klemp, JB, Dudhia, J, Gill, DO, Barker, DM, Wang, W & Powers, JG 2008b, *Adescription of the advanced research WRF version 3. NCAR Technical Notes-468+STR*, NCAR, Boulder, Colorado, USA, NCAR/TN-468+STR.

Sills, DML 1998, *Lake and land breezes in southwestern Ontario: Observations analyses and numerical modeling*, PhD. Thesis, York University.

Simpson, JE 1977, 'Inland penetration of sea breeze fronts', *Quarterly Journal of the Royal Meteorological Society,* vol. 103, no. 435, pp. 47-76.

Simpson, JE 1995, 'Notes and correspondence: Diurnal changes in sea-breeze direction', *Journal of Applied Meteorology,* vol. 35, pp. 1166-9.

Simpson, JE & Britter, RE 1980, 'A laboratory model of an atmospheric mesofront', *Quarterly Journal of the Royal Meteorological Society,* vol. 94, pp. 477-95.

Simpson, SE 1994, *Sea breeze and Local Wind*, Cambridge University Press, New York.

Sparrow, CJ 1968, 'Some Geographical aspects of air pollution in Auckland', *Journal of Clean Air Society of Australia and New Zealand,* vol. 22, no. 04.

Staley, DO 1957, 'The low-level sea breeze of northwest Washington', *Journal of Meteorology,* vol. 14, pp. 458-70.

Standards Australia 1987, *Ambient Air Guide for the Siting of Sampling Units*, Homebush, NSW.

Stephens, GL 1978, 'Radiation profiles in extended water clouds. Part II: Parameterization schemes', *Journal of Atmospheric Sciences,* vol. 35, no. 2123-2132.

Stull, RB 2000, *Meteorology for scientists and engineers,* 2nd edn, Brooks/Cole Thompson Learning, CA, USA.

Stull, RB 2003, *An introduction to boundary layer meteorology*, Kluwer Academic Publishers, Boston.

Sturman, A & Tapper, N 2006, *The weather and climate of Australia and New Zealand,* 2nd edn, Oxford University Press, South Melbourne.

Sturman, AP, McGowan, HA & Spronken-Simith, RA 1999, 'Mesoscale and local climates in New Zealand', *Progress in Physical Geography,* vol. 23, no. 4, pp. 611-35.

Sutton, C 1996, *Numerical modelling of sea breezes and pollutant dispersion*, Ph.D. Thesis, University of Auckland.

Sutton, CM 1992, *Numerical modelling of sea breezes in the Auckland region*, Dissertation Thesis, The University of Auckland.

Tabachnick, BG & Fidell, LS 2001, *Using multivariate statistics,* 4th. edn, Allyn & Bacon.

Talbot, C, Patrick, A, Leroy, C, Willlart, V, Delbarre, H & Khomenko, G 2007, 'Impact of a sea breeze on the boundary-layer dynamics and the atmospheric stratification in a coastal area of the North sea', *Boundary-Layer Meteorology,* vol. 125, pp. 133-54.

Taylor, R, Cochrane, P, Stephenson, B & Gibbs, N 1997, 'The state of our Air', in I Smith, A Saunders, D Swain & B Wall (eds), *The State of New Zealand's Environment*, MfE & GP Publications.

Thompson, RD 1998, *Atmospheric Processes and Systems,* 1st. edn, Routledge, London.

Tijm, ABC, Holtslag, AAM & Delden, AJV 1999, 'Observations and modeling of the sea breeze with the return current', *Monthly Weather Review,* vol. 127, no. 5, pp. 625-40.

University Corporation of Atmospheric Research 2008, *Thermally-forced Circulations I: Sea Breezes*. Retrieved 27-Nov, from http://www.meted.ucar.edu/mesoprim/seabreez/

Varvayanni, M, Helmis, CG, Amanatidis, GT, Asimakopoulas, DN, Bartzis, JG, Soilemes, A, Papadopoulas, KH & Kambezidis, HD 1993, 'Effect of onshore and offshore topography on sea breeze circulation: An observational study at Eastern Attica, Greece', *Pure and Applied Geophysics,* vol. 140, no. 4, pp. 681-720.

Venkatram, A 1977, 'A model of internal boundary layer development', *Boundary-Layer Meteorology,* vol. 11, pp. 419-37.

Walsh, JE 1974, 'Sea breeze theory and applications', *Journal of the Atmospheric Sciences,* vol. 31, pp. 2012-26.

Willmott, CJ 1981, 'On the validation of models', *Physical Geography,* vol. 2, pp. 184-94.

Wilson, GJ & Zawar-Reza, P 2006, 'Intraurban-scale dispersion modelling of particulate matter concentrations: Applications for exposure estimates in cohort studies', *Atmospheric Environment,* vol. 40, no. 6, pp. 1053-63.

WMO 2008, *Guide to Meteorological Instruments and Methods of Observation*, World Meteorological Organization, Geneva, Switzerland.

Wratt, DS, Hadfield, MG, Jones, MT & Johnson, GM 1990, 'Predicting the impact of a proposed gas fired power station on photochemical pollution levels around Auckland', *International Clean Air Conference*, pp. 159-64.

Xian, Z & Pielke, RA 1991a, 'The effects of width of land masses on the development of sea breezes', *Journal of Applied Meteorology,* vol. 30, no. 09, pp. 1280-304.

Xian, Z & Pielke, RA 1991b, 'The effects of width of landmasses on the development of sea breezes', *Journal of Applied Meteorology,* vol. 30, pp. 1280-304.

Yan, H & Anthes, R, A. 1988, 'The effect of variations in surface moisture on mesoscale circulations', *Monthly Weather Review,* vol. 116, pp. 192-208.

Yoshikado, H 1992, 'Numerical study of the daytime urban effect and its interaction with the sea breeze', *Journal of Applied Meteorology,* vol. 31, pp. 1146-64.

Zawar-Reza, P, Kingham, S & Pearce, J 2005a, 'Evaluation of a year-long dispersion modelling of $PM_{10}$ using the mesoscale model TAPM for Christchurch, New Zealand', *Science of The Total Environment,* vol. 349, no. 1-3, pp. 249-59.

Zawar-Reza, P, Titov, M & Sturman, AP 2005b, *Dispersion modelling of $PM_{10}$ for Christchurch, New Zealand: An intercomparison between MM5 and TAPM*, Centre for Atmospheric Research, University of Canterbury, Christchurch. Retrieved 15-Apr., from http://www.ucar.canterbury.ac.nz/

Zeileis, A, Meyer, D & Hornik, K 2007, 'Residual-based shading for visualizing (conditional) Independence', in *Computational and Graphical Statistics*, vol. 16. http://epub.wu-wien.ac.at, pp. 507-25, 28-Sep-09.

Zhong, S & Fast, JD 2003, 'An evaluation of the MM5, RAMS, and Meso-Eta models at subkilometer resolution using VTMX field campaign data in the Salt Lake Valley', *Monthly Weather Review,* vol. 131, pp. 1301-22.

Zhong, S, In, H & Clements, C 2007, 'Impact of turbulence, land surface, and radiation parameterizations on simulated boundary layer properties in a coastal environment', *Journal of Geophysical Research,* vol. 112, p. 14.

Zhong, S & Takle, ES 1992, 'An observational study of sea-and land breeze circulation in an area of complex coastal heating', *Journal of Applied Meteorology,* vol. 31, no. 12, pp. 1426-38.

Zhong, S & Takle, ES 1993, 'The effects of large-scale winds on the sea-land breeze circulations in an area of complex coastal heating', *Journal of Applied Meteorology,* vol. 32, pp. 1182-995.

Zilitinkevich, SS 1995, *Non-local turbulent transport: pollution dispersion aspects of coherent structure of convective flows, Air Pollution III- Volume I. Air Pollution Theory and Simulation*, Eds. H. Power, N. Moussiopoulos and C.A. Brebbia. Computational Mechanics Publications, Southampton, Boston.

# Appendix 4A

## List of Monitoring Stations in the Auckland Region

The meteorological parameters and pollutant used in this research have been listed corresponding to each monitoring station.

| No | Site Name | Pollutants Measured | Meteorological Parameters Measured |
|---|---|---|---|
| 1 | Auckland Air Port | | Wind speed, wind direction, ambient temperature, relative humidity |
| 2 | Whangarei | | Solar radiation |
| 3 | Leigh | | Wind speed, wind direction, ambient temperature, relative humidity, solar radiation |
| 4 | Paeroa | | Solar radiation |
| 5 | Pukekohe | $NO_x$ | Wind speed, wind direction, ambient temperature, relative humidity, solar radiation |
| 6 | Wiri | | solar radiation |
| 7 | Onehunga | | Solar radiation |
| 8 | Henderson (Lincoln Road) | $NO_x$ | Wind speed, wind direction, ambient temperature, relative humidity, solar radiation |
| 9 | Henderson (Te Pai Park) | | Wind speed, wind direction, ambient temperature, relative humidity Solar radiation |
| 10 | North Shore | | Wind speed, wind direction, solar radiation |
| 11 | Ruakura -I | | Solar radiation |
| 12 | Ruakura-II | | Solar radiation |
| 13 | Warkworth | | Solar radiation |
| 14 | Musick Point | $NO_x$ | Wind speed, wind direction, solar radiation |
| 15 | Kyber Pass | $NO_x$ | Wind speed, wind direction, ambient temperature, relative humidity, solar radiation |
| 16 | Pakuranga | $NO_x$ | Wind speed, wind direction, ambient temperature, relative humidity, solar radiation |
| 17 | Penrose | $NO_x$ | Wind speed, wind direction, ambient temperature, relative humidity, solar radiation |
| 18 | Mangere | | Wind speed, wind direction, ambient temperature, relative humidity, solar radiation |
| 19 | Toenepi | | Solar radiation |
| 20 | Whatawhata | | Solar radiation |
| 21 | Whangaparaoa | | Wind speed, wind direction, ambient temperature, relative humidity, solar radiation |
| 22 | Queen Street | $NO_x$ | Wind speed, wind direction, ambient temperature, relative humidity |
| 23 | Glen Eden | $NO_x$ | Wind speed, wind direction, ambient temperature, relative humidity |
| 24 | Arc Kumeu | | Solar radiation |
| 25 | Kingsland | $NO_x$ | Wind speed, wind direction, ambient temperature, relative humidity |
| 26 | Takapuna | $NO_x$ | Wind speed, wind direction, ambient temperature, relative humidity |

# Appendix 5A

**Combined summary statistics of 6 observation sites**

| Met. Var. | Scheme | Observed Mean | Modelled Mean | Observed Std. Dev. | Modelled Std. Dev. | Corr. Coeff. | IOA | RMSE | RMSE_S | RMSE_U |
|---|---|---|---|---|---|---|---|---|---|---|
| Wind speed (m s-1) | 101cg | 2.7 | 3.6 | 1.8 | 2.4 | 0.81 | 0.83 | 1.74 | 1.00 | 1.43 |
| | 101ch | 2.7 | 3.3 | 1.8 | 2.0 | 0.75 | 0.82 | 1.51 | 0.7 | 1.34 |
| | 101ci | 2.7 | 3.2 | 1.8 | 2.3 | 0.80 | 0.82 | 1.65 | 0.86 | 1.41 |
| | 101cj | 2.7 | 3.1 | 1.8 | 2.1 | 0.76 | 0.83 | 1.44 | 0.51 | 1.34 |
| | | | | | | | | | | |
| U velocity (m s-1) | 101cg | -0.2 | -0.6 | 2.3 | 2.9 | 0.83 | 0.89 | 1.70 | 0.44 | 1.64 |
| | 101ch | -0.2 | -0.6 | 2.3 | 2.6 | 0.79 | 0.88 | 1.66 | 0.52 | 1.58 |
| | 101ci | -0.2 | -0.6 | 2.3 | 2.8 | 0.70 | 0.83 | 1.59 | 0.42 | 1.54 |
| | 101cj | -0.2 | -0.6 | 2.3 | 2.6 | 0.80 | 0.88 | 1.61 | 0.51 | 1.53 |
| | | | | | | | | | | |
| V velocity (m s-1) | 101cg | 0.8 | 1.6 | 2.1 | 2.8 | 0.79 | 0.85 | 1.88 | 0.78 | 1.71 |
| | 101ch | 0.8 | 1.4 | 2.1 | 2.5 | 0.76 | 0.85 | 1.73 | 0.64 | 1.6 |
| | 101ci | 0.8 | 1.6 | 2.1 | 2.6 | 0.84 | 0.90 | 1.84 | 0.79 | 1.66 |
| | 101cj | 0.8 | 1.4 | 2.1 | 2.3 | 0.78 | 0.85 | 1.58 | 0.63 | 1.45 |
| | | | | | | | | | | |
| Air temperature (°C) | 101cg | 19.3 | 18.0 | 2.7 | 1.9 | 0.77 | 0.78 | 2.14 | 1.77 | 1.20 |
| | 101ch | 19.3 | 18.1 | 2.7 | 2.3 | 0.79 | 0.84 | 1.98 | 1.43 | 1.37 |
| | 101ci | 19.3 | 17.6 | 2.7 | 1.9 | 0.77 | 0.76 | 2.37 | 2.03 | 1.21 |
| | 101cj | 19.3 | 18.3 | 2.7 | 1.8 | 0.78 | 0.77 | 1.91 | 1.55 | 1.12 |
| | | | | | | | | | | |
| Relative humidity (%) | 101cg | 77.6 | 79.1 | 13.0 | 10.0 | 0.71 | 0.82 | 9.34 | 6.08 | 7.09 |
| | 101ch | 77.6 | 79.0 | 13.0 | 14.2 | 0.74 | 0.83 | 9.65 | 2.62 | 9.29 |
| | 101ci | 77.6 | 83.0 | 13.0 | 10.5 | 0.74 | 0.81 | 10.30 | 7.52 | 7.03 |
| | 101cj | 77.6 | 76.8 | 13.0 | 11.0 | 0.71 | 0.82 | 9.31 | 5.18 | 7.73 |

## Appendix 5B

# Parameterizations used in WRF(ARW) Model Simulations

Various parameterizations for land surface, turbulence, surface layer etc. provided in this appendix are reproduced from (Shamarock et al. 2008b) and (National Center for Atmospheric Research-USA 2008) as quick reference for the reader. For brevity most of the in-text citations have been removed from the text and only necessary references are retained.

## 1. Land Surface Schemes

The land-surface models (LSMs) use atmospheric information from the surface layer scheme, radiative forcing from the radiation scheme, and precipitation forcing from the microphysics and convective schemes, together with internal information on the land's state variables and land-surface properties, to provide heat and moisture fluxes over land points and sea-ice points. These fluxes provide a lower boundary condition for the vertical transport done in the PBL schemes (or the vertical diffusion scheme in the case where a PBL scheme is not run, such as in large-eddy mode). [Note that large-eddy mode with interactive surface fluxes is not yet available in the ARW, but is planned for the near future.] The land-surface models have various degrees of sophistication in dealing with thermal and moisture fluxes in multiple layers of the soil and also may handle vegetation, root, and canopy effects and surface snow-cover prediction. The land surface model provides no tendencies, but does update the land's state variables which include the ground (skin) temperature, soil temperature profile, soil moisture profile, snow cover, and possibly canopy properties. There is no horizontal interaction between neighboring points in the LSM, so it can be regarded as a one-dimensional column model for each WRF land grid-point, and many LSMs can be run in a stand-alone mode.

### 1.1 5-layer thermal diffusion

This simple LSM is based on the MM5 5-layer soil temperature model. Layers are 1, 2, 4, 8, and 16 cm thick. Below these layers, the temperature is fixed at a deep-layer

average. The energy budget includes radiation, sensible, and latent heat flux. It also allows for a snow-cover flag, but the snow cover is fixed in time. Soil moisture is also fixed with a landuse- and season-dependent constant value, and there are no explicit vegetation effects.

### 1.2 The Noah LSM

The Noah LSM is the successor to the OSU LSM. The scheme was developed jointly by NCAR and NCEP, and is a unified code for research and operational purposes, being almost identical to the code used in the NCEP North American Mesoscale Model (NAM). This has the benefit of being consistent with the time-dependent soil fields provided in the analysis datasets. This is a 4-layer soil temperature and moisture model with canopy moisture and snow cover prediction. The layer thickness are 10, 30, 60 and 100 cm (adding to 2 meters) from the top down. It includes root zone, evapotranspiration, soil drainage, and runoff, taking into account vegetation categories, monthly vegetation fraction, and soil texture. The scheme provides sensible and latent heat fluxes to the boundary-layer scheme. The Noah LSM additionally predicts soil ice, and fractional snow cover effects, has an improved urban treatment, and considers surface emissivity properties, which are all new since the OSU scheme.

## 2. Planetary Boundary Layer

The planetary boundary layer (PBL) is responsible for vertical sub-grid-scale fluxes due to eddy transports in the whole atmospheric column, not just the boundary layer. Thus, when a PBL scheme is activated, explicit vertical diffusion is de-activated with the assumption that the PBL scheme will handle this process. The most appropriate horizontal diffusion choices are those based on horizontal deformation or constant Kh values where horizontal and vertical mixing are treated independently. The surface fluxes are provided by the surface layer and land-surface schemes. The PBL schemes determine the flux profiles within the well-mixed boundary layer and the stable layer, and thus provide atmospheric tendencies of temperature, moisture (including clouds), and horizontal momentum in the entire atmospheric column. Most PBL schemes consider dry mixing, but can also include saturation effects in the vertical stability that determines the mixing. The schemes are one-dimensional, and assume that there is a

clear scale separation between sub-grid eddies and resolved eddies. This assumption will become less clear at grid sizes below a few hundred meters, where boundary layer eddies may start to be resolved, and in these situations the scheme should be replaced by a fully three-dimensional local sub-grid turbulence scheme such as the TKE diffusion scheme.

## 2.1 Yonsei University (YSU) PBL

The Yonsei University PBL is the next generation of the MRF PBL, also using the counter-gradient terms to represent fluxes due to non-local gradients. This adds to the MRF PBL an explicit treatment of the entrainment layer at the PBL top. The entrainment is made proportional to the surface buoyancy flux in line with results from studies with large-eddy models. The PBL top is defined using a critical bulk Richardson number of zero (compared to 0.5 in the MRF PBL), so is effectively dependent on the buoyancy profile, in which the PBL top is defined at the maximum entrainment layer (compared to the layer at which the diffusivity becomes zero). A smaller magnitude of the counter-gradient mixing in the YSU PBL produces a well-mixed boundary-layer profile, whereas there is a ronounced over-stable structure in the upper part of the mixed layer in the case of the MRF PBL. In version 3.0, an enhanced stable boundary-layer diffusion algorithm is also devised that allows deeper mixing in windier conditions.

## 2.2 Mellor-Yamada-Janjic (MYJ) PBL

This parameterization of turbulence in the PBL and in the free atmosphere represents a nonsingular implementation of the Mellor-Yamada Level 2.5 turbulence closure model through the full range of atmospheric turbulent regimes. In this implementation, an upper limit is imposed on the master length scale. This upper limit depends on the TKE as well as the buoyancy and shear of the driving flow. In the unstable range, the functional form of the upper limit is derived from the requirement that the TKE production be nonsingular in the case of growing turbulence. In the stable range, the upper limit is derived from the requirement that the ratio of the variance of the vertical velocity deviation and TKE cannot be smaller than that corresponding to the regime of

vanishing turbulence. The TKE production/dissipation differential equation is solved iteratively. The empirical constants have been revised as well.

## 3. Surface Layer

The surface layer schemes calculate friction velocities and exchange coefficients that enable the calculation of surface heat and moisture fluxes by the land-surface models and surface stress in the planetary boundary layer scheme. Over water surfaces, the surface fluxes and surface diagnostic fields are computed in the surface layer scheme itself. The schemes provide no tendencies, only the stability-dependent information about the surface layer for the land-surface and PBL schemes. Currently, each surface layer option is tied to particular boundary-layer options, but in the future more interchangeability and options may become available. Note that some boundary layer schemes (YSU and MRF) require the thickness of the surface layer in the model to be representative of the actual surface layer (e.g. 50-100 meters).

### 3.1 Similarity theory (MM5)

This scheme uses stability functions from to compute surface exchange coefficients for heat, moisture, and momentum. A convective velocity following is used to enhance surface fluxes of heat and moisture. No thermal roughness length parameterization is included in the current version of this scheme. A Charnock relation relates roughness length to friction velocity over water. This surface layer scheme must be run in conjunction with the MRF or YSU PBL schemes. In Version 3, there is an option to replace the Charnock relation for roughness length with a Donelan relation that has lower drag at hurricane force
wind speeds, and may be more suitable for hurricane simulations. Also for water points, the Beljaars formulation for convective velocity is replaced by one proportional only to the vertical thermal gradient to help in weak-wind situations.

### 3.2 Similarity theory (Eta)

The Eta surface layer scheme is based on similarity theory (Monin & Obukhov 1954). The scheme includes parameterizations of a viscous sub-layer. Over water surfaces, the viscous sub-layer is parameterized explicitly following (Janjic 1994). Over land, the

effects of the viscous sub-layer are taken into account through variable roughness height for temperature and humidity as proposed by Zilitinkevich (1995). The Beljaars (1994) correction is applied in order to avoid singularities in the case of an unstable surface layer and vanishing wind speed. The surface fluxes are computed by an iterative method. This surface layer scheme must be run in conjunction with the Eta (Mellor-Yamada-Janjic) PBL scheme, and is therefore sometimes referred to as the MYJ surface scheme.

## 4. Atmospheric Radiation

The radiation schemes provide atmospheric heating due to radiative flux divergence and surface downward longwave and shortwave radiation for the ground heat budget. Longwave radiation includes infrared or thermal radiation absorbed and emitted by gases and surfaces. Upward longwave radiative flux from the ground is determined by the surface emissivity that in turn depends upon land-use type, as well as the ground (skin) temperature. Shortwave radiation includes visible and surrounding wavelengths that make up the solar spectrum. Hence, the only source is the Sun, but processes include absorption, reflection, and scattering in the atmosphere and at surfaces. For shortwave radiation, the upward flux is the reflection due to surface albedo. Within the atmosphere the radiation responds to model-predicted cloud and water vapor distributions, as well as specified carbon dioxide, ozone, and (optionally) trace gas concentrations. All the radiation schemes in WRF currently are column (one-dimensional) schemes, so each column is treated independently, and the fluxes correspond to those in infinite horizontally uniform planes, which is a good approximation if the vertical thickness of the model layers is much less than the horizontal grid length. This assumption would become less accurate at high horizontal resolution.

### 4.1 Rapid Radiative Transfer Model (RRTM) Longwave

This RRTM, which is taken from MM5, is a spectral-band scheme that uses the correlated-k method. It uses pre-set tables to accurately represent longwave processes due to water vapor, ozone, CO2, and trace gases (if present), as well as accounting for cloud optical depth.

### 4.2 MM5 (Dudhia) Shortwave

This scheme is based is taken from MM5. It has a simple downward integration of solar flux, accounting for clear-air scattering, water vapor absorption, and cloud albedo and absorption. It uses look-up tables for clouds from Stephens (1978). In Version 3, the scheme has an option to account for terrain slope and shadowing effects on the surface solar flux.

## 5. Cumulus parameterization

These schemes are responsible for the sub-grid-scale effects of convective and/or shallow clouds. The schemes are intended to represent vertical fluxes due to unresolved updrafts and downdrafts and compensating motion outside the clouds. They operate only on individual columns where the scheme is triggered and provide vertical heating and moistening profiles. Some schemes additionally provide cloud and precipitation field tendencies in the column, and future schemes may provide momentum tendencies due to convective transport of momentum. The schemes all provide the convective component of surface rainfall. Cumulus parameterizations are theoretically only valid for coarser grid sizes, (e.g., greater than 10 km), where they are necessary to properly release latent heat on a realistic time scale in the convective columns. While the assumptions about the convective eddies being entirely sub-grid-scale break down for finer grid sizes, sometimes these schemes have been found to be helpful in triggering convection in 5–10 km grid applications. Generally, they should not be used when the model can resolve the convective eddies itself (e.g., 5 km grid).

### 5.1 Kain-Fritsch scheme

The modified version of the Kain-Fritsch scheme (KF-Eta) is based on (Kain & Fritsch 1990), but has been modified based on testing within the Eta model. As with the original KF scheme, it utilizes a simple cloud model with moist updrafts and downdrafts, including the effects of detrainment, entrainment, and relatively simple microphysics. It differs from the original KF scheme in the following ways:

- A minimum entrainment rate is imposed to suppress widespread convection in marginally unstable, relatively dry environments.

- Shallow (non precipitating) convection is allowed for any updraft that does not reach minimum cloud depth for precipitating clouds; this minimum depth varies as a function of cloud-base temperature.
- The entrainment rate is allowed to vary as a function of low-level convergence.
- Downdraft changes:
  - Source layer is the entire 150 – 200 mb deep layer just above cloud base.
  - Mass flux is specified as a fraction of updraft mass flux at cloud base. Fraction is a function of source layer RH rather than wind shear or other parameters, i.e., old precipitation efficiency relationship not used.
  - Detrainment is specified to occur in updraft source layer and below.

## 6. Microphysics

Microphysics includes explicitly resolved water vapor, cloud, and precipitation processes. The model is general enough to accommodate any number of mass mixing-ratio variables, and other quantities such as number concentrations. Four-dimensional arrays with three spatial indices and one species index are used to carry such scalars. Memory, i.e., the size of the fourth dimension in these arrays, is allocated depending on the needs of the scheme chosen, and advection of the species also applies to all those required by the microphysics option. In the current version of the ARW, microphysics is carried out at the end of the time-step as an adjustment process, and so does not provide tendencies. The rationale for this is that condensation adjustment should be at the end of the time-step to guarantee that the final saturation balance is accurate for the updated temperature and moisture. However, it is also important to have the latent heating forcing for potential temperature during the dynamical sub-steps, and this is done by saving the microphysical heating as an approximation for the next time-step. Currently, the sedimentation process is accounted for inside the individual microphysics modules, and, to prevent instability in the calculations of the vertical flux of precipitation, a smaller time step is allowed. The saturation adjustment is also included inside the microphysics. In the future, however, it might be separated into an individual subroutine to enable the remaining microphysics to be called less frequently than the model's advection step for efficiency. As a general rule, for grid sizes less than 10 km, where updrafts may be resolved, mixed-phase schemes should be used,

particularly in convective or icing situations. For coarser grids the added expense of these schemes is not worth it because riming is not likely to be well resolved.

### 6.1 Purdue Lin scheme

Six classes of hydrometeors are included: water vapor, cloud water, rain, cloud ice, snow, and graupel. All parameterization production terms are based on Lin et al. (1983) and Rutledge & Hobbs (1984) with some modifications, including saturation adjustment and ice sedimentation. This is a relatively sophisticated microphysics scheme in WRF, and it is most suitable for use in research studies. The scheme is taken from the Purdue cloud model.

## Appendix 5C

# Mean Sea Level Weather Charts for New Zealand

Mean sea level geopotential height charts for the simulation period from 17th March to 25th March 2006. The Weather charts are extracted form NCEP reanalysis pressure level data (NOAA Research 2009).

**a) 17 Mar 2006 1200 hrs NZST. Lev: 1000 hPa.**

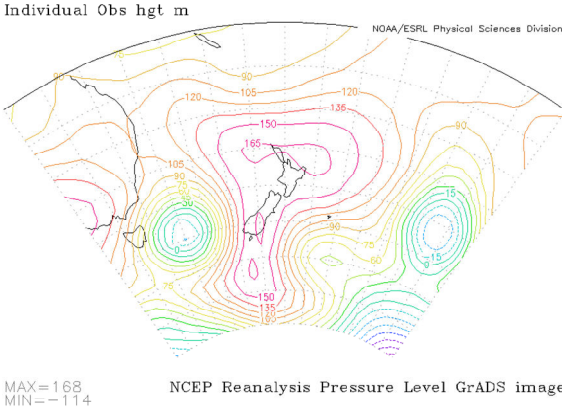


**b) 18 Mar 2006 0000 hrs NZST. Lev: 1000 hPa.**

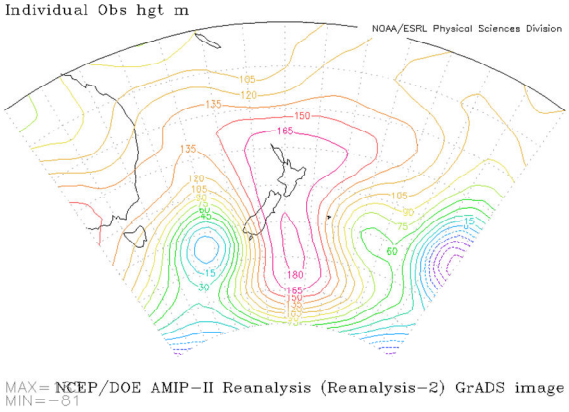


**c) 18 Mar 2006 1200 hrs NZST. Lev: 1000 hPa.**

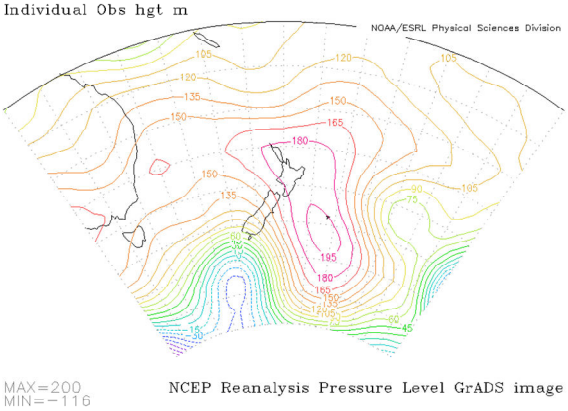


**d) 19 Mar 2006 0000 hrs NZST. Lev: 1000 hPa.**

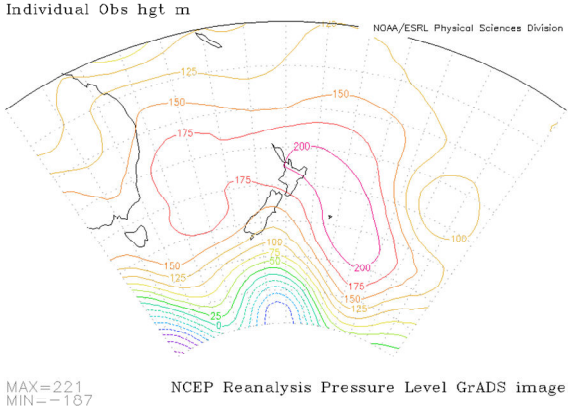


**e) 19 Mar 2006 1200 hrs NZST. Lev: 1000 hPa.**

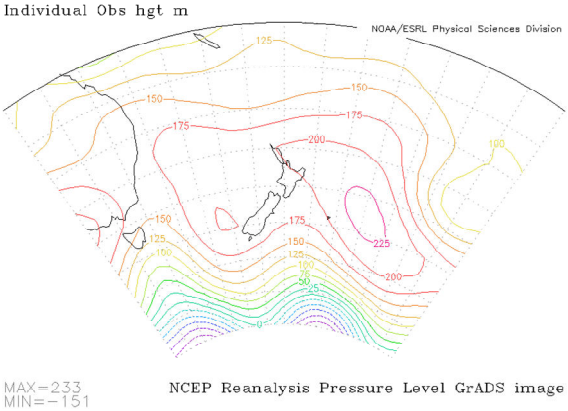


**f) 20 Mar 2006 0000 hrs NZST. Lev: 1000 hPa.**

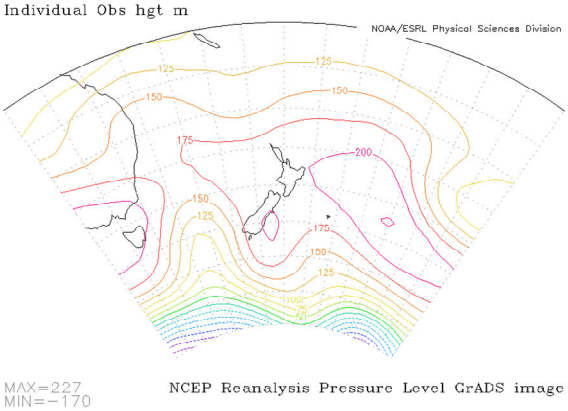

**g) 20 Mar 2006 1200 hrs NZST. Lev: 1000 hPa.**

Individual Obs hgt m

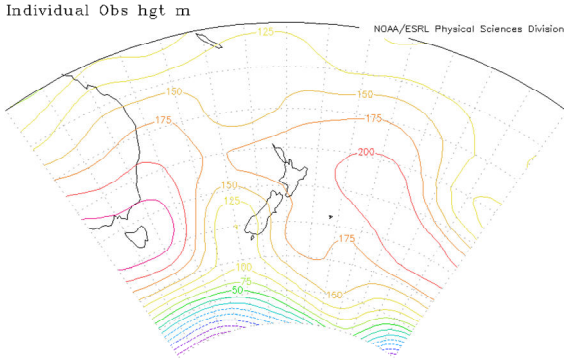


MAX=244
MIN=−139

NCEP Reanalysis Pressure Level GrADS image

**h) 21 Mar 2006 0000 hrs NZST. Lev: 1000 hPa.**

Individual Obs hgt m

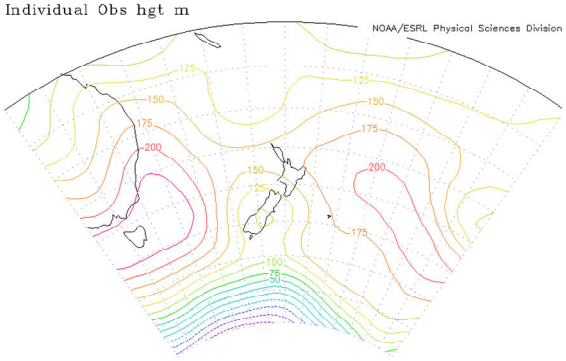


MAX=245
MIN=−109

NCEP Reanalysis Pressure Level GrADS image

**i) 21 Mar 2006 1200 hrs NZST. Lev: 1000 hPa.**

Individual Obs hgt m

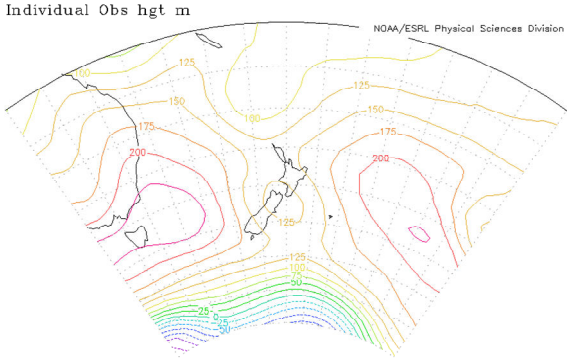


MAX=245
MIN=−165

NCEP Reanalysis Pressure Level GrADS image

**j) 22 Mar 2006 0000 hrs NZST. Lev: 1000 hPa.**

Individual Obs hgt m

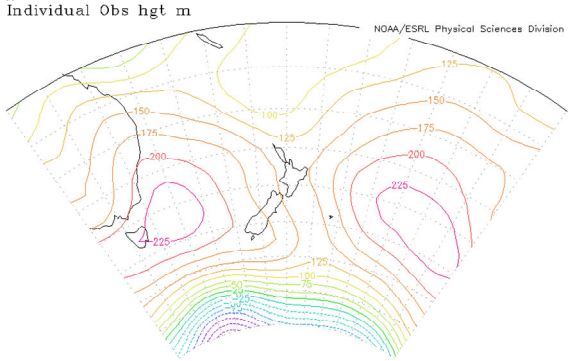


MAX=243
MIN=−186

NCEP Reanalysis Pressure Level GrADS image

**k) 22 Mar 2006 1200 hrs NZST. Lev: 1000 hPa.**

Individual Obs hgt m

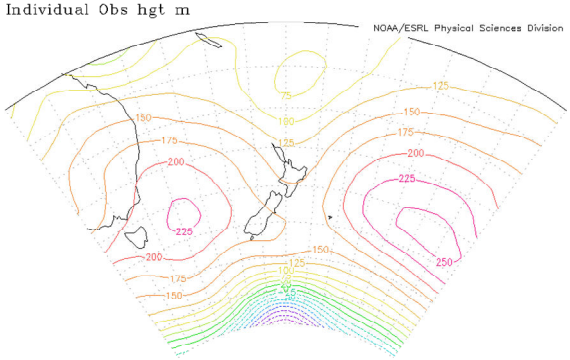


MAX=260
MIN=−224

NCEP Reanalysis Pressure Level GrADS image

**l) 23 Mar 2006 0000 hrs NZST. Lev: 1000 hPa.**

Individual Obs hgt m

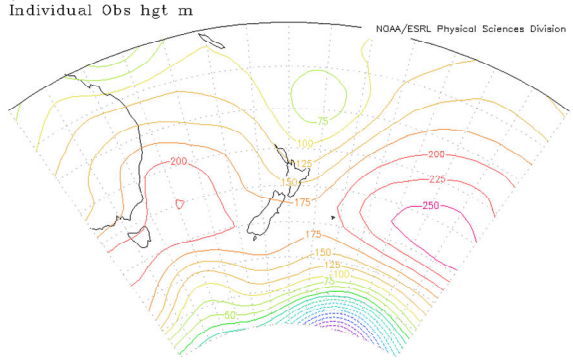


MAX=268
MIN=−226

NCEP Reanalysis Pressure Level GrADS image

**m) 23 Mar 2006 1200 hrs NZST. Lev: 1000 hPa.**

Individual Obs hgt m

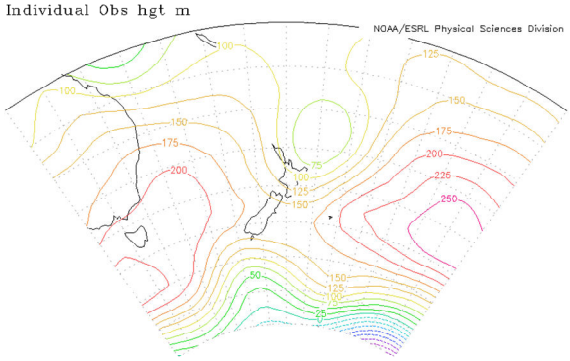


MAX=269
MIN=−203

NCEP Reanalysis Pressure Level GrADS image

**n) 24 Mar 2006 0000 hrs NZST. Lev: 1000 hPa.**

Individual Obs hgt m

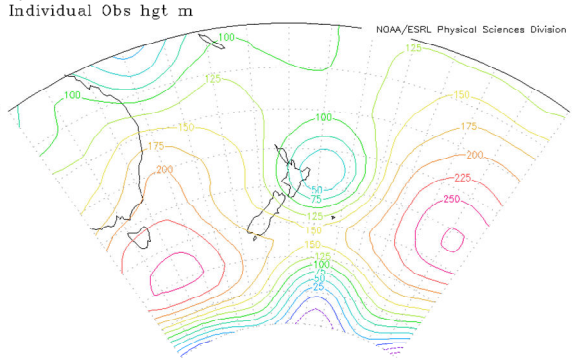


MAX=276
MIN=−76

NCEP Reanalysis Pressure Level GrADS image

**o) 24 Mar 2006 1200 hrs NZST. Lev: 1000 hPa.**

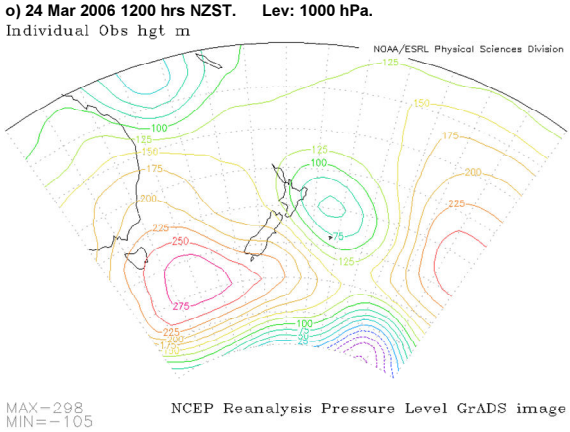


**p) 25 Mar 2006 0000 hrs NZST. Lev: 1000 hPa.**

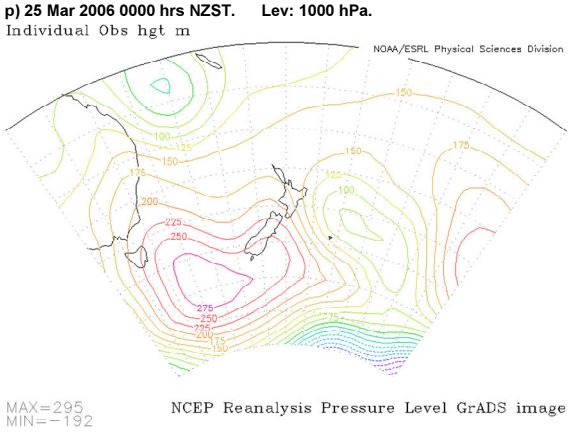


**q) 25 Mar 2006 1200 hrs NZST. Lev: 1000 hPa.**

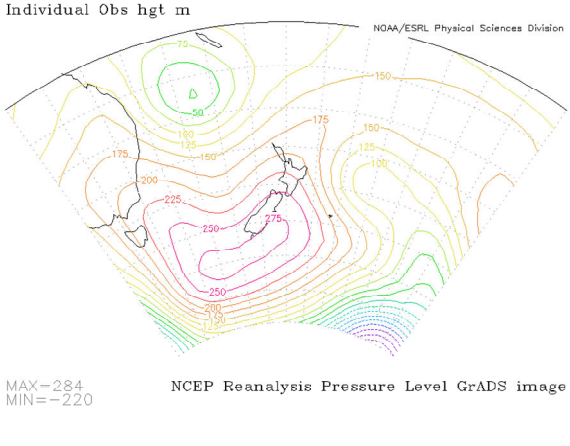


**r) 26 Mar 2006 0000 hrs NZST. Lev: 1000 hPa.**

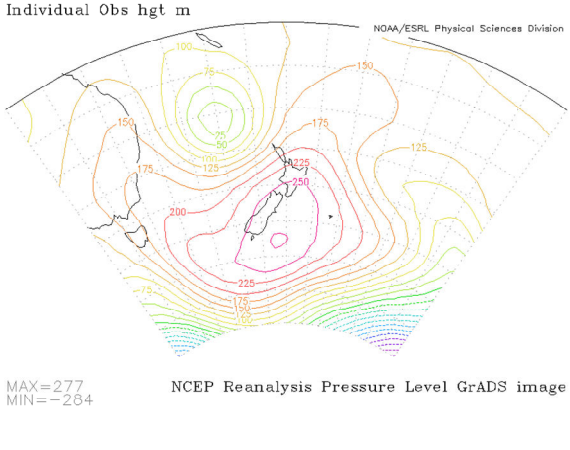

## Appendix 5D

# Statistical Methods used for WRF (ARW) and TAPM Performance Evaluation.

### 1. Pearson's Coefficient of Correlation (r)

Pearson's Correlation Coefficient describes co-linearity between the observed and predicted values.

$$\mathbf{r} = \frac{\sum_{i=1}^{N}(P_i - \overline{P}).(O_i - \overline{O})}{\left[\sum_{i=1}^{N}(P_i - \overline{P})^2 . \sum_{i=1}^{N}(O_i - \overline{O})^2\right]^{0.5}}$$

Where '$O_i$' is the observed value, '$P_i$' is the predicted values, '$\overline{O}$' is the observed mean and '$\overline{P}$' is the predicted mean value while '$N$' is the total number of cases or values in the sample.

### 2. Index of Agreement

The index of agreement is a dimensionless quantity and determines the degree to which observed values were accurately predicted by the modelled values.

$$IOA = 1 - \left[\frac{\sum_{i=1}^{N}(P_i - O_i)^2}{\sum_{i=1}^{N}\left(\left|P_i^{`}\right| + \left|O_i^{`}\right|\right)^2}\right]$$

Where $0 \le IOA \le 1$,

$P_i^{`} = P_i - \overline{O}$ and,

$O_i^{`} = O_i - \overline{O}$

## 3. Root Mean Squared Error

The root mean square error (RMSE) represents the average error produced by the model that refers to the average difference between observed and predicted values. The difference between P and O is squared that makes the statistic more conservative and more sensitive to extreme values.

$$\text{RMSE} = \left[ N^{-1}.\sum_{i=1}^{N}\left(P_i - O_i\right)^2 \right]^{0.5}$$

Since RMSE can not give information about the sources and/or types of error in the predicted data, it can be decomposed in to systematic and unsystematic parts as defined below

### 3.1 Systematic Root Mean Squared Error (RMSEs)

$$\text{RMSEs} = \left[ N^{-1}.\sum_{i=1}^{N}\left(\hat{P}_i - O_i\right)^2 \right]^{0.5}$$

Where $\hat{P}_i$ is regarded as the best estimate based on the least square regression of the form a + b* $O_i$ .

### 3.2 Unsystematic Root Mean Squared Error (RMSEu)

$$\text{RMSEu} = \left[ N^{-1}.\sum_{i=1}^{N}\left(P_i - \hat{P}_i\right)^2 \right]^{0.5}$$

## Appendix 5E

# Mean Sea Level Pressure Analysis for 24th March 2006

The MSLP Analysis charts for South Pacific Ocean are obtained from Bureau of Meteorology-Australian Government (2006).

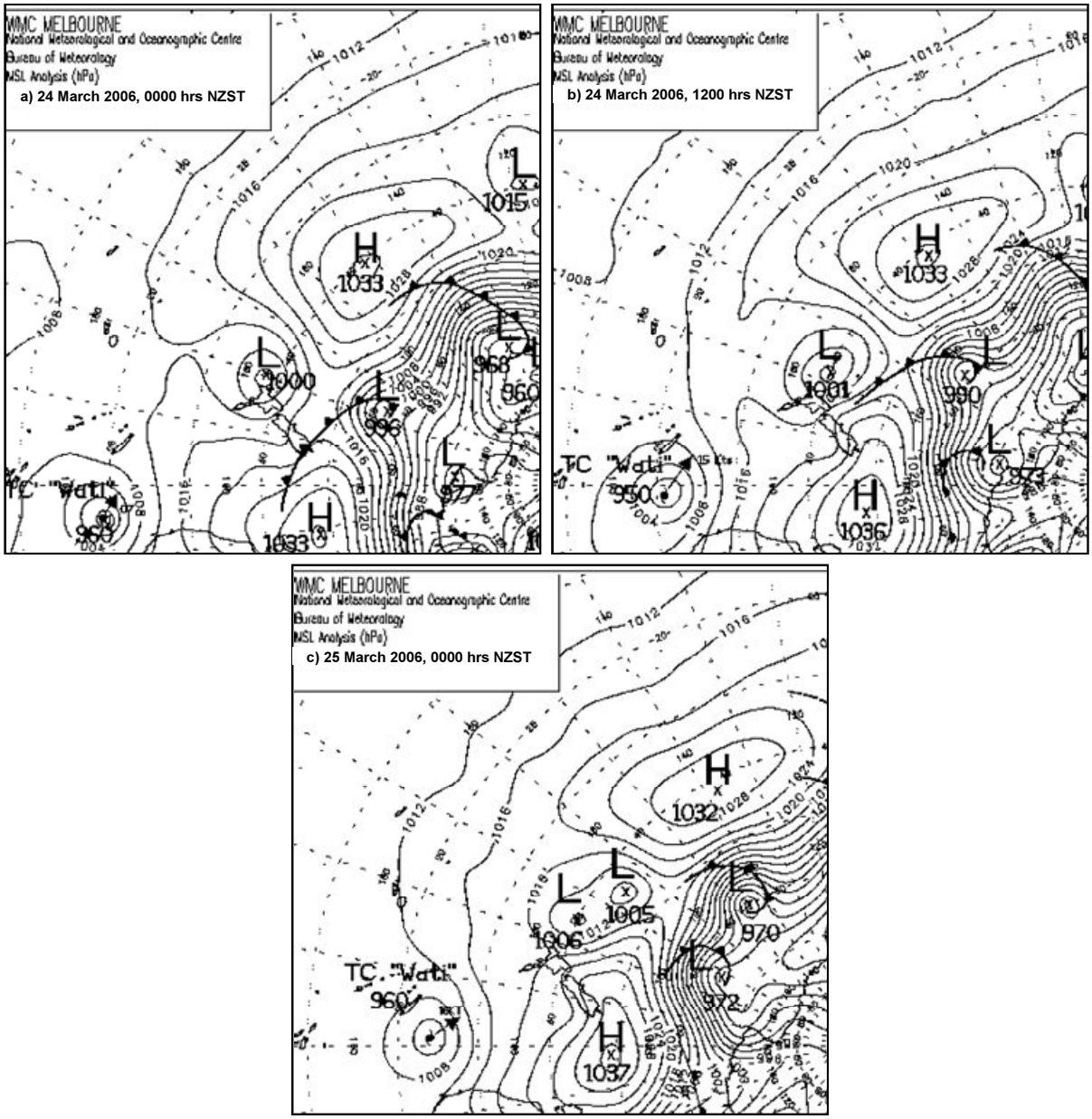


Bureau of Meteorology-Australian Government 2006, *MSLP Analysis Charts, Pacific Ocean*, from http://www.bom.gov.au/nmoc/MSL/index.shtml